10-2003

Development of a Design Guideline for Phase Construction of Steel Girder Bridges

Atorod Azizinamini
University of Nebraska - Lincoln, aazizinamini1@unl.edu

NDOR Research Project Number SPR-PL-1 (038) P530

FINAL REPORT

Development of a Design Guideline for Phase Construction of Steel Girder Bridges

Atorod Azizinamini, Ph.D., P.E.
Aaron J. Yakel
John P. Swendroski

National Bridge Research Organization (NaBRO)
(http://www.NaBRO.unl.edu)
Department of Civil Engineering
College of Engineering and Technology

W348 Nebraska Hall
Lincoln, Nebraska 68588-0531
Telephone (402) 472-5106
FAX (402) 472-6658

Sponsored By

Nebraska Department of Roads

October, 2003

University of Nebraska Lincoln

Table of Contents

List of Figures

List of Tables

APPENDIX C
Live Load Testing 307

Acknowledgement

Funding for this investigation was provided by the Nebraska Department of Roads. The authors would like to express their appreciation for this support. The authors would also like to express their thanks to Mr. Lyman Freemon, Gale Barnhill, and Sam Fallaha of the Bridge Division at the Nebraska Department of Roads (NDOR), and Curtis Smith of Capital Contractors for their assistance.

The opinions expressed in this report are those of the authors and do not necessarily represent the opinions of the sponsors.

Abstract

Although phased construction offers the benefit of maintained traffic flow during construction several problems have been observed. Problems such as differential elevation of the phases and premature deterioration of the closure region were examined in this project. The Dodge Street Bridge over I-480 in Omaha, Nebraska, was replaced utilizing phased construction. The bridge was instrumented and then monitored during and after its construction. The results obtained from this extensive monitoring along with other case studies and numerical modeling provided insight into the causes and potential remedies of the observed problems. A number of recommendations and design aids were developed to assist in the design and construction of a steel girder bridge using phased construction.

Executive Summary

Phased construction allows for the replacement of a bridge while maintaining traffic flow during the construction. A number of difficulties have been observed with the construction of bridges using phased construction. The main objective of this project was to develop recommendations for constructing steel girder bridges using the phased construction method which will alleviate the commonly encountered problems.

The first task was to identify those problems associated with the use of phased construction. The first problem identified is a potential for differential elevation between the phases at the time of closure. A number of factors, described in Chapter 2, can lead to this condition. The second problem commonly encountered on projects utilizing phased construction is a premature deterioration of the closure region. Again, this problem can have a number of causes and is discussed in Chapter 2.

Replacement of the Dodge Street Bridge over I-480 in Omaha, Nebraska provided an opportunity to monitor a phase construction project. Instrumentation was placed on the bridge to continuously monitor strains and deflections at various locations during construction and after. The monitoring is described in Chapter 3. In addition to the instrumentation and monitoring of Dodge Street over I-480, which provided the majority of data

for this project, two other projects that experienced significant problems utilizing phased construction are presented in Chapter 10.

Three-dimensional finite element modeling was carried out as is described in Chapter 4. The modeling was used to determine the source of deformations and isolate the impact which various factors have on the structure independent from one another.

One source of deformation which needs to be isolated is that attributable to temperature or seasonal fluctuation. Chapter 7 describes the methods used to deal with the movements due to temperature. An observation made was that vertical deflection is not directly correlated to temperature on a seasonal basis. Although there is a definite deflection trend from summer to winter, the deflection peak occurs about one month after the temperature peak.

The limited applicability of the AASHTO distribution factor equations with respect to number of girders was to be examined under this project. Since each phase of a phased construction project utilizes a fraction of the total girders in the structure a need for distribution factor equations which can accommodate a small number of girders is required. During the course of the project AASHTO provided recommendations for the calculation of distribution factors on structures with as few as three girders which rendered additional investigation unnecessary. Due to the torsional flexibility and lack of redundancy of a two girder system the recommended minimum number of girders in a phase expected to carry traffic is three. Note that this recommendation does not preclude the use of a two girder phase which is joined to the remaining structure prior to carrying traffic.

As the flexibility of the structure and predicted deflections increase, so too does the potential magnitude of error as well as corresponding need for additional provisions to assure a minimization of these errors. Therefore, the magnitude of dead load deflection appears to be a good, readily avail-

able, parameter to use in specifying the applicability of restrictions and advanced analysis requirements. Determination of limiting values beyond which a particular recommendation should apply was beyond the scope of this project as it will require time and field experience to develop reasonable limits. However, when appropriate, a qualitative assessment as to the sensitivity with respect to flexibility of a particular recommendation is provided.

It was found that maintaining symmetry of the cross section is very important to success in phased construction. Provisions for analysis are given in Chapter 5 in the event that an unequal number of girders is desired in each phase. However, the cross section of each phase should be made symmetric whenever possible and non-symmetric phase geometry should be prohibited as the anticipated dead load deflection grows large. The typical assumption that dead loads are evenly distributed is only valid for symmetric cross-sections. A number of problems arise with torsional loading and are exacerbated by the small number of girders often used in phase construction. The extreme situation is a one-sided closure, the use of which should be limited to cases with very low dead load deflections.

Care must be taken to ensure the end restraint conditions are the same for each phase. The construction sequence should be explicitly specified to ensure the order of operation is the same for both phases. If provisions for optional joints or details are provided ensure the same option is exercised on both phases. In addition, the construction of the first phase should not restrain the ends of the girders for the second phase and demolition of existing structures should not release restraint which was present during construction of the first phase. One particular recommendation is that a concrete end diaphragm encasing the girder ends should not be made continuous between the phases.

It was found that deflection over time was a key component to many causes of the identified problems. Therefore, if one were to be able to predict the deflections appropriate actions could be taken to avert problems. To this end, a computer program was developed to aid in this analysis and is described in Chapter 6.

As the predicted dead load deflection increases, an increasingly detailed time dependent deflection analysis should be performed. For a system with small deflections no analysis is necessary. A system with large dead load deflections should use the detailed time dependent analysis provided for in Chapter 6. The results of this analysis are then used to determine the anticipated stresses using the program described in Chapter 9. Systems anticipating a moderate amount of deflection could check the closure region stresses using a conservative value for time dependent deformation in lieu of the detailed analysis.

The cross frames within the closure region should be placed prior to joining the phases. After the closure region has been joined, a crane can no longer be used to place the cross frames requiring the frames to be placed by hand from below.

The cross frames joining the two phases is a potential topic for future research. There has been some speculation that these frames in this region may not be required at all or at least be of a minimal design. However, cross frames between the two phases may also help to protect the green concrete since one phase of the bridge is typically open to traffic during or immediately after the closure operation.

Although the designer seeks to eliminate differential elevation at time of closure there will be instances when a differential will exist. Two programs were developed to assist in this situation. The first determines the amount of slab tip deflection resulting from the addition of ballast on a single phase. The second program determines the deflections and stresses due

to the application of an uneven overlay. These programs cover the two most common methods for dealing with differential phase elevations.

The major findings with respect to the use of phase construction for steel girder bridges are summarized in the following list.

- Use AASHTO recommended distribution factors
  - Three girders are required to support traffic
- Ensure similar end restraint for phases
  - Control construction sequence
  - Require optional procedures are followed on both phases
- Maintain symmetry
  - Analysis for unequal number of girders
  - Maintain symmetry of phase geometry
- Perform time dependent deflection analysis
  - Detailed analysis with high dead load deflections
  - Reduced requirement for other cases
- Check stresses in closure due to differential time dependent deflection
- Place cross frames prior to joining closure region
- Suggested remediation strategies
  - Additional ballast
  - Uneven overlay

Several ancillary issues were addressed in response to communications with NDOR. The first dealt with the inability of some software used by NDOR to analyze structures utilizing a semi-integral abutment. An analysis method was developed in Chapter 5 which allows designers to model the semi-integral abutment using existing software.

The second issue examined the effect of pour sequencing on the predicted deflections. On large structures it is common to place and cure the concrete in the positive regions prior to the negative regions. This sequencing

means the positive region is composite when the negative region is placed. It was determined that ignoring the pouring sequence introduced no appreciable error.

The final issue examined was the longitudinal movement due to temperature and the impact the semi-integral abutments had on this movement. It was determined that the actual longitudinal deformation is 88% of the predicted value ignoring the effects of the abutments. The lower expected longitudinal movement reduces the required size of the expansion joint

Chapter

1 Introduction

Description and Motivation of Phase Construction

As America's infrastructure has aged, many bridges have reached or exceeded their design life. These bridges are in need of replacement with new designs that will serve in the coming years. One problem with completely removing some bridges while constructing the replacement is a lack of alternate traffic routes. In these situations it is necessary to keep the bridge partially open to traffic throughout construction of the new bridge. This bridge replacement technique, called staged or phase construction, involves replacing half of the bridge at a time and allowing traffic to flow on the other half. After the two phases of the new design are completed separately, they are joined by a closure pour to make the deck of the new bridge transversely continuous.

The replacement of an existing bridge while allowing the continuous flow of traffic is the reason for the popularity of Phase Construction. However, the AASHTO Bridge Design specifications do not specifically address potential problems and solutions for Phase Construction. Therefore, each state has its own unique approach for Phase Construction and the state of Nebraska is not an exception. Investigators for this project have had an opportunity to work closely with bridge engineers at NDOR to resolve problems related to bridges using phase construction. Phase construction is gaining popularity with NDOR and almost all new bridges are constructed using this concept.

1.1 OBJECTIVE

The main objective of this project was to develop guidelines for constructing bridges using the Phase Construction method. To accomplish this, four major facets of bridge design and construction to be impacted by the phase construction method have been identified and although there is some overlap these four have been separately addressed as such to the degree permissible. These four facets, analysis, deflections, constructability and closure pour are introduced in the following paragraphs.

Analysis of bridges using Phase Construction requires additional considerations beyond what AASHTO codes specify. For instance, the number of girders on each individual phase during construction is often less than 4 which invalidates the use of the distribution factors in the AASHTO specifications. Although beginning with the 1998 version the AASHTO specification has provided for the use of the lever rule in structures with 3 girders there are additional analysis requirements especially for phases with low numbers of girders. The problems with a low girder count are greatly exacerbated when symmetry is not maintained through the cross-section resulting in torsional deformations.

After the construction of the first phase and prior to the completion of the second, the first phase of the bridge experiences long term deflections due to creep and shrinkage causing challenging problems trying to match the elevations of the second half to the first half. As long as designers can estimate the final deflection of each girder these creep and shrinkage deflections can be accounted for and not pose a problem. However, problems arise when the predicted deflections are not close to those estimated by the engineers. An uneven deck surface results from not being able to predict the final deflection of each girder within reasonable accuracy. Repair costs are usually very high, in addition to the delays that occur before the bridge is opened to traffic.

The majority of problems observed during construction are related to the end conditions of the girders and sequence of construction. Determination of the end boundary condition is perhaps the single most important parameter for estimating the deflection of girders both over the short and long term. Therefore, one important task in the design and sequencing of a Phased Construction project is the identification and subsequent minimization of those factors which can tend to alter the end restraint condition between the construction of the two phases.

In many cases a middle strip is cast between the two phases referred to as the closure region. This segment, which is on the order of 4 to 6 feet wide, often experiences transverse and longitudinal cracking resulting in fast deterioration. Therefore, one objective of this project is to identify the causes for this cracking and through a combination of mitigating the causes and improving the closure region details reduce the amount of cracking and rate of deterioration. In certain circumstances the closure region may be eliminated all together in lieu of a one-sided closure. This situation is typically limited to short spans and criteria will be developed to determine when this type of closure is practical.

1.2 CONTENT OF REPORT

The first task addressed by the report is the identification of potential for problems associated with the Phase Construction method. These problems can largely be divided into two categories, short term and long term. In the short term, problems are typically constructability problems. The greatest of these being making the two phases arrive at the same elevation to allow for the completion of the closure operation. Long term concerns are typically performance issues, specifically the performance of the closure region.

The major physical task of this project was monitoring the replacement of the Dodge Street Bridge over I-480 in Omaha, Nebraska. Dodge Street is a major one-way arterial that carries commuters and goods out of the downtown business district. It would have been unacceptable to construct this bridge in one phase because of the volume of traffic it carries and the lack of an alternate route that could have absorbed the extra volume. The original bridge was a cast-in-place reinforced concrete box girder bridge. It had seven intermediate piers, eight spans, and the abutments were both skewed. The bridge was at the end of its life span and the concrete was beginning to degrade. The bridge carried four lanes of traffic, which allowed closure of two lanes to traffic for demolition and replacement, while keeping the other two lanes open. The new bridge at this site consists of eight two-span continuous composite girders, spaced at 2.87 m (9'5") spanning 72.09 m (236.5'). Each phase of construction consists of the placement of four girders and 7.6 m (25') of concrete deck. The closure pour is 1.01 m (40") wide. A more detailed description of the bridge and monitoring program can be found in Chapter 3.

Extensive finite element analyses were carried out using the Ansys analysis package. Chapter 4 describes the modeling techniques utilized and the accompanying verification accomplished by comparing the results to the

data obtained from the monitoring of the Dodge Street Bridge of I-480. This base model was then used as a benchmark for performing additional analyses and developing simplified analyses techniques.

The analysis techniques required to address many of the problems identified in Chapter 2 are developed in Chapter 5. In some instances such as bridges with horizontal curvature the recommendation is to perform a full three dimensional analysis. However, for many of the problems identified simple analysis techniques are available for addressing and evaluating the potential magnitude of the problems. Central to the analysis methods is the estimation of deformations. Immediate deformations are readily available during the course of the design process. However, short term and long term deflection predictions due to creep and shrinkage and also temperature effects are generally not estimated. However, these estimations are essential for the evaluation of phase construction project. Therefore, the analysis and prediction of long term deflections due to creep and shrinkage are addressed in Chapter 6 while the long term deflection due to temperature and other meteorological effects are addressed in Chapter 7.

There are a number of considerations which can aptly be considered construction issues and are addressed in Chapter 8. These are items such as construction sequencing and closure region detailing requirements.

A simple finite element analysis program has been developed based on the theory of discrete elastic foundations for the transverse analysis of cross-sections. Given the fact that many of the factors affecting the response are difficult to quantify combined with the knowledge that the impact of these factors are often of the same magnitude of the responses due to quantifiable factors the assumptions in the program are such as to provide for a simplified analysis rather than a more exact result. This will give the designer an approximation which can often be used to determine whether

or not a particular situation has a potential for problems and requires additional analysis.

The University of Nebraska in the past has been consulted on a couple of additional problems connected with the use of Phased Construction. Chapter 10 provides background information and the conclusions drawn from these investigations.

Contained in the Appendices is additional data obtained from the monitoring of the construction of the Dodge Street Bridge over I-480.

Chapter

2 Problem Identification

WHAT ARE THE PROBLEMS OBSERVED USING PHASED CONSTRUCTION

The problems encountered when using phased construction methods can be broken into two main categories. The first category deals with the short term constructability concerns while the other is concerned with the long term performance of the structure.

2.1 SHORT TERM CONSTRUCTABILITY CONCERNS

Many of the problems associated with phased construction occur during the construction itself. These problems can be broken into two categories. The first set of problems result in a condition where there is a differential elevation at the time of closure. That is, due to the various reasons which will be addressed in the following section, at the time of closure the first phase is at one elevation, while the second phase is at another. This can make it difficult; if not impossible to perform the closure region pour as

designed. The second set of problems manifest themselves as a torsional distortion of the individual phases. Again, this condition can make it difficult to perform the closure pour.

2.1.1 Differential Elevation at time of Closure

Figure 2-1 illustrates the problem of differential elevation at time of closure. The first and second phases are built as independent structures. The goal is that the two will be at the exact same elevation after completion such that they can be joined together into one structure as though it had been built all at one time. However, this goal is not always met. The following sections will identify some of the problems associated with the condition and possible sources which can lead to the condition.

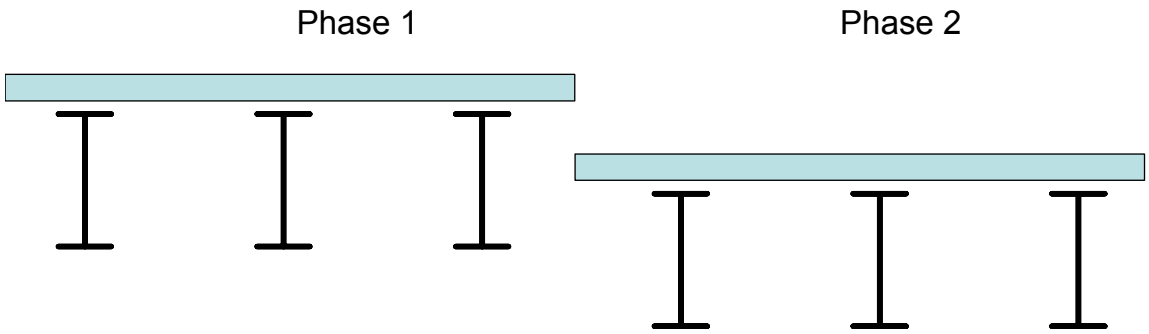

Figure 2-1: Differential Elevation

Problems associated with condition

The most immediate problem that arises due to the condition of differential elevation at the time of closure is difficulty in forming the closure region. The forms from one of the phases will not match the forms from the other phase leaving a gap where concrete could flow through. For small differentials, this problem could almost be ignored. However, as the differential increases, so to does the need for mitigation. Very large differentials may begin to interfere with the splicing of the transverse reinforcement as well.

A second problem which arises due to the differential elevation is an incorrect transverse deck profile. If the differential elevation is not eliminated prior to closure then the overlay may have to be modified to obtain the correct the profile and prevent poor drainage. Again, for small differences in elevation a slight modification to the overlay would be a simple remedy for this problem. However, for a large differential, the amount of modification to the overlay may become unacceptable. If the amount of additional overlay placed on the lower phase, becomes too great, the additional dead load may become a factor in the rating of the bridge. The amount of overlay placed on the higher phase may be reduced by some amount to offset the additional requirement. However, there is a limit to the reduction which can be made without adversely affecting the durability, life expectancy and performance of the thinner overlay.

The final problem associated with a differential elevation at the time of closure is the additional difficulty of installing the cross frames in the bay between the two phases. Although slotted holes can accommodate some amount of differential, there is a limit to the length of the slot. For a 7/8" diameter bolt, the AASHTO Specification limits the length of a long slot to 2-3/16".

Common causes

There are a number of possible sources of differential elevation. Several will be identified in this section. While some of the differential elevation stems from sources that are easy to quantify and therefore compensate for, other sources are very difficult to identify let alone quantify.

One of the easiest sources to identify is differential elevation due to construction errors or tolerances. Specifically these can include errors in the surveying of girder seat elevations, differences in camber, and splice fit-up tolerances. These can all result in differences between the phases, however are generally considered negligible and do not contribute since any dis-

crepancies are taken care of by varying the amount of shim, or pad depth between the girder and slab. Of course, this operation could also be a source of error.

Several other easily identified factors that can contribute to differential elevation are design oversights and construction sequencing. These two are related in that the specified construction sequencing, or lack thereof, is part of the design. One common source of differential elevation arises from allowing the contractor to make decisions in sequencing which can impact the deflections. An example of this would be the timing of the approach slab pour. As the approach slab is doweled to the turndown, which in turn encases the girder ends, the approach slab coupled with the backfill behind the turndown can lend partial rotation restraint to the end of the girder. If the approach slab is present during the deck pour of one phase and not the other, the end restraint condition would not be equal and one would not expect the same deflections as a result of the deck pour.

A more difficult source of differential elevation is associated with time dependent deflections which occur between the construction of the two phases. These movements are generally attributed to creep and shrinkage, or possible settlement and loss of restraint behind the turndown. These items are not as easily quantified since it requires continuous monitoring and careful record keeping to know when quasi-transient loads such as temporary barriers are placed and moved around. These loads are classified as quasi-transient since they are not permanent loads; however, they are not live loads. Since they act for a relatively longer period of time, often on green concrete, they have the potential for contributing significantly to creep deflections.

Finally, the most difficult to predict potential source of differential elevation is due to temperature and seasonal effects. Temperature can affect the deflection of the bridge both in the long and short term. Unequal heating

of the bridge due to sunlight can also result in short term movements which must be taken into account. Humidity and precipitation can forestall, and even temporarily reverse the predicted shrinkage behavior of the concrete.

2.1.2 Torsional Distortion of Individual Phases

Figure 2-2 illustrates a torsional distortion of one of the phases. Torsional distortion can also occur in both phases depending on the cause of the distortion, the direction of the distortion may be the same, or opposite between the phases.

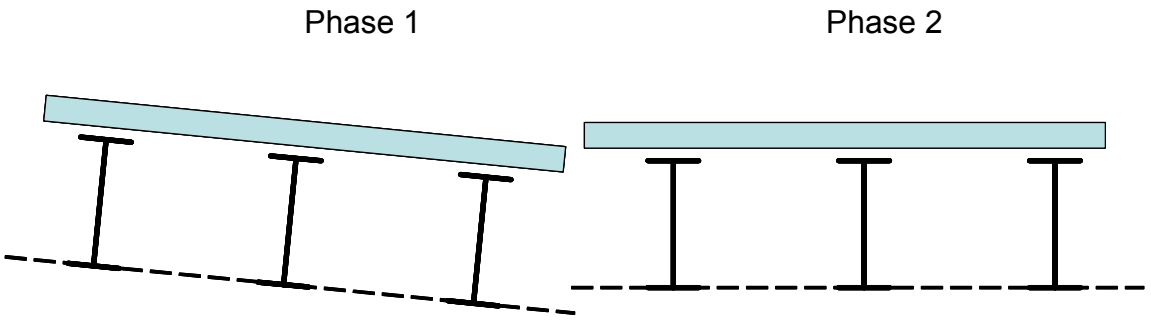

Figure 2-2: Torsional Distortion

Problems associated with condition

Many of the problems associated with torsional distortion of individual phases are similar to those associated with a differential elevation at the time of closure.

Again these include difficulty in forming the closure region. The forms from one of the phases will not match the forms from the other phase leaving a gap where concrete could flow through. An incorrect transverse deck profile is a second problem which can arise due to the torsional distortion. This can result in poor drainage and require additional overlay to correct. Also, difficulty installing the cross frames in the bay between the two phases may occur.

One additional possible cause for concern is the potential for gross instability and even possible collapse. This problem would only be exhibited in very un-symmetric cross-sections or those on a horizontal curve.

CAUSES

Some of the potential causes of torsional distortion are related to design. An un-symmetric placement of the deck over the girder pattern can result in rotation. Although the final design with all girders may be symmetric, one of the phases may be made un-symmetric to accommodate the design criteria.

Placement of the temporary and permanent barriers can cause a rotation within a phase. Although cross-frames are thought to help in distributing the load transversely between the girders, experiments and 3-Dimensional analysis show that this is not always accomplished.

Along the lines of the previous cause are any other un-symmetric loads, permanent, or more likely, temporary construction loads.

2.2 LONG TERM PERFORMANCE CONCERNS

Although the completed structure after phased construction is similar to a structure constructed entirely at one time there are some differences in the long term performance which arise due to the phased construction methods utilized.

2.2.1 ADDITIONAL DIFFERENTIAL DEFLECTION AFTER CLOSURE

Due to the very definition of phased construction, one phase of the bridge will be older than the other. Therefore, the older phase has had more time to allow its dead loads to “settle in” and has seen the presence of live loading for a much longer period of time prior to connection of the two phases. Therefore, after the closure operation has been performed, there is catch up period where the newer phase is attempting to undergo the same “set-

tling in" that the first phase has already performed. However, the movement of the second phase is now restrained by its connection to the first phase.

PROBLEMS ASSOCIATED WITH CONDITION

There are several problems associated with this additional deflection. The first is an incorrect transverse profile. After the closure operation is performed and the overlay placed such that the desired profile has been obtained, additional deflection of one of the phases distorts this desired profile. Although the magnitudes of such distortions are expected to be small, the condition could manifest itself as drainage problems resulting in hazardous ponding during rains, or patches of ice due to melt-water refreezing during the winter.

As the second phase attempts to deflect after the two have been joined, it is restrained by its connection to the other. This connection is made up of a strip of concrete and the cross-frames between the two phases. The restraint of the relative deflection provided by this connection will result in increased stresses in the closure region and cross frames. Large stress in the closure region could lead to cracking and premature deterioration of the closure region. Large stresses in the cross frames could result in fatigue problems at the connection between the cross frame and the girder. Loads in the cross frame can result in a biaxial state of bending applied to the tension flange resulting in a larger state of stress.

CAUSES

The most apparent cause of additional defection is due to creep and shrinkage. The first phase, usually being at least 3 months older than the second at the time of closure, has had time for a majority of creep and shrinkage deflections to occur. Figure 2-3 shows a typical creep and shrinkage response versus time. The second phase, having been cast on the order of several weeks before closure, will still be expected to experience an additional amount of deflection over time.

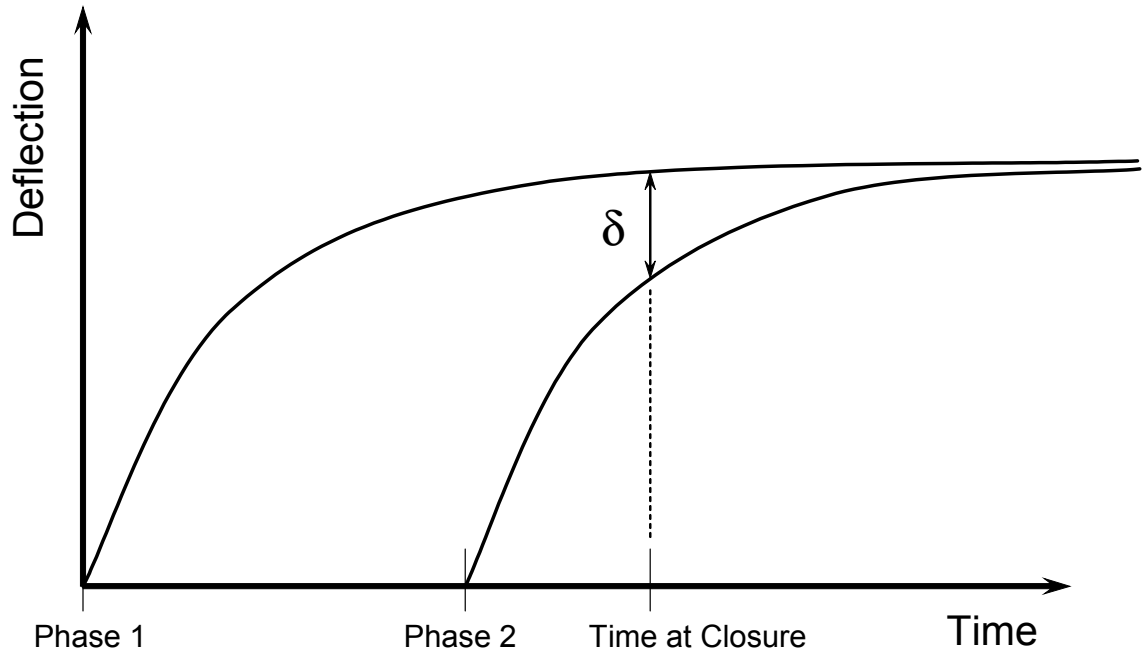

Figure 2-3: Creep and Shrinkage over Time

This condition can be exacerbated by an unequal addition of dead loads tending to drive the creep deflection on the newer phase. These loads can be caused by the addition of permanent barriers and utility attachments. Although symmetric barriers and attachments may exist on the first phase, this need not be true. Another source of additional loading can be due the application of additional overlay to compensate for an incorrect transverse profile as discussed in Section 8.3.

A final possible cause for the additional relative deflection is due to settlement. As the bridge responds to live loading and temperature effects, the soil behind the turndowns and abutments can become increasingly compacted. When the bridge contracts due to cold weather, contact can be lost between the soil and the turndown, reducing the end restraint condition. The potential for this phenomenon is greater for the first phase as it has been in place for a longer period of time than the second phase. This can result in a differential response between the two phases.

2.2.2 Premature Deterioration of Longitudinal Closure Region

The strongest, most durable deck is comprised of a single monolithic slab of concrete. Any break in that monolithic slab serves as an incipiency for deterioration. Therefore, it is not surprising that one concern in the use of phased construction is for the premature deterioration of the closure region which requires two, or in some cases only one, cold joint running longitudinally the full length of the bridge.

Problems associated with condition

The problems are those typically associated with deteriorating concrete including formation of potholes and spalling of concrete from the underside of the bridge. Also of concern is corrosion of the deck steel due to exposure to de-icing chemicals

Causes

As was previously mentioned, the most prevalent cause for premature deterioration of the longitudinal closure region of a bridge constructed using phased construction is the presence of one or two longitudinal cold joints between the phases. Although one would expect deterioration to take place in any concrete structure over time there is increased concern in the case of a bridge constructed using phased construction over the rapid onset of the condition.

A second cause which can lead to premature deterioration is excessive stresses. This can be due to differential deflection of the phases relative to each other after completion of the closure pour as discussed in Section 2.2.1. If these stresses exceed the cracking stress of the concrete, cracks will form allowing penetration of water eventually causing freeze-thaw cycle damage to the closure region.

Chapter

3 Monitoring Program Overview

INSTRUMENTATION OF THE DODGE STREET BRIDGE OVER I-480

Since much of the report will rely on references to the monitoring of the Dodge Street Bridge over I-480 in Omaha, Nebraska, an overview and introduction to the monitoring program is presented in this Chapter. Additional details of the monitoring is provided in Appendix A. The thesis, *Field Monitoring of a Staged Construction Project*, contains extensive information as well (Swendroski 2001).

3.1 EXPERIMENTAL PROGRAM OVERVIEW

Replacement of Dodge Street over I-480 in Omaha, Nebraska provided an opportunity to monitor a phase construction project. Each construction phase was monitored to gain behavioral insights. Gages were used to monitor steel strains, concrete strains, and deflections. Both short-term data,

during construction events, and long term-data were investigated. Live load tests were performed to determine distribution factors as will be described in more detail in Appendix C.

Monitoring of Dodge Street Bridge is an ongoing project. This report concerns the construction, gaging, and analysis of data collected from October 20, 1999 through May 5, 2002. Data has been analyzed to investigate long-term data trends including creep, shrinkage, and temperature effects. Data from the two phases is compared to verify similar behavior. Design assumptions are investigated to determine their validity.

3.1.1 Challenges Faced in Field Monitoring

Several challenges were encountered in field monitoring. Gages were either placed in the field or at Lincoln Steel, where the girders were fabricated. Although proper procedures were followed to ensure gages were applied properly this makes the task cumbersome. Once gages are placed, wires from the gage to the data acquisition unit must be placed in the field. After installation on the bridge, girders are over 20 feet off the ground which made this process difficult and dangerous. Instrumentation locations are somewhat limited as frames to monitor deflection had to be placed so they would not interfere with construction equipment or I-480 traffic that runs under the bridge. Several large television transmission towers are also present near the bridge. Radio waves can interfere with the transmission of electrical signals through gage wires. Shielded wires were used to eliminate the problem.

Many construction events affect the loading on bridge girders, such as placement of heavy temporary barriers and removal of formwork. In order to understand the strain data collected from each girder, it is desirable to know exactly when these events occur. Unfortunately there is significant uncertainty regarding construction timing. As the bridge is 60 miles away it is not possible to be there continuously observing construction. Also,

construction occurs at a rapid pace and not even the contractor knows in advance when certain events will occur so the drive to be there could be made. Communication with the construction manager enables dates of events to be obtained, however beginning and end times are not recorded. For instance, barriers may have been placed on June 4, 2001 but the start and ending times must be determined from analyzing data. As formwork removal takes a very long time, up to two months, it is impossible to determine the affect removing this load has.

The fact that monitoring occurs in an uncontrollable environment, versus a laboratory for example, also adds challenges. A laboratory environment stays relatively stable allowing the direct observation of long-term concrete affects. In the field, temperature and weather change. Not only does temperature increase or decrease seasonally but the temperature profile across the girder changes daily as the sun warms the deck faster than girders. These temperature changes affect bridge behavior. Environmental affects must be removed to directly observe how various construction events and long-term concrete behavior effect strains and deflections. These environmental affects have been studied and presented. Attempts have been made to remove these effects to more directly observe time dependent concrete effects but more work should be done to better understand this behavior. Finally, live load is present during monitoring as the phases carry traffic. This will cause some variation in readings and make it more difficult to directly observe long-term concrete behavior. Ideally this would not be present but there is no way to uncouple the live load effects.

3.2 Bridge Description

Replacement of Dodge Street Bridge over I-480 in Omaha, Nebraska provided an opportunity to monitor a project built utilizing staged construction. Dodge Street (US Highway 6) is a major arterial and complete closure to traffic during construction was not feasible. The new bridge, which is a

two span continuous steel plate girder bridge, replaces a 1963 eight span cast-in-place reinforced concrete box girder bridge. The new bridge will carry the same four traffic lanes and two pedestrian sidewalks as the old bridge. The completed new bridge consists of eight continuous steel plate girders spaced 9 ft., 5 in. apart spanning two equal 236.5 ft. spans. Each construction phase consisted of four girders topped by a 7.0 in. deep by 34ft. 10in. wide deck built compositely with the girders. The width of the closure pour joining the two phases is 40 in. After the closure pour, an overlay brought the final deck thickness to 8.5 in. and permanent railings were slip-formed. All plate girders were hybrid. Over the pier, girders utilize HPS-70W steel (High Performance Weathering Steel with 70 ksi yield strength) for both flanges. In the positive moment section, only the tension flanges use HPS-70W steel while the compression flanges use A709-50W steel. A709-50W steel was selected for web materials.

3.2.1 GIRDERS

The eight girders for the completed bridge are identical and change section properties at five locations as shown in Figure 3-1. The girders are longitudinally symmetric about the pier. There are 4 field splices, two on each side of the pier, so each girder was manufactured in five sections. Girder spacing is 9 ft. 5 in. on center. Girders are named according to letter designation. Girders E, G, H and J are contained in Phase I while A, B, C, and D are in Phase II. The five field sections are designated by girder letter and section number, such as A3.

Girder camber accounts for dead load deflections and the substantial vertical roadway curvature, accommodating nearly 7 ft of elevation difference between east and west abutments. The west abutment is higher than the east. Figure 3-2 contains the blocking diagram from the bridge design and Figure 3-3 contains the blocking ordinates.

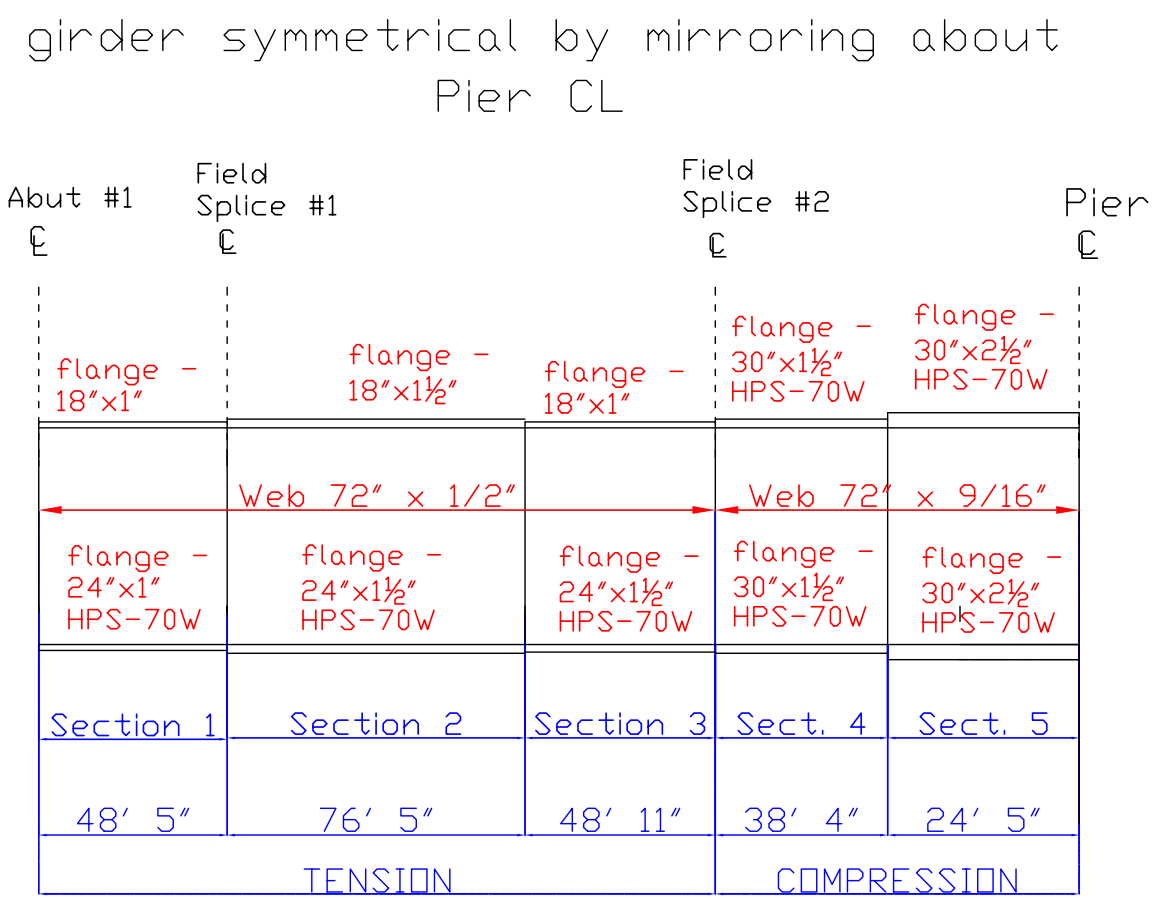

Figure 3-1: Girder plate dimensions. Note symmetry about the Pier CL. All steel is A709-50W unless noted otherwise.

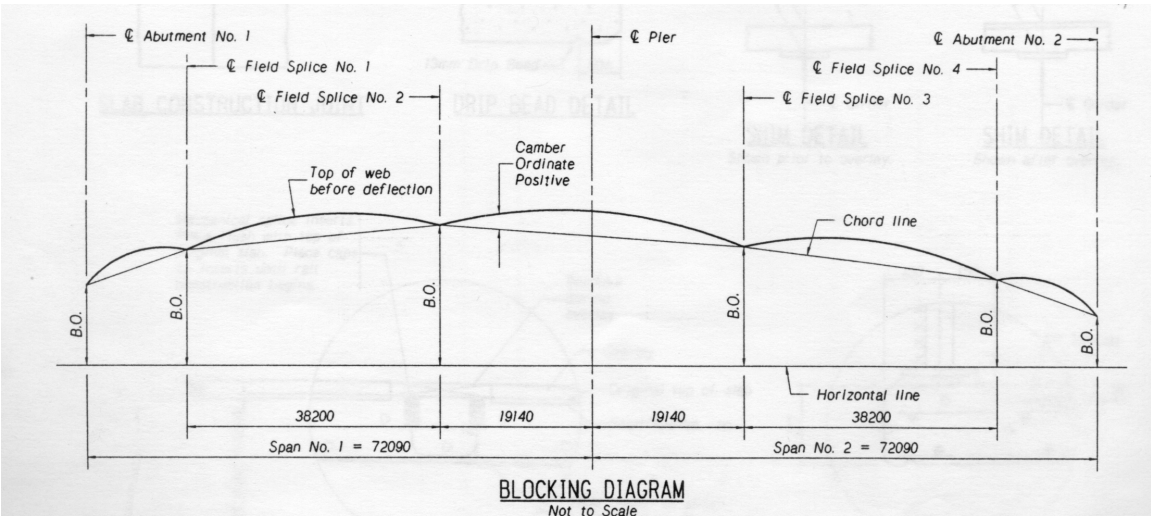

Figure 3-2: Blocking diagram for girders. Units are in mm.

DEFLECTION, CAMBER, AND BLOCKING ORDINATES FOR GIRDERS

Tenth Point	Deflection Ordinate (mm)	Camber Ordinate (mm)	Blocking Ordinate (mm)
1.0	0	0	2117
1.1	121	15	
1.2	217	2	
FS 1	220	0	2762
1.3	274	150	
1.4	293	234	
1.5	273	240	
1.6	221	176	
1.7	147	53	
FS 2	120	0	3165
1.8	73	11	
1.9	20	14	
2.0	0	13	2897
2.1	20	14	
2.2	73	11	
FS 3	120	0	2603
2.3	147	53	
2.4	221	176	
2.5	273	240	
2.6	293	234	
2.7	274	150	
FS 4	220	0	1078
2.8	217	2	
2.9	121	15	
3.0	0	0	0

Figure 3-3: Blocking ordinates for girders. Units are in mm.

Figure 3-4: Shear Studs on the top flange. Picture is taken looking West. From right to left are Girders E, G, H, and J during erection for Phase I.

Shear studs welded to the top flange will provide composite action with the deck. The shear studs are M7/8 x 5" with three per row spaced 24" between rows. An example of the shear stud placement can be seen in Figure 3-4.

3.2.2 Cross Frames

Figures 3-5 and 3-6 show cross frame locations and orientations. Cross frames were placed to provide compression flange bracing during construction and transverse continuity. Cross frame locations are symmetric about the pier.

3.2.3 Deck

The slab for the completed bridge consists of three parts. The first two parts are the slabs cast in Phases I and II. These slabs are 7.0 in. thick by 34ft. 10in. wide built compositely with the girders. The third completed deck section is the closure region which is 7 in. thick by 40 in. wide and connects the two phases as shown in Figure 3-7.

Once the three sections of the deck are completed an overlay seals the joints and brings the total deck thickness to 8.5 in. as shown in Figure 3-7.

3.2.4 Permanent Railings

Once the overlay is complete, NDOR standard closed concrete rails are slip-formed on each side separating two 9 ft. sidewalks from 54 ft. of clear roadway. Figure 3-8 is a cross section of the completed bridge.

3.3 Construction Sequence

The purpose of Staged construction is to maintain traffic flow while an existing bridge is being replaced. To perform this task on Dodge Street over I-480, several steps were taken. First, the southern half of the existing bridge was removed allowing the construction of Phase I. During this time temporary barriers were placed on the remaining half of the existing bridge allowing for two lanes of traffic and a pedestrian sidewalk.

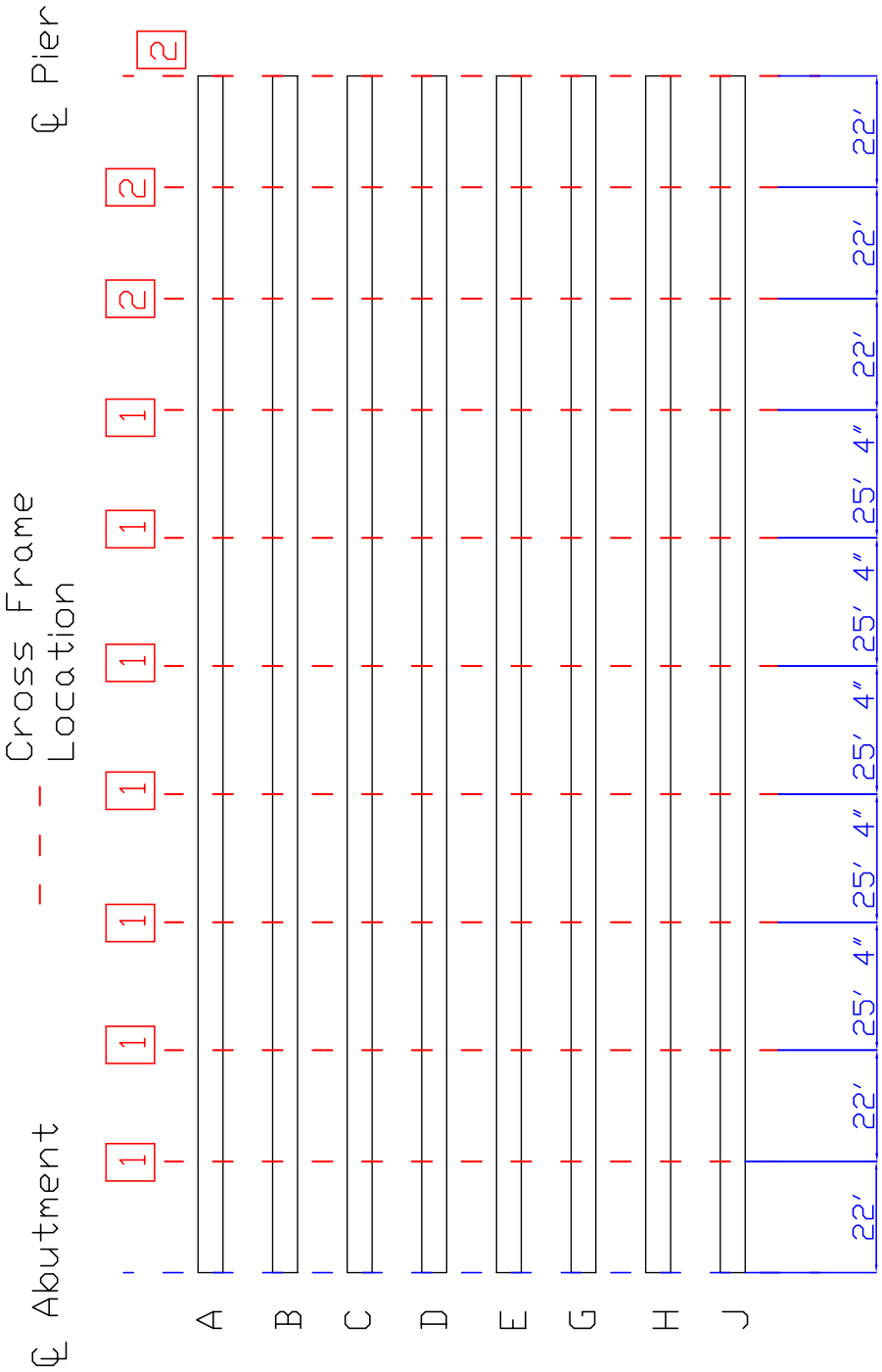

Figure 3-5: Location of Cross Frames. Refer to Figure 2.6 for orientation.

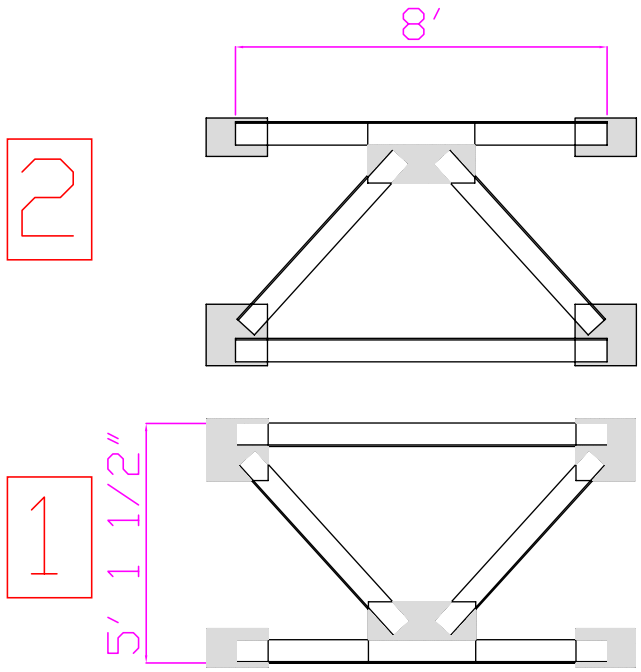

Figure 3-6: Orientation of Cross Frames. All members are L6x6x3/8

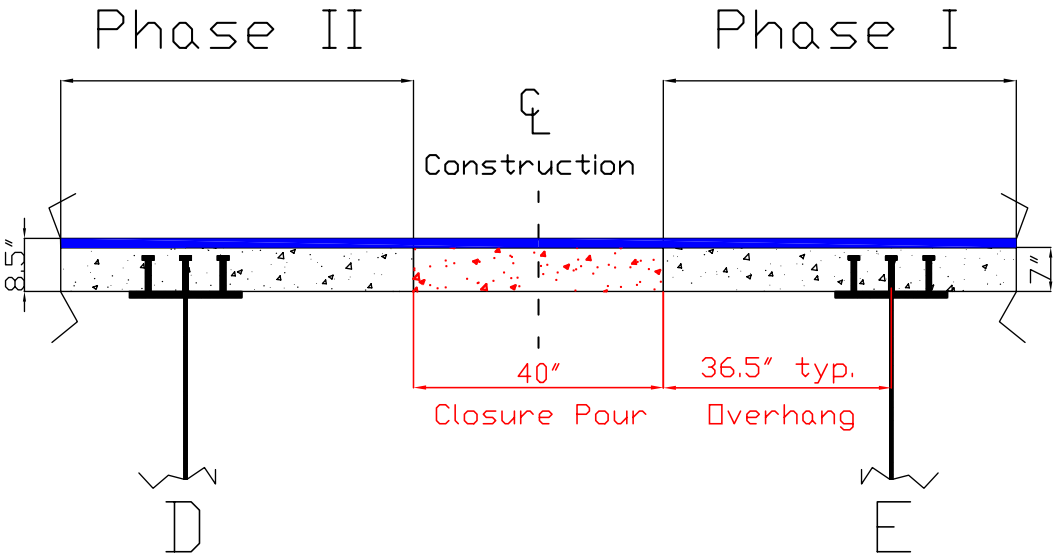

Figure 3-7: Deck thickness

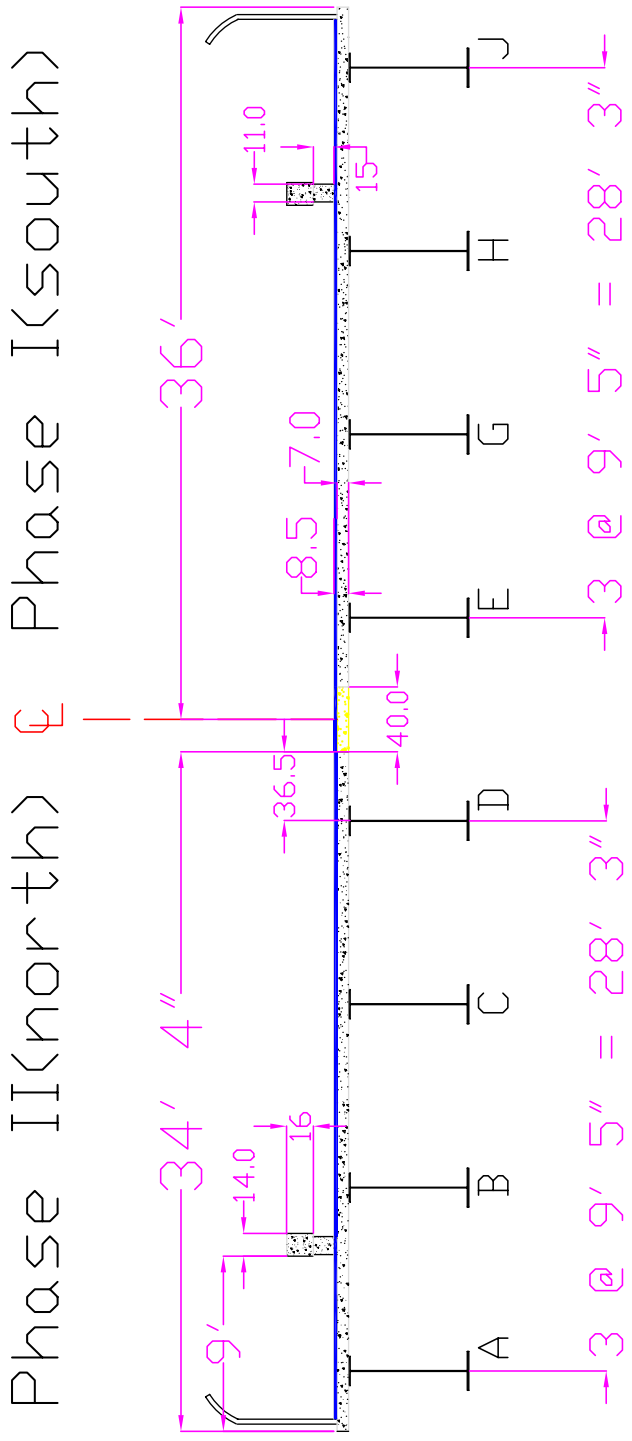

Figure 3-8: Completed bridge cross section. Note the phases are symmetric about the centerline. All dimensions are inches unless noted otherwise.

Once Phase I was completed, temporary barriers were placed and traffic was switched onto the completed phase. The remaining half of the old bridge was then demolished. Phase II was constructed while Phase I carried traffic.

Once Phase II's deck was complete, the entire bridge was closed for 2 days while the closure pour operation joined the phases. Temporary barriers were used to maintain traffic flow while the overlay was placed first on the North side then on the South side. Next, permanent barriers were slip-formed utilizing temporary barriers to maintain traffic flow. Finally, all four traffic lanes and both pedestrian sidewalks were opened.

3.3.1 Construction of Phase I

After the southern half of the existing bridge had been removed and traffic was being carried on the existing bridge's remaining half, Phase I construction started. The first operations were those concerning the substructure: pile driving, constructing the concrete pier, and pile cap pouring. Once these operations were complete superstructure work could begin.

Girder Erection

Figure 3-9 is a graphical representation of the erection sequence. The like shaded girder sections were erected simultaneously and in the order indicated below the figure. Table 3-1 includes the dates girder sections were erected.

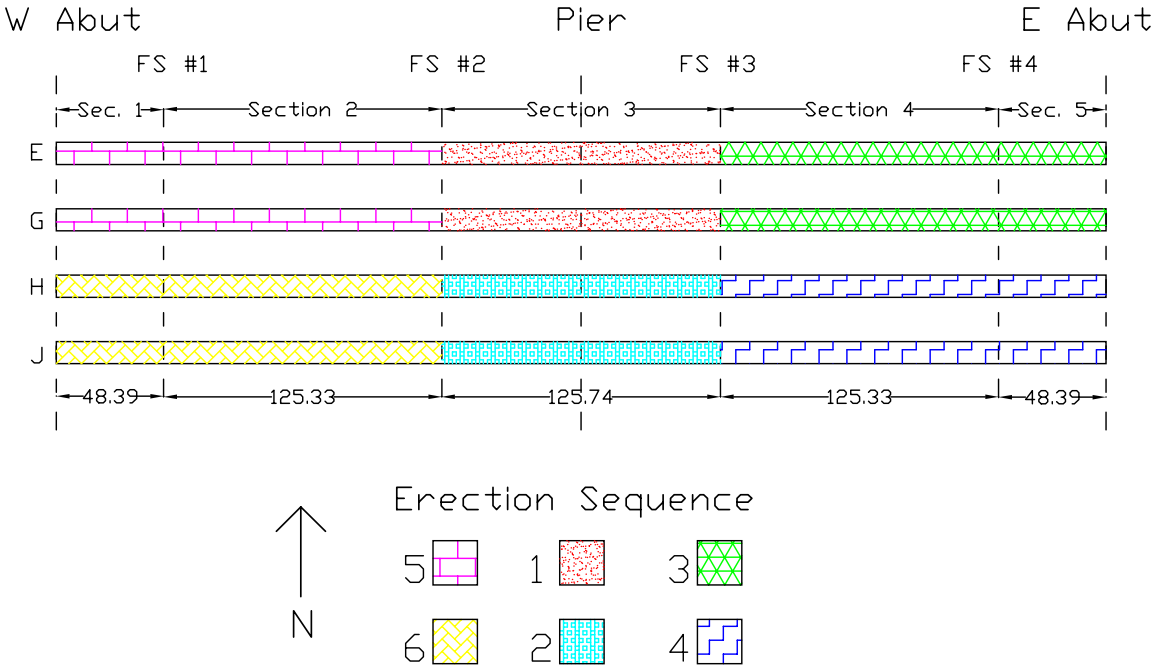

Figure 3-9: Girder erection sequence for Phase I

Event	Date Started	Date Completed
Pour of Pier		6/21/99
East Abutment Poured		7/15/99
West Abutment Poured		7/28/99
Girder Placement	8/31/99	9/14/99
Girders E3 and G3		8/31/99
Girders H3 and J3		9/1/99
Girders E4-E5 and G4-G5		9/3/99
Girders H4-H5 and J4-J5		9/8/99
Girders E1-E2 and G1-G2		9/10/99
Girders H1-H2 and J1-J2		9/14/99
Deck Formwork Placed	9/18/99	10/7/99
Rebar Placed for deck	10/4/99	10/13/99
Positive Region Pour		10/20/99
Negative Region Pour		10/28/99
Pedestrian Fencing Installed	11/5/99	11/9/99
Placement of Traffic Barriers on Ph. I	11/5/99	11/12/99
South Side Temporary		11/5/99
North Side Temporary		11/12/99
Phase I Opened to Traffic		11/15/99

Table 3-1: Construction Time Table for Phase I

Phase I girders were erected as follows. Sections E3 and G3 were connected by their cross frames while on the ground and placed on the pier. Temporary shoring supported the girders so wind would not blow them off. Next, Sections H3 and J3 were connected on the ground and placed on the pier. While in the air, cross frames between Girders G and H were placed. Now all girder sections over the pier were in place as seen in Figure 3-10. In the figure Girder J is in forefront. Note the temporary shoring supporting the West (left) side.

Figure 3-10: Girder sections E3, G3, H3, and J3 placed over the pier

East span girder sections were erected after the pier sections were in place. While on the ground, sections 4 and 5 were spliced together for Girders E and G. The cross frames connecting Girder E to G and the cross frames that connect Girder G to H were placed before lifting. This unit was then spliced with girder section 3 while in the air and placed on the East abutment girder seats. Girder sections 4 and 5 of Girders H and J were placed in the same way. Figures 3-11 and 3-12 show these sections in place. Note in Figure 3-11 that Girder E is on the left and girder G is to the right. Also note the girders supported by the East abutment and cross frames ready to accept Girder H. Splice to section 3 is not visible.

Figure 3-11: Girder sections 4 and 5 of the East span

Figure 3-12: All four girders for East span in place.

The final girder sections erected for Phase I were those for the West Span. Sections 1 and 2 of Girders E and G were spliced together. The cross frames connecting them were placed along with the cross frames to accept Girder H. This unit was then spliced with girder section 3 in the air and placed on the West abutment girder seats. Girder sections 1 and 2 of Girders H and J were placed in the same way. Figure 3-13 shows the West span girders in place. Note in the figure that the west abutment and the temporary shoring to support section 3 has been removed as it is no longer needed. Girder J is in forefront. Posts on top of the girders are for the safety of construction workers.

Figure 3-13: West span girders in place

Girder sections were spliced in the field using 22.2mm ASTM A325M bolts. Each side of the splice contained 2 lines of 5 bolts in top flange splices, 2 lines of 23 bolts in web splices, and 2 lines of 10 bolts in bottom flange splices. Splice plates utilized A709-50W steel. Top flange splice plates were 0.625" thick, web splice plates were 0.5" thick, and bottom flange splice plates were 1.0" thick. Filler plates were of appropriate size. A typical splice is shown in Figure 3-14.

Figure 3-14: Girder splice

DECK POURING SEQUENCE

Once girder erection is complete the deck formwork and rebar can be placed. Forming the deck with plywood and metal hangers was carried out between 9/18/1999 to 10/7/1999. Placement of rebar took place between 10/4/1999 and 10/13/1999.

The concrete deck for Phases I and II was cast in the following sequence. Starting at a distance of 167' 4" from each abutment, concrete was poured simultaneously using two crews working towards each abutment as seen in Figure 3-15. The pour was 7" thick and 34' 4" wide. This pour is referred to as the positive region pour. The pour was performed 10/20/99 for Phase I.

The remaining portion of the deck was cast after the positive region concrete reached its 28 day design strength. This pour had a 138' 4" length. The pour started on the East span and ended on the West span. This “neg-

ative region pour" can be seen in Figure 3-16. This portion of the deck was poured 10/28/99 for Phase I.

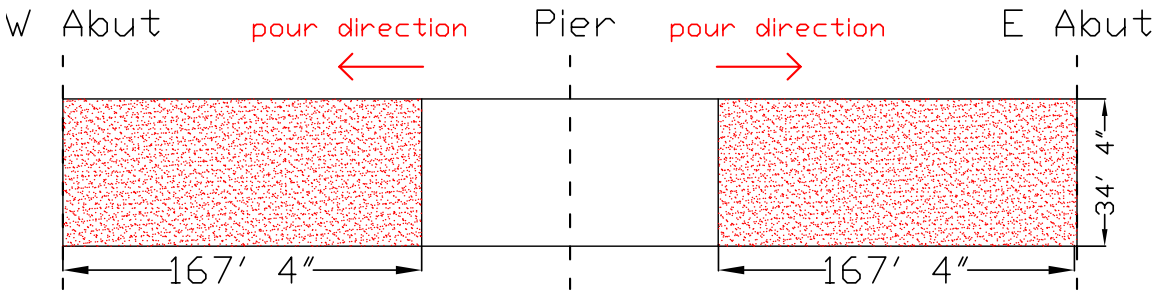

Figure 3-15: Positive region pour.

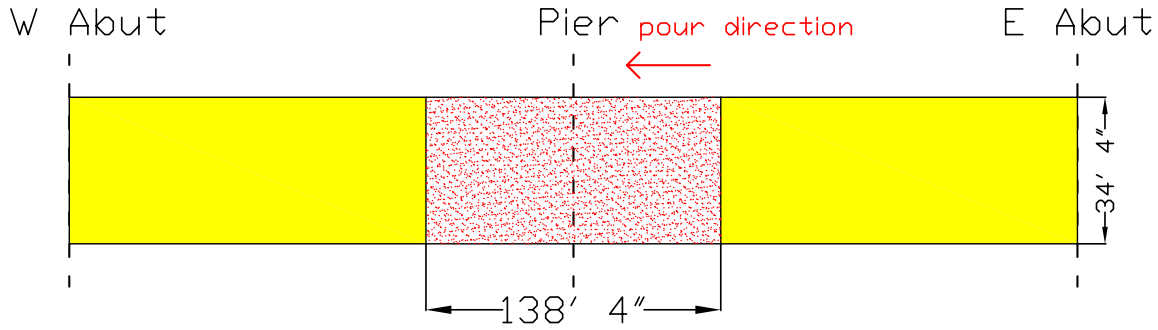

Figure 3-16: Negative region pour

Temporary Guardrail and Fencing

With the deck of Phase I complete it is nearly ready to carry traffic. Before that is possible pedestrian fencing must be placed and temporary barriers located to separate traffic lanes from the sidewalk. The fencing was placed on the South side of Phase I from 11/5/99 to 11/9/99. Temporary barriers were placed on the Southern side of Phase I on 11/5/99. On 11/12/99 temporary barriers were placed on the North side, near the closure pour location. Barrier locations are shown in Figure 3-17. In the figure Girder E is on the North side and is closest to the closure region. The remaining half of the existing bridge would be North (right) of Girder E.

Phase I opens to Traffic

On 11/15/99 traffic was switched from the Northern half of the existing bridge to Phase I. Once Phase I was opened to traffic the formwork was

removed from all regions except the closure region. After Phase I was carrying the traffic the remaining half of the existing bridge was demolished as seen in Figure 3-18.

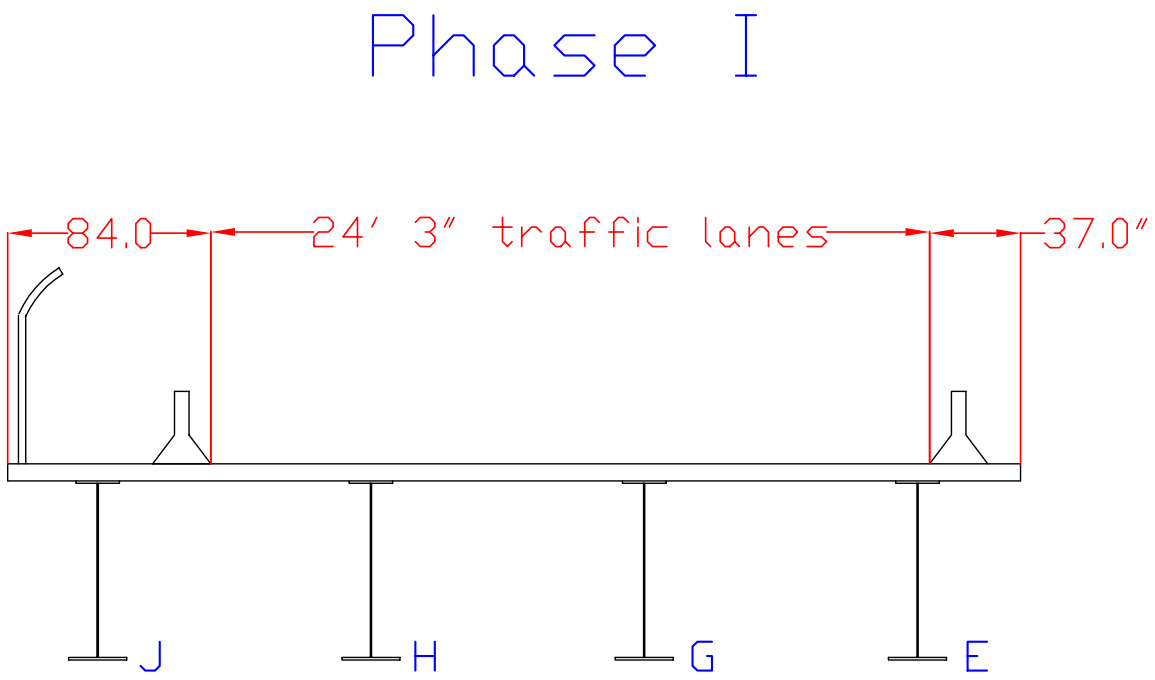

Figure 3-17: Location of Temporary barriers.

Figure 3-18: Demolition of the Northern half of the existing bridge

3.3.2 Phase II Construction

After demolition of the existing bridge's northern half was completed, Phase II construction commenced. Again, the first operations were those concerning the substructure: pile driving, constructing the concrete pier, and pile cap pouring. Once these operations were complete superstructure work could begin. As the two phases are mirror images about the project centerline, construction steps were very similar. Therefore, an in-depth summary of Phase II's construction up to closure is unwarranted.

Girder Erection

Girders for Phase II were placed in a similar manner to those of Phase I with two joined by cross frames were set at once. The only difference was that the West span girders were placed before the East span girders. The order of placement can be seen in Figure 3-19 and Table 3-2 shows the dates of erection.

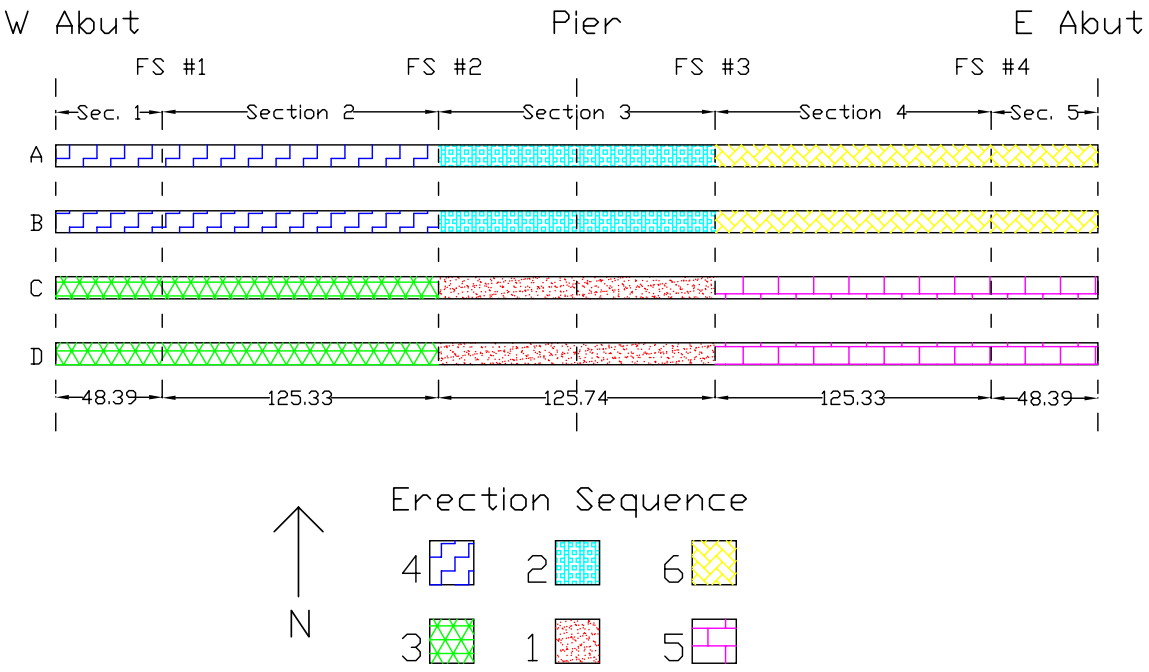

Figure 3-19: Girder erection sequence for Phase II.

Event	Started	Completed
Pour of Pier		12/28/1999
East Abutment Poured	1/19/00	1/21/00
West Abutment Poured	1/27/00	1/28/00
Girder Placement	2/1/00	2/21/00
Girders C3, D3, A3, and B3	2/1/00	2/5/00
Girders C1-C2 and D1-D2		2/8/00
Girders A1-A2 and B1-B2		2/13/00
Girders C4-C5 and D4-D5		2/20/00
Girders A4-A5 and B4-B5		2/21/00
Deck Formwork Placed	3/1/00	3/14/00
Positive Region Pour	4/18/00 8am	4/18/00 11am
Negative Region Pour	4/26/00 7am	4/26/00 9am
Live Load Tests	5/3/00	5/4/00
Bridge Closed to all Traffic		5/5/00 at 11pm
Closure Pour	5/6/00 5:15am	5/6/00 7:05am
Phase I Re-opened to Traffic		5/7/00 at 3pm
Overlay on Phase 2	5/22/00 2:25am	5/22/00 8:15am
Placement of Permanent N Side Barrier	6-2-00 2pm	6-2-00 4:30pm
Placement of Fence and Handrail on Phase II	6-5-00	6-8-00
Handrail Attached on Phase 2 Permanent Rail	6-12-00 6:30am	6-12-00 3pm
N Side Overhang Slab Formwork Removed	6-8-00 7pm	6-9-00 2am
Temporary Barriers Placed on S Side Phase 2	6-13-00 6am	6-13-00 9:30am
Phase 2 Opened to Traffic	6-13-00 10:30am	
Temporary Barriers Removed from Phase 1	6-13-00 10:30am	6-13-00 4pm
Formwork Removal from Phase II	6-18-00 11pm	6-19-00 3:30am
Final Cross Frames Placed between Phases	6-19-00 3:30am	6-19-00 5am
Formwork Removal from Phase 2 completed	6-19-00 11pm	6-20-00 6am
South Bridge Overlay	6-30-00 5am	6-30-00 10:30
South Bridge Sidewalk Overlay	7-8-00 7am	7-8-00 10am
Prep of Phase I bridge for concrete railing	7-10-00	7-13-00
Placement of Phase I permanent Barrier	7-14-00 8am	7-14-00 10 am
Bridge Completely opened to Traffic		8-10-00 3:30pm

Table 3-2: Construction Time Table for Phase II

DECK POURING SEQUENCE

Once girder erection was complete the deck formwork and rebar was placed. Deck forming was carried out between 3/1/2000 to 3/14/2000. Placement of rebar took place between 4/2/2000 and 4/9/2000.

The concrete deck for Phase II was cast in the same sequence as Phase I. The positive region pour was performed 4/18/2000 and is shown in

Figure 3-20. The negative region pour was performed on 4/26/2000 and can be seen in Figure 3-21.

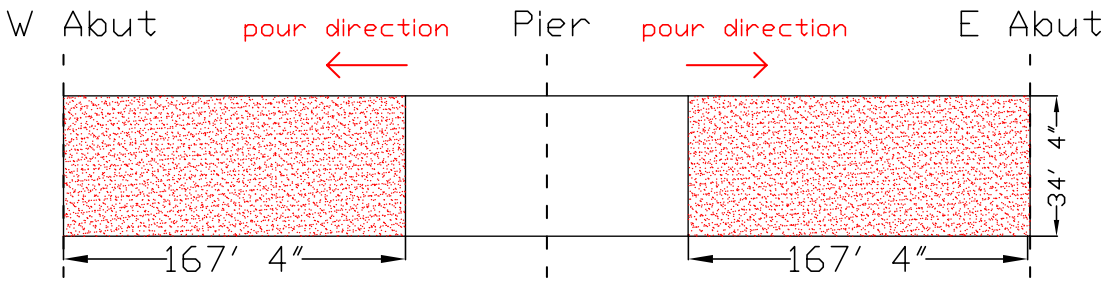

Figure 3-20: Positive region pour.

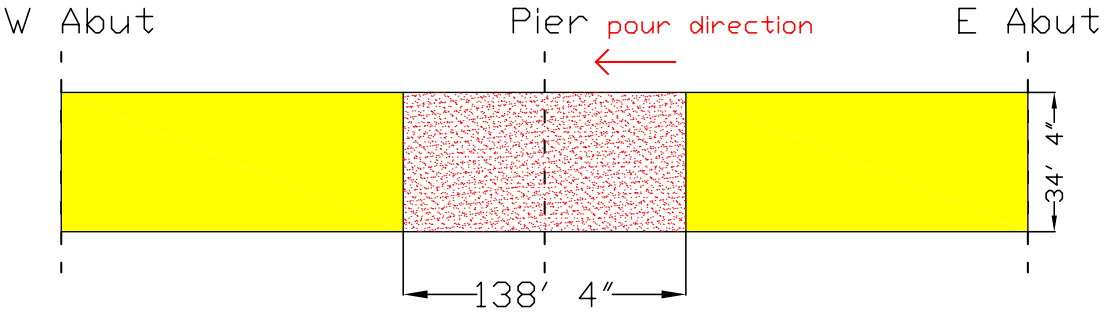

Figure 3-21: Negative region pour

3.3.3 Closure Pour

Before connecting the two phases with the closure pour, several things were done. First the construction crew removed some of the formwork from Phase II but left the overhangs needed for the closure concrete. Then some of the cross frames between Girders D and E were placed. All of the cross frames between these girders could not be placed because a differential elevation existed and cross frame bolt holes did not line up with those on the girders. The cross frames that were installed prior to the closure pour are shown in Figure 3-22. The other cross frames were placed after the closure operation. Longitudinal rebar was also placed in the closure region to provide strength. Transverse rebar consisted of extensions from the Phase I and II slabs. No additional rebar was placed in the transverse direction, rather, the bars extending from the Phase I and II slabs were lapped and tied together.

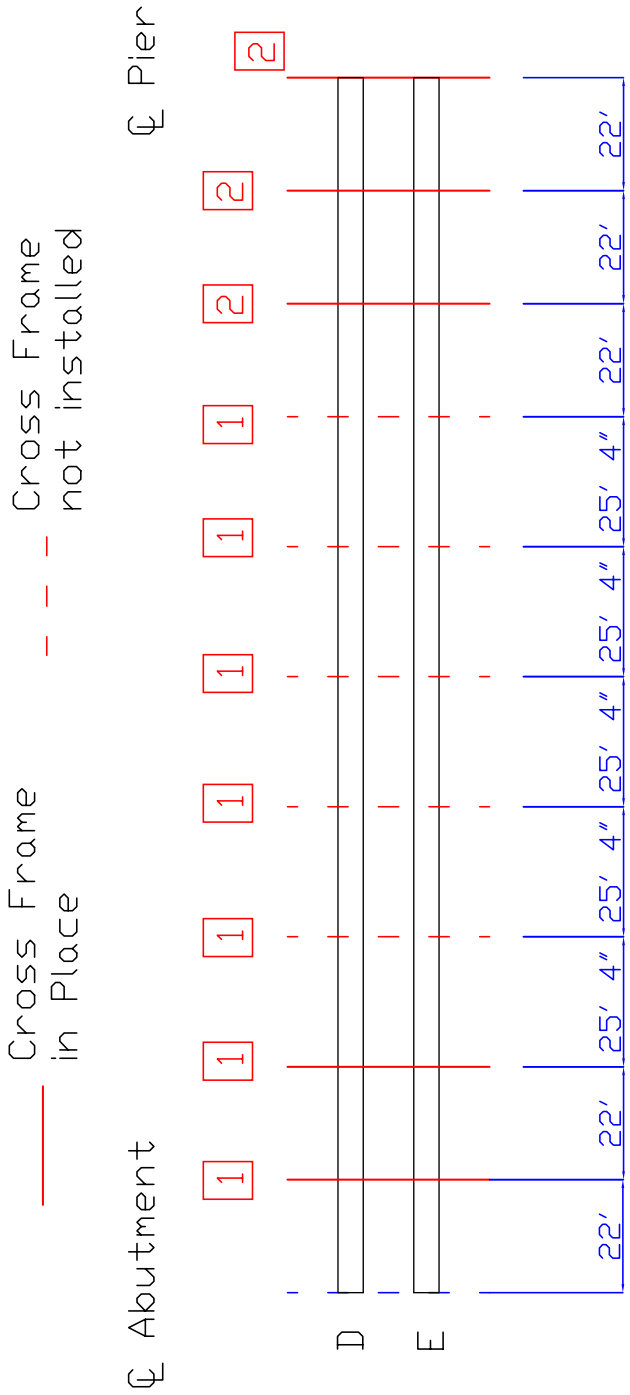

Figure 3-22: Cross frames that were installed at time of closure pour.

To perform the closure pour both phases were closed to traffic from 11pm May 5, 2000 to 3pm May 7, 2000. This was the only time during construction that traffic was entirely closed down. After the bridge was closed, all temporary barriers were removed from Phase I. The elevation of each phase was then obtained to determine the differential between the phases. Because Phase II was significantly higher than Phase I on the East span, barriers were placed on Phase II's East span as shown in Figure 3-23. These barriers reduced the differential elevation to 0.75" on the East Span. Barriers were placed from East abutment to pier. This reduced the differential elevation and was deemed an acceptable solution by Nebraska Department of Roads bridge engineers. The closure region formwork was then adjusted by turning the leveling screw in the overhang brackets and plywood was screwed together to remove any gap in the forms.

Concrete placement began 5:15am on May 6, 2000. Concrete trucks were not allowed on the bridge so concrete was either pumped or carted where it was needed with wheelbarrows. The closure pour was 40" wide and ran the entire bridge length. Pouring started at the East abutment and ended at the West abutment. The depth depended on the amount of differential elevation and was approximately the same as the Phase I and II decks, 7". Figure 3-24 shows the pour as it was being performed. The two decks from Phase I and II are clearly seen in the figure. Note transverse rebar tied together. This rebar consists of extensions of the rebar from the Phase I and II slabs to provide continuity. Longitudinal rebar was placed before the pour commenced. Figure 3-25 indicates the pouring direction.

After the concrete surface was finished it was covered with a curing agent and covered with wet burlap for 48 hours. The pour ended at 7:05am May 6, 2000.

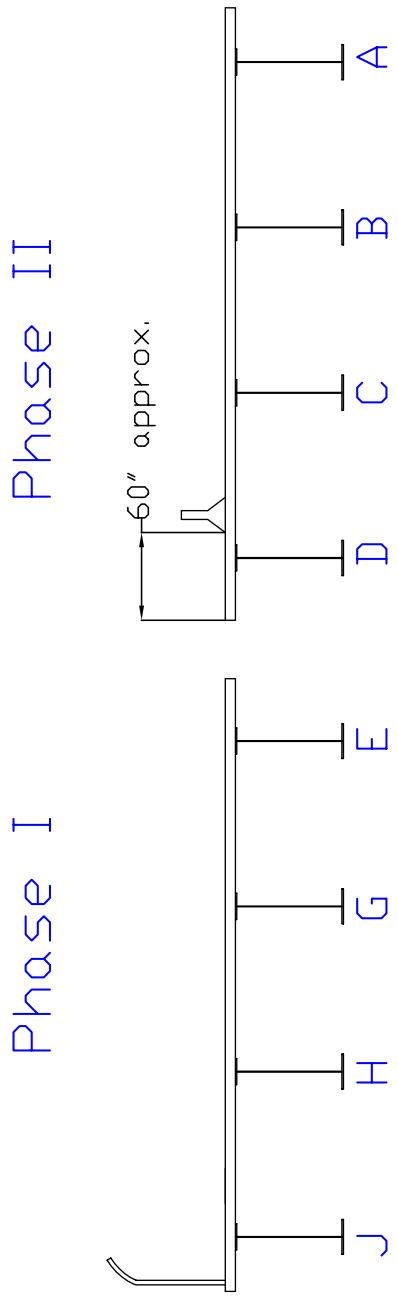

Figure 3-23: Location of barriers on Phase II

Figure 3-24: Closure pour

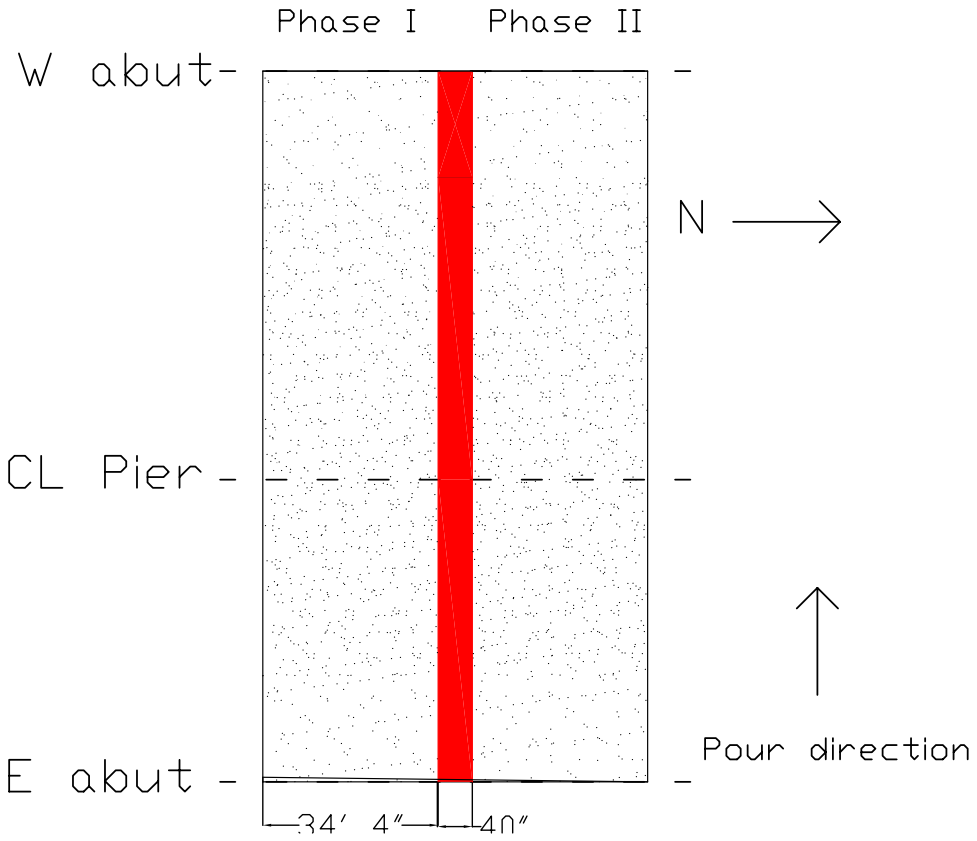

Figure 3-25: Direction of closure pour

Phase I was re-opened to traffic on May 7, 2000 at 3pm. Barriers were removed from Phase II and placed on Phase I as shown in Figure 3-26. This allowed only 32 hours for closure concrete to cure before barriers on the East span of Phase II were removed. Data recorded during the closure operation will be presented later.

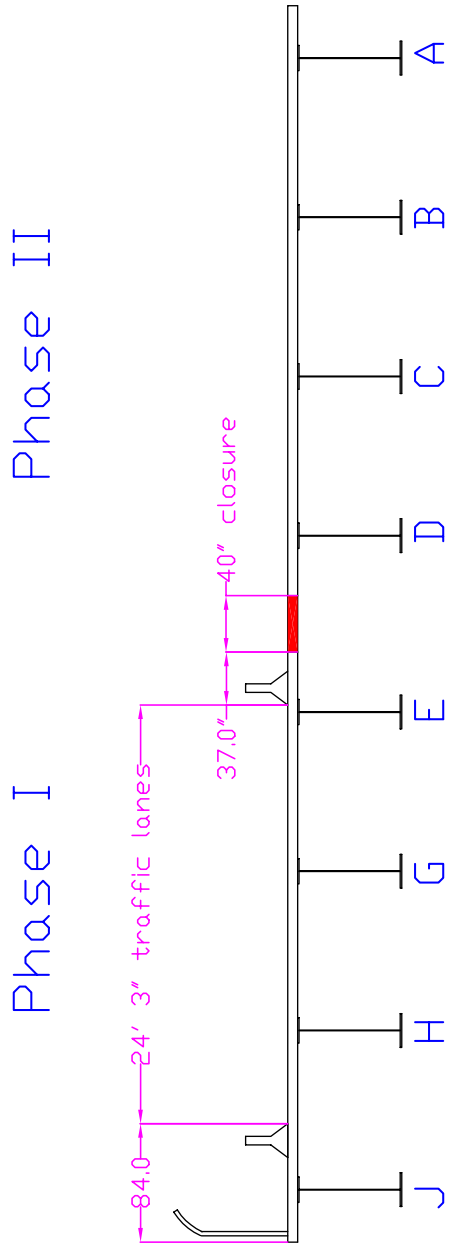

Figure 3-26: Phase I and II after closure pour

3.3.4 Overlay and Barriers

Once the primary structure had been completed, a few tasked remained including overlay of both phases and installation of the permanent barriers.

Phase II Overlay

As traffic was once again on Phase I the Phase II overlay was placed. Before this could be done the deck of Phase II was prepared. This consisted of sandblasting 1/8” from the deck, blowing away dust using compressed air, and washing the surface with water. Wet burlap was then carefully placed from the West abutment to the East abutment. This was done in such a way that workers and trucks never stepped on the prepared surface. Instead they walked on wet burlap until the pour began.

Two concrete trucks were always on the bridge during the pour. They both backed down the bridge from the West abutment. One concrete truck contained a grout that was brushed onto the deck to help the overlay adhere to the original surface. The other concrete truck contained the overlay concrete. These trucks unloaded directly onto the bridge. The pour started at the East abutment and ended at the West. Burlap was pulled up as trucks drove forward to expose the prepared surface. A finishing machine and several workers did the finishing work. After work on a region was complete it was recovered with burlap and sprinklers placed. The overlay was kept moist for 7 days to reduce shrinkage cracks and insure the best possible bond between the original deck and overlay.

The overlay of Phase II started at 2:25am May 22, 2000 and ended at 8:15am the same day. The final deck thickness was 8.5 in. yielding an approximate overlay thickness of 1.75 in. The area overlaid was one half the deck width, from Phase II's edge to the closure region's center, as seen in Figure 3-27.

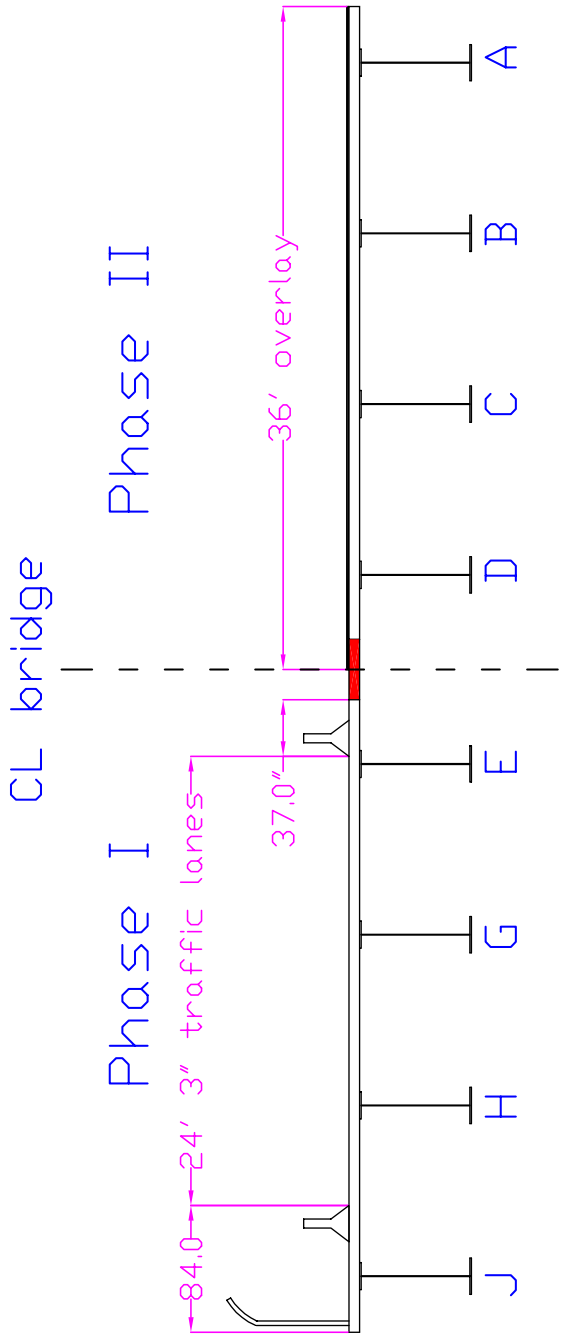

Figure 3-27: Configuration of bridge after Phase II overlay. Note bridges are joined by closure pour which has already occurred.

PHASE II PERMANENT RAILING

With the overlay on Phase II completed and traffic still being carried on Phase I the permanent barrier on Phase II was placed. After the reinforcing steel was in place, the rail was slip-formed from the West to the East abutment from 2:00pm to 4:30pm on June 2, 2000. The rail was coated with a curing agent and left uncovered. Figure 3-28 shows the machine to slip form the rail and the reinforcing steel in place.

Figure 3-28: Phase II permanent barrier before casting. Note dowels epoxied into deck

After the railing cured pedestrian fencing was placed on Phase II and temporary barriers placed so traffic could be switched over and Phase I completed. A cross section of the bridge before the Phase I overlay is seen in Figure 3-29.

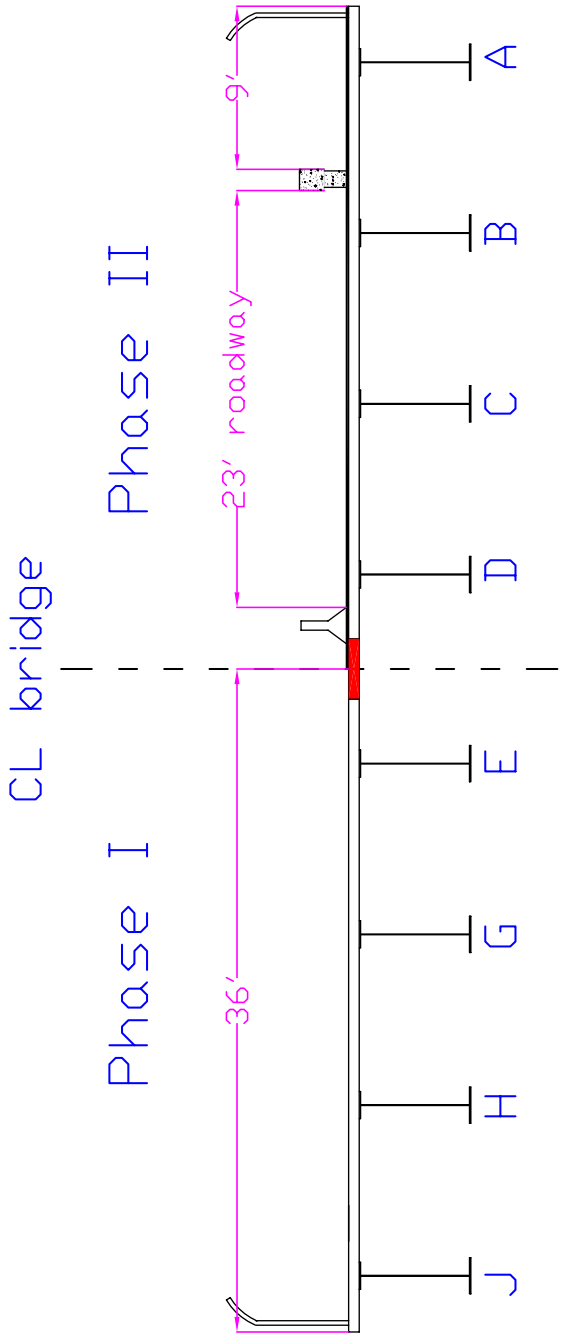

Figure 3-29: Configuration of bridge before Phase I overlay. Note traffic is being carried on Phase II as it is complete.

PHASE I OVERLAY

The Phase I overlay was very similar to that of Phase II. The deck preparations were performed in the same fashion and the concrete was placed the same way from East to West. The only difference is that Phase I had the pedestrian fencing in place at the time of the pour. Therefore the finishing machine rail had to be placed on the deck and the whole width could not be overlain at once. The majority of the overlay was placed from 5:00am to 10:30am on June 30, 2000. The remaining sidewalk overlay portion was completed on July 8, 2000 from 7:00am to 10:00am. As the sidewalk overlay was a small region all finishing work was done by hand. Both the main deck and sidewalk overlays were kept moist for one week to ensure a good bond with the original deck and to reduce shrinkage cracking. Figure 3-30 shows the bridge cross section after the Phase I overlay was complete.

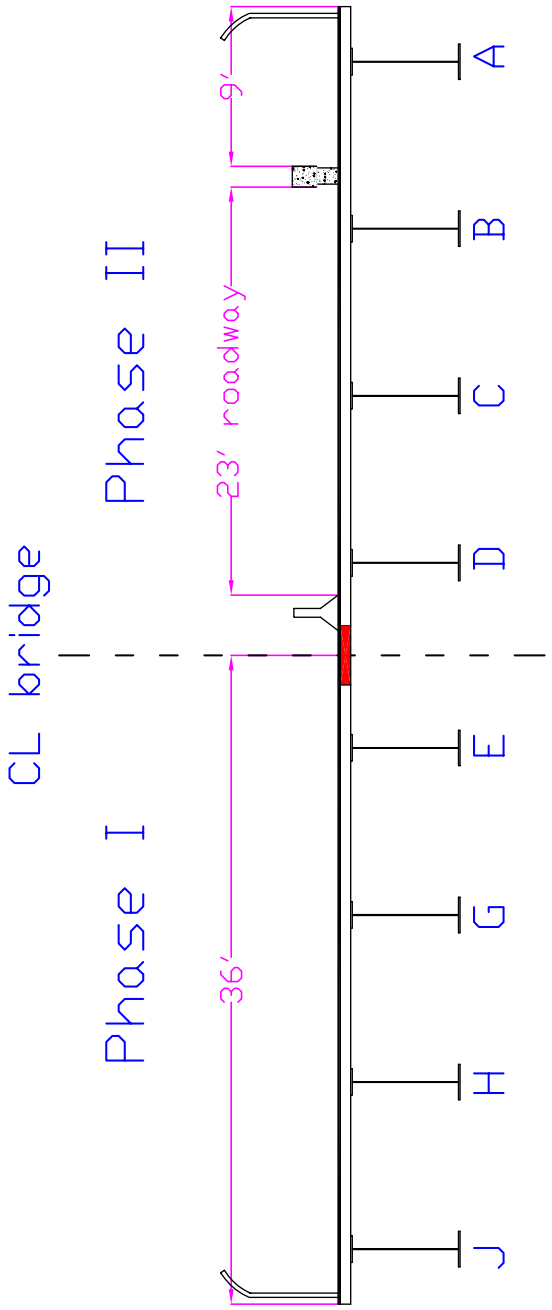

Figure 3-30: Configuration of Bridge after Phase I overlay.

PHASE I PERMANENT RAILING

Permanent rail for Phase I was cast on July 14, 2000 from 8:00am to 10:00am. This railing was also slip-formed from the West Abutment to the East abutment as was Phase I. A photo of the finished rail is seen in Figure 3-31.

Figure 3-31: Finished permanent barrier. Note truck on bridge is grinding surface.

COMPLETION OF PROJECT

Before the bridge could be opened to traffic some of the deck had to be ground to bring the surface profile to the design 2% cross slope. During this operation the temporary barriers were removed from the bridge and traffic was limited to one phase or the other by barrels as seen on the left side of Figure 3-31.

Both phases of the bridge were officially opened to traffic on August 10, 2000 at 3:30pm. Construction lasted 14 months from the time the Phase I pier was poured. A completed cross section of the bridge is shown in Figure 3-32.

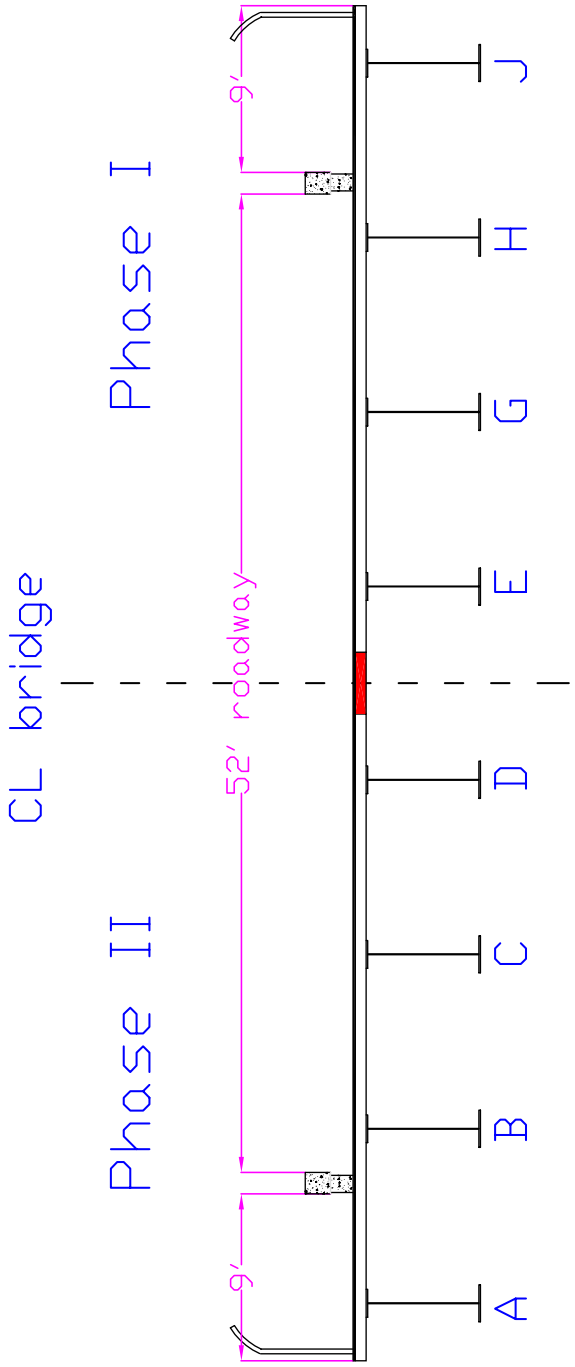

Figure 3-32: Completed bridge. Four traffic lanes and two sidewalks are clearly seen. Overall width of construction is 72'.

3.4 INSTRUMENTATION

The necessary data to obtain an understanding of the bridge behavior can be divided into two categories: strain and deflection. This data will provide information necessary to understand system behavior during short-term construction events such as deck casting, concrete barrier placement, closure pour, and live load tests. The data will also provide information necessary to understand long term bridge behavior such as creep, shrinkage, weather, and thermal effects.

3.4.1 DEVICES AND SENSORS USED IN MONITORING

Proper choice of instruments is essential for obtaining the required data. The strain data can be sub-divided into two categories: steel strain and concrete strain. The desired deflection data can also be divided into two categories: vertical girder deflection and longitudinal girder movement. A description of each instrument chosen to obtain the desired data follows.

Redundant instrumentation to obtain the desired data adds to the project cost and produces massive data files. Therefore, a cost effective instrumentation strategy was devised by judiciously selecting the location of gages.

Using the 1997 AASHTO LRFD Bridge Design Manual, the bridge as designed by the Nebraska Department of Roads (NDoR) was analyzed. From the dead and live load analyses the positioning of the gages was determined as described below. It was desirable to place gages on the East span because the distance to the ground is only 20' versus nearly 50' on the West span.

STEEL STRAIN SENSORS

Spot-Weldable Vibrating Wire(VW) sensors produced by Slope Indicator CO. of Bothell, WA were used to obtain data involving steel girder strain. The gauge consists of a steel wire held in tension inside a tube. The tube is mounted on a stainless steel flange, which is welded to a structural mem-

ber's surface using specialized equipment. Sensors placed over each gauge read the frequency at which the wire vibrates after the sensor plucks the wire. This frequency varies with the tension in the wire and can therefore be converted to a strain measurement. The reader also contains a thermistor that measures local temperature. An example of this gage can be seen in Figure 3-33. Vibrating wire gages were chosen for this project instead of typical electrical strain gages because of the monitoring duration. An electrical gage could not withstand constant excitation for over two years and reliable readings would be lost. Vibrating wire gages on the other hand have excellent long-term performance and can be expected to perform for many years.

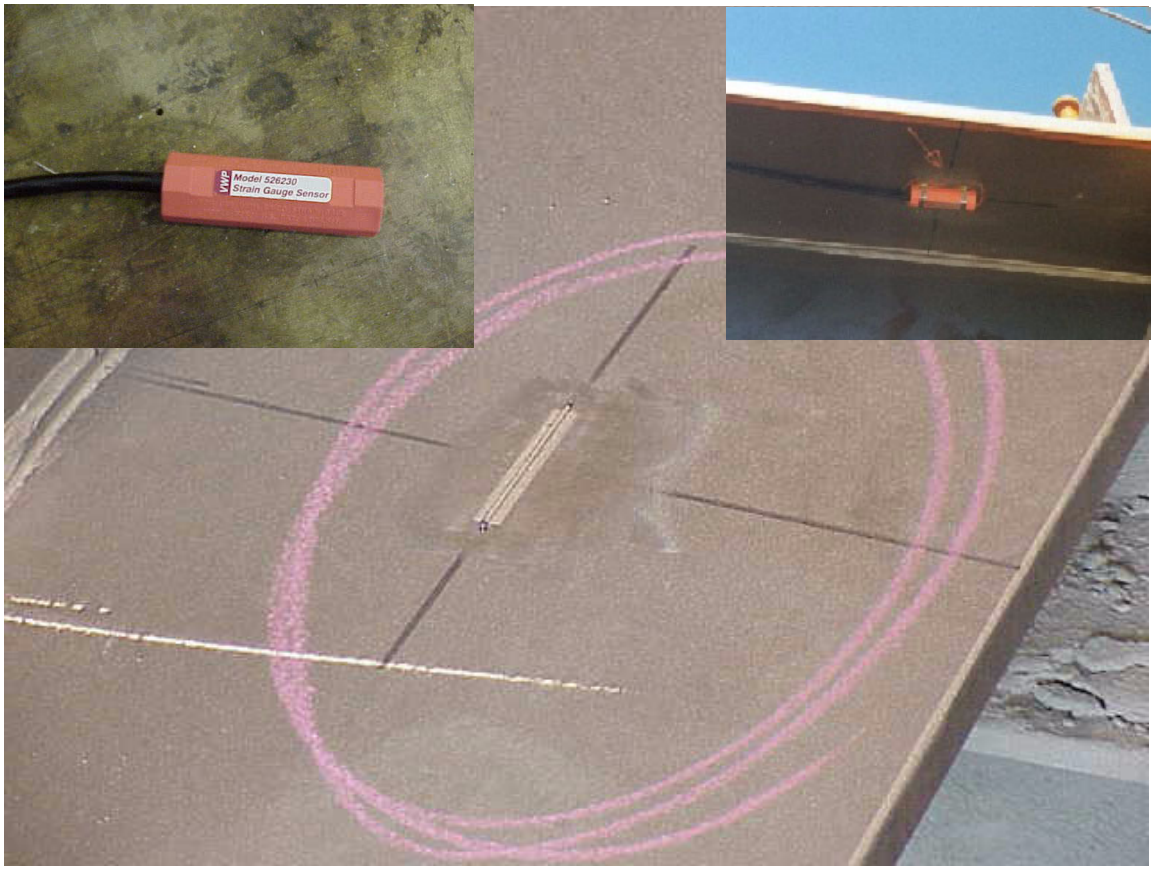

Figure 3-33: Steel strain gage and reader. Clockwise from upper left: reader, gage and reader in place, gage after being placed on reader.

The location of maximum positive bending moment from the Strength I combination was chosen as a gaging location. These strain readings will relate to the bending moment experienced by the girders. To obtain the amount of negative moment carried by girders, strain gages were also placed 2' East of the pier centerline. The gages could not be placed directly at the pier because of the bearing stiffeners there. Finally, spot-weldable gages were placed near the abutments so the amount of end restraint could later be determined and compared to the simple support assumed for design. Strain gages attached to the flanges were centered on the flange at their respective position.

Two cross frames for Phase II and were also gaged. These strain readings will indicate how effective cross frames are in transmitting load in the transverse direction as the phases deflect relative to each other. The cross frames chosen to be gaged were the ones closest to the maximum positive moment section (Section 2).

CONCRETE STRAIN SENSORS

Embedment Strain Gauges, model 52630126, produced by Slope Indicator CO. of Bothell, WA were used to obtain the strain in the concrete. The VS Embedment strain gauge is a steel tube with flanges at either end. Inside the body is a steel strap and a magnetic coil. The strap is held in tension between the two flanges, and the coil magnetically “plucks” the steel strap, which then vibrates at a frequency that can then be converted to a strain reading. The gages also contain a thermistor to record local temperature. The gages are tied to rebar before concrete placement. Figure 3-34 shows two of these gages tied to rebar in the closure region.

To obtain concrete strain data, gages were placed at several locations and orientations in the deck. Additionally, one gage was placed in a control specimen 7" deep x 6" wide x 18" long, as seen in Figure 3-35, that was placed near the DAS to obtain the concrete's free shrinkage behavior.

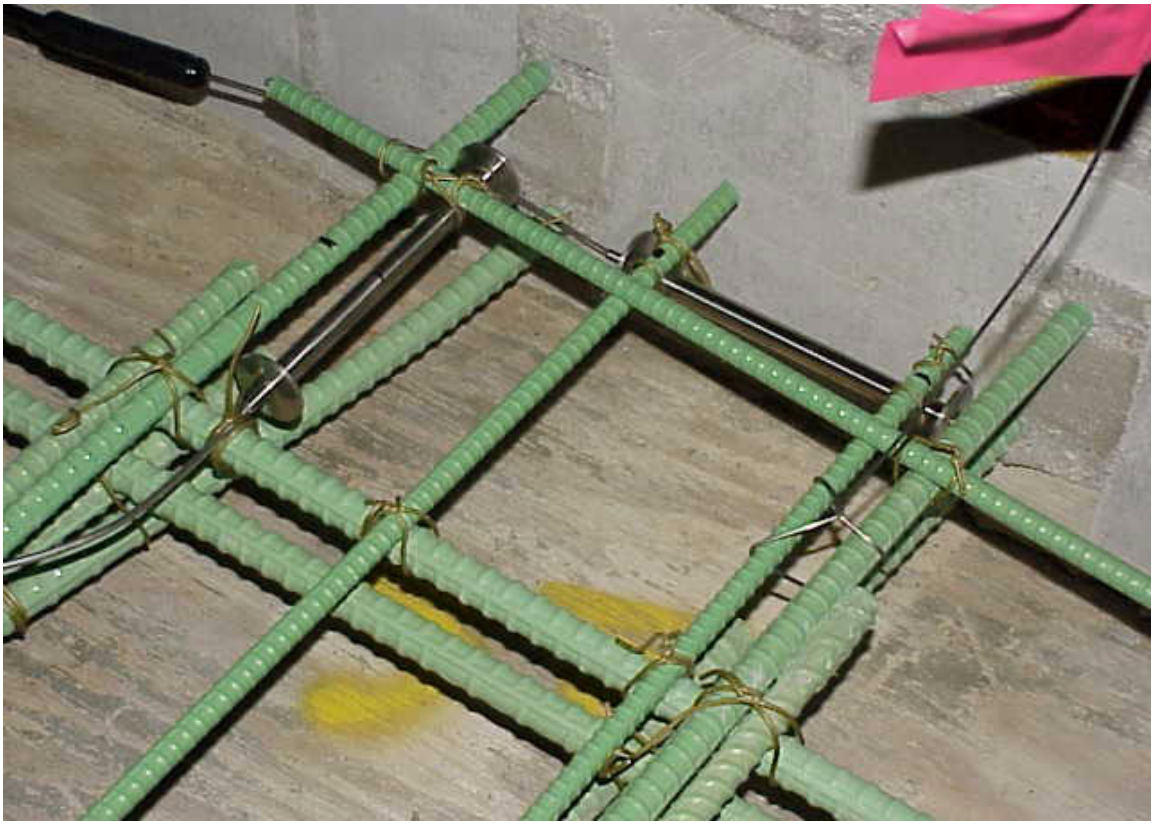

Figure 3-34: Concrete Embedment gage in place. These gages record concrete strain.

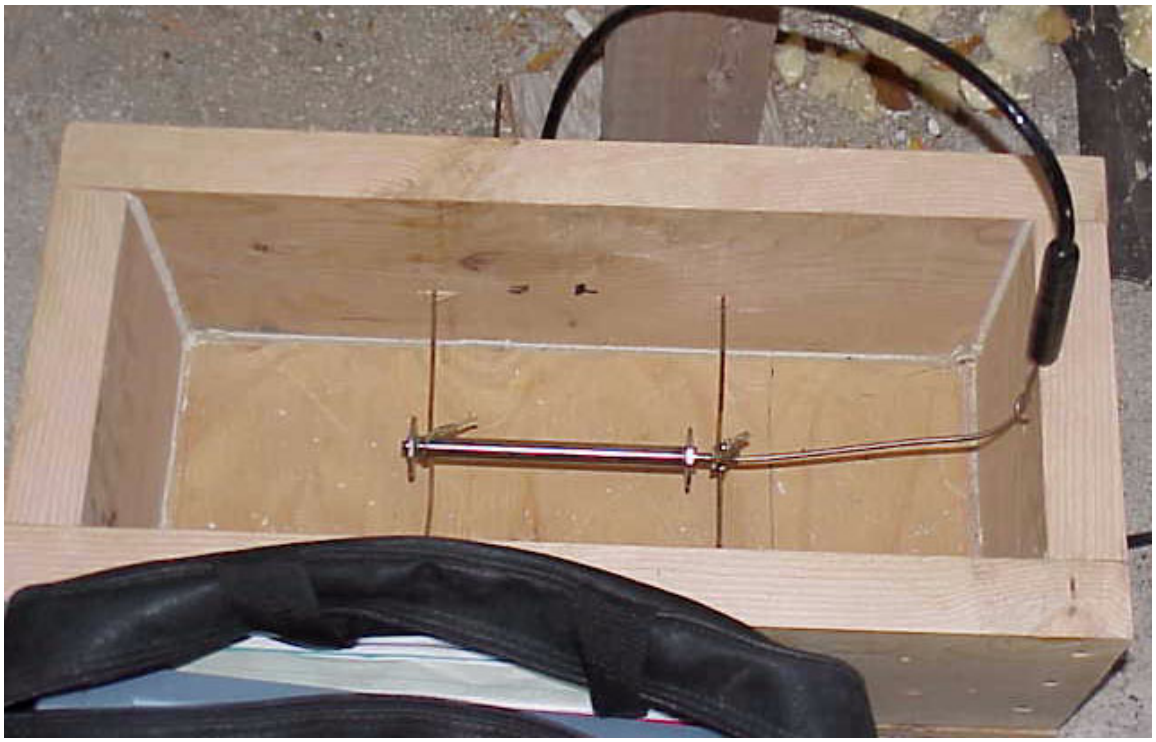

Figure 3-35: Embedment Gage in Free Shrinkage Control Specimen

Gages were placed in the closure pour because it joins the two phases and can carry high strains and crack if differential settlement between the phases occurs. The gages will also provide long-term data on the closure region concrete behavior as it creeps and shrinks.

VERTICAL GIRDER DEFLECTION

The vertical girder deflections were measured using RAYELCO Linear Motion Transducers manufactured by MagneTek of Simi Valley, CA. These gages contain a potentiometer that is connected to a wire spool. A known voltage is sent to the potentiometer and by reading the return voltage the length of stretched wire is computed. The free end of the spooled wire is connected to a fixed point and the potentiometer is fixed to the deflecting structure, or vice-versa. By choosing a datum at an appropriate time the change in deflection can be interpreted from subsequent readings. The devices were mounted to a piece of steel and then protected from the environment by constructing a covering over them. Care was taken so the covering would not disturb their normal function. The unit in its protective covering clamped to the bridge girder can be seen in Figure 3-36.

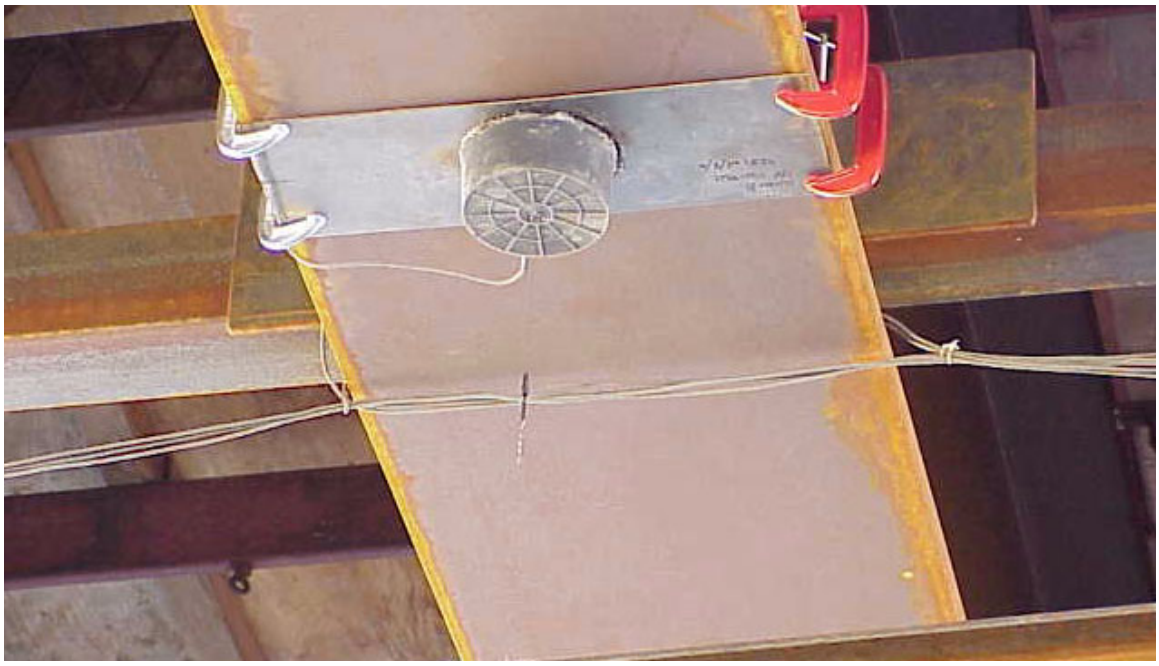

Figure 3-36: Potentiometer connected to the girder and fixed frame.

To obtain meaningful vertical displacement data it is desirable to measure deflection at the predicted location of maximum deflection, 0.4L. Potentiometers (pots) could not be placed exactly at this location because there is a roadway underneath the bridge. Therefore they were placed as close to the roadway as possible while still in a location that would not interfere with construction. The pots are tightly clamped to the underside of the girders while the other end is connected to a rigid test frame, which has its base embedded in concrete at a depth below the frost line. The pots monitor deflection during significant construction events and also long-term behavior. This data will indicate the amount of differential deflection occurring between the phases.

LONGITUDINAL DISPLACEMENTS

Girders D and E were instrumented at each abutment to measure the longitudinal displacement of each phase. These girders were chosen because they are adjacent to the closure pour and should have the most effect on the closure region behavior. This data allows comparisons between the behaviors of the two phases.

Longitudinal girder movements were measured at the abutments using VWP Displacement Transducers (crackmeters) produced by Slope Indicator CO. of Bothell, WA. The device is mounted with one end on the girder's bottom flange and the other on a surface that is assumed not to move, the pile cap in this case. The device operates on the same frequency principle as previously mentioned gages but these instruments relate frequency to displacement. As with the other Slope indicator products, local temperature is also recorded. An example of these units during service can be seen in Figure 3-37. In the figure, note the right end connected to the galvanized angle that has been screwed into pile cap and the left end which is connected to an angle which has been clamped to girder flange.

Figure 3-37: Crackmeter connected to girder flange

3.4.2 DATA ACQUISITION SYSTEM (DAS)

To acquire the necessary data, a DAS that can perform the essential tasks while remaining flexible to changing needs is essential. These tasks include taking readings from sensors at appropriate intervals, recording the readings in non-volatile memory, and the ability to download data files for analysis. Readings in non-volatile memory are stored such that system power can be lost and previously stored readings are preserved.

The DAS for this task was produced by Slope Indicator CO. and consists of many different modules. The CR10X is the primary module that controls the system and stores the system's instructions. It controls the other modules and dictates when readings are taken and how data is recorded into memory using the other modules. Gages are connected to the AM416 Relay Multiplexers which excite the gages and read the responses. The AVW100

module switches between multiplexers so the channels are excited in correct order. Power is provided through the PS12LA battery/battery charger. Data is recorded in the CR10X's internal 128k of memory. Finally, the SC32A Optically Isolated RS232 Interface allows the user to interface with the DAS using a computer and a 9-pin connector. The individual modules are manufactured by Campbell Scientific, INC. of Logan, Utah and are assembled by Slope Indicator to meet the project's needs.

Two multiplexers provided adequate resources to acquire data from the 24 vibrating wire gages and 5 potentiometers required for Phase I monitoring. Once Phase II began, the system had to be upgraded. Four additional multiplexers were added providing channels for up to 48 more vibrating wire gages and 16 potentiometers. A COM 100 Cellular Phone Package and a COM 200 Telephone Modem were added so data could be retrieved remotely. A solar panel, manufactured by Solarex of Frederick, MD, was connected to the PS12LA battery/battery charger to provide power during the day and to charge the battery for night usage. Finally a SM4M Storage module was added providing an additional 4 Megabytes of non-volatile memory allowing for longer intervals between downloading data. Figure 3-38 is a schematic of the final DAS.

To control, communicate, and access the system's memory Slope Indicator CO provides a program package, PC208W Datalogger Support Software. The package serves several functions. One is to allow the user to provide the DAS with information concerning gage to channel relationships and at what frequency to excite gages. This information is contained in a program which is uploaded to the CR10X. The program also contains information concerning what data to record into memory so it can be accessed later. Another important function of the package is to download data stored in memory. The user can also set the DAS's clock and instruct it to take readings at set intervals or upon command.

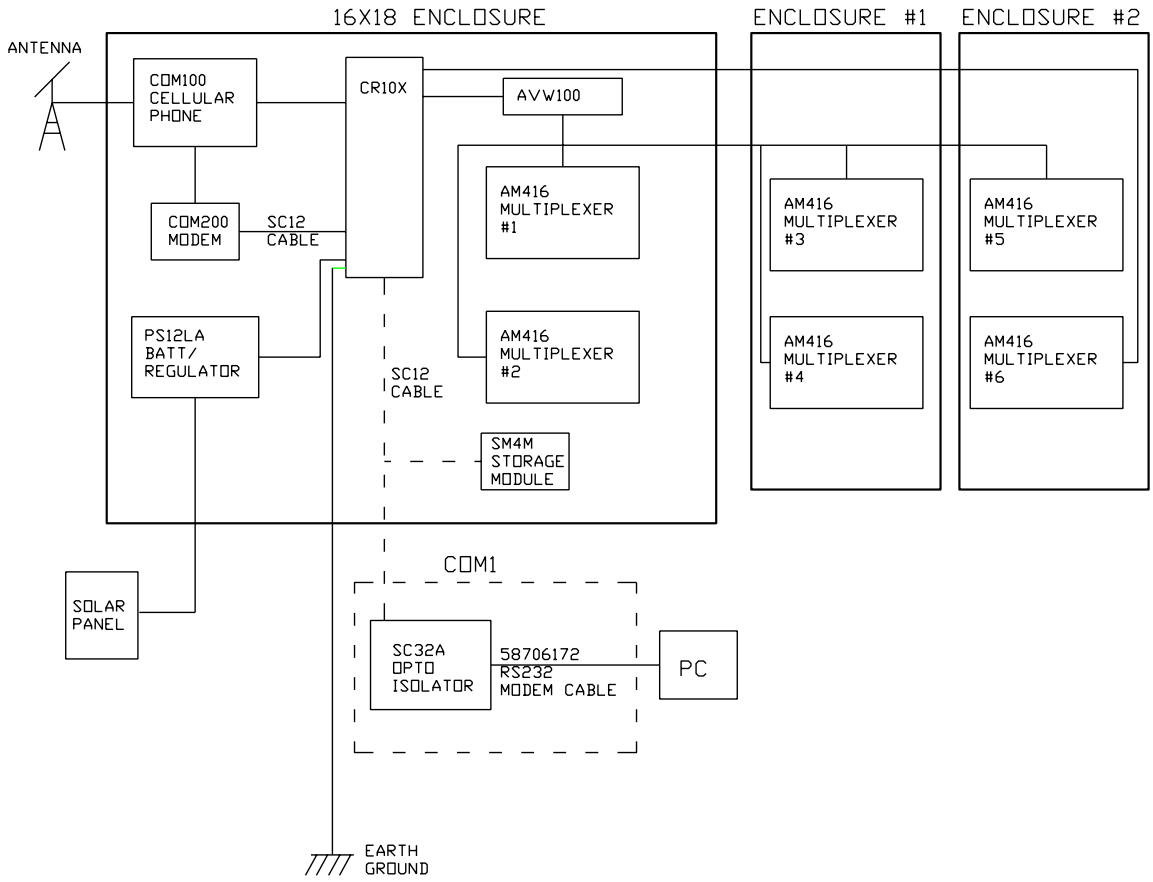

Figure 3-38: Data Acquisition System (DAS) for Dodge Street over I-480

Chapter

4 Finite Element Modeling

Development and Verification of 3-Dimensional Finite Element Model

Full three-dimensional modeling of Dodge Street was performed using Ansys, version 5.6.1. The goal was to develop and validate a model against the results obtained from the field testing. Once a validated model had been obtained it could be used in a variety of ways.

First, detailed stress, strain, and deformation information is available at all points in the model, not just at the gage locations from field testing. Although gage locations are selected to correspond with points of significance, such as a location expecting a maximum response, often the location of the true maximum is in a slightly different location. With the finite element model, these locations can be determined exactly. In addition, the response due to a single condition can be isolated from the system noise and analyzed more clearly.

Second, the model can be utilized to run hypothetical “what if” studies. These can be useful in determining the allowable limits of a given parameter such as determining how much additional shrinkage deflection is allowable after the closure pour has been performed.

Finally, the modeling techniques developed can be employed to model systems utilizing similar construction details, but with different dimensions. The assumption is that the modeling techniques will yield accurate results for systems which are somewhat similar to the actual bridge used in the calibration procedure. When performing a parametric study where key variables are set at different values, the impact of a given parameter on the system response can be determined.

4.1 General Model Description

The model developed is a full 3-dimensional model. Material properties were obtained from drawings and test results. The geometry of the bridge was built according to the drawings used in construction so the dimensions are based on the drawings rather than the actual job.

The steel girders are modeled using shells (Ansys SHELL43) for the web and beam elements (Ansys BEAM44) for the top and bottom flange. SHELL43 has six degrees of freedom at each node: translations in the nodal x, y, and z directions and rotations about the nodal x, y, and z axes. The deformation shapes are linear in both in-plane directions. For the out-of-plane motion, it uses a mixed interpolation of tensorial components. BEAM44 is a uniaxial element with tension, compression, torsion, and bending capabilities. The element has six degrees of freedom at each node: translations in the nodal x, y, and z directions and rotations about the nodal x, y, and z-axes. The effect of shear deformation is also available as an option. This element allows the end nodes to be offset from the centroidal axis of the beam.

Use of beam elements for the flanges greatly simplifies the model and reduces its size. Preliminary investigations were done using shells for both the web and flanges. However, to sufficiently discretize the flanges without producing ill-shaped elements required relatively small element sizes, especially in the region of flange transitions. This flange discretization then had to be matched by the deck elements. The result was an enormous number of elements. When the model utilizing beam elements was compared with the all shell model, a difference of less than 1% was observed. Based on this finding, the beam flange model was chosen over the all shell model.

The deck was modeled using shell elements (Ansys SHELL43). The deck was attached to the top of the girder through the use of constraint equations which couple the degrees of freedom (DOF's) at the web flange juncture to the DOF's at the midsurface of the deck. Modeling of the wet concrete during the casting operations was accomplished by wet concrete weight was modeled by taking a very small elastic modulus for deck concrete. Since the positive region and negative region were cast in different times for positive and negative steps, the positive region weight was first applied and then its stiffness activated with its real value. Then the negative region weight was applied with a small elastic modulus for concrete in that region. Once both region weights were applied and the analysis was done the concrete elastic modulus was set to its actual value and other loads such as temporary barriers load, live load, or temperature are applied on the full composite model composed of the steel girders and concrete deck. The maximum mesh size for deck and girders is 20 inches which was shown to be accurate enough with a sensitivity analysis.

End diaphragms were modeled by using both shell elements (Ansys SHELL43) and solid elements (Ansys SOLID45) which have 24 degrees of freedom. By doing some sample analyses it was shown that there is no sig-

nificant difference between the two models so most of analyses were done using the shell model, which has fewer degrees of freedom.

Intermediate stiffeners and Cross-Frame members were modeled with beam elements, Ansys BEAM44 and BEAM188. The intermediate stiffeners were defined as a beam running the depth of the web. In locations where the stiffener was one-sided, the offset option of the beam element was utilized.

Although the end supports are assumed to be hinges and rollers in these types of bridges, for more precise study different end conditions and support restraints were utilized in the model. Four different conditions are in the model: fixed ends, unrestrained ends, partially restrained using link elements, Ansys LINK10 and LINK8, and applying point loads on the ends, which resemble soil reactions on the abutments. Figure 4-1 shows the finite element model with the deck removed for clarity.

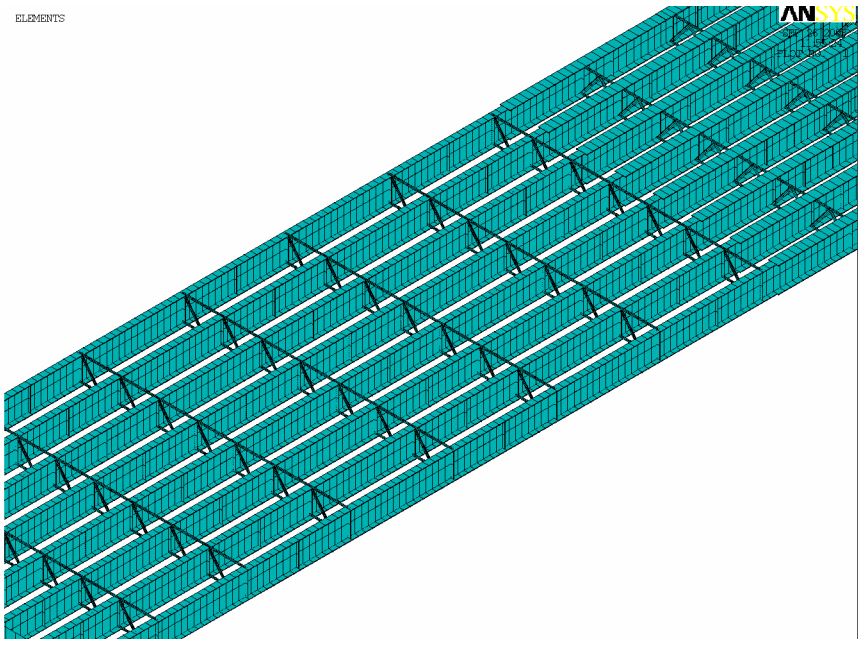

Figure 4-1: Finite Element Model

4.2 MODEL VERIFICATION

4.2.1 INDIVIDUAL PHASE CONSTRUCTION SEQUENCE

The analysis process was accomplished according to the following construction sequence:

1. Positive concrete pour for one phase including 4 girders.
2. Negative region pour for one phase including 4 girders.
3. Applying some temporary loads such as barriers on the 4-girder model

Once the 4-girder model was built, wet concrete weight was modeled by using a very small elastic modulus for deck concrete. Since the positive region and the negative region were cast at different times for positive and negative steps, the positive region weight was first applied and then its stiffness developed into its full composite value and the negative region weight was then applied with a small elastic modulus for concrete in that region. Once both regions' weights were applied and the analysis was done, the concrete elastic modulus was set to its test result value and other loads and effects like temporary barrier loads, live loads or temperature effects were applied on the composite model of the steel girders and concrete deck.

Comparing the results of analysis and site measurement for the deck pour showed different results. One of the most important reasons for this discrepancy comes from the end restraints so the end restraints must be changed so that the results match. By trying different models a model was developed which yields relatively good results in different gage locations such as potentiometers, strain gages and crack meters. This model shows a different stiffness for the top flange and bottom flange in the abutment, which is in contact with the soil and the approach slab. This makes sense since tension and compression behavior of soil is different. There are some other factors which were taken into account to get close to empirical

results such as modeling vertical curve, crown in the bridge, and the edge step. A summary of results is shown in Table 4-1.

Deflection Source	Deflection (in)				Avg Error
	A	B	C	D	
Semi-Rigid, Edge Step, Vertical Curve, Crown	-4.76	-4.80	-4.83	-4.84	6.64%
Simply Supported, Edge Step, Vertical Curve, Crown	-4.98	-5.02	-5.05	-5.07	11.58%
Fixed Ends, Edge Step, Vertical Curve, Crown	-2.74	-2.78	-2.81	-2.82	38.17%
Site Measurement Phase I	-4.59	-4.62	-4.86	-4.93	5.34%
Site Measurement Phase II	-4.03	-4.21	-4.30	-4.53	5.34%
Site Measurement Average Phase I &II	-4.31	-4.41	-4.58	-4.73	0.00

Table 4-1: Summary of Finite Element Comparison with Experimental Results

By changing the end stiffness, the average condition that satisfies all of the gage data was chosen. It can be observed that even measured data from each phase has about 11% difference, however both phases are almost the same so a percentage of error within 11% is ignorable. This error comes from different factors such as different end restraints, variability in the thickness of the deck, instrumentation errors, and other environmental effects like temperature. Generally it can be observed that a bridge with semi-rigid connections has the best result in comparison with measured data. The same process for the negative region pour shows an 8.87% error for the semi-rigid model. The difference between the negative and positive pour results can be explained by the fact that during the positive pour, due to the freedom of the steel girder top flange the rigidity of the ends are less than the negative pour period when the turndown and diaphragm have already hardened and the rigidity should be higher.

For modeling end restraint some linear spring by link elements were added to the top and bottom flanges. Table 4-2 shows the spring characteristics. The lengths of the springs were chosen based on the distances of the ends of the girders to the lever beam and the area of each spring is the girder

spacing multiplied by the turndown height. Comparing to the soil elastic modulus the assumed elastic modulus indicates a very stiff soil type which is reasonable when considering the compactness and confinement of back-fill. More parametric studies are needed for recommending a range of soil elastic moduli for modeling end rigidity for practical design uses.

	Element Type	Elastic Modulus	Length	Area
Top Spring	LINK8	50 ksi	1524 in.	83225 in2
Bottom Spring	LINK10 (comp. only)	25 ksi	1524 in.	83225 in2

Table 4-2: End Restraint Spring Properties

4.2.2 Live Load Testing

Each phase was tested separately in the live load test. As mentioned, in self weight loading the results of the tests were compared with different types of modeling, especially those concerned with end rigidity. It was shown that the partially restrained model gives the best results with those of the live load tests. Some of the results for each phase have been summarized in Table 4-3. It can be observed that there is some error between analysis and the tests which, as described before, is inevitable because there is about 10% error between the two phases' test data, which are completely symmetric according to the drawings. Also error is higher for smaller quantities because of instrumentation errors so for heavier loading such as side by side trucks the results seem to be more accurate.

4.2.3 Closure Operation Modeling

Long Term Effects Modeling

The full model of the bridge was built including 8 girders and closure region. A uniform strain of 400 με was applied to half of the bridge for investigating non even shrinkage effects on the bridge. This amount of strain was applied by considering an equivalent temperature that could

Test Lane	Measured Parameter	Results	Girder Line E & D	G & C	H & B	J & A	Mean Error
South	Deflection (in)	Test	0.20	0.38	0.58	0.73	5.9%
		Model	0.17	0.35	0.55	0.74	
	Strain (με) Vx2,2b	Test	18.0	25.0	32.0	42.0	16.3%
		Model	10.4	21.5	30.4	40.4	
North	Deflection (in)	Test	0.66	0.57	0.44	0.32	5.3%
		Model	0.72	0.58	0.42	0.25	
	Strain (με) Vx2,2b	Test	47.0	33.0	25.0	17.0	2.3%
		Model	39.2	29.4	25.6	19.8	
Middle	Deflection (in)	Test	0.43	0.46	0.44	0.41	4.5%
		Model	0.41	0.45	0.47	0.48	
	Strain (με) Exx	Test	-7.0	-12.0	-13.0	-13.0	38.3%
		Model	-13.48	-14.1	-15.1	-16.5	
	Strain (με) Vx2,2b	Test	25.5	22.0	23.0	26.5	7.0%
		Model	25.3	23.8	24.3	29.1	
Side by Side	Deflection (in)	Test	0.98	0.98	0.96	0.92	1.1%
		Model	0.83	0.92	0.99	1.06	
	Strain (με) Exx	Test	-34.2	-28.4	-32.3	-32.3	1.4%
		Model	-26.7	-29.5	-32.8	-36.0	
	Strain (με) Vx2,2b	Test	60.5	56.1	58.3	59.1	6.8%
		Model	49.5	50.9	56.0	60.2	

Table 4-3: Modelling Comparison with Finite Element Results

produce the same strain on the concrete deck. The result of this analysis has been shown in Table 4-4 for the 4-girder model.

Midspan Response	GIRDER A	GIRDER B	GIRDER C	GIRDER D
Deflection (in)	-0.31	-0.39	-0.39	-0.31
Bottom Flange Strain (με)	16.4	20.6	20.6	16.4

Table 4-4: response of 4-girder model to uniform deck strain

The 8-girder model results have been shown in Table 4-5 when pseudo shrinkage strain was applied only on one phase. In Table 4-5 deflection variations match with those predicted but it should be noted that top

flange strain that is measured in longitudinal direction is induced more due to longitudinal shrinkage.

Response Location	A	B	C	D	E	F	G	H
DEFLECTION POTS (IN)	-0.22	-0.34	-0.38	-0.34	-0.24	-0.11	0.02	0.14
STRAIN TOP FLANGE SEC2	347	358	367	377	-15.2	-7.6	0.68	9.2
STRAIN BOT FLANGE SEC2	-6.2	12.3	25.8	29.2	24.1	13.8	0.66	-12.8
STRAIN TOP FLANGE SEC3	399	414	415	410	-0.69	-10.7	-17.1	-23.5
STRAIN BOT FLANGE SEC3	36.4	-42.0	-63.2	-60.5	-38.8	-16.7	-3.4	12.2

Table 4-5: Response of 8-girder model to uniform deck strain (με unless noted)

Strain in the embedment gages and cross frames are shown in Table 4-6. Embedment gauges 18 and 20, which are in the closure region in the transverse direction, show strain less than 400 με. This indicates shrinkage shortening is redistributed in the whole bridge. The maximum total strain in the embedment gages is 415 με which is more than cracking strain of concrete.

Embedment Gage	**E1**	**E2**	**E3**	**E4**	**E5**
Strain	380	377	-92	367	-92
Embedment Gage	**E6**	**E7**	**E8**	**E9**	**E10**
Strain	-92	347	41	42	42
Embedment Gage	**E11**	**E15**	**E16**	**E17**	**E18**
Strain	399	183	381	380	-87
Embedment Gage	**E19**	**E20**	**E21**		
Strain	193	-61	402		
Cross Frame Gage	**XCD1**	**XCD2**	**XCD3**	**XCD4**	**XCD5**
Strain	-290	5	-9	-16	-6
Cross Frame Gage	**XDE1**	**XDE2**	**XDE3**	**XDE4**	**XDE5**
Strain	-10	-.04	-0.4	-18	-18

Table 4-6: Response of Deck and Cross-Frames to Differential Deformation

Chapter

5 Analysis

Methods of Analysis During Design

There are several additional considerations which must be taken into account during the analysis phase when designing a bridge to be constructed using phased construction. These can be broken into several categories. Cross-section considerations include items which affect the cross-section design, its profile and how the deck is distributed on top of the girder pattern. Distribution factors are needed for various stages of the construction. As was discussed in Section 2.1, the key to success in phased construction is making the two phases be at the correct elevation for the closure operation. It is therefore obvious that an accurate prediction of deflection is required. Obtaining a more accurate predication of deflection requires consideration of the actual end restraint conditions than what is currently done. Similarly, assumptions as to the impact of deck pour sequencing on deflections must be investigated.

5.1 Cross-Section Considerations

The cross-section considerations investigated are symmetry within a given phase, symmetry between the two phases, skew and horizontal curvature.

5.1.1 Symmetry within a given phase

Just like the final bridge, one should strive to attain symmetry within each individual phase. The fewer girders carrying the load, the more susceptible the system is to torsional distortion. As an individual phase may be comprised of only a few girders, it may be highly susceptible to distortion. Often times in phased construction, however, there is pressure to go with an un-symmetric system. For example, a wider deck may be desired on one phase to accommodate the temporary traffic during construction. When symmetry cannot be maintained within a phase, a more detailed analysis may be required.

Deflection Prediction when non-symmetric

Two options are proposed for performing this analysis. The first is a simplified 3-dimensional model. As the level of deformation due to sources which are difficult to predict is of the same magnitude as the predictable magnitude, an exact analysis is not of much utility. Therefore, a simple grillage type model would be sufficient. Alternatively a simplified method has been developed in utilizing a discrete elastic foundation concept. This method has been utilized in a finite element program which will be further elaborated upon in Chapter 9.

5.1.2 Symmetry between Phases (Tributary Area)

Another symmetry condition which must be checked for in the design of a bridge to be constructed using phased construction is tributary area or total dead weight within a given phase. Two circumstances can give rise to this situation. The first is quite obvious; if the two phases have the same number of girders, yet one has a wider deck. The second case is not quite as obvious. If the phases have an unequal number of girders, even if the

final system and individual phase overhangs are symmetric, the tributary area to each girder may not be equal. This condition is illustrated in Figure 5-1.

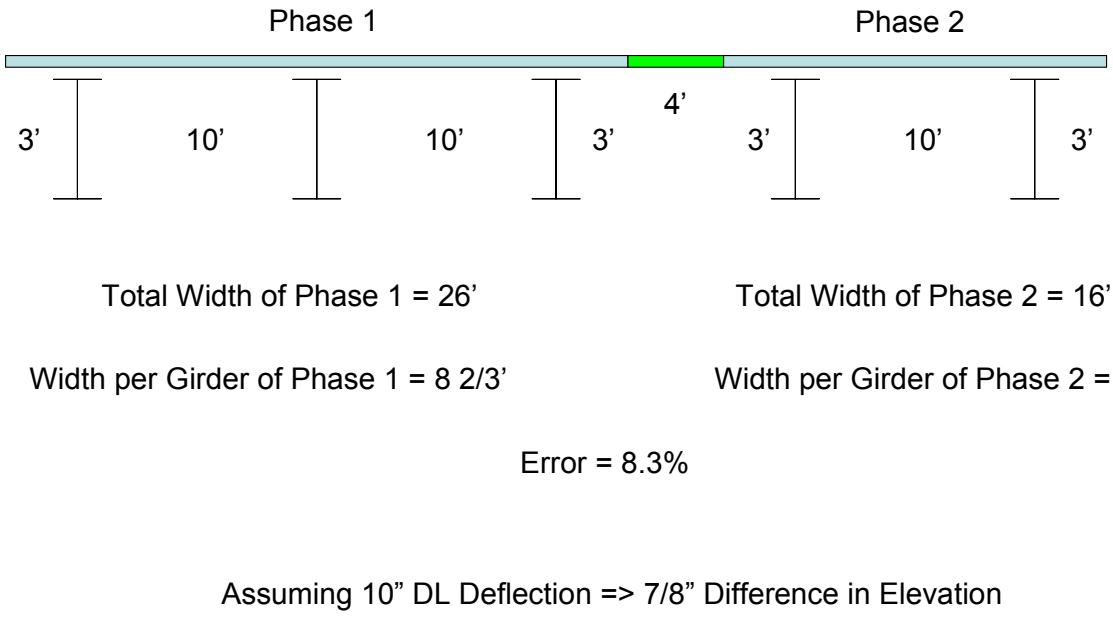

Figure 5-1: Example of Asymmetry Between Phases

As long as this condition is recognized, it is quite simple to calculate the differential deflection during design. The first method would be to run an individual analysis on each phase to obtain the differential deflection directly.

A second, approximate method of analysis, given by Equation 5-1, assumes that the dead load deflections come entirely from the deck pour.

$$\%\Delta = \frac{NG}{W}\left[\frac{W_1}{N_1} - \frac{W_2}{N_2}\right] \tag{5-1}$$

Where

$\%\Delta$ = Differential Deflection as percent of total Deflection

NG = Number of Girders

W = Total Width of Bridge

Ni = Number of Girders in i^{th} Phase

W_i = Width of i^{th} Phase

Applying Equation 5-1 to the bridge shown in Figure 5-1, the predicted error is 7.25% of the total dead load deflection as calculated for the finished bridge. This number is different from the number shown in the figure because the percentage in the figure is based on deflections calculated using Phase II as a basis. Equation 5-1 used the deflection calculated from a bridge of width W and NG girders.

5.1.3 Skew

The effects that skew angle has on the deflection profile of a bridge are most pronounced near the ends of the bridge. Near the ends of a bridge the elevation differentials experienced in phase construction would most often be due to construction tolerances and errors, the source of which has nothing to do with the use of phase construction.

Further, for medium to long bridges the impact of skew near midspan is nonexistent. However, most of the concerns associated with phased construction increase with span length. Therefore, skew is not considered a factor which impacts the use of phased construction. Should a concern arise in a particular instance a simple three-dimensional grillage analysis should suffice in determining the effects.

5.1.4 Horizontal Curvature

Bridges with horizontal curvature that are to be constructed using phased construction require detailed three dimensional analyses. Horizontally curved bridges using phase construction have experienced differential elevations of six to eight inches. The main cause of this is that the torsional properties of each individual phase are significantly different from the torsional properties of the entire system.

5.2 Distribution Factors

At the outset of this project the AASHTO LRFD equations for distribution factors were not applicable to bridges with fewer than four girders. Since

the bridge width is divided amongst two phases the number of girders within each phase is often very low. Therefore, one of the goals of this research was to determine the adequacy of the current LRFD equations for use with fewer than four girders or recommended alternate provisions for such structures. However, during the course of the project the AASHTO LRFD Specification was revised to make the distribution factor equations applicable to bridges with as few as three girders through the use of the lever rule provisions.

The results of procedures used to experimentally obtain the distribution factors from live load testing of the Dodge Street Bridge are provided in the following section.

5.2.1 Experimental Verification

Distribution factors are used in design to approximate the percent of live load carried by girders. Live load tests were performed on Phases I and II so design distribution factors could be compared to test results. The phases were constructed symmetrically so comparisons can also be made between phases to determine if they behave similarly. Tests were performed before the closure pour joined the phases.

On May 3, 2000 tests were performed on Phase I. Phase I was closed for 3 hours for testing. At this time there were temporary barriers in place that will not influence the results. On May 4, 2000 live load tests were performed on Phase II. No temporary barriers were in place on this phase.

The 1998 AASHTO LRFD Bridge Design Specifications were used to compute design live load distribution factors. Tables 5-1 and 5-2 show the calculated design values:

	1 lane loaded	2 lanes loaded
Int. girder	0.4036	0.6279

Table 5-1: Live Load distribution factors from code, interior girder

	Lever rule 1 lane loaded (w/o 1.2MPF)	Special Formula in Commentary (w/o 1.2MPF for L and R lanes)			2 lanes loaded
		Left lane	Right lane	Both lanes	
Ext. girder	1.0726	0.5619	0.4372	0.9991	0.4812

Table 5-2: Live Load distribution factors from code, exterior girder.

Trucks traversed the bridge in many locations and configurations to simulate traffic. These configurations are presented in Appendix C. The maximum experimentally calculated distribution factors from these tests for Phase I and II are in Tables 5-3 and 5-4 respectively. The distribution factor was obtained for several locations along the length of the bridge. The location where the distribution was a maximum is presented in Tables 5-3 and 5-4. These locations can be seen in Figures C-11 and C-12 on page 316 in Appendix C.

Test	J	H	G	E
Lane A	.3683 @ Max -E	.3835 @ Max + E	.2126 @ E4	.1596 @ E7
Lane C	.0675 @ E2	.2002 @ Max - E	.3379 @ Max + E	.4926 @ Max + E
A and C superimposed	.4287 @ E2	.5321 @ Max + E	.5262 @ Max + E	.6448 @ E7
A and C (side by side)	.5180 @ E2	.5446 @ Max + E	.5380 @ Max + E	.5490 @ E7
Middle	.2782 @ Max - E	.2872 @ E6	.3084 @ E6	.2680 @ Max - E

Table 5-3: Experimentally calculated distribution factor(DF) for Phase I

In Tables 5-3 and 5-4 Lane A is the lane away from the closure region and Lane C is near the closure region. Results from testing lane A and lane C were superimposed to obtain the effect of loading both lanes simultaneously. This can be compared to the lane A and C loaded test. The location where the maximum distribution factor occurred is also shown. Truck positions and locations will be outlined later in this section. Girders A, D, E, and J are exterior girders while Girders B, C, G, and H are interior girders

Test	D	C	B	A
Lane A	.1511 @ E7	.2179 @ E7	.3542 @ Max + E	.3856 @ max – E
Lane C	.4431 @ Max + E	.3223 @ Max + E	.2414 @ E4	.1351 @ Max - E
A and C superimposed	.5637 @ Max + E	.5271 @ Max + E	.5358 @ E6	.5827 @ E2
A and C (side by side)	.5274 @ E2	.5134 @ Max + E	.5604 @ E6	.5684 @ E2
Middle	.2653 @ Max - E	.3175 @ Max + E	.2722 @ Max + E	.2944 @ Max - E
Train C	.4315 @ E6-W1/W2	.3333 @ E6-W1/W2	.2272 @ E4-W3/W4	.0891 @ E7-CL/W1
Train Middle	.2833 @ E4-W3/W4	.2933 @ E6-W1/W2	.2799 @ E6-W1/W2	.2599 @ E7-CL/W1

Table 5-4: Experimentally calculated distribution factor(DF) for Phase II.

Tables 5-5 and 5-6 compare design values to experimental results for interior and exterior girder distribution factors respectively. From these tables it is clear experimental interior girder distribution factors are close to design values. For exterior girders with one lane loaded the lever rule grossly overestimates the distribution factor. The overestimation is even larger considering that the 1.2 MPF used in design is not included in the calculations. For exterior girders with two lanes loaded the commentary equation overestimates the distribution factor. Consequently, girders designed based on the lever rule and commentary equations will be over proportioned for the live load they experience.

Design		Experimental	
1 lane loaded	2 lanes loaded	1 lane loaded	2 lanes loaded
0.4036	0.6279	0.3835	0.5604

Table 5-5: Design calculated distribution factors and experimental results (Interior)

5.3 End Restraint

A very common construction detail used in Nebraska is that of a semi-integral abutment. By semi-integral it is meant that the ends of the girders are

Design				Experimental	
1 lane loaded		2 lanes loaded		1 lane loaded	2 lanes loaded
Lever rule	commentary	eg	commentary		
1.0726	0.5619	0.4812	0.9991	0.4926	0.4287 to 0.6448

Table 5-6: Design calculated distribution factors and experimental results (Exterior)

embedded in the turndown, however, excessive measures are not taken to ensure moment transfer. Although there is not full fixity, there is some amount of rotational restraint applied to the girder ends. During the design process, this partial restraint is conservatively ignored.

Although ignoring the partial restraint will result in a conservative and prudent estimation of strength, an improved estimation can be of value in the construction of a bridge utilizing phases. In general, the potential errors and misalignment of the phases increase with the magnitude of dead load deflections. The partial restraint provided by the semi-integral abutment will reduce the dead load deflections. Therefore, this restraint will be beneficial to the phased construction project. However, corrective measures, such as modified camber, taken based on predicted deflections ignoring the partial restraint may overshoot the required modifications due to the reduction in deflections as a consequence of the semi-integral abutment.

5.3.1 Analysis Technique

The actual restraint condition must lie between a simple support condition and full fixity. This can be expressed as a percentage of fixity given by Equation 5-2.

$$f = \frac{\delta_s - \delta}{\delta_s - \delta_f} \tag{5-2}$$

Where

f = Percent Fixity

δ = Actual Deflection

δ_s = Deflection assuming simple support condition

δ_f = Deflection assuming fixed support condition

If it is assumed that a given construction detail will give a predictable percentage of fixity then the actual deflection can be calculated from Equation 5-2 obtained by solving Equation 5-2 for δ.

$$\delta = \delta_s - f\left(\delta_s - \delta_f\right) \tag{5-3}$$

The deflection obtained by Equation 5-3 can now be used to assess the phased construction design. The final step is to monitor the observed deflections from actual details to assign an amount of fixity which a given detail will develop. This information may already be available in construction records. Further, this fixity is not specific to phase construction.

5.3.2 Results from Dodge Street

The average girder deformation due to placement of the deck obtained from finite element analysis assuming pinned ends is 5.0 inches. Assuming fully fixed ends results in a predicted deflection of 2.8 inches. The average deflection obtained from the actual placement of the deck was 4.8 and 4.3 inches for phases one and two respectively.

Using Equation 5-2 yields 9% and 32% end fixity for phases one and two respectively with an average end fixity of 20%. Note that this assumes that the difference in deflections from phase one to two is solely a result in different end fixity conditions.

5.3.3 Live Load deflection Analysis

For some range of spans the controlling limit state in design is often a deflection criterion under service loads. This criteria is optional in the AASHTO code, however, the State of Nebraska utilizes a deflection limit of L/800.

The previously described method of analysis could also be utilized in estimating the live load deflections. The partial restraint could still be ignored with regards to determining the loads such that the strength of the system remains conservative. However, some advantage could be gained in meeting the deflection criteria.

Much of the design is performed with the help of computer analysis programs. Once the desired level of fixity is determined, an equivalent rotational stiffness required to achieve that level of fixity if needed. However, many of the computer programs used by the Nebraska Department of Roads do not have the capability of modeling a rotation spring which is required to implement the rotational stiffness. One solution is to simulate the rotational springs at the supports by extending the bridge an additional span beyond the end of the bridge.

What is now required is a method for determining the required length of the additional span. A program has been developed to accomplish this task. The front end of the program consists of a Visual Basic for Applications Add-In to Excel. The front end provides a convenient interface allowing the problem input to be carried out in an Excel spreadsheet. The VBA front end then calls a Dynamic Link Library written in FORTRAN to perform the analysis. The results are then passed back to the VBA program which will then generate a resulting chart in Excel.

Program Details

The Visual Basic add-in handles the bookkeeping associated with calling the analysis routine. This includes displaying and controlling the dialog box, associating the data on the spreadsheet with the variables required for the analysis routine, and actually performing the calls. The add-in also includes the capability of generating plots which are useful in verifying the resulting solution.

The real algorithm is contained within the FORTRAN DLL. There are three primary units within the program. At the heart is a simple finite element code for analyzing continuous beams. The finite element code is wrapped by an evaluation unit which takes as input all the loading and geometrical information and evaluates the deflections. Finally, there is a control structure which handles the search for the desired condition. There is also a stub routine to the evaluation structure which can be called directly from the Excel add-in used to evaluate the stiffness condition for a structure with prescribed side spans. This is used when the evaluation mode is selected in the dialog box.

THE FLOW THROUGH THE PROGRAM IS AS FOLLOWS:

The user inputs the beam segment and spanning data in an Excel spreadsheet. The program can accept an arbitrary number of segments within each span to accommodate section changes. The data required for each segment are the length and flexural stiffness (EI). A stub has been incorporated allowing for the future addition of a module which would allow the section properties to be calculated from the section profile. However, this has not been implemented at this time. For each end of the beam, the user provides the desired percent of fixity, the flexural stiffness of the extra spans, and an initial guess for the required length. In most realistic situations, the value of the initial length is not terribly critical to the success of the algorithm, although an initial length which is shorter than the correct value will probably converge slightly faster. One situation which can require a better initial length is a beam with highly unbalanced spans.

Additionally, an option box can be checked which will activate an automated evaluation of the seed length values. In most common applications, this method should yield good results. If convergence is not obtained then one may be required to manually select values.

The next step is an initial evaluation of the degree of fixity provided by the assumed span lengths. If either of the computed fixity ratios is too large, indicating excessive stiffness the algorithm begins a loop over two steps. The first step is activated if both of the spans are too stiff in which case each span is lengthened by 10%. This first step is repeated until one of the spans is long enough. Once one of the spans is long enough the second step reduces the length of the span which is too long by 5% while leaving the other intact. The algorithm then returns to the first step, looping over both steps until both ends are flexible enough that the degree of fixity is less than that which had been requested.

Once the previous requirements have been satisfied, the algorithm begins an iterative refinement stage. During each iteration the length of the extensions are multiplied by the value of one plus the evaluated fixity ratio minus the requested fixity ratio at the respective end. This is repeated until convergence within the specified tolerance is obtained.

PROGRAM INPUT

A screen shot of a typical input scenario is shown in Figure 5-2. The input dialog is shown in Figure 5-3.

The first input the program requires is the geometrical properties and span information of the cross-section segments. Each segment is described by a line of data. The segments must be listed in sequential order from one end to the other. Although the results are independent of the assumed direction, for demonstration purposes, the first span will be assumed to be located towards the left. The first column of each segment data is the length of the segment. The second column indicates which span the segment is in. In Figure 5-4, each span is composed of two segments. The final column for each beam segment is the flexural stiffness, or EI value. This analysis can be done on either a per-girder basis, or full section basis

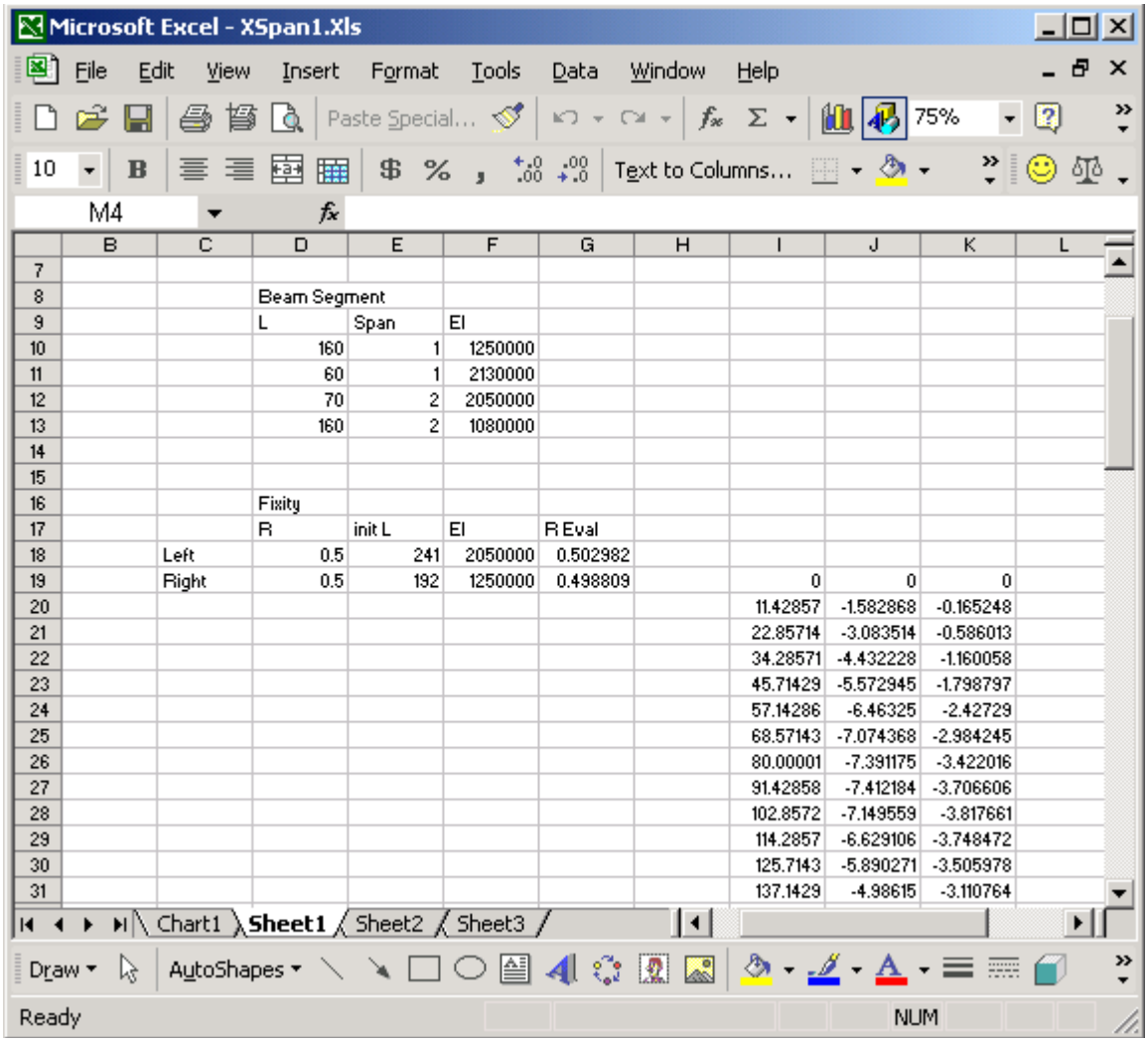

Figure 5-2: Excel Screen Shot Showing Typical Input

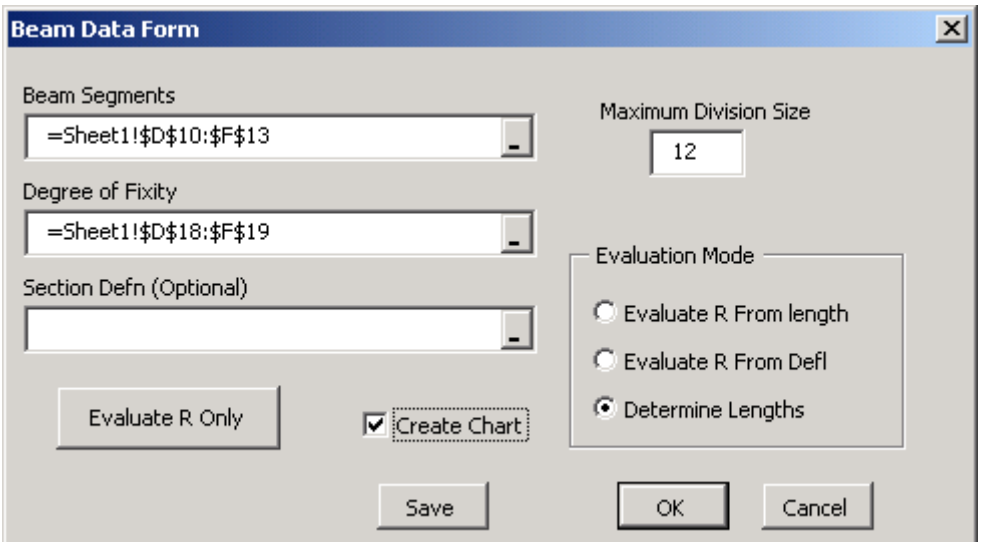

Figure 5-3: Analysis Control Dialog

depending on the available information. The range containing the segment data is then entered into the dialog.

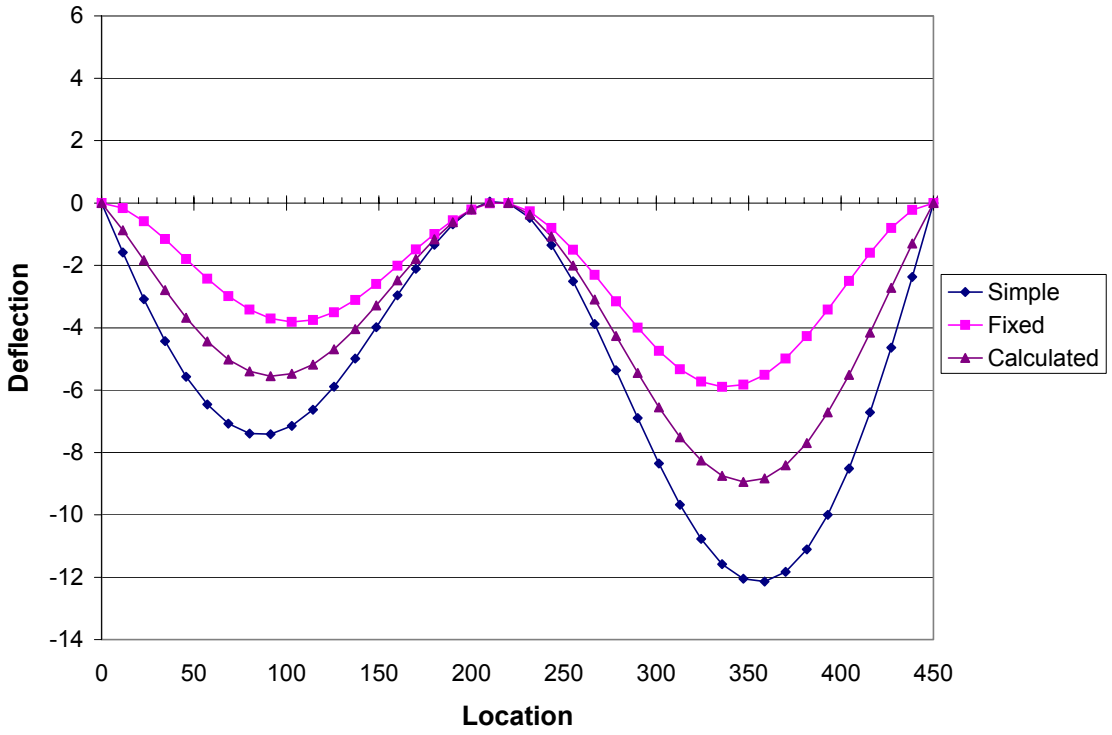

Figure 5-4: Example of Partial Fixity Analysis

The next information is the fixity requirements. There are two lines of data, one for each end of the girder. The first column is the desired level of fixity. The second column is the specified initial starting length. If this is left blank, the program will use an automatically determined initial length. The final column is the rotational stiffness of the beam extension. The fourth column shown in Figure 5-2 is an output column reporting the evaluated fixity ratio. The calculated lengths are also output to the second column replacing the starting length values. If the calculation mode is chosen to be evaluation only, which is done by clicking the evaluation mode toggle, then the length column is not modified and only the evaluated level of fixity is updated.

Several other options are available in the dialog. The first is the maximum division size. The default value of 12 should be ok for most applications, however, for beams with extreme dimensions or entry in alternative units could require this value to be modified.

Diagnostic plots can also be generated to verify visually that the desired solution has been obtained. The output location of the data required to generate the charts can be specified as well.

5.4 POUR SEQUENCING

Predicted deflections are needed to compare against field deflections during positive and negative region pours. To obtain predicted values finite element models were constructed using SAP 2000. The models only considered a single girder with an applied loading equal to one fourth of the total concrete placed. This load is computed using Equation 5-4.

$$\text{Applied load} = \tfrac{1}{4} * 34' - 4" * 7.0" * 150 \text{ pcf} \Rightarrow 0.06259 \text{ lb/in} \quad (5\text{-}4)$$

Where

34' - 4" = pour width

7.0" = pour depth

150 pcf = concrete unit weight

Another design assumption is that vertical curvature of girders can be ignored. To investigate if this assumption is valid two models were created. The first is a perfectly straight girder and the second model considers the vertical curvature. In both models girders change section properties at appropriate locations as seen in Figure 5-5.

When composite section properties are needed for negative region pours the effective flange width of composite sections is consistent with AASHTO design provisions. The compressive strength of concrete is taken to be the design compressive strength, 4350 ksi (40 Mpa). At abutments roller sup-

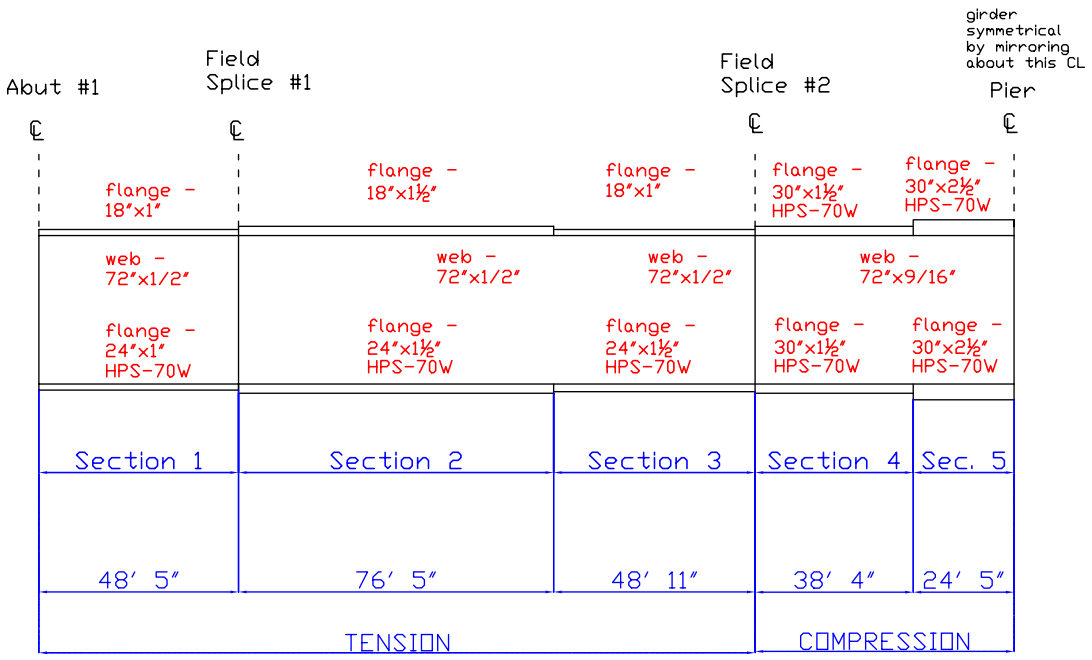

Figure 5-5: Girder Dimensions

ports are assumed and the pier is assumed to be a pin connection. These are also commonly used design assumptions.

First the assumption that ignoring vertical curvature does not cause significant error will be investigated. Finally predicted deflection values for both pours will be compared to field observations.

5.4.1 Straight and Curved Model Comparison

Positive region pours placed 167'-4” of wet concrete on each span. The curved and straight girder model with this load is shown in Figures 5-6 and 5-7. During this pour girders are non-composite and sectional properties of each model reflect this.

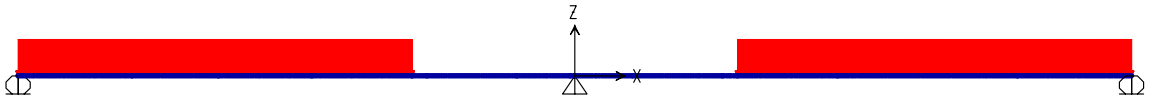

Figure 5-6: Straight girder model during positive region pours. Loaded region is 167' 4" from each abutment.

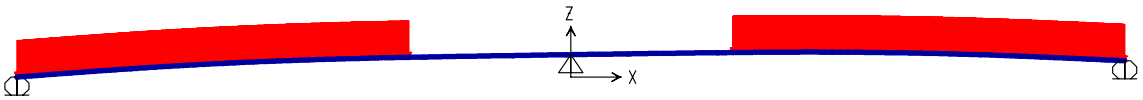

Figure 5-7: Curved girder model during positive region pours. Loaded region is 167' 4" from each abutment.

Deflection results from these models are compared in Figures 5-8 and 5-9. The location of field measured deflection is included in these figures.

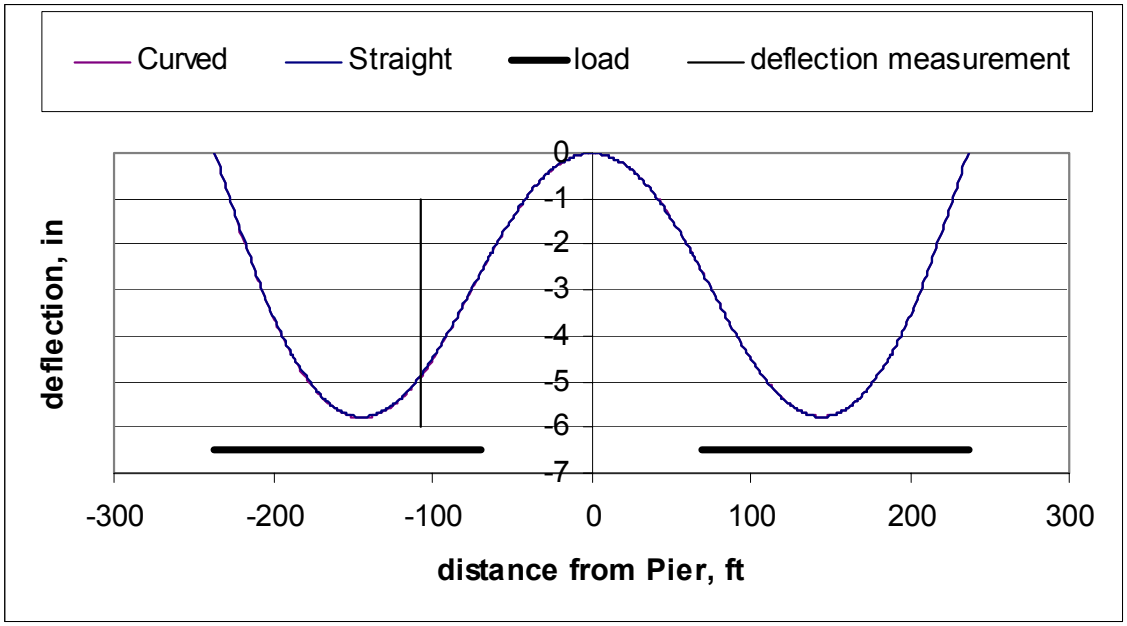

Figure 5-8: Results of Positive Pour Modeling Curved and Straight Models

Figure 5-9 shows the difference of curved and straight girder model deflections. Ignoring curvature during positive region pours results in less than 0.02" error.

Figures 5-10 and 5-11 show the straight and curved girder models for the negative region pours. This pour could not be performed until the positive region concrete reached its design compressive strength. Therefore,

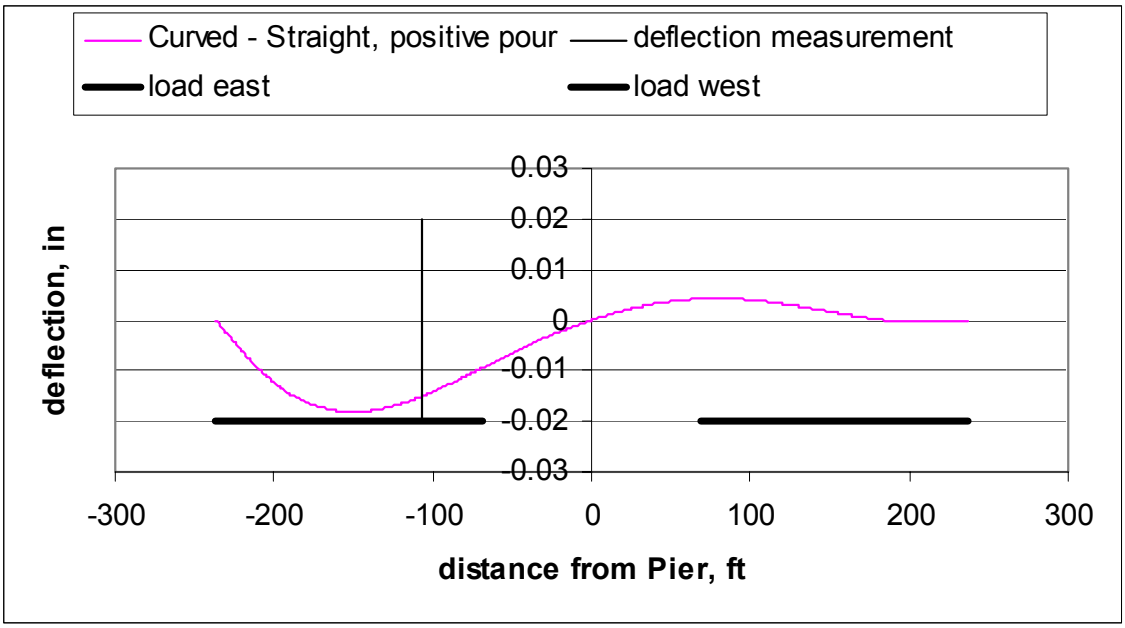

Figure 5-9: Deflection Difference between Straight and Curved Model Results

regions with concrete already in place are assumed composite in both models.

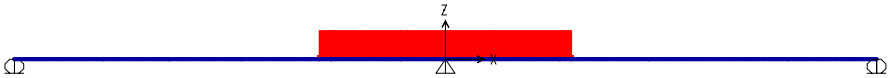

Figure 5-10: Straight girder model during negative region pours. Loaded region is 130' 4" wide

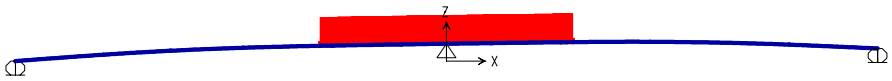

Figure 5-11: Curved girder model during negative region pours. Loaded region is 130' 4" wide

Deflection results from these models are compared in Figures 5-12 and 5-13.

From the figures, ignoring curvature during negative region pours results in less than 0.001" deflection. From these results, ignoring curvature does not induce significant error in predicted deflections.

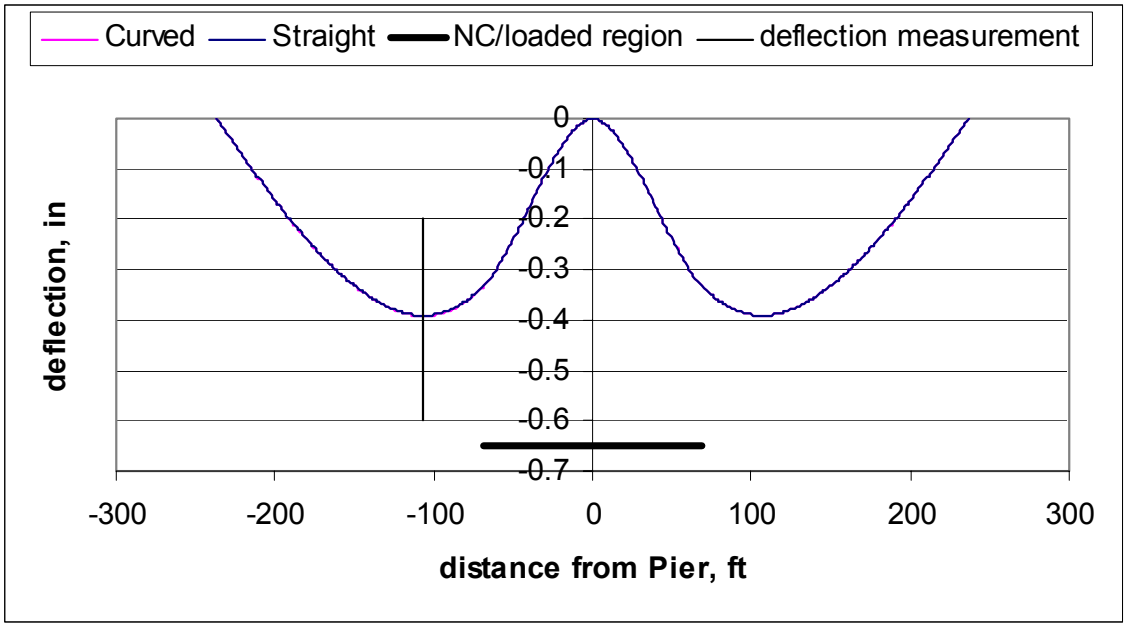

Figure 5-12: Deflection results from straight and curved models

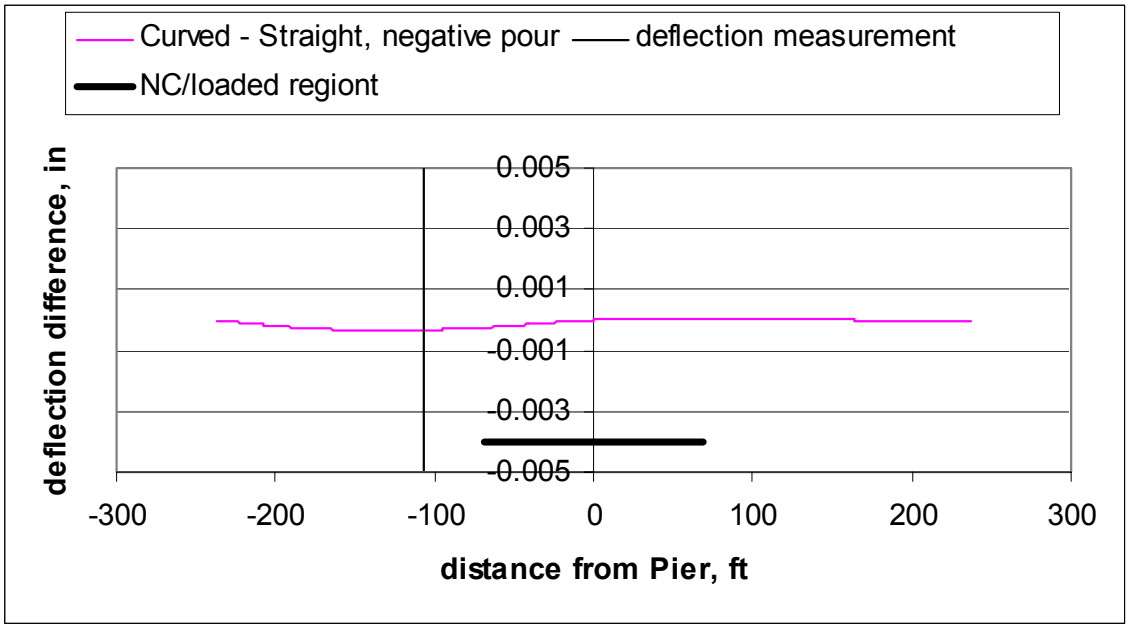

Figure 5-13: Comparison of Curved and Straight girder model deflections

In reality the concrete pour is performed in two stages. Often in design pouring sequence is ignored to compute deflection. The straight and curved models can also be used to determine error from ignoring pouring sequence. To determine this error both models are fully loaded along their

length. Results from these analyses are compared to superposition of individual pour deflections. The fully loaded models are shown in Figures 5-14 and 5-15.

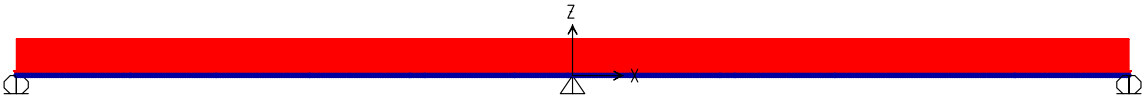

Figure 5-14: Fully loaded straight girder model

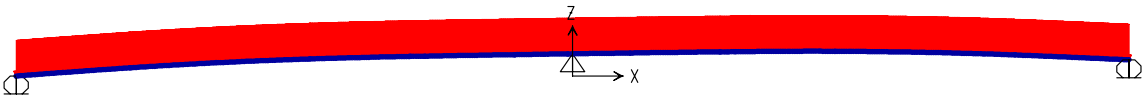

Figure 5-15: Fully loaded curved model

Figures 5-16 and 5-17 compare results from placing the concrete in one pour and the pouring sequence.

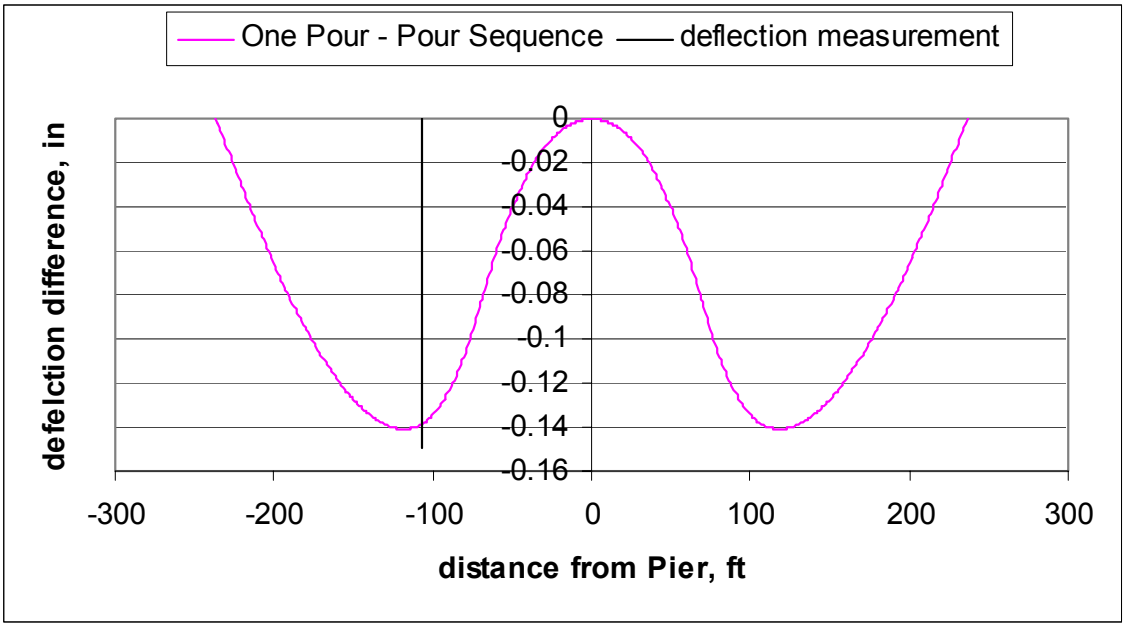

Figure 5-16: Comparison of placing all concrete at once and modeling the pour sequence for straight girders

Ignoring the pouring sequence only introduces 0.14" of error. Compared to the 6" of expected deflection this is only 2% error. Therefore ignoring the pouring sequence introduces no significant error.

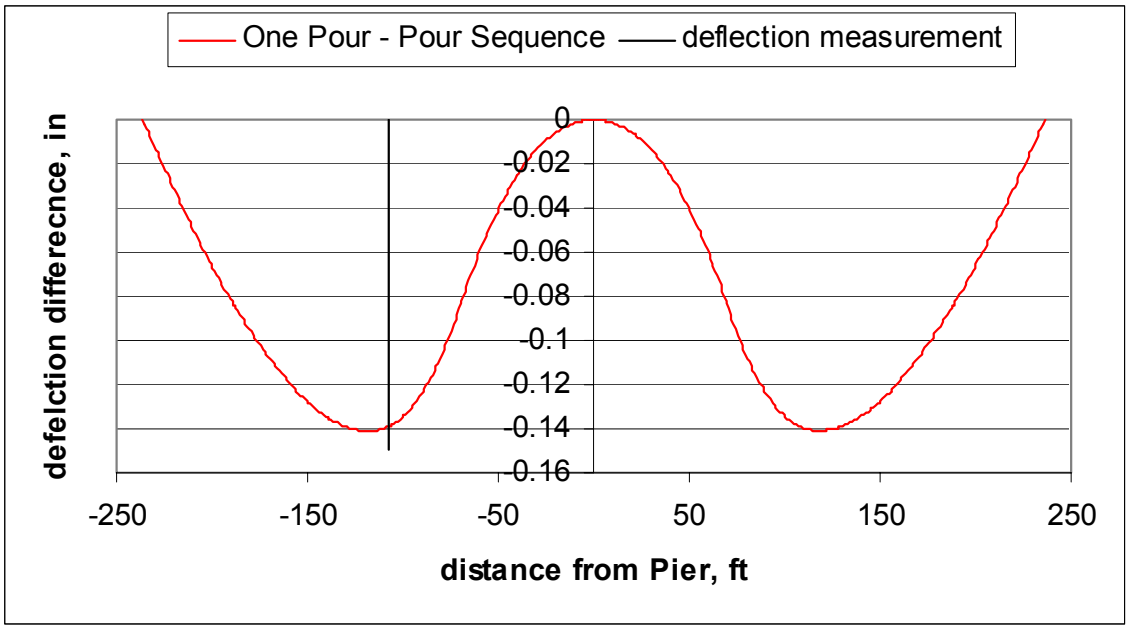

Figure 5-17: Comparison of placing all concrete at once and modeling the pour sequence for curved girders

In conclusion, the maximum possible error will occur if both curvature and pouring sequence are ignored. To compute this error results from the straight model with all concrete placed at once are used. These results can be compared to deflections from curved models by superimposing deflections from the pouring sequence. This maximum error is shown in Figure 5-18. The maximum error is still small compared to the 6" expected deflection from superimposing curved model results. In design ignoring the pouring sequence and curvature will introduce no significant error.

5.4.2 Field Deflections versus Predicted Deflections

Predicted values used to compare against field deflections will be obtained from the curved models. These models more accurately reflect the girders.

Predicted deflection for the positive region pour is -4.899". Field deflections are summarized in Table 5-7. Girders farthest from the closure on the left side of Table 5-7.

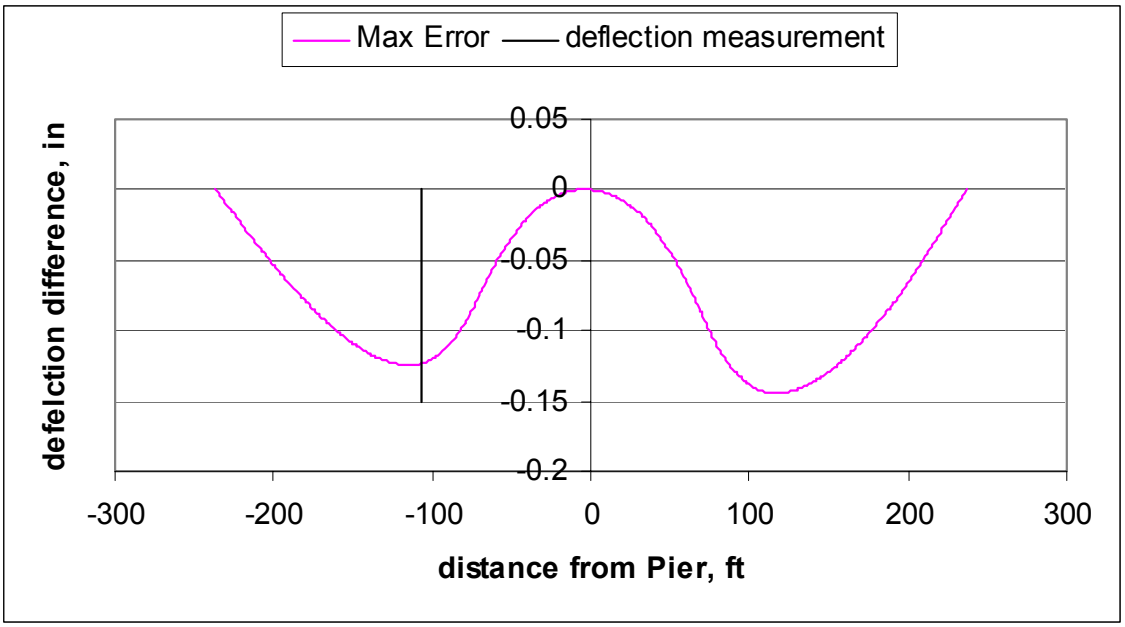

Figure 5-18: Maximum error in pour sequence modeling

Girder J	Girder H	Girder G	Girder E
-4.932	-4.855	-4.615	-4.593
Girder A	**Girder B**	**Girder C**	**Girder D**
-4.932	-4.754	-4.664	-4.473

Table 5-7: Positive region pour deflections.

Girder deflections farthest from the closure are closer to the predicted value. The maximum deviation from predicted deflection is 0.426" or 9%. This is still close considering the complexity of each phases behavior.

Predicted deflection for the negative region pour is -0.391". Field deflections are summarized in Table 5-8. Girders farthest from the closure on the left side of Table 5-8.

All girders deflected similarly except for Girder H. The error for Girder H is 0.129" or 33%. The average error for the other girders is 0.046" or 12%. More work needs to be done with finite element modeling to understand behavior during these pours. End conditions are most likely not truly rollers and pins as assumed. This will affect predicted deflections.

Girder J	Girder H	Girder G	Girder E
-0.453	-0.520	-0.424	-0.454
Girder A	**Girder B**	**Girder C**	**Girder D**
-0.442	-0.426	-0.423	-0.435

Table 5-8: Negative region pour deflections.

NOTE ON DIFFERENTIAL ELEVATIONS

Girder elevations were only measured at one location. It is possible for this measurement location to show nearly no differential elevation while at other points it may be significant.

5.5 INTRODUCTION TO LONG TERM DEFLECTION

The material contained within Chapter 6 entitled Long Term Deflection Prediction essentially should be included in the current analysis chapter. However, it is much too involved and has therefore been treated separately.

Chapter

6 Long Term Deflection Prediction

DEFLECTIONS WHICH ACCUMULATE OVER TIME DUE TO CREEP AND SHRINKAGE

When constructing a bridge utilizing phased construction there are two distinct needs for knowing long term deflection behavior. First, since there is a substantial period of time between the construction of the phases the initial phase has time to accumulate time dependent deformations prior to the completion of the final phase. Having an estimate of these deformations allows the designer to determine if the deformations are significant and if they are indeed significant, what level of accommodation must be provided so the two phases are at the same elevation when it is time for the closure operation to be completed. Second, once the two phases are joined by the closure region the newer phase will still be expected to deform over time more so than the older phase. However, now that the two phases have been joined this relative deformation will be restrained which in turn will

give rise to additional stresses in the elements providing the connection, namely the closure region and cross-frames. Therefore, an estimate of the magnitude of relative deformation will allow the designer to evaluate the additional stresses in the connecting elements and determine whether any additional steps need to be taken.

Within this chapter the theory behind time dependent deformation is presented. A finite element program has been developed utilizing the age adjusted effective modulus method suitable for the analysis of continuous two-span bridges. Also presented in this chapter are the results from several experimental investigations to verify the theory and finite element program.

6.1 THEORY

The following section presents the basic creep and shrinkage behavior of concrete. Methods for time history analysis are then presented after which the theory is specialized for the analysis of continuous composite concrete-steel girders.

6.1.1 MATERIAL BEHAVIOR

When a concrete specimen is subjected to load, its response is both immediate and time-dependent. Under sustained load, the deformation of a specimen gradually increases with time and eventually may be many times greater than its instantaneous value.

If temperature and stress remain constant, the gradual development of strain with time is caused by creep and shrinkage. Creep strain is produced by sustained stress, whilst shrinkage strain is independent of stress. These inelastic and time-dependent strains cause increases in deformation and curvature.

TYPICAL CONCRETE STRAINS

At any time t, the total concrete strain $\varepsilon(t)$ in a uniaxially loaded specimen consists of a number of components, which include the instantaneous strain $\varepsilon_e(t)$, the creep strain $\varepsilon_c(t)$, the shrinkage strain $\varepsilon_{sh}(t)$, and the temperature strain $\varepsilon_T(t)$. It is usual to assume that all four components are independent and may be calculated separately and summed to obtain the total strain:

$$\varepsilon(t) = \varepsilon_e(t) + \varepsilon_c(t) + \varepsilon_{sh}(t) + \varepsilon_T(t) \tag{6-1}$$

Where

ε = Total Strain

ε_e = Instantaneous strain

ε_c = Creep strain

ε_{sh} = Shrinkage strain

ε_T = Temperature strain

Consider a concrete specimen subjected to a constant, sustained compressive stress σ_0. The instantaneous strain that occurs immediately on application of the stress may be considered to be elastic at low stress levels, and therefore:

$$\varepsilon_e(t) = \frac{\sigma_0}{E_c(t)} \tag{6-2}$$

Where

σ_0 = Constant, sustained compressive stress

E_c = Modulus of elasticity of concrete

CREEP

The capacity of concrete to creep is usually defined in terms of the creep coefficient, ϕ. Under a constant sustained stress, ϕ is the ratio of the creep strain at time t to the instantaneous elastic strain. Since creep strain

depends on the age of the concrete at the time of first loading, so too does the creep coefficient. Therefore:

$$\phi(t,\tau) = \frac{\varepsilon_c(t,\tau)}{\varepsilon_e(\tau)} \tag{6-3}$$

Where

$\phi(t,\tau)$ = Creep coefficient

τ = Time of loading

Figure 6-1 shows the effect of age at first loading on the creep-time curves of identical specimens first loaded at τ_0, τ_1, and τ_2. The older concrete is when loaded, the smaller is the final creep strain.

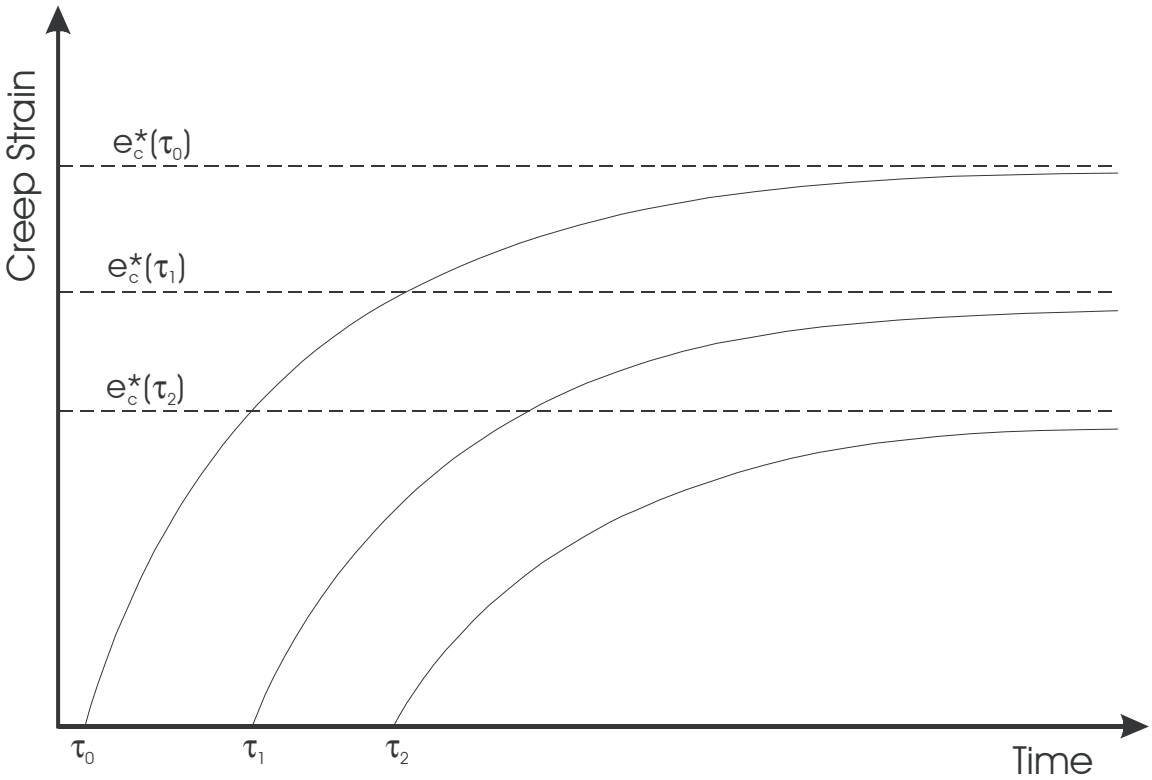

Figure 6-1: Effect of age at first loading on creep strains

SHRINKAGE

Shrinkage is defined as the time-dependent strain measured at constant temperature in an unloaded and unrestrained specimen. Since shrinkage is to a large extent caused by drying, shrinkage strains vary through the

thickness of structural members and are highest at the surfaces exposed to the atmosphere.

DEFORMATION OF CONCRETE

As discussed earlier, the total strain at any time t at a point in a uniaxially loaded specimen at constant temperature may be expressed as follows:

$$\varepsilon(t) = \varepsilon_e(t) + \varepsilon_c(t) + \varepsilon_{sh}(t) \tag{6-4}$$

The strain components in a specimen loaded with a constant sustained compressive stress first applied at time τ are shown in Figure 6-2. Immediately after the concrete sets or at the end of moist curing, shrinkage strains begin to develop and continue to increase at a decreasing rate. On application of the stress, a sudden jump in the strain diagram (instantaneous strain) is followed by an additional increase in strain due to creep.

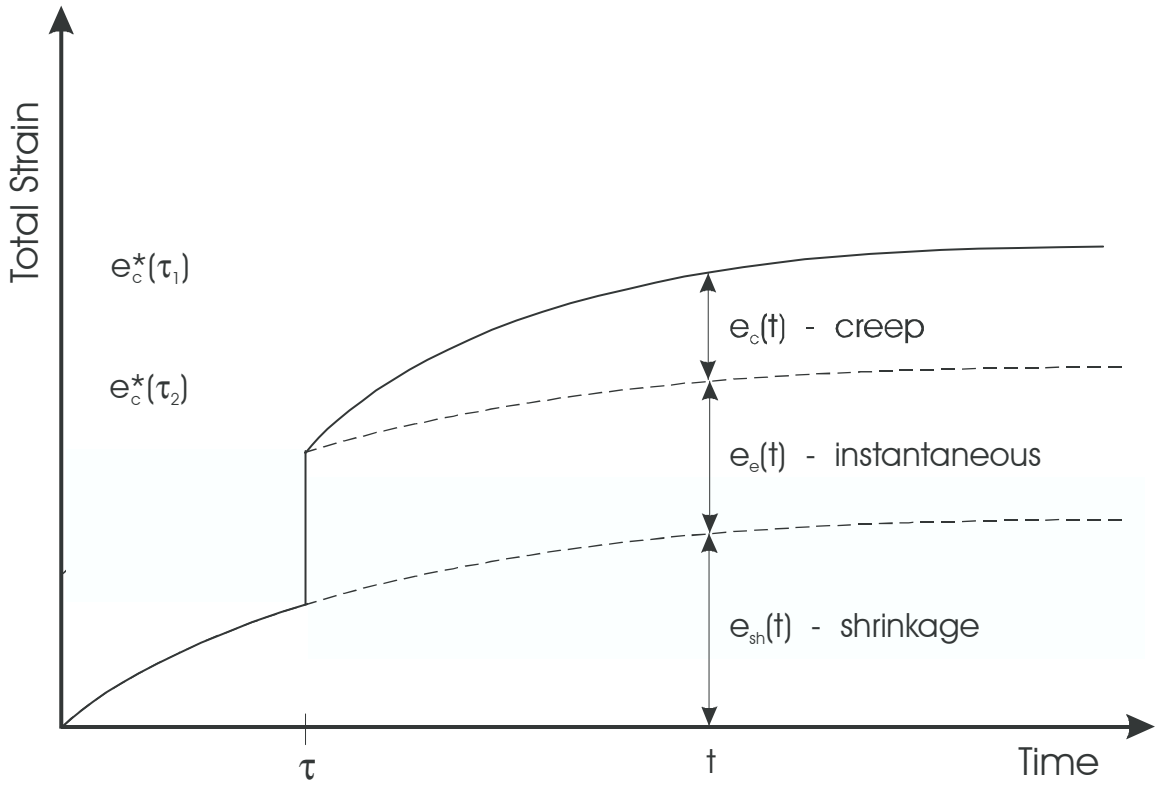

Figure 6-2: Concrete strain components under sustained stress

The prediction of the time-dependent behavior of a member requires the accurate prediction of each of these strain components at crucial locations. This requires knowledge of the stress history, in addition to accurate data for the material properties. The stress history depends both on the applied load and on the boundary conditions of the problem.

METHODS FOR PREDICTING CREEP COEFFICIENT AND SHRINKAGE

Potentially the most accurate means for predicting the final creep coefficient and shrinkage strain, ϕ^* and ε_{sh}^* (where the * denotes values at time infinity), is to extrapolate from short-term test results. Creep is measured over a relatively short period in specimens subjected to constant stress. Shrinkage is measured over a similar period in companion unloaded specimens. Various mathematical expressions for the shape of the creep and shrinkage curves are available from which long-term values may be predicted from short-term measurements. The longer the period of measurement, the more accurate are the long-term predictions.

6.1.1.0.1 Predictions from short-term tests

Numerous expressions have been proposed for the development of creep and shrinkage with time. Exponential, hyperbolic, logarithmic and power expression have been used to model the development of both creep and shrinkage.

Combinations of these types of expressions which provide much better predictions of long-term creep are also available. The hyperbolic-power expression used by ACI and developed by Meyers et al (1970) is an example:

$$\phi(t,\tau) = \frac{\alpha(t-\tau)^{\gamma}}{\beta + (t-\tau)^{\gamma}} \tag{6-5}$$

Where

α = Final creep coefficient, $\phi^*(\infty,\tau)$

The ACI suggests (ACI 1978):

$$\beta = 10.0 \text{ and } \gamma = 0.6 \tag{6-6}$$

When t-τ = 28 days, the relationship between the 28-day and final creep coefficient is obtained from Equation 6-5 as:

$$\phi(\tau + 28, \tau) = \frac{\phi^*(\infty, \tau)}{2.35} \tag{6-7}$$

By substituting Equation 6-7 into Equation 6-5, the long-term creep coefficient may be obtained from 28 day measurements:

$$\phi(t, \tau) = \phi(\tau + 28, \tau)\frac{2.35(t-\tau)^{0.6}}{10 + (t-\tau)^{0.6}} \tag{6-8}$$

6.1.2 METHODS FOR TIME ANALYSIS

The time analysis of a concrete structure involves the determination of strains, stresses, curvatures and deflections at critical points and at critical times during the life of the structure. To accurately predict time dependent behavior, two basic prerequisites are required:

1. Reliable data for the creep and shrinkage characteristics of the particular concrete mix
2. Analytical procedures for the inclusion of these time-dependent deformations in the analysis and design of the structure.

The creep and shrinkage characteristics of concrete are highly variable and are never exactly known. In addition, it will be seen in this chapter that the methods for the time analysis of concrete structures are plagued by simplifying assumptions and approximations. Accurate numerical predication of time-dependent behavior is therefore not possible. However, it is possible to establish upper and lower limits to behavior in order to determine whether or not time effects are critical in any particular situation and, if required, to adjust a design to reduce undesirable long-term deformations.

CONSTITUTIVE RELATIONS

If the concrete stress σ at a point in a structure remains constant with time, the determination of each of the strain components in Equation 6-4 presents no problem.

$$\varepsilon(t,\tau) = \varepsilon_e(t,\tau) + \varepsilon_c(t,\tau) + \varepsilon_{sh}(t) \tag{6-9}$$

$$= \frac{\sigma}{E_c(\tau)} + \frac{\sigma}{E_c(\tau)}\phi(t,\tau) + \varepsilon_{sh}(t) \tag{6-10}$$

Where

σ = Concrete stress at any point

Numerical values of $\phi(t,\tau)$ and $\varepsilon_{sh}(t)$ may be obtained from test data or the predictive models discussed earlier.

If the instantaneous and creep components of strain in Equation 6-10 are combined, a reduced or effective modulus for concrete, $E_e(t,\tau)$, can be obtained as follows:

$$\varepsilon(t,\tau) = \frac{\sigma}{E_c(\tau)}[1 + \phi(t,\tau)] + \varepsilon_{sh}(t) \tag{6-11}$$

$$= \frac{\sigma}{E_e(t,\tau)} + \varepsilon_{sh}(t) \tag{6-12}$$

Where: $$E_e(t,\tau) = \frac{E_c(\tau)}{[1 + \phi(t,\tau)]} \tag{6-13}$$

This is the simplest and oldest techniques for including creep in structural analysis and is Faber's effective modulus method, EMM (Faber 1927).

According to EMM, the creep strain at time t (Equation 6-12) depends only on the current stress σ and is independent of the previous stress history. This, of course, is not so. Aging of concrete has been ignored.

If the concrete stress at a point varies with time, the determination of creep strain becomes more difficult. In reinforced concrete structures, even under constant sustained loads, stresses are rarely constant. Creep and shrinkage see to that. Equation 6-10 can no longer be used to predict deformation; the stress history and the effects of aging must be included.

AGE ADJUSTED EFFECTIVE MODULUS METHOD (AEMM)

Consider the two concrete stress histories and the corresponding creep-time curves shown in Figure 6-3. The creep strain at any time t ($>\tau_0$) produced by the gradually applied stress is significantly smaller than that resulting from the suddenly applied stress, as shown. This is due to aging. The earlier a concrete specimen is loaded, the greater is the final creep strain.

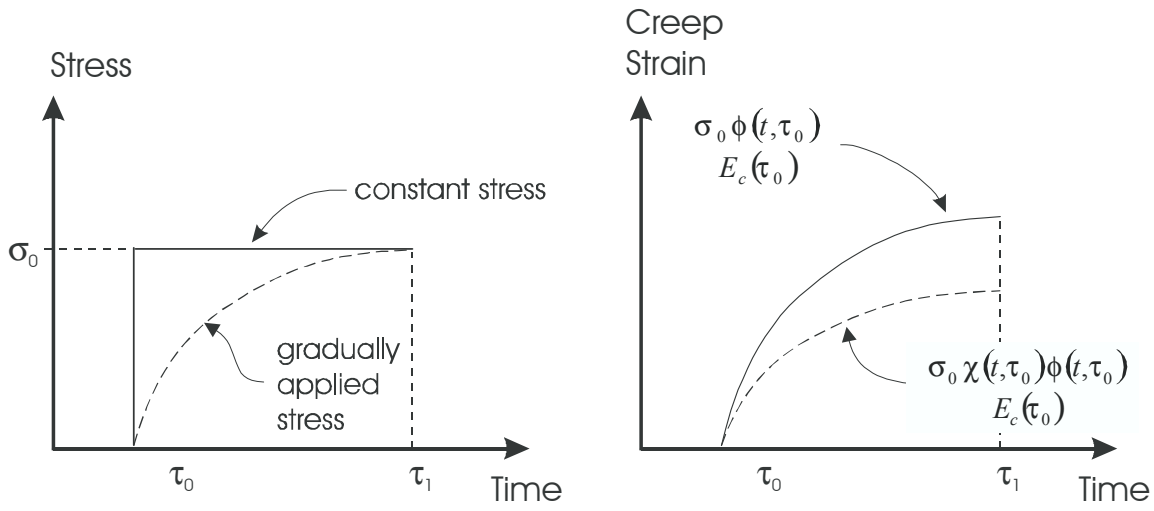

Figure 6-3: Creep due to both constant and variable stress history

A reduced creep coefficient can therefore be used to calculate creep strain, if stress is gradually applied.

Let this reduced creep coefficient be $\chi(t,\tau_0)\phi(t,\tau_0)$. The coefficient $\chi(t,\tau_0)$ is called the aging coefficient and its magnitude generally falls within the range 0.6 to 0.9. In most practical situations, the final aging coefficient $\chi(\infty,\tau_0) = \chi^*(\tau_0) = 0.75$ to 0.85.

The creep strain at time t due to a stress $\sigma(t)$, which has been gradually applied over the time interval $t-\tau_0$, may be expressed as:

$$\varepsilon_c(t) = \frac{\sigma(t)}{E_c(\tau_0)} \chi(t,\tau_0)\,\phi(t,\tau_0) \qquad (6\text{-}14)$$

Where

$\chi(t,\tau_0)$ = Aging Coefficient

Now, consider the typical concrete stress history shown in Figure 6-4. An initial stress σ_0, applied at time τ_0, is gradually reduced with time. The change of stress is:

$$\Delta\sigma(t) = \sigma(t) - \sigma_0 \qquad (6\text{-}15)$$

Where

$\Delta\sigma(t)$ = Change in stress over time

This may be due to a change of external loads, or resistance to creep and shrinkage, or variations of temperature, or a combination of these and is usually unknown at the beginning of an analysis.

The total strain at time t may be expressed as the sum of the strains produced by σ_0 (instantaneous and creep), the sum of the strain produced by

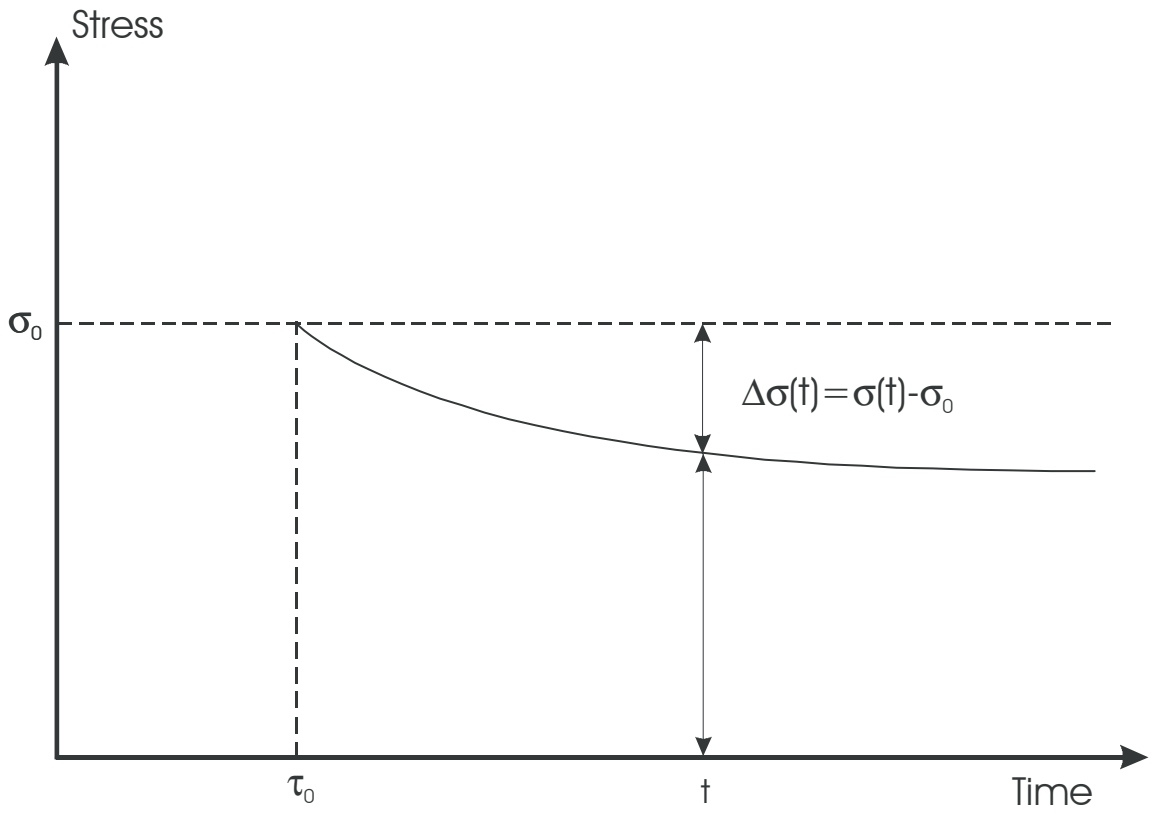

Figure 6-4: Gradually Reducing Stress History

the gradually applied stress increment, $\Delta\sigma(t)$ (instantaneous and creep), and the shrinkage strain:

$$\varepsilon(t)=\frac{\sigma_0}{E_c(\tau_0)}[1+\phi(t,\tau_0)]+\frac{\Delta\sigma(t)}{E_c(\tau_0)}[1+\chi(t,\tau_0)\,\phi(t,\tau_0)]+\varepsilon_{sh}(t) \tag{6-16}$$

$$\varepsilon(t)=\frac{\sigma_0}{E_e(t,\tau_0)}+\frac{\Delta\sigma(t)}{\overline{E}_e(t,\tau_0)}+\varepsilon_{sh}(t) \tag{6-17}$$

Where

$\overline{E}_e(t,\tau_0)$ = Age adjusted modulus

Equation 6-18 is a constitutive relationship which may be used in structural analysis to include the time dependent effects of creep and shrinkage. $\overline{E}_e$ is the age adjusted modulus and is equal to:

$$\overline{E}_e(t,\tau_0) = \frac{E_c(\tau_0)}{1+\chi(t,\tau_0)\,\phi(t,\tau_0)} \tag{6-18}$$

6.1.3 TIME-DEPENDENT ANALYSIS OF COMPOSITE SECTIONS

While the underlying theory is applicable to a much wider range of cross-sectional types, the development here will be limited to those comprised of a concrete deck connected to an underlying steel I-Girder joist. This configuration has a single axis of symmetry and may be subjected to a combination of axial force and bending moment about its axis of symmetry. In addition to the rolled or fabricated steel joist, the cross-section may contain layers of steel reinforcement within the concrete deck.

Throughout this work, compressive forces, stresses and deformations are positive. Positive bending moments produce tensile stresses in the bottom fibers of a horizontal beam, and the corresponding curvature is also positive.

SHORT TERM ANALYSIS

Assuming linear-elastic behavior of both steel and concrete analysis is performed on the transformed section shown in Figure 6-5. Expressions are developed for strain and stress by taking the top fiber of the cross-section as the reference level.

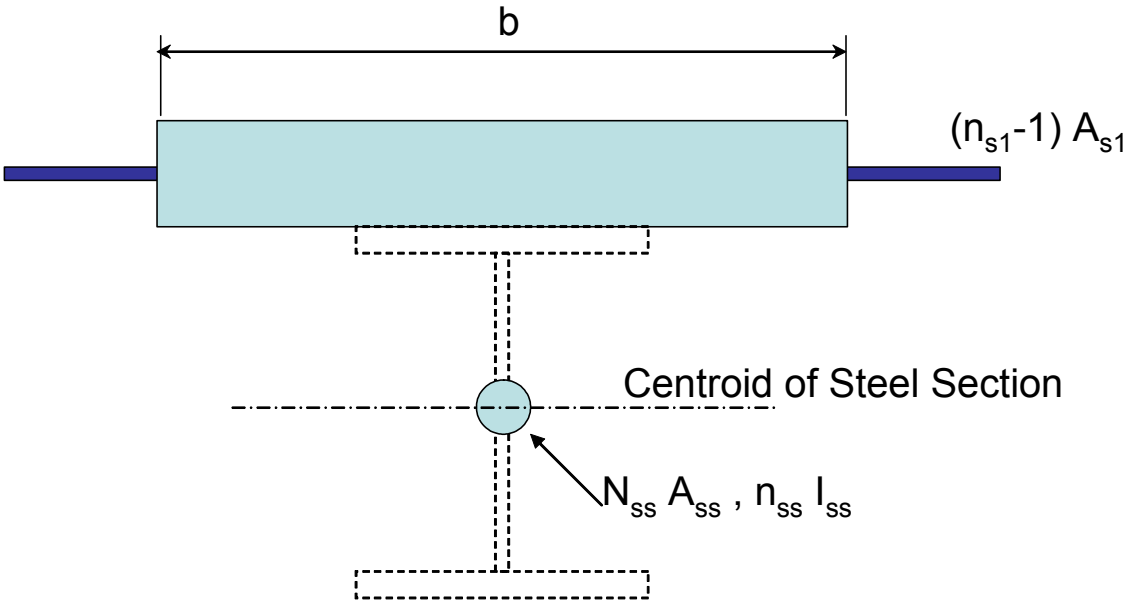

Figure 6-5: Transformed Section

Strain at distance y below top surface is:

$$\varepsilon_i = \varepsilon_{0i} - y\rho_i \tag{6-19}$$

Where

ε_i = Strain at distance y below top surface

ε_{0i} = Short term strain at top fiber

y = Distance below top surface

ρ_i = Initial curvature

The initial stress distribution can be formulated as follows:

$$\sigma_i = E_c\varepsilon_i = E_c\left(\varepsilon_{0i} - y\rho_i\right) \tag{6-20}$$

Where

σ_i = Initial stress at distance y below top surface

Thus:

$$N = \int \sigma_i \, dA = E_c \varepsilon_{0i} A - E_c \rho_i B \tag{6-21}$$

Where

N = Axial Force

A = Area of the transformed section

B = First moment of the transformed area about the top surface

And:

$$M_i = \int \sigma_i \, y \, dA = -E_c \varepsilon_{0i} B + E_c \rho_i I \tag{6-22}$$

Where

M_i = Moment

I = Second moment of the transformed area about the top surface

And:

$$M_i = \begin{cases} M \\ M - N d_N \end{cases} \tag{6-23}$$

Where

M = For pure bending

$M - Nd_N$ = For combined axial force and bending

d_N = Depth to resultant axial force

Solving Equations 6-21 and 6-22 for ε_{0i} and ρ_i yields:

$$\varepsilon_{0i} = \frac{B M_i + I N}{E_c \left(A I - B^2 \right)} \tag{6-24}$$

$$\rho_i = \frac{A M_i + B N}{E_c \left(A I - B^2 \right)} \tag{6-25}$$

For the transformed section shown in Figure 6-5:

$$A = b\,D_c + (n_{s1} - 1)A_{s1} + n_{ss}A_{ss} \tag{6-26}$$

$$B = \frac{1}{2}b\,D_c^2 + (n_{s1} - 1)A_{s1}d_{s1} + n_{ss}A_{ss}d_{ss} \tag{6-27}$$

$$I = \frac{1}{3}b\,D_c^3 + (n_{s1} - 1)A_{s1}d_{s1}^2 + n_{ss}\left(I_{ss} + A_{ss}d_{ss}^2\right) \tag{6-28}$$

Where

b = Effective slab width

D_c = Depth of concrete slab

n_{s1} = Modular ratio for steel reinforcement

A_{s1} = Cross-sectional area of steel reinforcement

d_{s1} = Depth to steel reinforcement

A_{ss} = Cross-sectional area of steel section

d_{ss} = Depth to centroid of steel section from top of slab

I_{ss} = Moment of inertia of steel section

n_{ss} = Modular ratio for steel section

Initial concrete and steel stresses are obtained from strain diagram as follows:

$$\sigma_i = E_c(e_{0i} - y\,\rho_i) \tag{6-29}$$

$$\sigma_{si} = E_s(e_{0i} - y\,\rho_i) \tag{6-30}$$

$$\sigma_{s1i} = E_s(e_{0i} - d_{s1}\,\rho_i) \tag{6-31}$$

Where

σ_{si} = Initial stress of steel section

σ_{s1i} = Initial stress of steel reinforcement

TIME DEPENDENT ANALYSIS USING AGE ADJUSTED EFFECTIVE MODULUS METHOD

The change in strain that occurs on a composite section due to creep and shrinkage in the concrete is shown in Figure 6-6. As the concrete shortens with time, the top fibers of the steel section and the bonded reinforcement

within the slab deck are compressed. There is thus a buildup of compression in the bonded steel and an equal and opposite decrease in compression, or increase in tension, in the concrete slab.

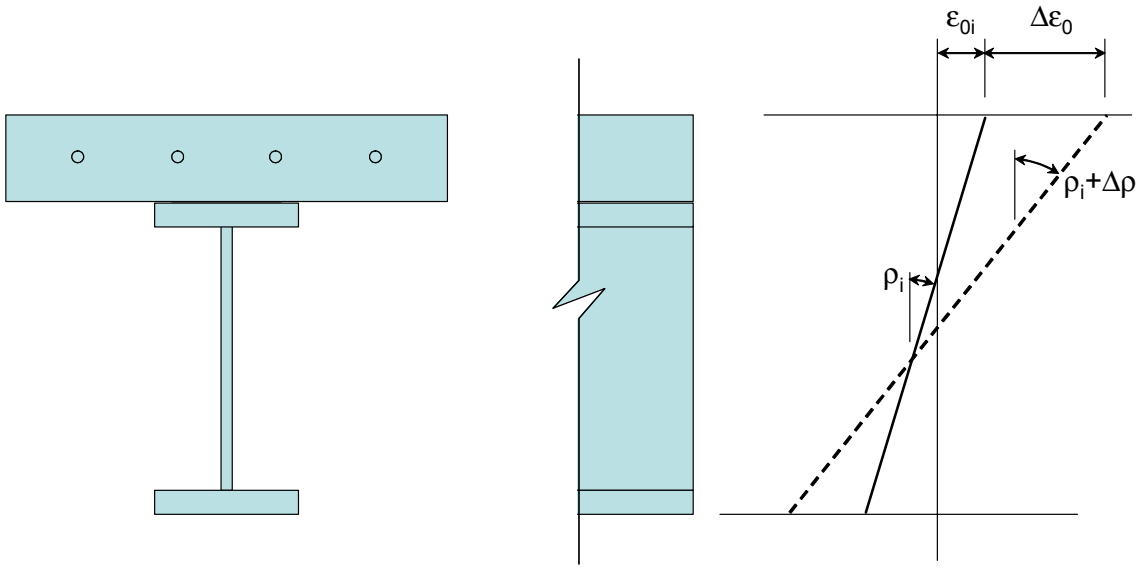

Figure 6-6: Change in strain due to creep and shrinkage

A useful approach to the time-analysis of any cross-section using the AEMM involves the use of a relaxation solution procedure first proposed by Bresler and Selna (1964).

6.1.3.0.1 Relaxation Solution Procedure

During any time interval, the strain distribution is assumed to remain unchanged. If the total strain is held constant, but the creep and shrinkage components change, then the instantaneous component of strain must change by an equal and opposite amount. As the instantaneous strain changes, so does the concrete stress. The stress in the concrete deck is therefore allowed to vary freely due to relaxation. As a result, the internal actions change and equilibrium is not maintained. To restore equilibrium, and axial force ΔN and a bending moment ΔM must be applied to the section.

The increments of top fiber strain and curvature produced by the axial force ΔN and the moment ΔM, gradually applied about the top reference level, may be obtained from the following equations (which are similar to Equations 6-24 and 6-25):

$$\Delta\varepsilon_0 = \frac{\overline{B}_e \Delta M + \bar{I}_e \Delta N}{\overline{E}_e\left(\overline{A}_e \bar{I}_e - \overline{B}_e^2\right)} \tag{6-32}$$

$$\Delta\rho = \frac{\overline{A}_e \Delta M + \overline{B}_e \Delta N}{\overline{E}_e\left(\overline{A}_e \bar{I}_e - \overline{B}_e^2\right)} \tag{6-33}$$

Where

$\Delta\varepsilon_0$ = Change in top fiber strain

ΔM = Restraining moment due to relaxation of the section

ΔN = Restraining axial force due to relaxation of the section

$\overline{A}_e$ = Area of the age-adjusted transformed section

$\overline{B}_e$ = First moment of the area of the age-adjusted transformed section about the top surface

$\bar{I}_e$ = Second moment of the area of the age-adjusted transformed section about the top surface

$\overline{E}_e$ = The age-adjusted effective modulus

6.1.3.0.2 Calculation of ΔN and ΔM

If creep were not restrained in any way, the top fiber strain and curvature would increase to $\phi(t,\tau_0)\varepsilon_{0i}$ and $\phi(t,\tau_0)\rho_i$, respectively, during the time interval $(t-\tau_0)$. The restraint forces required to prevent this deformation are obtained from Equations 6-21 and 6-22 to give:

$$-\Delta N_{creep} = -\overline{E}_e \phi \left(A_c \varepsilon_{0i} - B_c \rho_i \right) \tag{6-34}$$

$$-\Delta M_{creep} = -\overline{E}_e \phi \left(-B_c \varepsilon_{0i} + I_c \rho_i \right) \tag{6-35}$$

Where

ΔN_{creep} = Restraining axial force due to creep

ΔM_{creep} = Restraining moment due to creep

A_c = Area of the concrete section

B_c = First moment of the concrete section

I_c = Second moment of the concrete section

Where A_c, B_c, and I_c refer to the concrete section (ignoring steel) since only the concrete is creeping.

If shrinkage is uniform over the depth of the slab and completely unrestrained, then the curvature is zero, and:

$$\text{Shrinkage induced top fiber strain} = \varepsilon_{sh}\left(t - \tau_0\right) \tag{6-36}$$

The restraining forces required to prevent this uniform deformation are shown in Equations 6-37 and 6-38:

$$-\Delta N_{shrinkage} = -\overline{E}_e \varepsilon_{sh} A_c \tag{6-37}$$

$$-\Delta M_{shrinkage} = +\overline{E}_e \varepsilon_{sh} B_c \tag{6-38}$$

Where

$\Delta M_{shrinkage}$ = Restraining force to prevent deformation

$\Delta N_{shrinkage}$ = Restraining moment to prevent deformation

The total restraining forces are then:

$$-\Delta N_{creep} = -\overline{E}_e\left[\phi\left(A_c\varepsilon_{0i} - B_c\rho_i\right) + \varepsilon_{sh}A_c\right] \quad (6\text{-}39)$$

$$-\Delta M_{creep} = -\overline{E}_e\left[\phi\left(-B_c\varepsilon_{0i} + I_c\rho_i\right) - \varepsilon_{sh}B_c\right] \quad (6\text{-}40)$$

By substituting Equations 6-39 and 6-40 into Equations 6-32 and 6-33 the change of the strain distribution with time is established ($\Delta\varepsilon_0$, $\Delta\rho$, in Figure 6-6).

6.1.3.0.3 Calculation of Stresses

Actual change of concrete stress, $\Delta\sigma$, that occurs during the time interval due to the effects of creep and shrinkage is:

$$\Delta\sigma = \Delta\sigma_{relaxation} + \Delta\sigma_{restore} \quad (6\text{-}41)$$

$$= -\overline{E}_e\left[\phi\left(\varepsilon_{0i} - y\rho_i\right) + \varepsilon_{sh}\right] + \overline{E}_e\left(\Delta\varepsilon_0 - y\,\Delta\rho\right) \quad (6\text{-}42)$$

Where

$\Delta\sigma$ = Actual change in concrete stress

$\Delta\sigma_{relaxation}$ = Loss of stress in concrete at any distance below the top fiber due to relaxation (while the state of strain is initially frozen)

$\Delta\sigma_{restore}$ = Change of stress when ΔN and ΔM are applied to the section to restore equilibrium

Time dependent change of steel stress in the slab reinforcement and at any point on the steel I-section ($y>D_c$) is, respectively:

$$\Delta\sigma_{ss} = E_{ss}\left(\Delta\varepsilon_0 - y\,\Delta\rho\right) \quad (6\text{-}43)$$

$$\Delta\sigma_{s1} = E_{s1}\left(\Delta\varepsilon_0 - d_{s1}\,\Delta\rho\right) \quad (6\text{-}44)$$

Where

$\Delta\sigma_{ss}$ = Time dependent change of stress in slab reinforcement

E_{ss} = Modulus of elasticity of slab reinforcement

$\Delta\sigma_{s1}$ = Time dependent change of stress in steel section

E_{s1} = Modulus of elasticity of steel section

CROSS-SECTION SUBJECTED TO A CONSTANT SUSTAINED MOMENT WITH ZERO AXIAL FORCE (ALTERNATIVE FORMULA)

The total strain at the top fiber is the sum of the short-term and time-dependent values:

$$\varepsilon_0 = \varepsilon_{0i} + \Delta\varepsilon_0 \tag{6-45}$$

Where

ε_0 = Final strain at top fiber

And the final curvature is:

$$\rho = \rho_i + \Delta\rho \tag{6-46}$$

Where

ρ = Final curvature

For a cross-section subjected to a constant sustained moment M, with zero axial force, the curvature-moment relationship at any time is linear and may be written as:

$$\rho = \alpha + B\,M \tag{6-47}$$

By substituting Equations 6-24 and 6-25 into Equations 6-39 and 6-40 and using the resulting expressions for ΔN and ΔM in Equation 6-33, the following expressions for the constants α and β in Equation 6-47 are obtained:

$$\alpha = \varepsilon_{sh}\frac{\overline{B}_e A_c - \overline{A}_e B_c}{\overline{A}_e \overline{I}_e - \overline{B}_e^2} \tag{6-48}$$

$$\beta = \frac{1}{E_c\left(A\,I - B^2\right)}\left[A + \phi\frac{A_c B\overline{B}_e - B_c A\overline{B}_e - B_c B\overline{A}_e + I_c A\overline{A}_e}{\left(\overline{A}_e \overline{I}_e - \overline{B}_e^2\right)}\right] \tag{6-49}$$

For short-term loading

$$\alpha = 0 \qquad \beta = \frac{A}{E_c\left(A\,I - B^2\right)} \tag{6-50}$$

6.1.4 CONTINUOUS CONCRETE-STEEL GIRDER

In a statically indeterminate beam, such as a continuous composite beam, creep and shrinkage cause a gradual redistribution of moments throughout any period of sustained load. Therefore, in addition to the initial moment M, each cross-section is subjected to a time-dependent increment of moment δM (not to be confused with ΔM), and Equation 6-47 becomes:

$$\rho(x) = \alpha + \beta\, M(x) + \gamma\, \delta M(x) \tag{6-51}$$

Where

ρ(x) = Curvature at distance x from end of girder

δM(x) = Time-dependent increment of moment at distance x

x = Distance from end of girder

The increment of curvature δρ caused by δM is expressed as γ·δM and the constant γ is obtained from Equation 6-33:

$$\delta\rho = \frac{\overline{A}_e}{\overline{E}_e\left(\overline{A}_e\overline{I}_e - \overline{B}_e^2\right)}\delta M \tag{6-52}$$

Where

δρ = Increment of curvature caused by δM

Thus:

$$\gamma = \frac{\overline{A}_e}{\overline{E}_e\left(\overline{A}_e\overline{I}_e - \overline{B}_e^2\right)} \tag{6-53}$$

Where

γ = A constant

The increment of top fiber strain associated with δM is obtained from Equations 6-32 and 6-53:

$$\delta\varepsilon_0 = \frac{\overline{B}_e \gamma}{\overline{A}_e} \delta M \tag{6-54}$$

Where

$\delta\varepsilon_0$ = Increment of top fiber strain associated with δM

The final top strain is found by:

$$\varepsilon_0 = \varepsilon_{0i} + \Delta\varepsilon_0 + \delta\varepsilon_0 \tag{6-55}$$

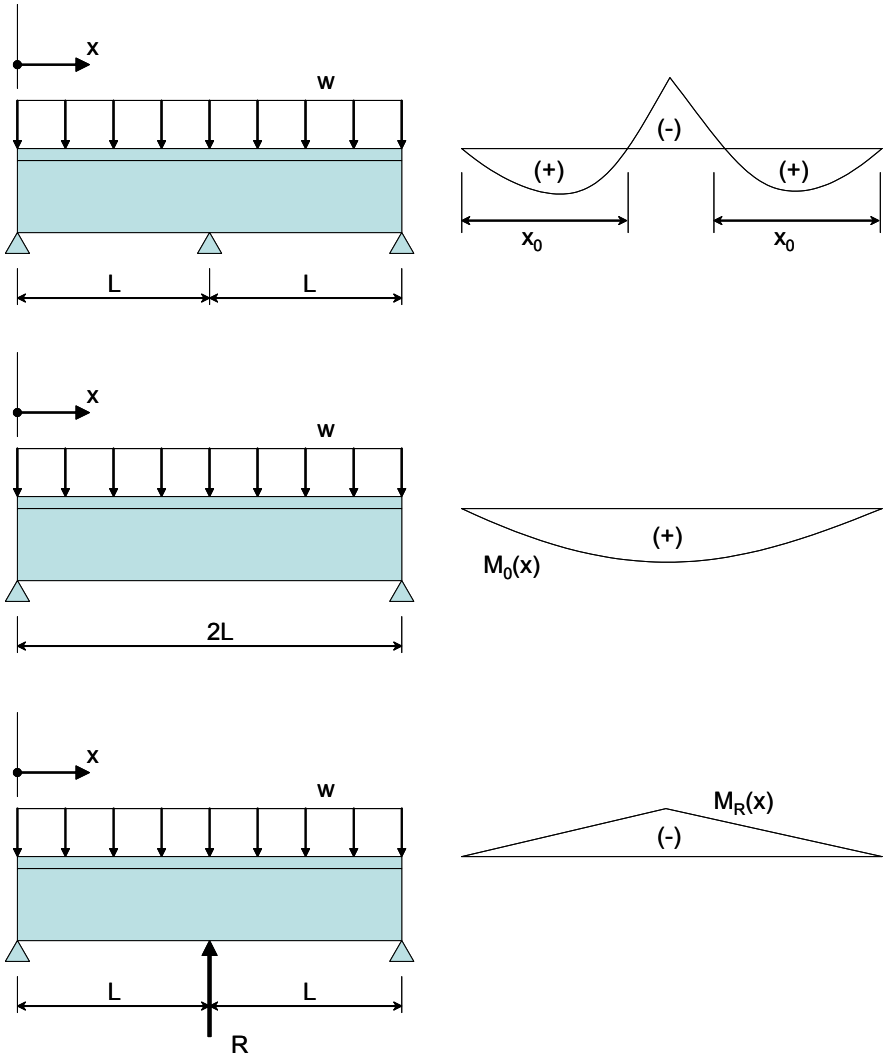

Figure 6-7: Two-span, one-fold indeterminate beam

LONGITUDINAL MOMENT ANALYSIS (UNCRACKED SECTION)

The distribution of moments along a continuous beam and the deflection at any point may be obtained using the principle of virtual work.

Consider the uniformly loaded, one-fold indeterminate beam shown in Figure 6-7. The reaction at the internal support is selected as the redundant force, and after releasing the internal support, the statically determinate primary structure and the primary bending moment $M_0(x)$ caused by the external load w are shown. The redundant force R and the corresponding redundant moment $M_r(x)$ are also shown. The total moment diagram is obtained by adding $M_0(x)$ and $M_r(x)$, with the moment changing sign at some distance $x=x_0$ from the external support.

Under uniformly distributed load w, the total moment M(x) in the left span is (when x=L):

$$M(x) = M_0(x) + M_r(x) = wLx - w\frac{x^2}{2} - R\frac{x}{2} \qquad (6\text{-}56)$$

Where

$M(x)$ = Total moment at distance x from end of girder

$M_o(x)$ = Primary bending moment at distance x caused by distributed load w

$M_r(x)$ = Bending moment at distance x caused by redundant force R

R = Redundant reaction

w = Uniform load

L = Span length

When $x<x_0$ the member is subjected to sagging bending, and where $x_0<x\leq L$, the member is in hogging bending. When $x=x_0$, $M(x_0)=0$ and from Equation 6-56:

$$x_0 = 2L - \frac{R}{w} \qquad (6\text{-}57)$$

If a unit upward vertical force is applied at the primary beam at the position of central support (x=L), then the resulting moment diagram $M_{bar}(x)$ has the same shape as shown in Figure 6-7c, and for x=L:

$$\overline{M}(x) = \frac{-x}{2} \tag{6-58}$$

Where

$\overline{M}(x)$ = Moment at distance x due to unit upward force at location of central support

Using the principle of virtual work, the deflection of the real beam at the position of the internal support (which is zero) is given by:

$$u(L) = 2\int_0^L \rho(x)\overline{M}(x)dx = 0 \tag{6-59}$$

Where

u(L) = Deflection at location of center support

Where $\rho(x)$ is given by Equation 6-51.

6.1.4.0.1 Steel Girder Composed of different segments

If the steel girder is composed of different segments with different section properties then the values of α, β, and γ in Equation 6-51, which depend on section properties, are different for each segment.

Let α_i, β_i, and γ_i represent the values corresponding to segment i of the girder (i=1,2,…,n).

To determine the short-term response, immediately after the application of the load w, Equation 6-51 reduces to:

$$\rho(x) = \beta M(x) \tag{6-60}$$

And Equation 6-59 becomes:

$$u(L) = -\int_0^L x\,\beta\left(wLx - w\frac{x^2}{2} - R_0\frac{x}{2}\right)dx = 0 \tag{6-61}$$

Where

R_0 = Redundant reaction due to short-term loading

The integral can be divided as:

$$\sum_{i=1}^{n}\int_{x_{i-1}}^{x_i} x\,\beta_i\left(wLx - w\frac{x^2}{2} - R_0\frac{x}{2}\right)dx \tag{6-62}$$

From which, upon integration and simplification:

$$R_0 = \frac{\sum_{i=1}^{n} w\beta_i\left\{\left(L\frac{x_i^3}{3} - \frac{x_i^4}{8}\right) - \left(L\frac{x_{i-1}^3}{3} - \frac{x_{i-1}^4}{8}\right)\right\}}{\sum_{i=1}^{n}\beta_i\left(\frac{x_i^3}{6} - \frac{x_{i-1}^3}{6}\right)} \tag{6-63}$$

During a period of sustained load, the redundant reaction changes by an amount δR, and therefore the moment in the left span changes by:

$$\delta M(x) = -\frac{x}{2}\delta R \tag{6-64}$$

Where

δR = Change in redundant reaction during sustained load

The curvature on each section is given by Equation 6-51, in which the moment M is the value immediately after the short-term analysis and is given by Equation 6-56:

$$M(x) = wLx - w\frac{x^2}{2} - R_0\frac{x}{2} \tag{6-65}$$

Expanding Equation 6-59 gives:

$$\sum_{i=1}^{n}\int_{x_{i-1}}^{x_i} x\left\{\alpha_i+\beta_i\left(wLx-w\frac{x^2}{2}-R_0\frac{x}{2}\right)+\gamma_i\left(-\frac{x}{2}\delta R\right)\right\}dx \tag{6-66}$$

Which reduces to:

$$\delta R=\frac{\sum_{i=1}^{n}\alpha_i\left(\frac{x_i^2}{2}-\frac{x_{i-1}^2}{2}\right)}{\sum_{i=1}^{n}\gamma_i\left(\frac{x_i^3}{6}-\frac{x_{i-1}^3}{6}\right)} \tag{6-67}$$

The long-term value of the redundant is, therefore:

$$R=R_0+\delta R \tag{6-68}$$

The time dependent change of the top fiber strain, curvature, concrete stresses, and steel stresses on any cross-section may now be determined.

FINAL STRAINS AND STRESSES

The increment of top fiber strain associated with δM is obtained from Equation 6-54, and the final top fiber strain is found by adding $\delta\varepsilon_0$ to Equation 6-45:

$$\varepsilon_0=\varepsilon_{0i}+\Delta\varepsilon_0+\delta\varepsilon_0 \tag{6-69}$$

The final concrete and steel stresses are calculated by adding the increments $\delta\sigma_c$, $\delta\sigma_s$, and $\delta\sigma_{s1}$ to Equations [6-29 + 6-42], [6-30 + 6-43], and [6-31 + 6-44] respectively, where:

$$\delta\sigma_c=E_c\left(\delta\varepsilon_0-y\,\delta\rho\right),\quad y\le D_c \tag{6-70}$$

$$\delta\sigma_s=E_s\left(\delta\varepsilon_0-y\,\delta\rho\right),\quad y>D_c \tag{6-71}$$

$$\delta\sigma_{s1} = E_s\left(\delta\varepsilon_0 - d_{s1}\,\delta\rho\right) \tag{6-72}$$

Where

$\delta\sigma_c$ = Incremental stress in concrete

$\delta\sigma_s$ = Incremental stress in slab reinforcement

$\delta\sigma_{s1}$ = Incremental stress in steel girder

DEFLECTION CALCULATIONS

At any time after loading, when the redundant R_0 and δR have been determined, the variation of displacements, u(x), is obtained by integrating the curvature twice. The curvature, $\rho(x)$, at any point is obtained from the moments using Equation 6-51. Performing the integrations, and noting that:

$$\left.\frac{du(x)}{dx}\right|_{x=L} = \theta(x)\big|_{x=L} = 0 \tag{6-73}$$

Produces (6-74)

$$u(x) = \int_0^x \int_0^x \rho(x)dx\,dx - \int_0^x \int_0^L \rho(x)dx\,dx \tag{6-75}$$

The integration can be carried out numerically using Simpson's rule with each span length divided into $2 \cdot n$ intervals.

6.2 PROGRAM DEVELOPMENT

The program developed is capable of determining the deflection profile versus time of a balanced two span concrete slab on steel girder bridge system. Unlimited section changes are permitted along the length of the bridge, however they are assumed to be symmetric about the center support location. Shrinkage is accounted for in the program by providing a shrinkage strain history. This can be an approximate one based on empirical models, or experimental shrinkage data can be entered as well. Creep is handled in a similar manner, where the creep coefficient time history is provided along with the loading history.

6.2.1 COMPUTER PROGRAM

A computer program, 2-span.for, was developed in Fortran to analyze the short term and time-dependent behavior of a continuous two equal span steel-reinforced concrete bridge. The age adjusted effective modulus method AEMM is used for the analysis. The program calculates strains, curvature, and stresses in the continuous composite beam due to time dependent effects.

The values of shrinkage strain (obtained from controlled specimens), creep coefficient, and aging coefficient are first read for a particular time. Values regarding the beam dimensions, externally applied loads including dead weight of the concrete slab, section properties and elastic moduli for concrete and steel are read in the next step.

Values of R_0 and δR are calculated from Equations 6-63 and 6-67 from which M(x) and $\delta M(x)$ are calculated from Equations 6-65 and 6-64 respectively, along the length of span at different increments dx. The incremental value dx is defined by the user. Having M(x) and $\delta M(x)$ calculated the curvature r(x) is computed from Equation 6-51 along the beam span.

The Simpson rule of integration is then used twice to calculate the variation of displacements v(x) along the length of the span Equation 6-75.

The process outlined above predicts the deflection of the beam at the particular time under consideration. Top fiber concrete strain, and stresses in concrete, reinforcing steel and steel section are also computed based on Equations 6-29, 6-30, 6-31, 6-42, 6-43, 6-44, 6-55, 6-70, 6-71, and 6-72, and reported in an output file.

To predict the behavior of the beam at another time the procedure may be repeated with new values of shrinkage strain, creep coefficient and coefficient corresponding to that particular date.

DATA INPUT

6.2.1.0.1 Bridge Geometry

Information about bridge geometry is provided through the input file named in1.dt. An example input file is shown in Figure 6-8.

```
2883.      ; L         , span length
5          ; NSEG      , no. of segments
10.        ; DX        , increment of x
0.0        ; wo        , uniformly distributed load on the beam
0.0        ; N         , mag. of the applied axial force
114.8      ; B         , flange width
0.0        ; BW        , web width
7.0        ; T         , flange thickness
7.0        ; D         , overall depth of concrete
2          ; N1        , no. of layers of non-prestressed
2.0        ; AS1       , steel area of non-prestressed in layer 1
2.5        ; DS1       , depth of steel in layer 1
3.1        ; AS2       , steel area of non-prestressed in layer 2
5.5        ; DS2       , depth of steel in layer 2
4.58e+06   ; EC        , elastic modulus for concrete
29.e+06    ; ES        , elastic modulus for reinforcing steel
29.e+06    ; ES        , elastic modulus for steel section
78.        ; SA        , segment steel area              (repeat for each segment ****
70895.     ; SI        , segment steel moment of inertia  (repeat for each segment ****
46.81      ; SD        , segment depth of steel centroid  (repeat for each segment ****
74.0       ; D1        , segment depth of steel section   (repeat for each segment ****
0.0        ; XA        , segment start coordinate         (repeat for each segment ****
590.       ; XB        , segment end coordinate           (repeat for each segment ****
99.0       ;           , Start Segment 2
99544.
47.84
75.
590.
1522.
84.        ;           , Start Segment 3
77456.
49.25
74.25
1522.
2118.
130.5      ;           , Start Segment 4
139063.
44.5
75.
2118.
2585.
190.5      ;           , Start Segment 5
225708.
45.5
77.
2585.
2883.
```

Figure 6-8: Example Geometry Input File in1.dt

The material time dependent parameters are given in the file in2.dt. This first line indicates the number of days, nd, for which data is provided in the

file. The remaining of the file is nd sets of data indicating the day number, creep coefficient, aging coefficient and shrinkage strain for that each day. An abbreviated example is shown in Figure 6-9.

```
33          Number of Days
0           Day
0.0         Creep Coefficient
0.0         aging Coefficient
0.0e-6      Shrinkage Strain
1           Day
0.182
.8
93.e-6
2           Day
0.263
.8
133.e-6
```

Figure 6-9: Example Geometry Input File in1.dt

6.2.2 RESULTS OUTPUT

Results are available in several forms depending on the analyst's needs. The first output file, out.dt, gives the resulting deflection. Each row corresponds to a day specified in the input file in2.dt while each column corresponds to a location along the bridge as specified by the variable dx in the input file, in1.dt.

The second output file, c1.out, contains tabular data for each day listing the final top strain and curvature along with the concrete stresses at the top and bottom of the slab.

The final output file, c2.out, contains detailed verbose results which would normally only be used for verification and program debugging.

It should be noted that the instantaneous deflection due to the distributed loading is added to the results for all time regardless of when the load was assumed to be applied in the determination of the creep coefficient, however, additional deflections due to creep are only dependent on the supplied creep coefficient and therefore do not arise unless the creep coefficient is greater than zero. One can separate the effects by setting appropriate factors equal to zero depending on the results desired.

6.3 VERIFICATION

Data obtained from the monitoring of the Dodge Street Bridge over I-480 was used to verify the analysis techniques and accompanying program.

6.3.1 BRIDGE DESCRIPTION

The Dodge Street Bridge over I-480 is a continuous bridge with two equal spans. The bridge is composed of eight identical welded plate steel girders and a reinforced concrete deck. Each span is 72090 mm with girders spaced at 2883 mm center to center.

Each girder is symmetric about the center support and composed of different segments with different plate width and thicknesses shown in Figure 6-10. The reinforced concrete deck is 7" thick with two layers of reinforcement. The top layer includes #4 bars at 12" spacing while the bottom layer includes #5 bars at 12" spacing.

For the purpose of deflection analysis, an interior girder was isolated with the appropriate concrete slab as shown in Figure 6-11. Calculation of section properties for each segment of the steel-girder, concrete slab, and modulus of elasticity of concrete at age 28-day are presented in the following section.

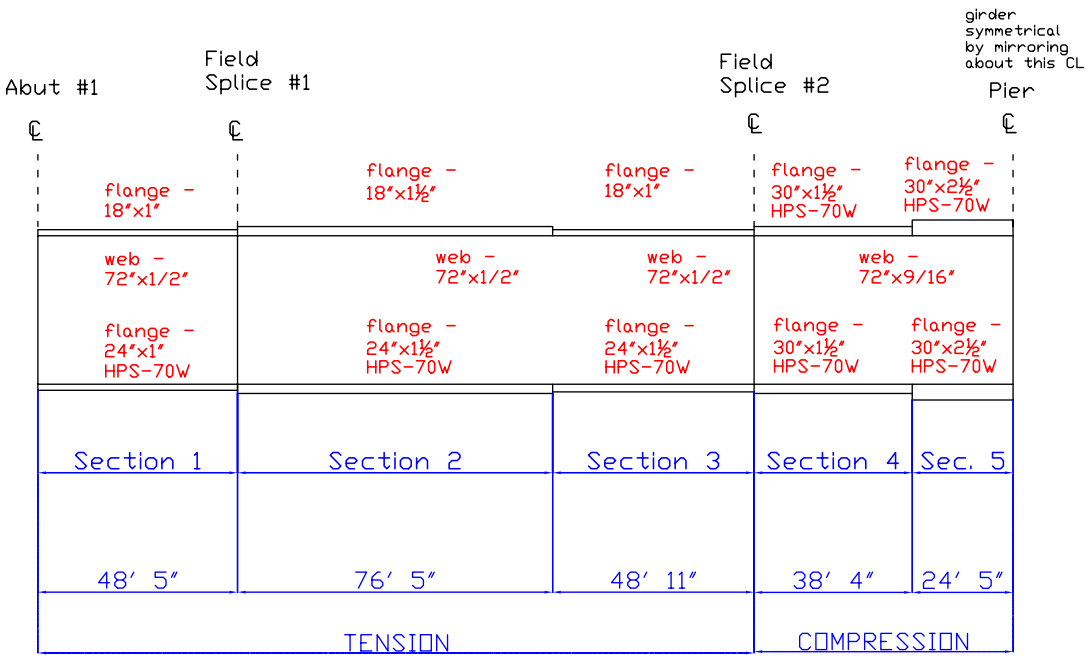

Figure 6-10: Girder elevation

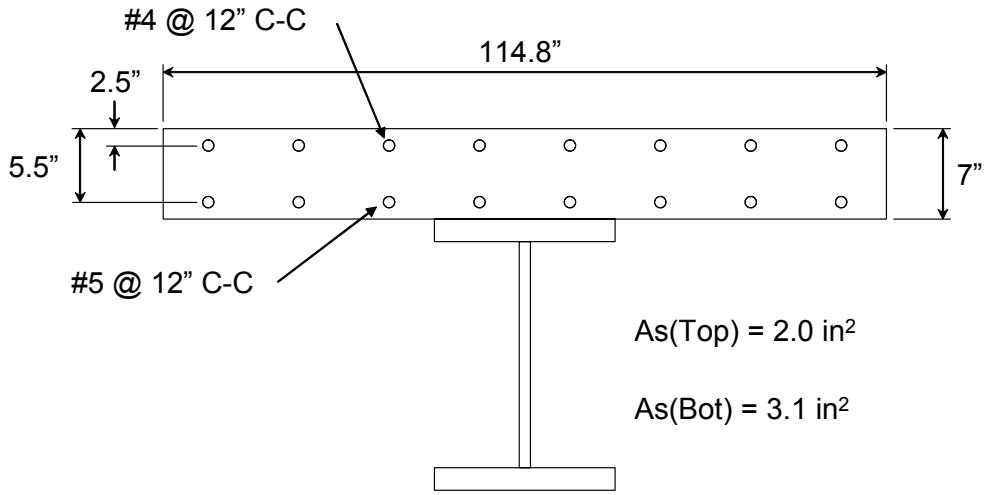

Figure 6-11: Interior girder cross section (Not to Scale)

6.3.2 Section Properties

The section properties of the steel girder such as the area of steel, centroid of section and moment of inertia about centroidal axis of the section are listed in Table 6-1.

The value of f'_c was determined by conducting compression tests on two cylinders cast at the time of the first pour. The specimens were 28 days

Sec	Start (mm)	Length (mm)	Asteel (in^2)	Yc From Bot (in)	I In^4
1	0	14750	78	34.19	70895
2	14750	8400	99	34.16	99544
3	23150	14900	99	34.16	99544
4	38050	14900	84	32	77456
5	52950	11690	130.5	37.5	139063
6	64640	7450	190.5	38.5	225708

Table 6-1: Steel girder section properties

old when the test was performed. The average compressive strength of the 28 day cylinders was 6,478 psi. The resulting predicted modulus of elasticity was calculated to be 4,580 ksi. This value was used throughout the analysis. The elastic modulus of steel was assumed to be equal to 29,000 ksi.

The dead loads applied to the steel girder are 69.75 pounds per linear inch due to the slab and 15.83 pounds per linear inch due to the barriers per girder.

6.3.3 Control Specimens

The concrete deck was cast at two different times. First, the positive moment regions from the two ends were cast on 10/20/1999. The negative moment region was then cast eight days later on 10/28/1999.

Several control specimens for the study of unrestrained shrinkage and creep strains were cast from different trucks at the time of each pour. The following provide a description of the curing process and the shrinkage and creep strain data obtained from these specimens.

Demac points were placed on the surface of all specimens for the purpose of measurements. Demac points are fixed reference points the distance between which is measured using a special caliper with 12" base gage length to monitor deformations.

FIRST POUR

Three of the prism shaped specimens, referred to as 1, 2, and 3, were placed in a moist room for a period of six days. Three others, referred to as specimens 4, 5, and 6, remained in the structural laboratory at room temperature.

Initial readings for the air cured specimens were taken on 10/22/1999, two days after casting. The moist cured specimens' initial readings were taken the day they the specimens were removed from the moist room. The day of initial reading is referred to as day zero in subsequent analyses. Readings were taken each day for the first month, then each week for the next five weeks, then finally, once a month for the next six months.

Variations of unrestrained shrinkage strains versus time for these control specimens are shown in Figure 6-12. Figures 6-13 and 6-14 show the average unrestrained shrinkage strains for the moist cured and air cured specimens respectively.

A number of control specimen cylinders were also cast from the concrete mix of the first pour. Three of these cylinders were used to determine the change of creep strains versus time. These specimens are referred to as CR1, CR2, and CR3. Two other cylinders, referred to as SH1 and SH2 served as companion unloaded specimens for shrinkage measurements. No measurements were taken from these specimens until 10/29/1999, 10 days after casting. Figure 6-15 represents the change in shrinkage strain with respect to time for SH1 and SH2.

To obtain the creep behavior of the concrete mix, specimens CR1, CR2, and CR3 were subjected to constant sustained loads at age 28 days. Two of the hydraulic rams providing the sustained loads leaked in the case of CR1 and CR2. These were fixed and the loads were adjusted accordingly. A continuous reading, however, was obtained for CR3. Figure 6-16 shows the behavior of creep and shrinkage versus time for CR3. The average shrink-

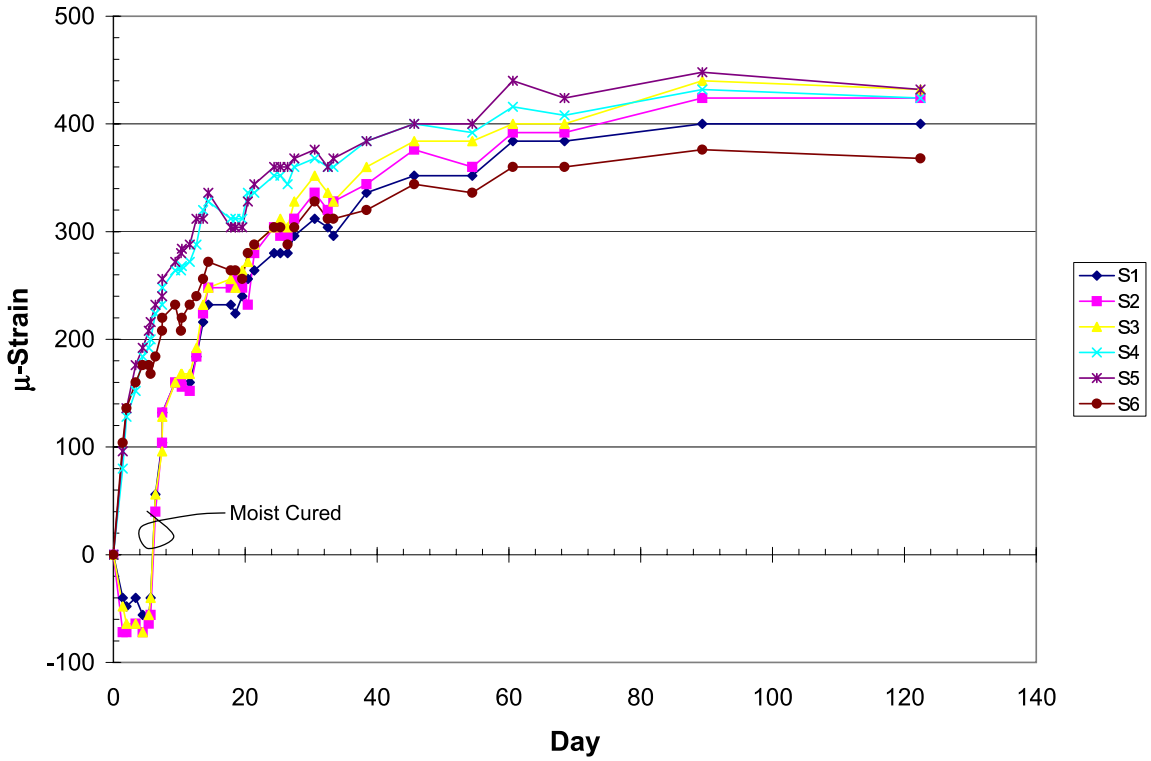

Figure 6-12: Concrete strain components under sustained stress

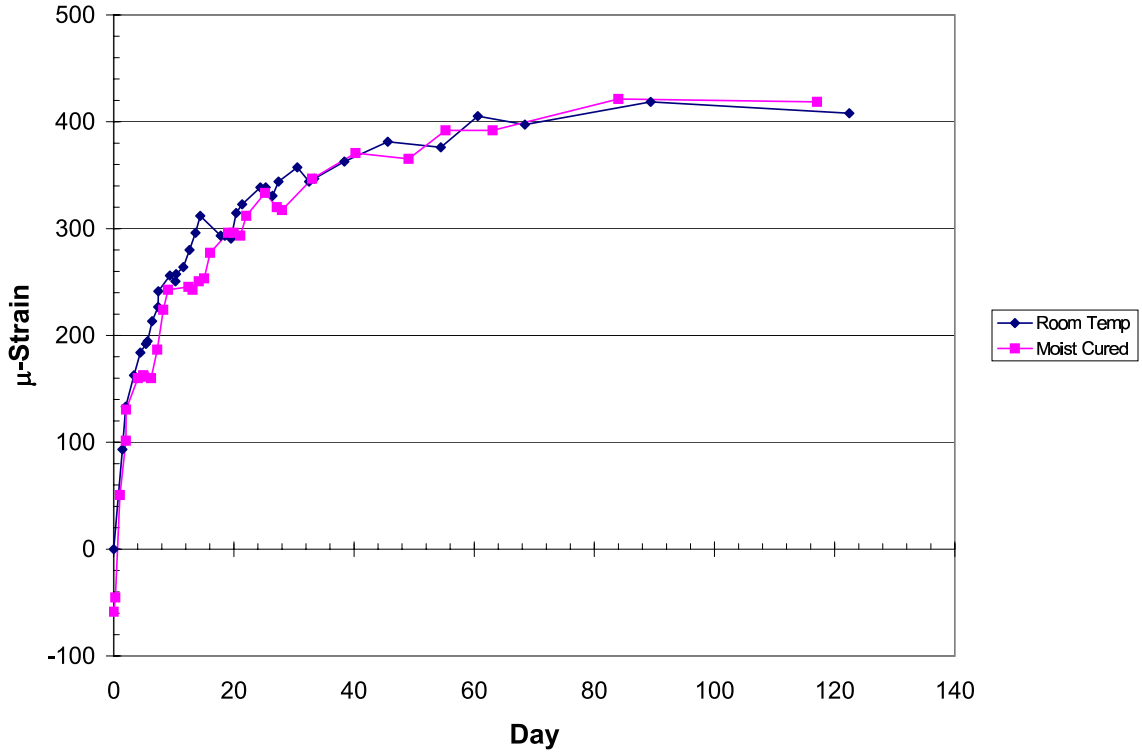

Figure 6-13: Average shrinkage strain - moist cured specimens

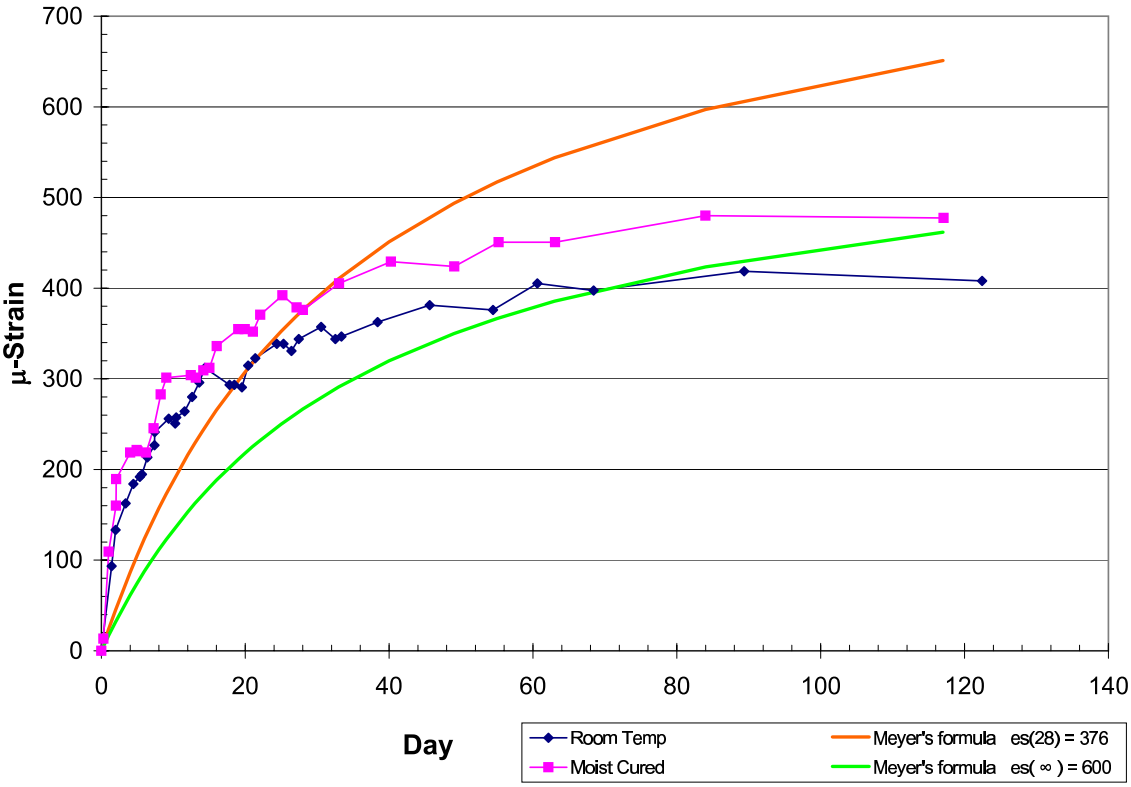

Figure 6-14: Average shrinkage strain - air cured specimens

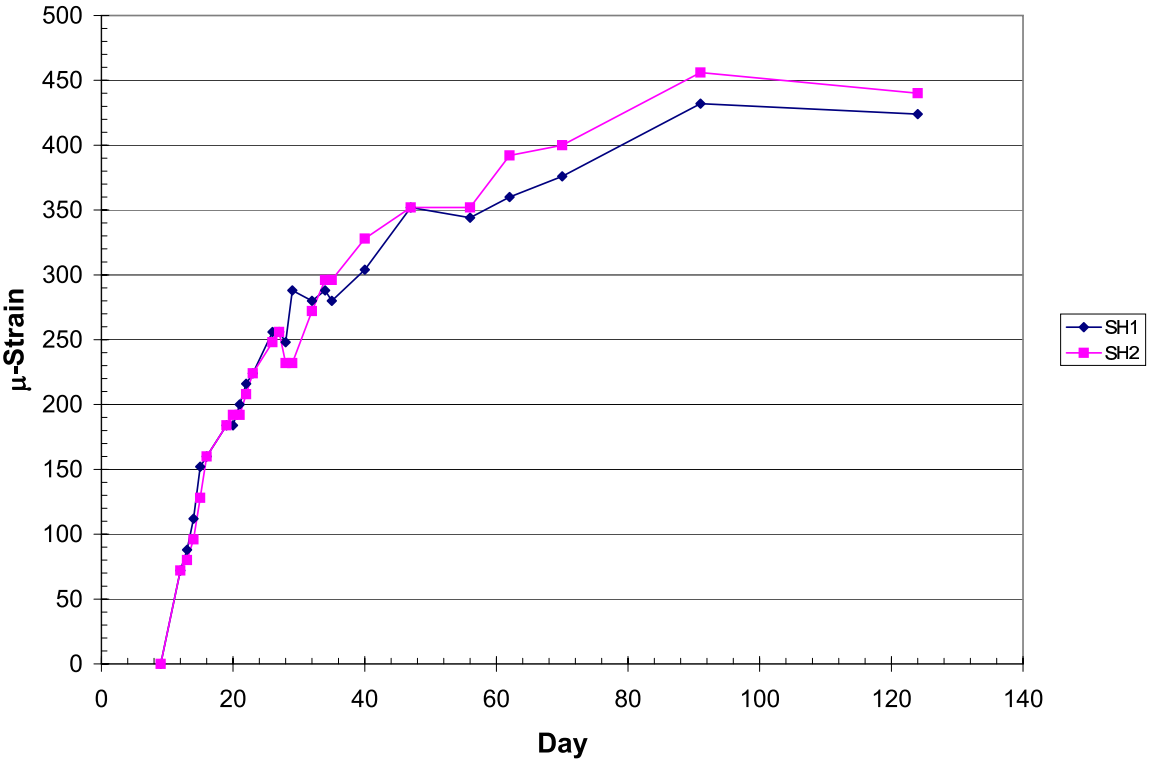

Figure 6-15: Companion Shrinkage Specimen Results

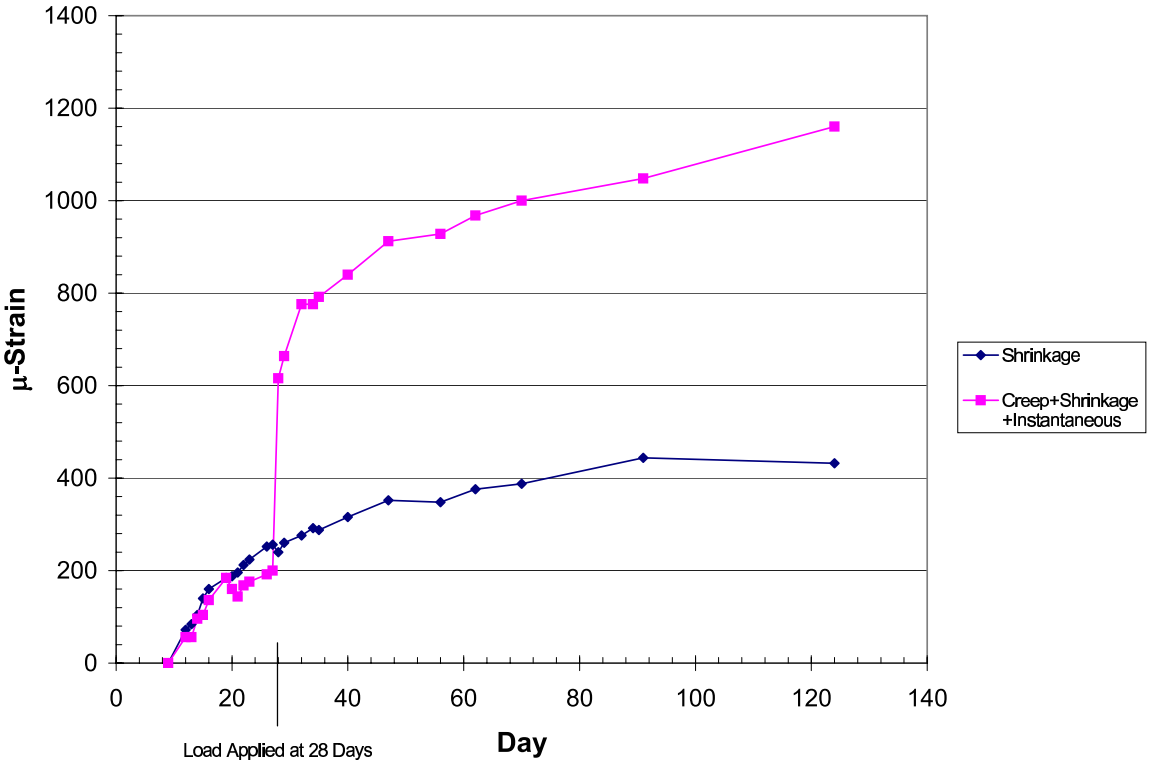

Figure 6-16: Control specimen shrinkage strain plot

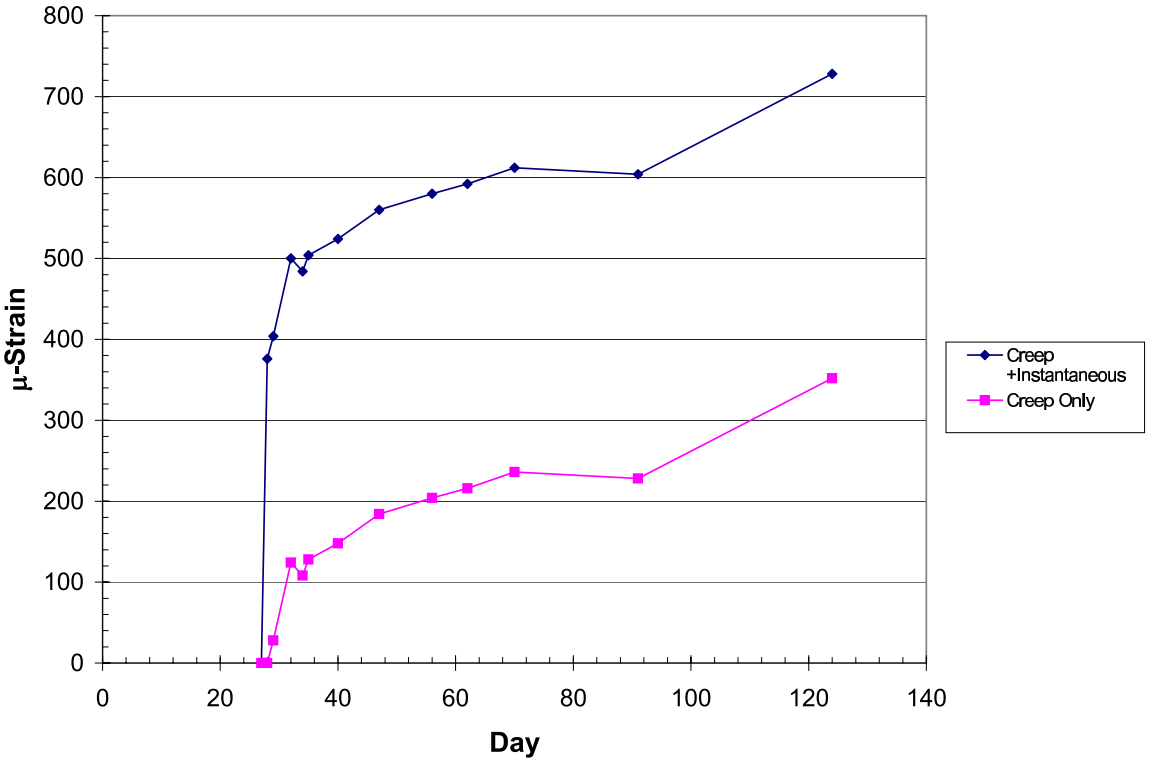

Figure 6-17: Average shrinkage strain plot

age strain of the unloaded companion specimens, SH1 and SH2, are also shown in this figure. Figure 6-17 shows the creep strain of CR3 versus time, which was obtained by subtracting the average shrinkage of the unloaded companion specimens from the CR3 curve.

The creep data obtained from loading specimen CR3 were compared with the empirical equation for creep coefficient (Equation 6-8) suggested by ACI presented in Section 6.1.1. Based on the measurements taken from specimen CR3 at τ=28:

$$\phi(\tau+28,\tau)=\phi(56,28)=0.543 \tag{6-76}$$

With this value for ϕ(56,28), the creep coefficient was calculated versus time using Equation 6-8. The predicted values of creep coefficients and those obtained from test specimen are shown graphically in Figure 6-18.

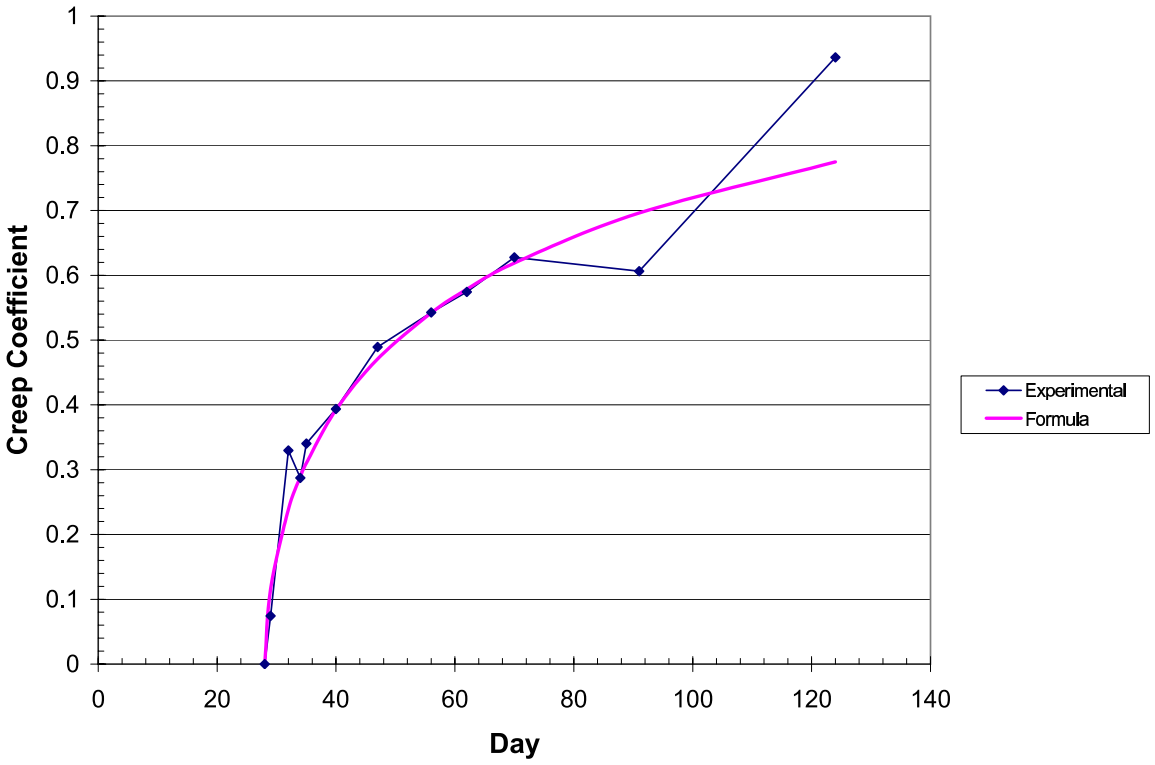

Figure 6-18: Predicted values of creep coefficients

SECOND POUR

Several specimens were made from the concrete mix used to cast the negative moment region of the deck on 10/28/99.

Four prisms, referred to as specimens 7, 8, 9, and 10 were placed in the moist room on 10/29/99 and removed from the moist room on 11/1/99. The starting shrinkage date, day zero, for these specimens was taken as 11/1/99 after been removed from the moist room. Figure 6-19 shows the variations of shrinkage strains with respect to time. The average shrinkage strains of these four specimens are shown in Figure 6-20.

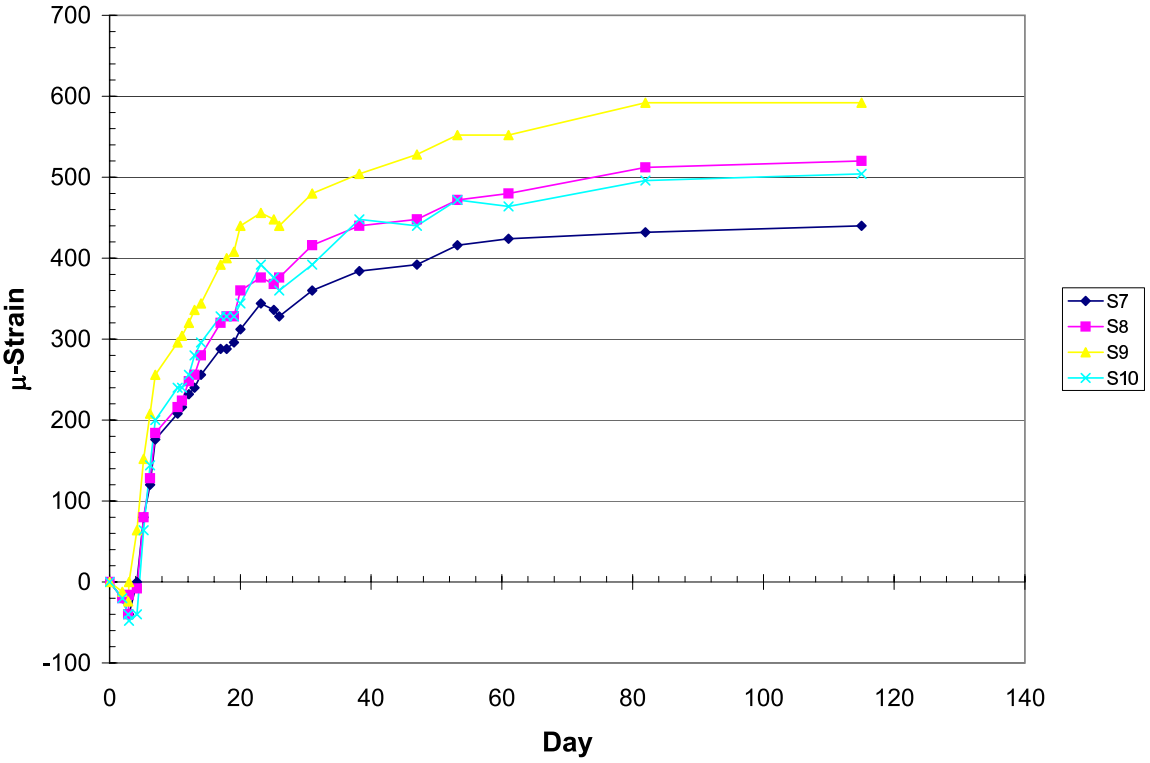

Figure 6-19: Shrinkage strains over time

The shrinkage strain data obtained from measurements taken from control specimens and presented in the previous sections construct the basis for prediction of the bridge deflection due to the time-dependent effects of creep and shrinkage.

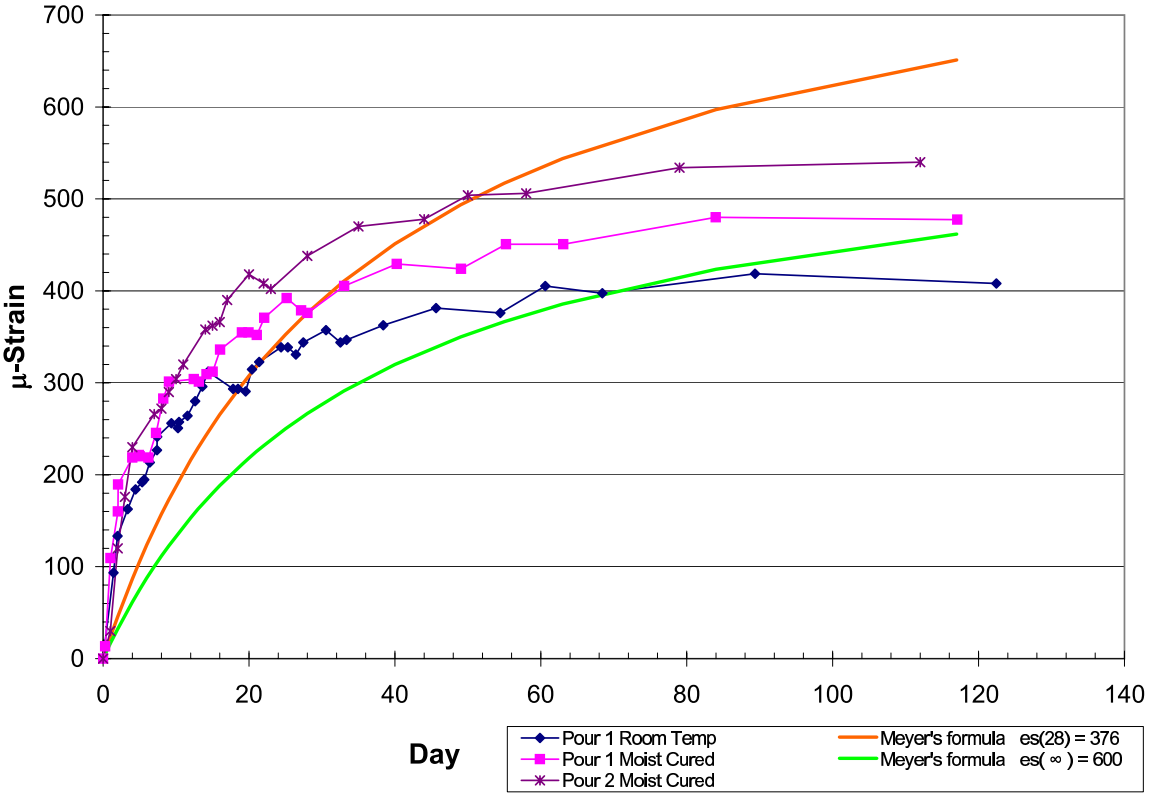

Figure 6-20: Comparison of results with Meyer's formula

6.3.4 Deflection Prediction

To predict the deflection of the Dodge Street bridge due to time dependent effects of shrinkage and creep, a computer program was prepared based on the theory developed in Section 6.1. The details and the performance of the program is presented in the following section.

Samples of input and output files have been included for the case of the Dodge street bridge in the following section.

The shrinkage, creep, and aging data utilized in this analysis are as follows:

- Input shrinkage data are average unrestrained shrinkage strains obtained from the control specimens from the positive region pour.
- Creep coefficients were estimated from the ACI empirical model Equation 6-5 assuming the concrete age at loading was 20 days. No other adjustments were made for humidity, slump, or other

such factors. The experimental results from test specimens, Figure 6-18, could not be used since the age at loading is 28 days for that sample.

- A constant value of 0.8 was assumed for the aging coefficient throughout.

The zero point for predicting the deflections due to creep and shrinkage was taken as the end of the positive region pour. The negative region pour occurred eight days later and the first round of barrier placement began seven days after this with a second round of barriers placed yet another seven days later. To simplify the analysis, the entire pour was assumed to occur at the zero point and all the load was assumed to be placed twenty days after the pour. Figure 6-21 shows the results of this analysis with the various deflection sources identified. Of particular note is the curve labeled "All" as this is the final predicted deflection including the effects of creep, shrinkage, and elastic components.

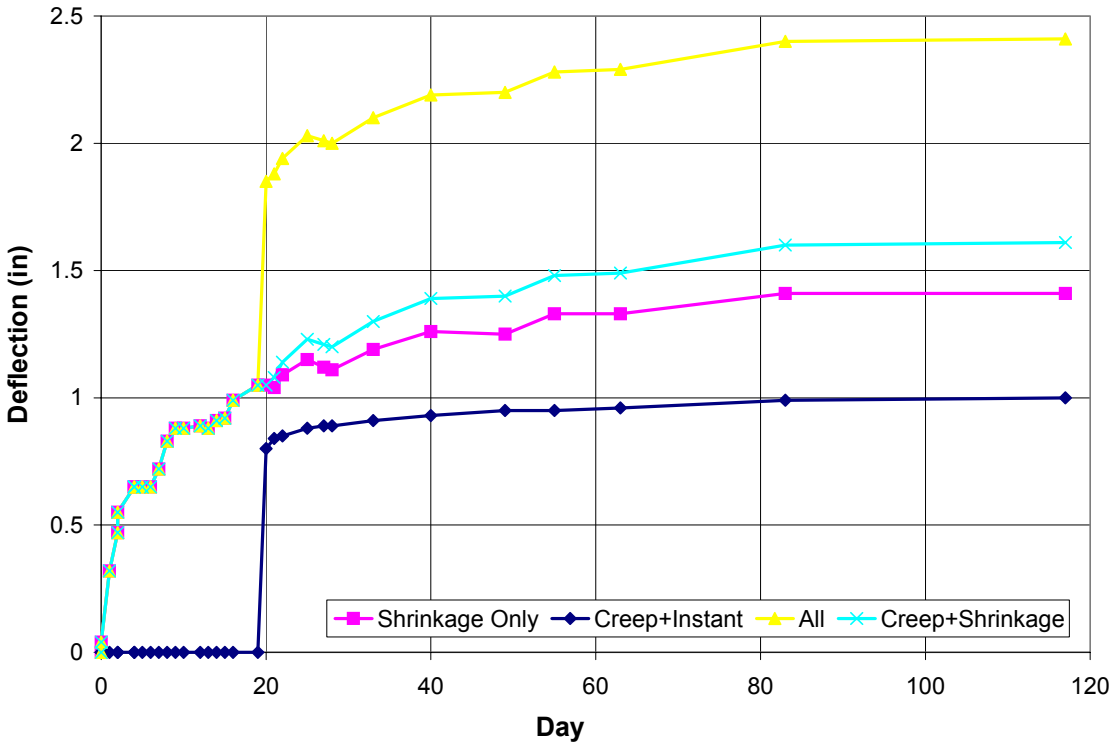

Figure 6-21: Comparison of calculated deflection and actual deflection

The following Figure 6-22 compares the total deflections due to instantaneous, creep and shrinkage effects against the experimental results obtained from the Dodge Street Bridge.

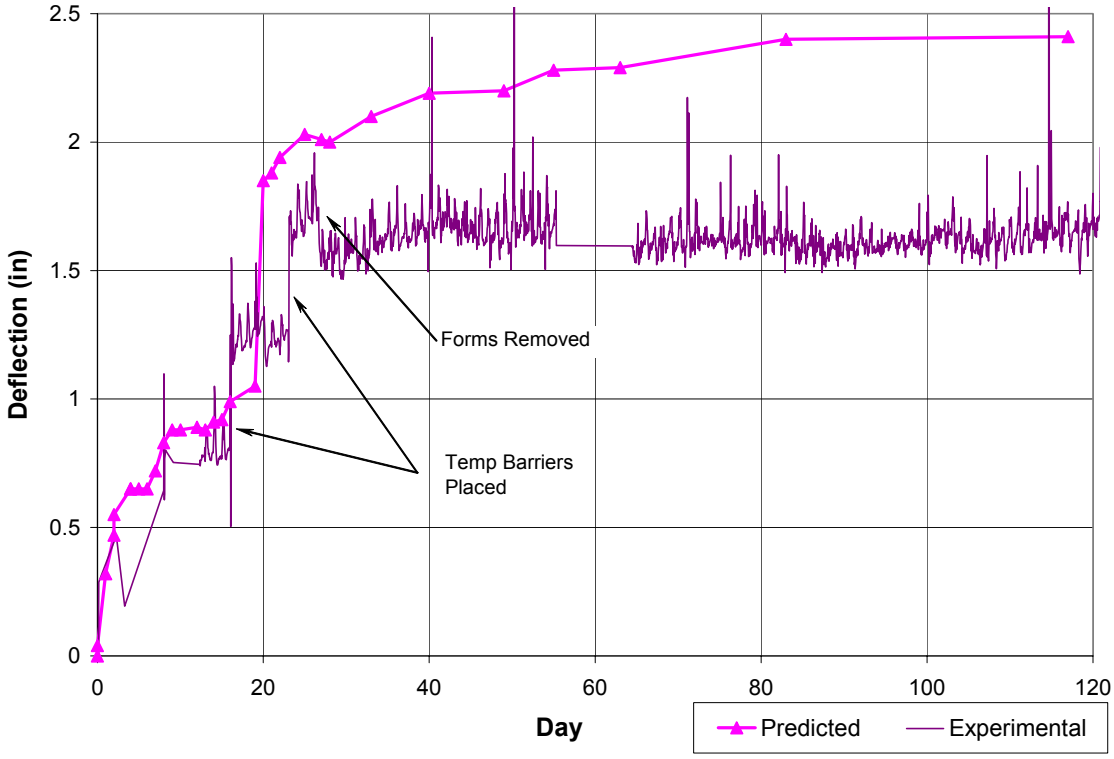

Figure 6-22: Comparison of calculated deflection and actual deflection

It can be observed in Figure 6-22 that the experimental deflections are similar to the predicted. The removal of forms was not taken into account in predicting the deflection profile. The form removal process was not well documented such as how much was removed and how quickly. However, the date the process began is known and a definite reduction in deflection is observed to occur around this date. It is assumed that if the form removal were taken into account the predicted deflections would have been even closer to the observed values.

6.3.5 Simplified Alternate Analysis

As has been mentioned previously, the uncertainty of the input parameters does not justify an overly detailed analysis. Therefore, it can be recom-

mended that the simplest analysis methods available would suffice. As such, use of the approximate creep and shrinkage coefficient values are recommended.

Such an analysis can be accomplished using the analysis program by specifying an alternate IN2.DT file. The line corresponding to number of days should be set to zero, which indicates the use of the alternate form. An example of this input file is shown in Figure 6-23 below.

```
0          Zero indicates alternate Input
1.0        Creep Coefficient Modifier (Usually 1.0) Modifies Equation xxxx
0.8        Aging Coefficient
20         Age at Loading
600.0e-6   Maximum Free Shrinkage Strain
35         Shrinkage Rate Modifier (Usually 35)  See Equation xxxx
120        Length of Analysis (Days)
```

Figure 6-23: Example Geometry Input File in1.dt

The creep coefficient is obtained using Equation 6-8 which only required the age at loading. A multiplicative modifier is provided which allows the value to be scaled up or down if desired. The shrinkage data needed is the maximum free shrinkage; often take as 600 ms, and shrinkage rate modifier. The shrinkage rate modifier is observed in the denominator of Meyer's formula. The lower this value is, the more quickly the shrinkage strain is developed. This value can be modified based on experience or test data whichever is appropriate. As was seen in Figures 6-14 and 6-20, the shrinkage strain developed much more rapidly than Meyer's formula would predict, thereby suggesting that a smaller value be utilized.

Figure 6-24 shows the results of the simplified analysis. The curve Creep+Shrinkage uses the experimental shrinkage results as a basis for analysis while the Simplified analysis uses Meyer's formula with the recommended values. The modified shrinkage model uses a maximum strain of 520 ms, and a rate value of 10.

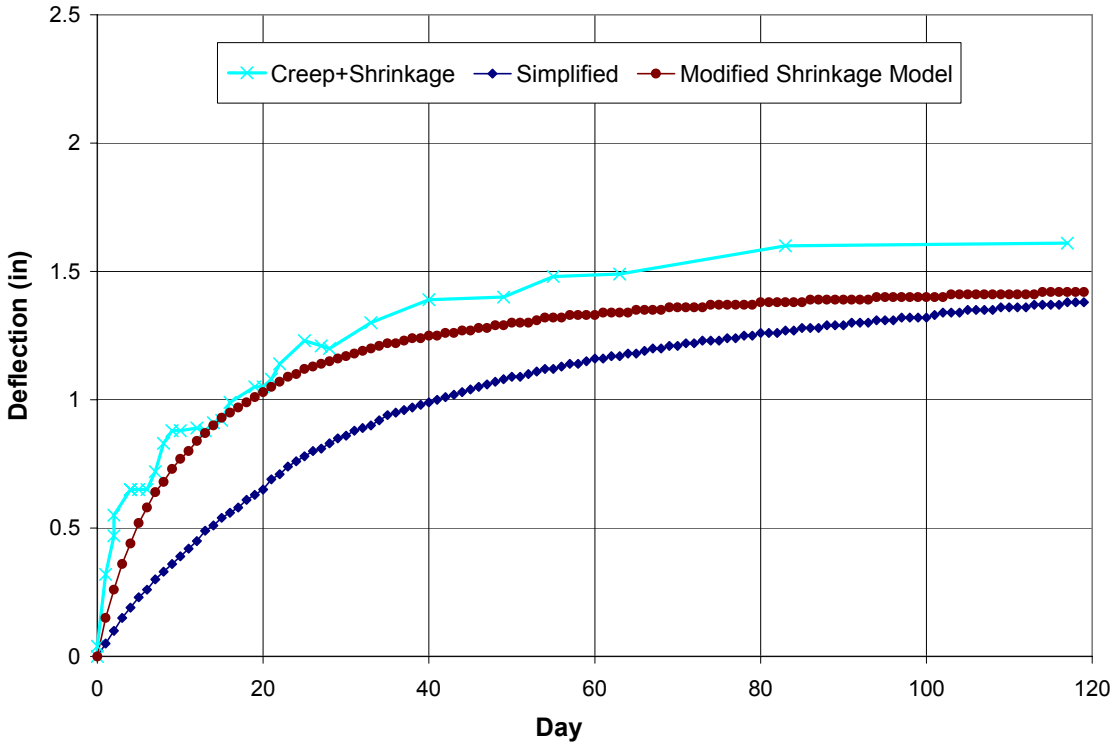

Figure 6-24: Results of simplified analysis

It can be seen in the figure that the various methods show very little difference after a few months. Therefore, for consideration of the differential elevation at time of closure, the result of the analysis is largely dependent on the specification of a value for maximum shrinkage since the time between phases is usually quite large. However, for determination of the additional relative deflection after the closure pour the rate of shrinkage is important. The shrinkage induced deflections developed more quickly on the Dodge Street Bridge than the simplified analysis would predict. Therefore, there would have been less differential elevation experienced after the pour than was predicted.

Chapter

7 Temperature

Longitudinal and Vertical Deformation Due to Temperature and Other Meteorological Factors

During the summer days the sun heats the top of the slab and the bridge deflection is upwards. Since the sun heats the deck directly while the girders below are shielded, a thermal gradient is introduced through the depth of the bridge. An increase in temperature causes the material the bridge is made of to expand. Since the sun is heating the top of the bridge, the top of the bridge expands, or elongates more than the bottom. The result is in an upward bending of the bridge. This effect is illustrated in Figure 7-1.

In addition to deflection due to thermal gradient, deflection can also be in response to a change in ambient temperature. Two potential mechanisms have been identified which explain this occurrence.

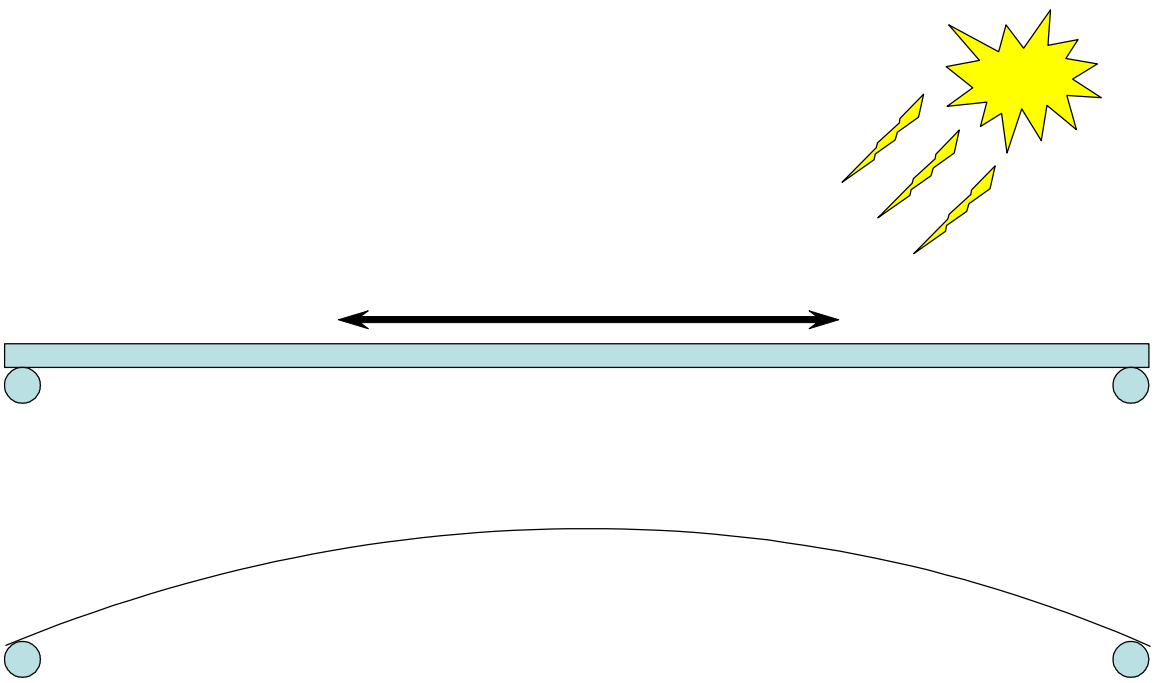

Figure 7-1: Deflection due to thermal gradient

The first explanation is the different coefficients of thermal expansion for steel and concrete. The values are 6.5 and 5.5 micro strain per degree Fahrenheit for steel and concrete respectively. Therefore, the steel elongates 1.0 micro strain per degree Fahrenheit more than the concrete. Since the steel is on the bottom of the structure, the bottom of the bridge elongates more than the top and the bridge deflects downwards. Notice that this is in the opposite direction as the movement due to temperature gradient. This phenomenon is illustrated in Figure 7-2.

The second mechanism requires the presence of at least partial end restraint at the end of the girders which acts eccentric to the girder as shown in Figure 7-3. As the girder expands the deck is restrained from expansion while the steel girder is not. Therefore, the bottom of the bridge is free to elongate more than the top. Again, the bridge deflection is downwards.

The temperature during a sunny summer day can be seen in Figure 7-4. The data in Figure 7-4 is from an interior girder taken around June 23, 2000.

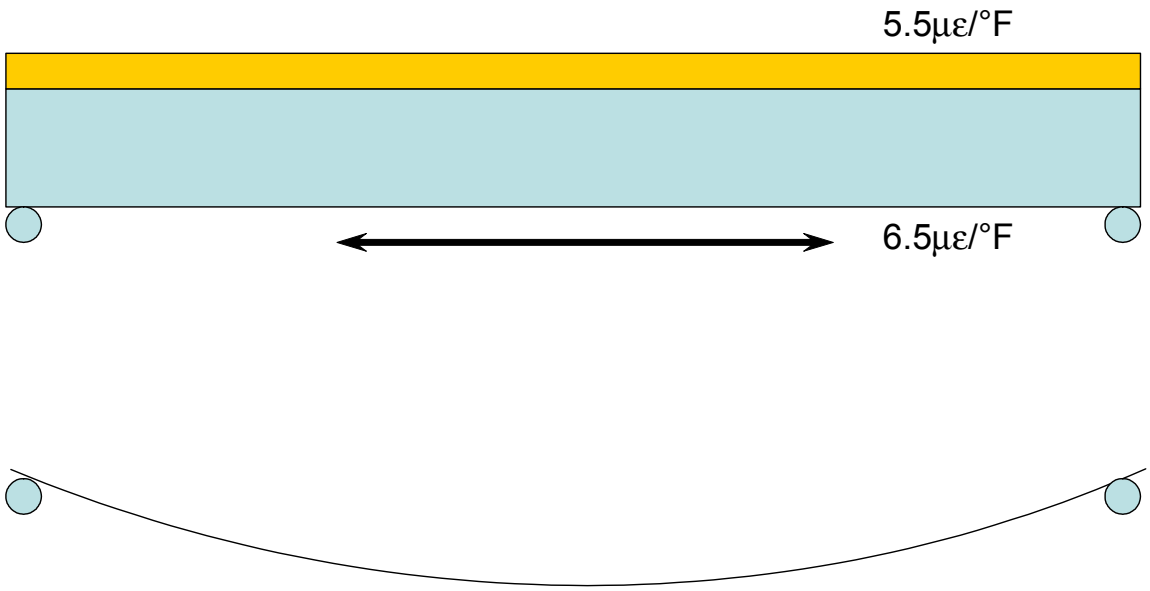

Figure 7-2: Deflection due to Uniform Temperature (Different Expansion Coefficient)

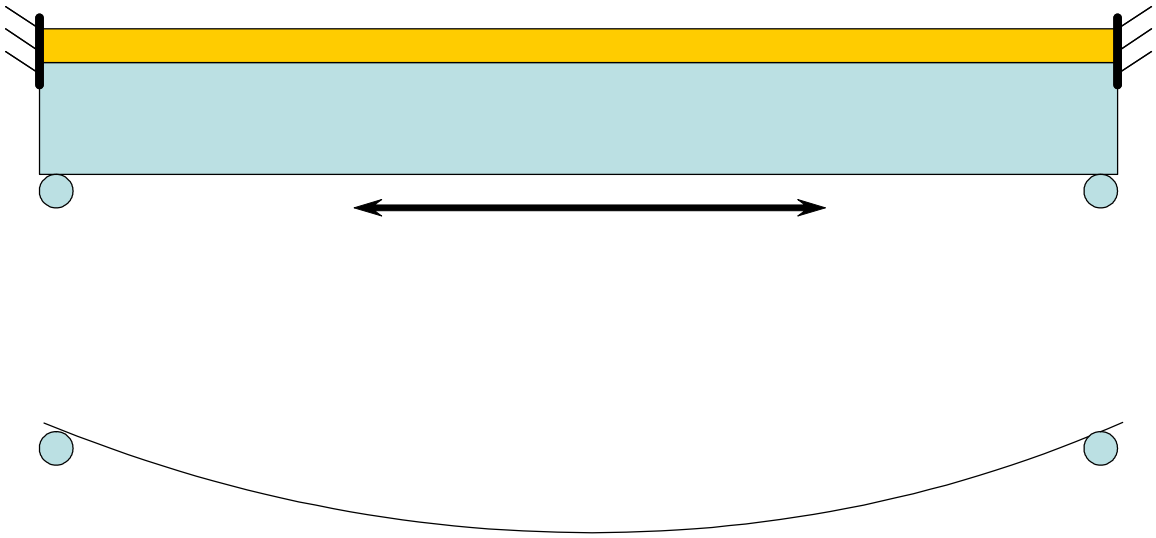

Figure 7-3: Deflection due to Uniform Temperature (End Restraint)

The numbers along the x-axis are the number of days since the beginning of the project with midnight falling on the whole numbers. It can be seen from the figure that the temperature in the slab can be a great deal higher than the temperature of the steel. This is due to solar heating. The temperature of the bottom flange follows very closely the ambient temperature. Further, due to conductive heating of the steel by the slab the top flange

temperature remains higher than the bottom flange. Finally, note that the temperature of the slab remains well above the temperature of the steel well into the morning hours. The entire system generally reaches a uniform temperature around 4:00 am.

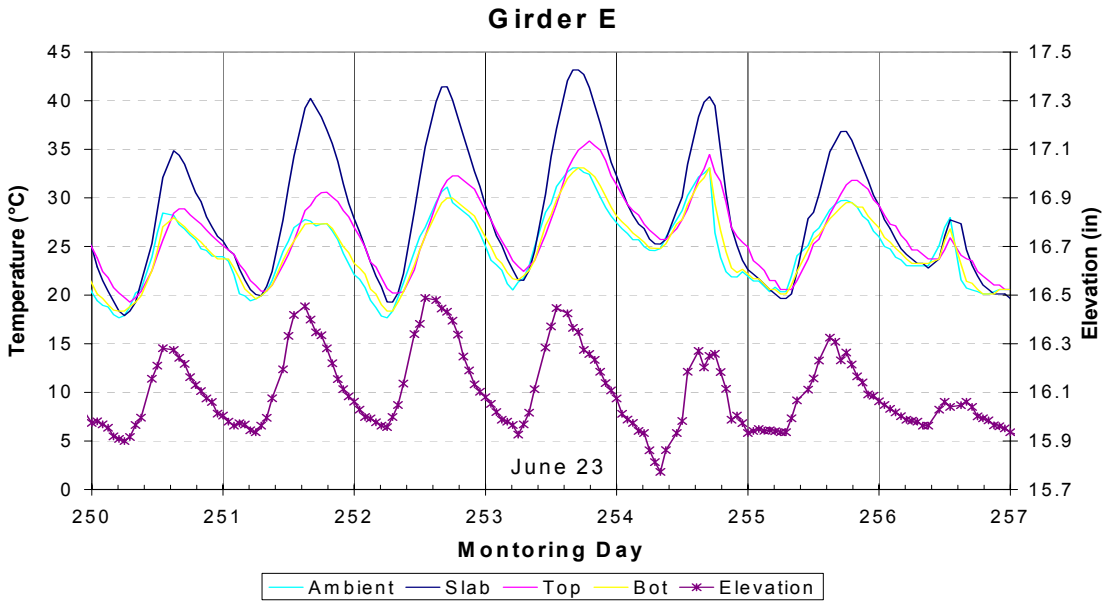

Figure 7-4: Vertical Movement due to daily temperature fluctuation

Figure 7-5 illustrates the gradient through the depth of the girder at 5:00pm on June 23, 2000. Also shown in the figure is the thermal gradient specified by the AASHTO LRFD Specification. Instrumentation was not provided to obtain the temperature through the entire depth of the slab, however, the temperature obtained at mid-depth does coincide well with the prescribed value. The predicted value at the top flange is well below the observed value. The higher temperature of the top flange is due to the conductive heating of the steel. It is assumed that the zone of elevated temperature is small and is therefore ignored by the predictive equations.

The elevation of Girder E has also been shown in Figure 7-4. The values along the right y-axis are the elevation in inches as measured from an arbitrary reference height. It can be seen that both the temperature gradient

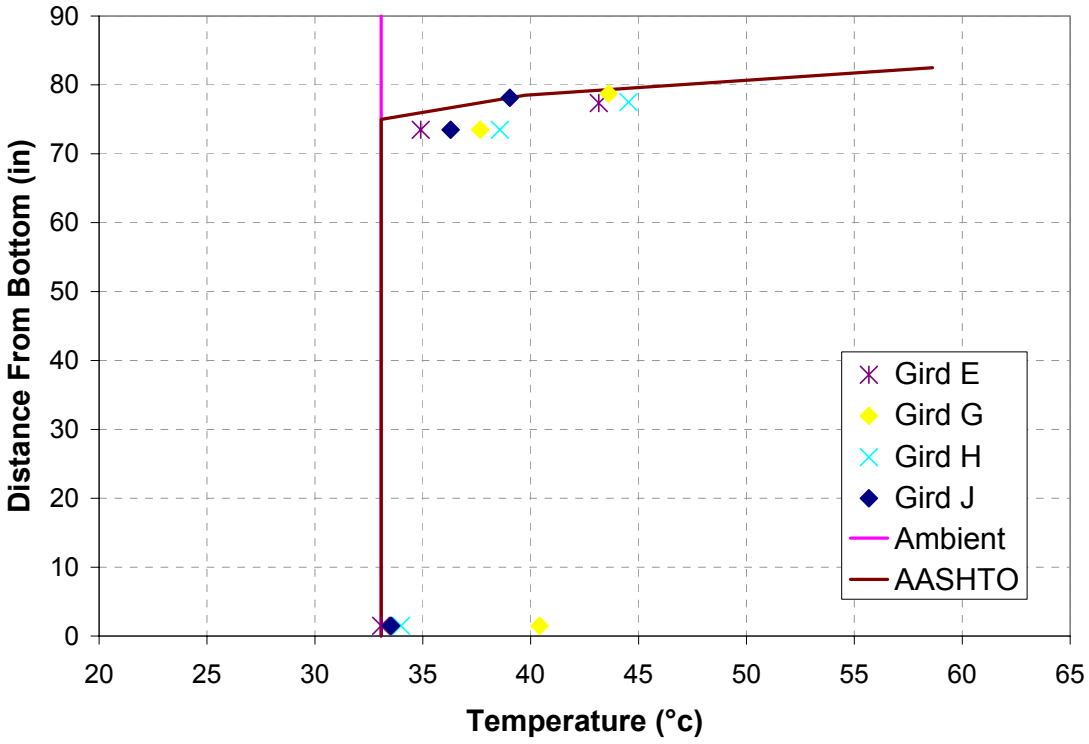

Figure 7-5: Gradient through depth of girder.

and deflection peak around 5:00 in the afternoon. The elevation increases over the course of the afternoon meaning the bridge deflects upwards.

It is of particular interest to observe the elevation of the girder at the time when the temperature is uniform over the depth of the girder. During the week presented in Figure 7-4 the early morning uniform temperature on most days was around 20˚ Celsius. At that same time the elevation of the girder was around 15.95 inches. However, on the morning of the 24th the uniform temperature was found to be 5˚ higher at 25˚ Celsius. On this day the elevation was at 15.75 inches. This demonstrates that as the uniform temperature increases the bridge deflects downwards.

The week of data presented in Figure 7-4 demonstrates well the primary deflection modes in response to temperature. It should be emphasized that the movement due to temperature movement due to an increase in temperature gradient is in the opposite direction as the movement due to an

increase in the uniform temperature. During the course of a typical day both the ambient temperature and temperature gradient increase during the afternoon and decrease during the evening resulting in opposing deflections. In a practical sense this is a good thing since the two effects oppose each other lessening the overall movement due to temperature. However, this situation is difficult to account for in analyzing the data obtained from the field testing.

Three general methods were proposed for dealing with the temperature effects. The first was to fully account for all thermal effects utilizing simulation and analysis techniques. It was determined that due to the complex interaction between the various factors including additional meteorological factors not yet mentioned such as humidity, drought and precipitation this alternative was too costly given the ultimate objectives of the project.

The second alternative was to ignore the presence of the moment gradient and deal solely with the average ambient temperature at the time of a reading. As was shown in the preceding section, during the afternoon as the average ambient temperature is increasing thus forcing the bridge downwards, the thermal gradient is increasing thus forcing the bridge upwards. It is quite apparent from Figure 7-4 that the thermal gradient effects are much greater than the ambient temperature effects on a day to day basis. On a good sunny day one can expect to see an approximate upwards deflection of 0.6 inches. However the approximate change in elevation observed through the seasonal thermal change is 0.5 inches. Therefore, since the magnitude of movement is the same for the two effects it would be incorrect to ignore either.

The third alternative was to separate the effects and consider them separately. Studying the effect of moment gradient can be done by examining the data obtained from individual days. The goal in particular is to find a sunny day during which the ambient temperature remains relatively con-

stant. This minimizes the effects of change in ambient temperature while exposing the response of the bridge to thermal gradient. The procedure for isolation of the bridge response to ambient temperature in absence of moment gradient is less straight forward and will be discussed in the following section.

7.1 Elimination of Thermal Gradient

After completion of the second phase there were 75 sensors capable of indicating temperature however the results from each and every gage is not necessarily accurate. Looking at a two week period of time in Figure 7-6 one can see that the temperature data can be quite noisy. This noise can come from a number of sources including but not limited to communication problems, interference, faulty gages, loads and vibration, and moisture in the wiring.

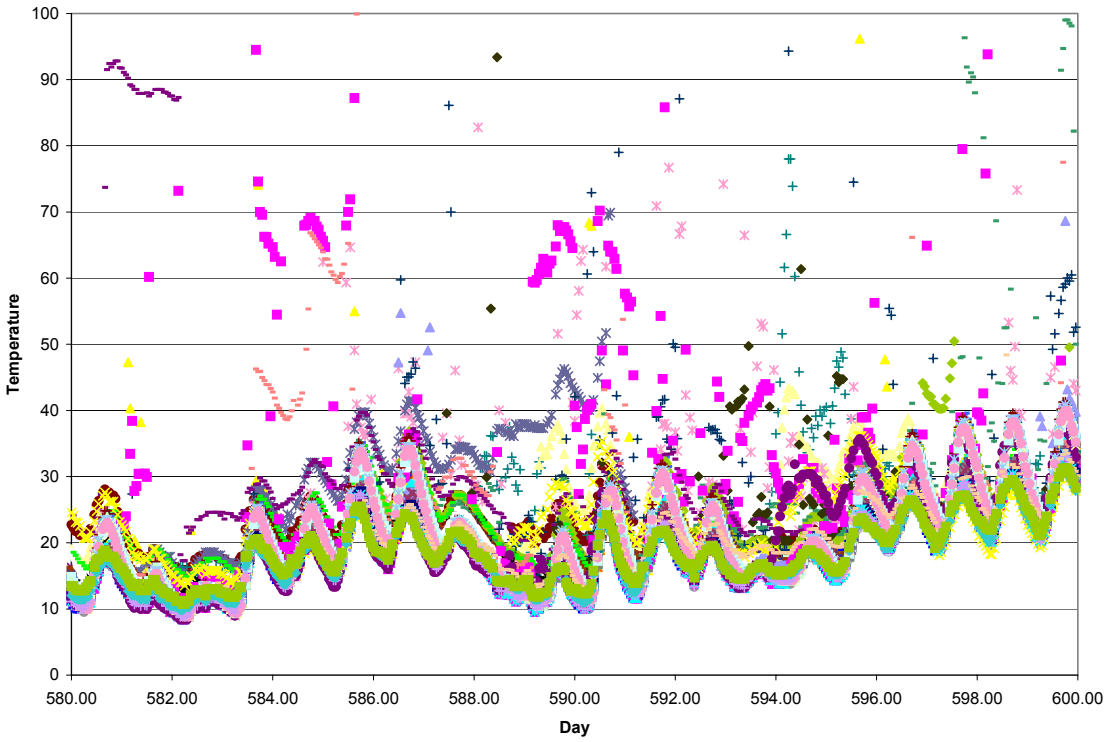

Figure 7-6: Raw Temperature Data

It was seen in the previous section that there is a short period of time during which the thermal gradient is at a minimum each day. The goal of filtering is to isolate that period of time and obtain the temperature and bridge response corresponding to a constant uniform temperature for each day. It would also be desirable to reduce to overall volume of data.

The first step in filtering the temperature data is to limit the time period used in the analysis. The time period chosen is from 3:00 am to 9:00 am resulting in seven readings for each day. The plots such as Figure 7-7 which shows all gages over a one day period indicate that the temperature is most stable during this period of time with the gages showing a small spread in values.

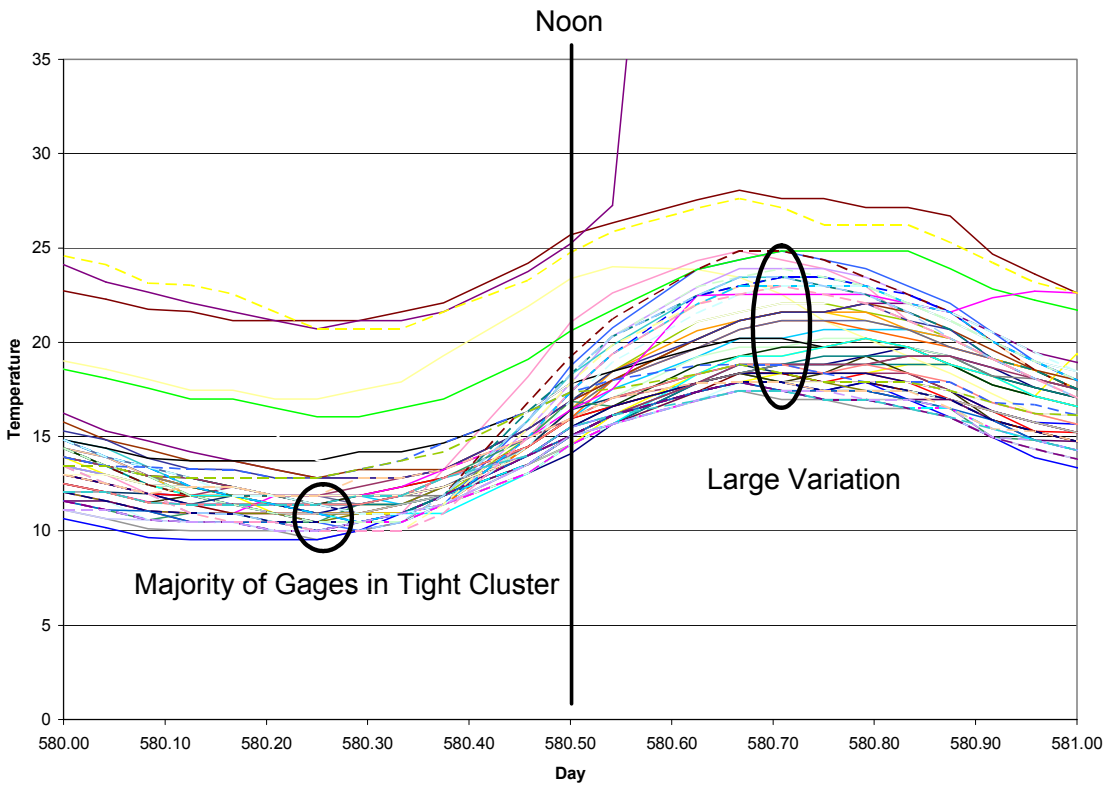

Figure 7-7: Variation in Temperature During Day

The next step is to eliminate the obvious outliers. These are the values which are so far out of range that they are obviously due to systemic error.

Since future filtering steps will further eliminate outlier points the limits at this point can be very generous. These limit points have been chosen to be -30 and 50 degrees Celsius. Any reading which falls outside these limits is eliminated from the data set. Figure 7-9 shows the same twenty days displayed in Figure 7-8 after imposing the time and extreme value limits.

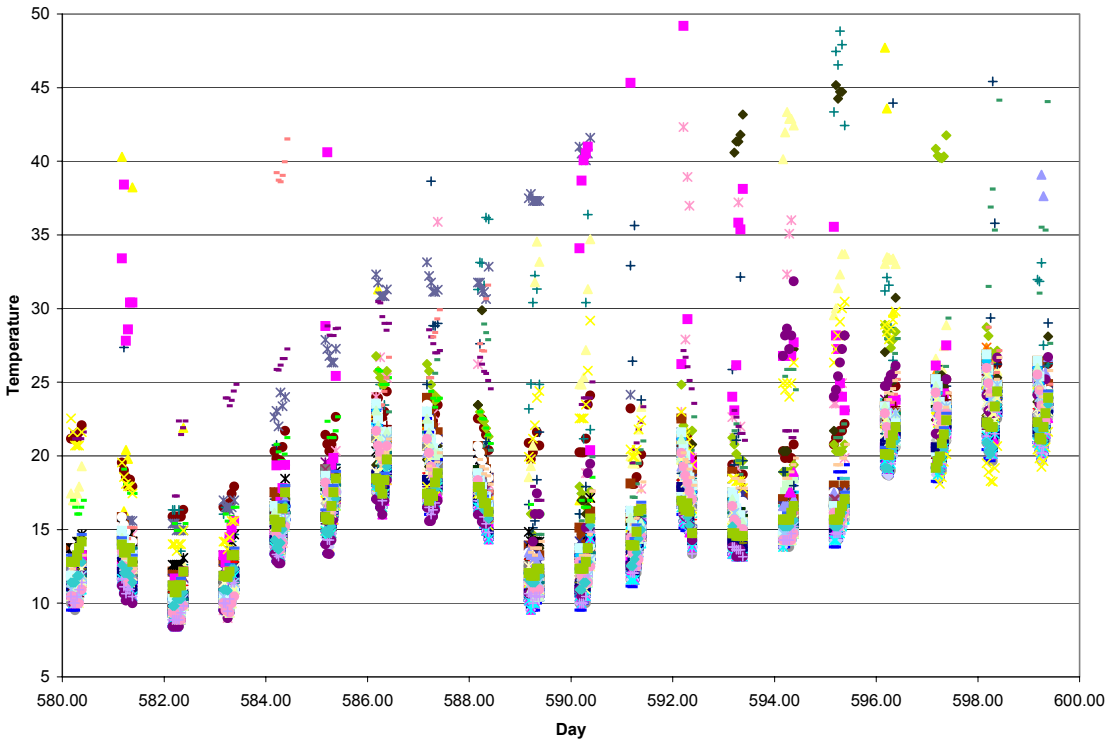

Figure 7-8: Temperature Data after elimination of obvious outliers

The next step is to further refine the elimination of outlier data points. This step is based on the following premise. If the temperature is constant, and has been for some time, one would expect all 75 gages to give approximately the same value. Based on this, the average value and standard deviation is calculated for each reading. If the standard deviation is less than three degrees then the reading is acceptable. However, if the standard deviation is over three degrees then the individual gage reading which is furthest from the mean is eliminated and the mean and standard deviation is recalculated. This is repeated until the three degree standard deviation cri-

terion is satisfied. At this point if there are at least ten gages remaining in the data set then the average value from the remaining gages is determined to be the average uniform temperature of the structure for the time of that reading. This is then repeated for each hour such that a single temperature is obtained for each hour. Figure 7-9 shows the results of this filter for the twenty days referenced previously. Since the outliers have been removed the data falls in a much tighter band and the limits in the plot have been adjusted accordingly to provide more detail.

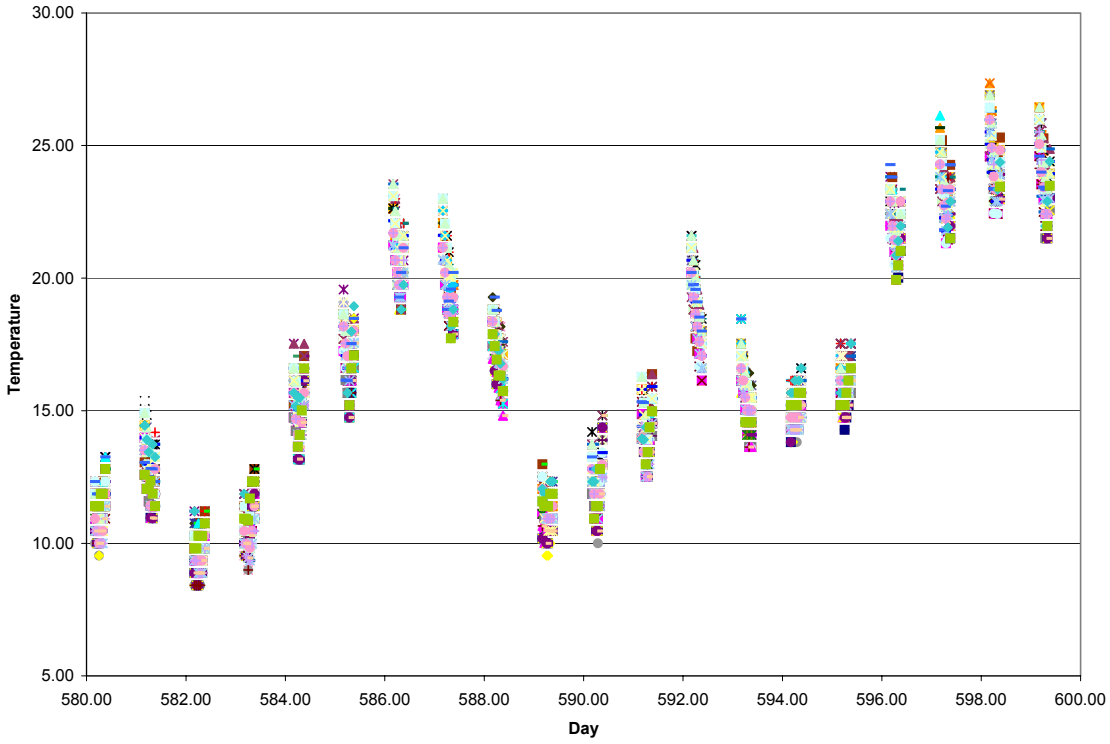

Figure 7-9: Temperature Data after filtering

The next step in the filtering process is to reduce to data down to a single temperature reading per day. The criteria for this operation are that the temperature range during the day must not exceed three degrees and the number of hourly reading remaining during that day be greater than or equal to five. The first criterion assures that the temperature is not changing too rapidly during the period of time. This is because the steel changes

temperature quickly and closely follows the ambient temperature while the concrete slab has more thermal inertia requiring more time to respond to rapidly changing temperatures. The second criterion requires that there are a sufficient number of readings available to provide a statistically relevant result. If the specified criteria are met then a centrally weighted average is performed with the resulting temperature being the temperature for that day. These temperatures are shown in Figure 7-10 for the twenty days being examined. The days in Figure 7-10 without a large marker indicating the final daily temperature are those days which violated the prescribed criteria.

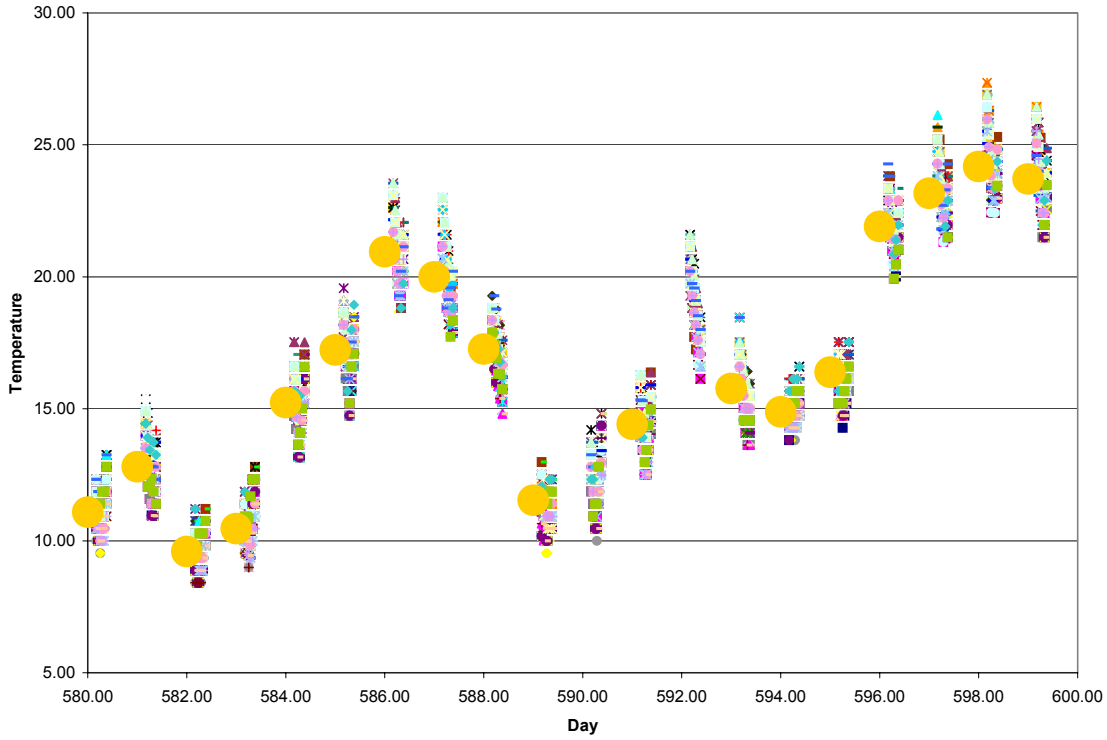

Figure 7-10: Temperature Data after Averaging Process

The final step in the temperature filtering process is to obtain daily values for the bridge response variables such as deflection, and strain. Minimal filtering is performed on the response variables. For each gage generous extreme outlier limits have been specified and the excessive values elimi-

nated from the data set. Once the extreme values have been removed a centrally weighted average is performed on the admissible hourly reading values for each day. The resulting value is the response variable value for that day.

The result of temperature filtering has thus reduced the full data set into a single temperature and the corresponding response data for each day. The values are from a period each day when the thermal gradient through the depth is at a minimum. Days during which the temperature is changing rapidly have been discarded and central averaging has been utilized to further reduce the effect of variability in the response variables.

7.2 Longitudinal Response due to Uniform Temperature Change

Once the effects of moment gradient had been removed using the procedure described above one could begin investigating the movements which could be attributable to a uniform change in temperature. There are four gages capable of monitoring the longitudinal deformation. One gage is placed at each end of girders E and D. A more detailed description of the instrumentation is given in Chapter 3. To begin examining the influence of temperature on longitudinal movement the longitudinal position has been plotted versus daily temperature for all data collected in Figure 7-11. The zero position for each gage is the arbitrarily chosen initial position when the gage was installed. This serves to separate the data and make each gage distinguishable from the others.

Inspecting Figure 7-11 one should notice an apparent linear relation for each of the gages. Further, a pairing of the data is observed with respect to which end of girder the gages are on. Figures 7-12 and 7-13 separate the pairs for the west abutment and east abutment respectively.

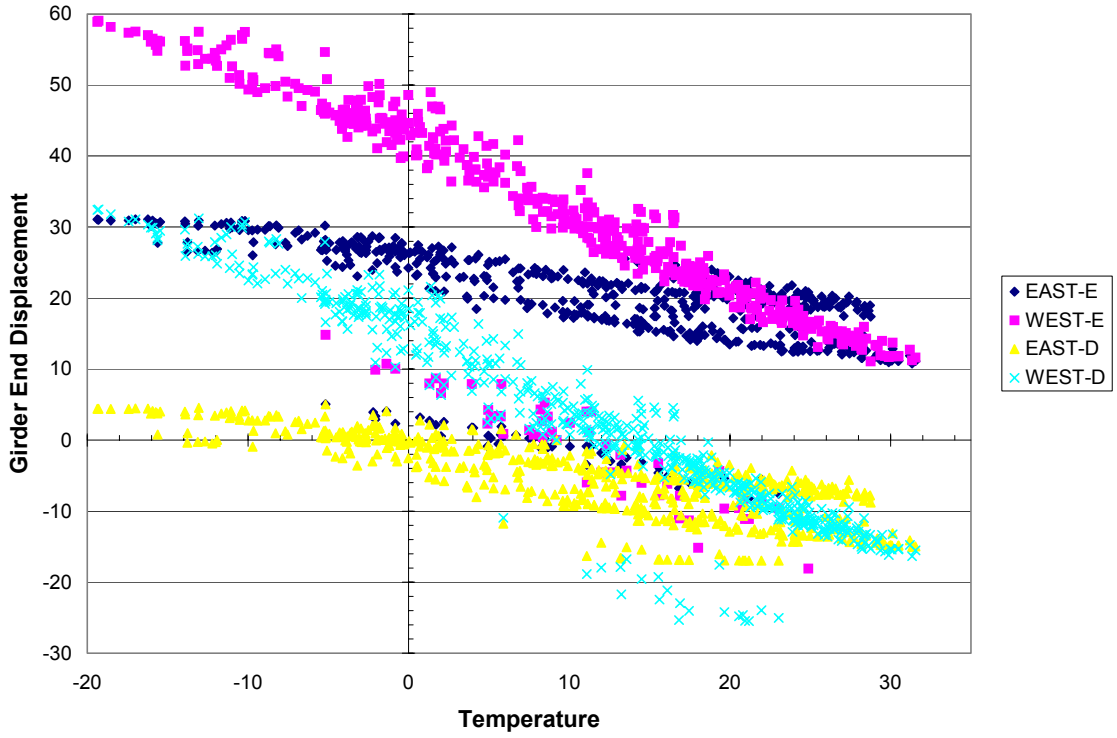

Figure 7-11: Longitudinal Movement versus Temperature

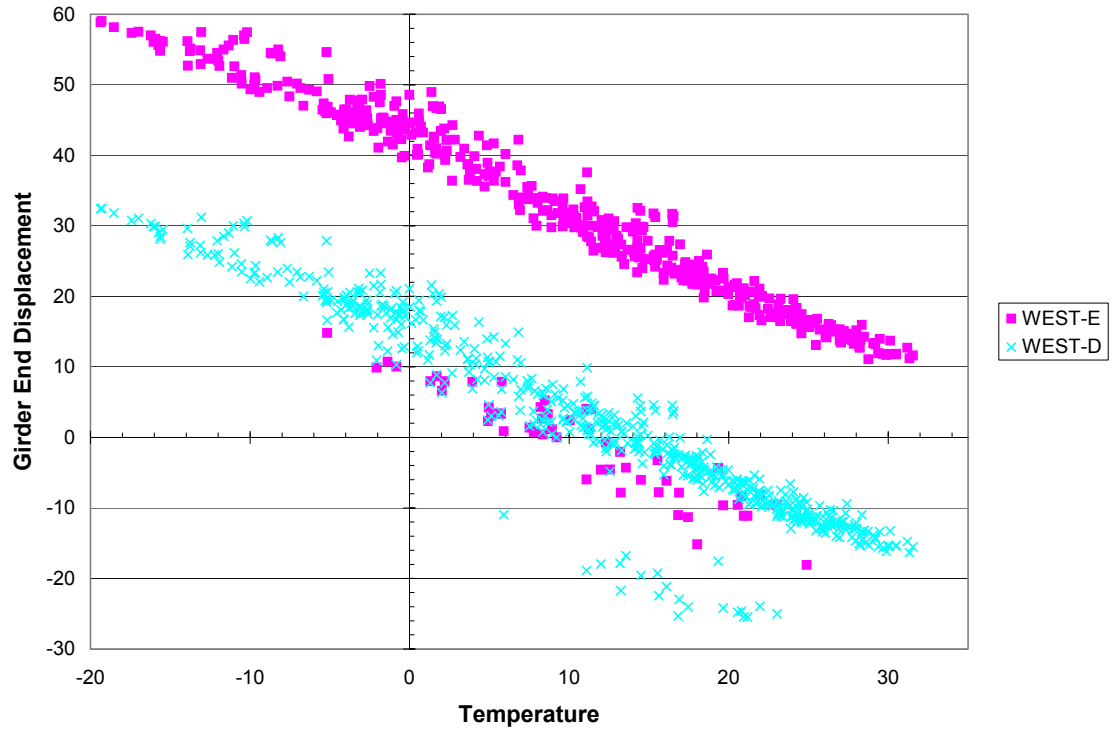

Figure 7-12: Longitudinal Movement versus Temperature (West End)

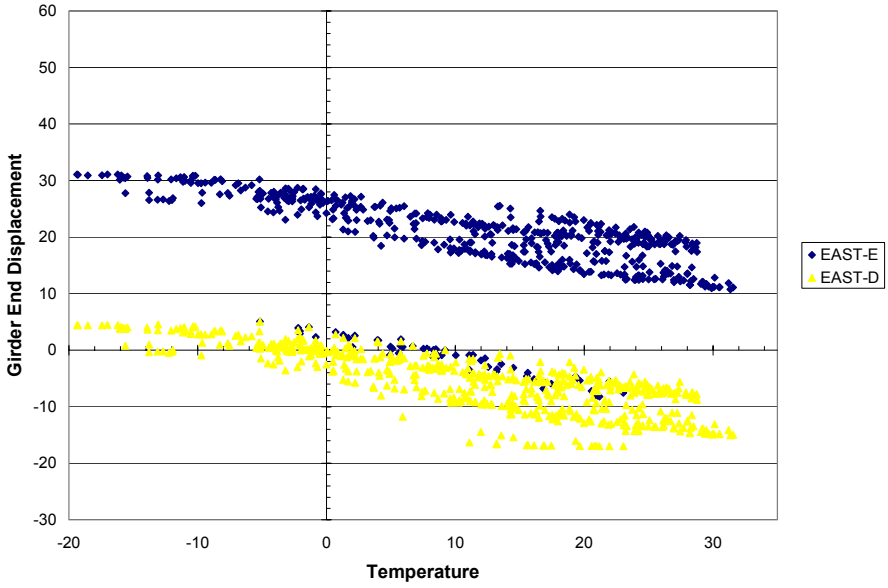

Figure 7-13: Longitudinal Movement versus Temperature (East End)

From inspection of the two previous figures one observes the deflection of the west end of the bridge caused by a change in temperature is larger than the deflection of the east end of the bridge subjected to the same temperature change. While there is insufficient instrumentation to verify, one hypothesis is that the difference in behavior between the two ends of the bridge is due to the vertical curve of the roadway as depicted in Figure 7-14. The supposition is that the lower end provides a rigid base off of which the rest of the bridge pushes off of. This is similar to a vertical metal rod resting on a table and subjected to a temperature change. The bottom remains fixed while the top of the bar experiences all the deformation.

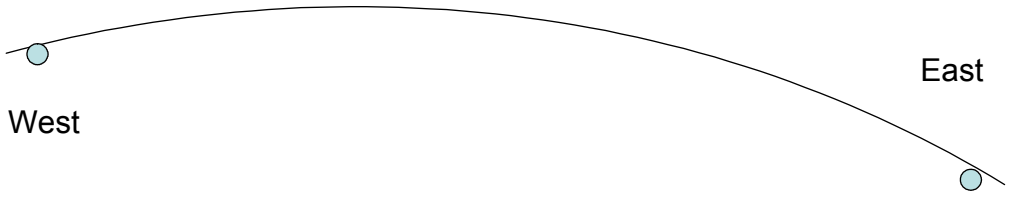

Figure 7-14: Bridge Vertical Alignment

Of greater significance than which end deforms more or less than the other is the total elongation or contraction of the bridge in response to temperature fluctuations. To obtain this value the deformation from the west end has been added to the deformation of the east end. The resulting data versus the average daily temperature has been plotted in Figure 7-15 for girders D and E. As was done with the position data, the reference point for zero deformation is arbitrary which separates the two data series on the same plot.

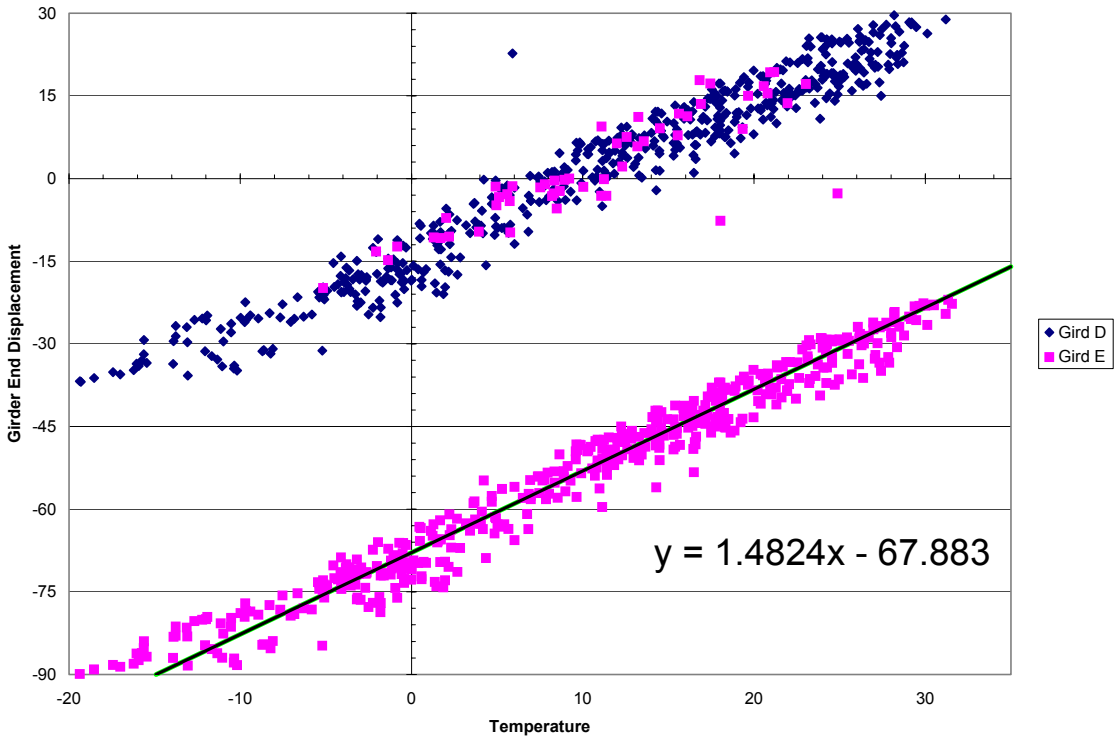

Figure 7-15: Girder Shortening versus Temperature

A linear regression for the girder contraction versus temperature data from Girder E is shown in Figure 7-15. As the intercept is arbitrary the slope is of interest. Equation 7-1 gives an approximation for the longitudinal movement due to a change in temperature.

The coefficient of thermal expansion of steel is 11.7×10^{-6} mm per mm per degree Celsius. Multiplying this value by the total bridge length of 144,180

$$\delta = \Delta_T \alpha L \tag{7-1}$$

Where

δ = Longitudinal movement due to temperature change

Δ_T = Change in temperature

α = Coefficient of thermal expansion

L = Length of girder

mm gives the rate of deformation with respect to change in temperature. Comparing the resulting value of 1.68 mm/˚C to the slope of the line in Figure 7-15, 1.48 mm/˚C it can be seen that the predicted rate of deformation with respect to temperature change is very close to the actual value being in error by 13.5%.

Nebraska is located within the Cold Climate region as specified in the AASHTO Specifications. The assumed temperature extremes used for design is from -30˚ to 120˚ F for a range of 150˚ F. Therefore, the full predicted deformation for design would be 141 mm while the actual deformation of the bridge due to the specified temperature variation is 124 mm.

7.3 VERTICAL DEFORMATION DUE TO TEMPERATURE CHANGE

In the previous section it was found that the longitudinal deformation correlated well with the change in average daily temperature and matched well with the theoretical prediction. This same exercise will now be performed considering the vertical deformation. Vertical deflection of each of the eight girders is measured near 0.4L in the East span using potentiometers. The resulting data along with temperature for all time is plotted in Figure 7-16.

It is apparent from this figure that several of the gages have been unstable at various times. It can be seen however that the deflection trends for each of the girders are similar. For these reasons two girders, G and H have been

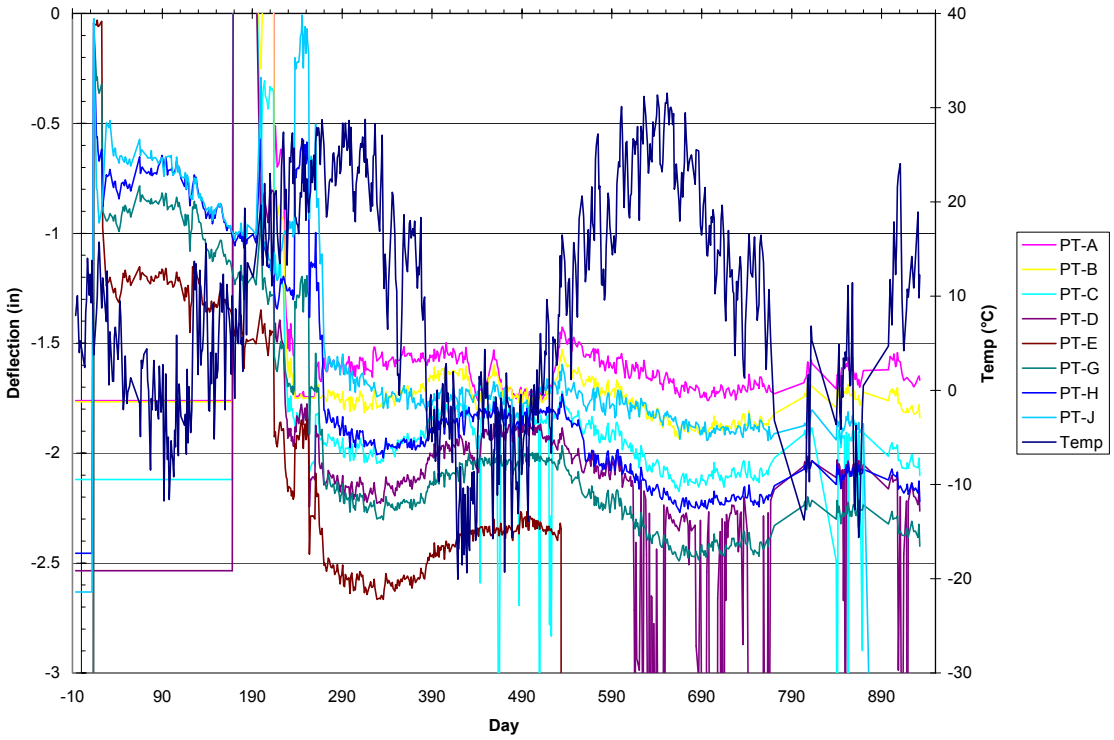

Figure 7-16: Vertical Movement over Time

isolated and will be investigated in more detail. These are shown in Figure 7-17.

The deflections occurring prior to the end of construction require a more detailed analysis as the loading and stiffness of the system continually changes during the construction process. Further, insufficient data has been collected to investigate trends extending beyond one year in duration. Therefore, the data has been clipped one year past the end of construction. The resulting data is shown in Figure 7-18.

Despite the obvious seasonal deflection trend the deformation peaks do not correspond with the observed peaks in temperature. In fact, the deformation appears to peak approximately one month after the temperature. When the vertical deflection is plotted versus the daily average temperature as shown in Figure 7-19 one can see that there is no apparent relationship.

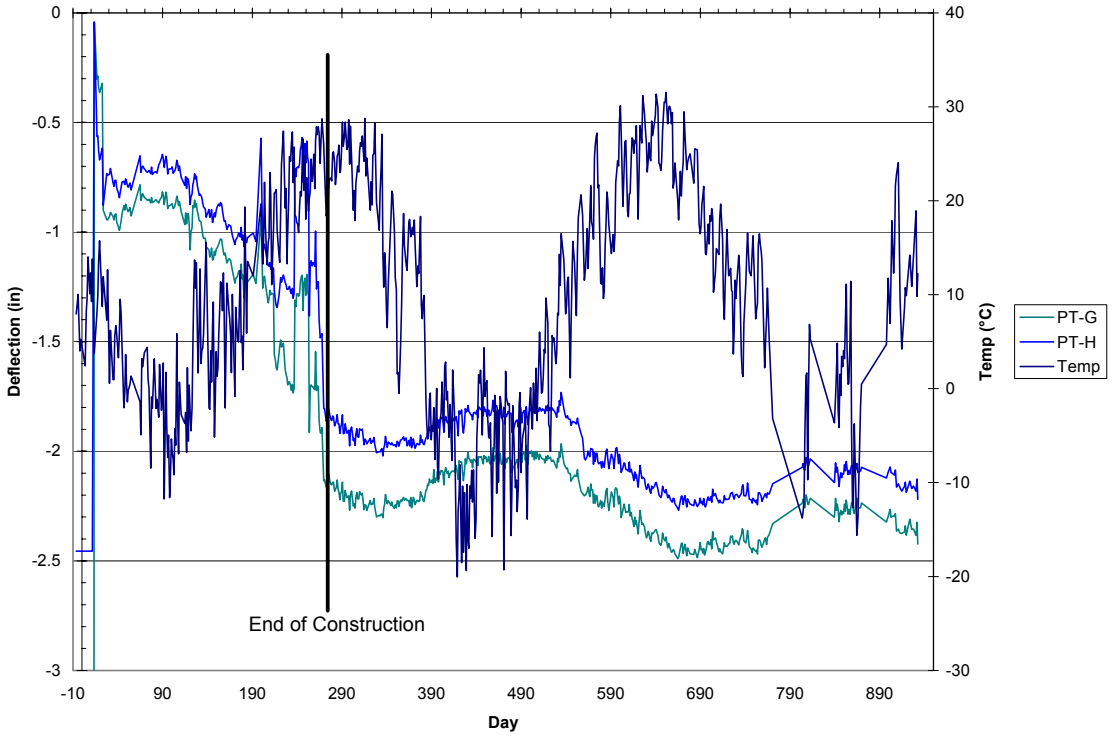

Figure 7-17: Vertical Movement Gages G and H Only

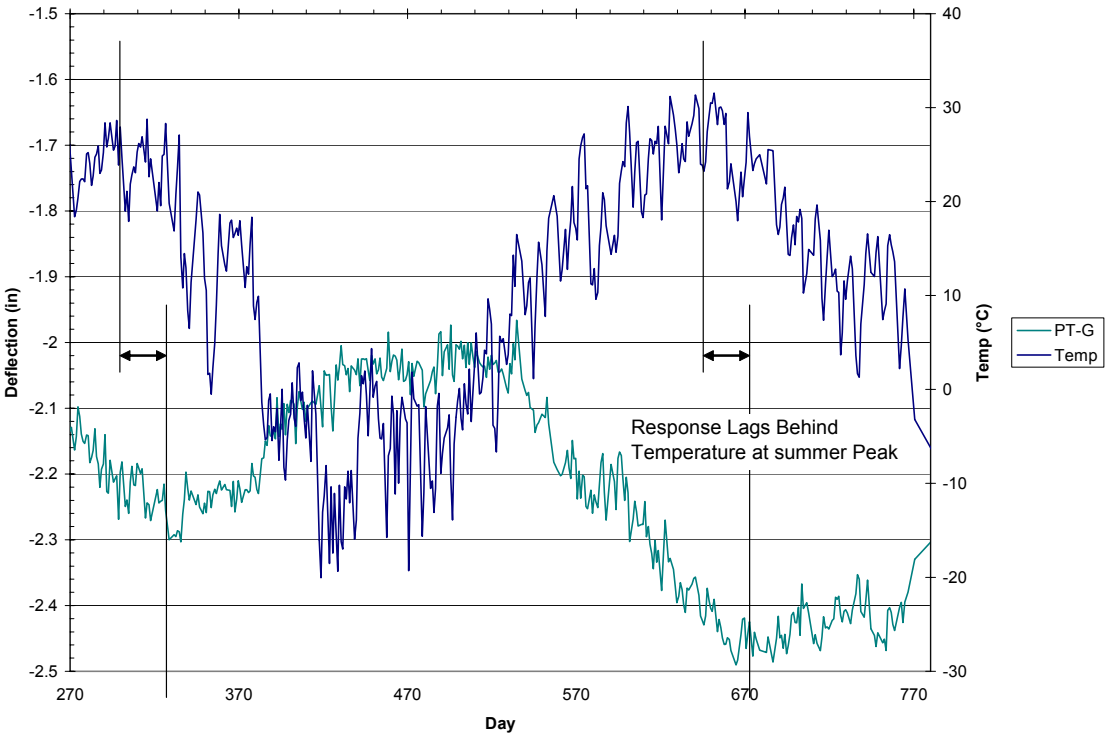

Figure 7-18: Vertical Movement Girder G Post Construction Only

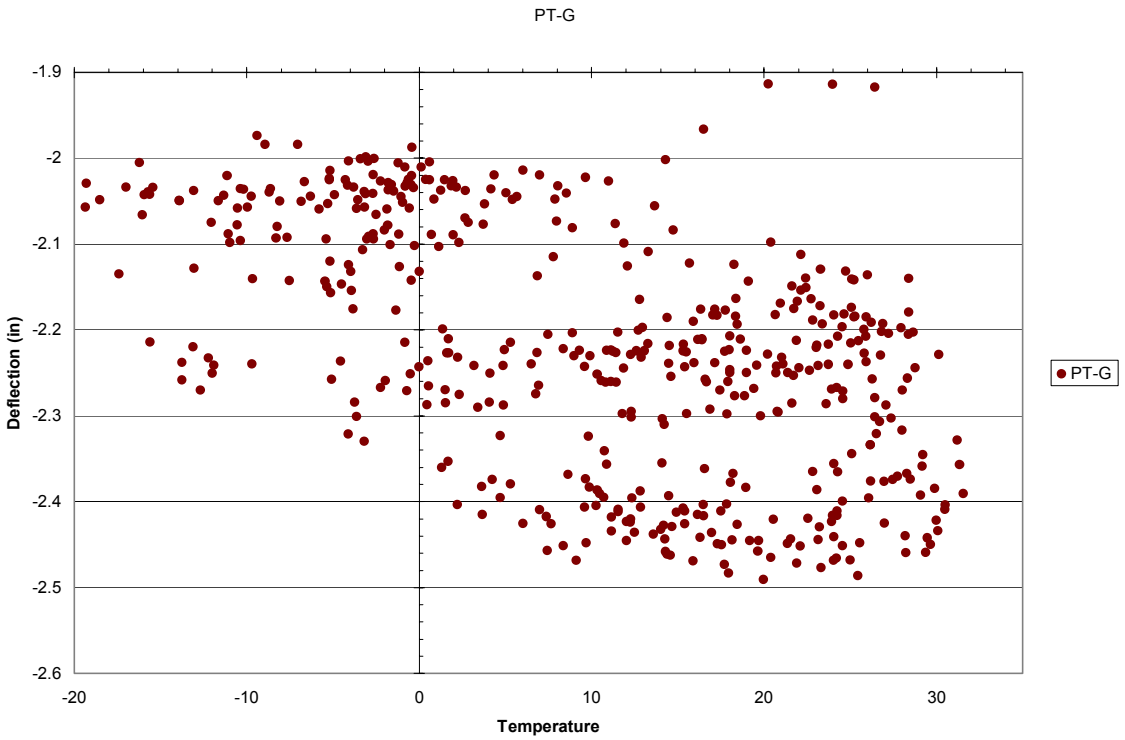

Figure 7-19: Deflection versus Temperature

The conclusion which the data suggests is that temperature is not the only factor driving the seasonal variation in vertical deflection. It is quite evident that there is seasonal variation in the deflection history. Therefore, it is suggested that an additional parameter also varies seasonally and operates in conjunction with the temperature to drive the deflection changes. In the next section one possible parameter will be suggested.

7.4 Other Meteorological Considerations

The meteorological parameter which keeps arising as a likely culprit is humidity and precipitation. Just as shrinkage occurs when concrete cures and loses moisture, exposing dry cured concrete to humidity can result in a re-expansion. Humidity, like temperature, fluctuates with the seasons with summers being humid and moist and the winters dry. It would be expected, however that as the concrete deck expanded during the moist

summer months the vertical deflection would tend upwards. It is seen in Figure 7-18 that during the summer months the bridge actually moves downwards. This could suggest that temperature is the predominate factor with the humidity movement being of lesser importance however, significant enough to force a shift in the peak deflection.

Although weather data was not collected on site, historic meteorological data is available from a number of sources. Figure 7-20 shows the daily precipitation as observed over the period of interest.

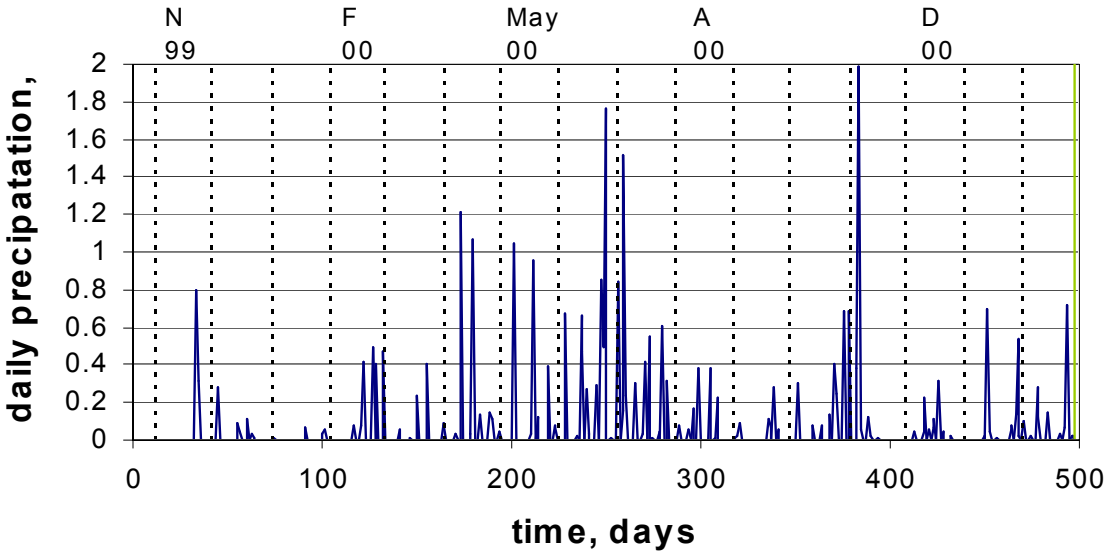

Figure 7-20: Precipitation over period of interest

Chapter

8 Construction Issues

Elements Specific to Phased Construcion

A number of the details that arise at construction time can have an impact on the success or failure of a phased construction project. Within this chapter, a number of these will be explored.

Although some aspects of construction sequencing are specifically called out in plans, there are a number of decisions that the contractor can make with respect to sequencing. Some of the decisions can have detrimental consequences on a phased construction project while they would have no impact on a traditionally constructed bridge.

No matter how carefully the system has been analyzed nor how many safe-guards have been put in place, there will always be some misalignment of the phases. One questions is how large of a differential elevation can be tolerated?

Finally, if it is determined that the amount of misalignment is excessive, what are the potential remediation alternatives available?

8.1 Construction Sequencing

One of the enduring themes of phased construction is to maintain similitude between the construction of the two phases. The sequence of construction events can weigh heavily on the level of similarity between the two phases. In particular, two controllable factors which can potentially contribute to a variation in the level of end restraint during the construction of the phases are sequencing of the approach slab and connectivity of the turndown between the phases.

8.1.1 Approach Slab

Figures 8-1 and 8-2 illustrate a common end bearing detail including the approach slab. The approach slab is a highly reinforced slab spanning between a grade beam and the turndown. Both the deck slab and the approach slab are doweled into the turndown although there is not continuous reinforcement between the two. The paving section is doweled into the grade beam while the approach slab is not. The ends of the girder are encased in the turndown as well. Through the web of the girder are placed steel reinforcing bars. By virtue of the connection detail at the turndown it is expected that tensile force carried in the deck, or top flange during deck casting, can be transferred into approach slab. While the approach slab is meant to move freely on the grade beam it is still expected that the approach slab is capable of anchoring some amount of force due its weight and the friction between the slab and the ground. At the same time, backfill behind turndown has the capability of resisting compressive forces near the lower portion of the steel girder. These two forces, tension near the top

and compression near the bottom form a couple which is capable of providing rotational restraint to the girder.

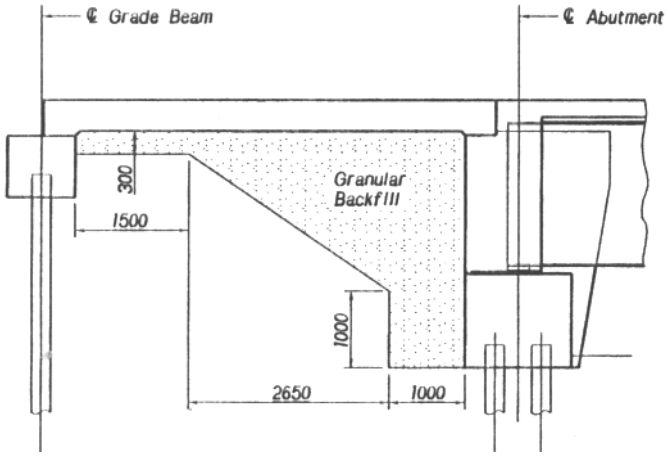

Figure 8-1: Approach Slab Detail

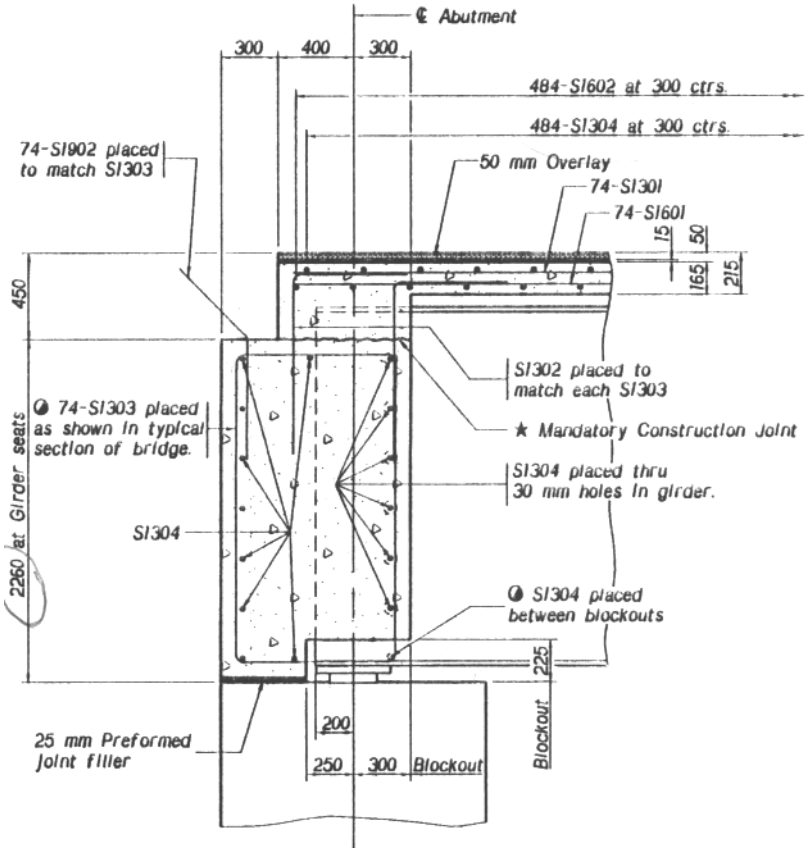

Figure 8-2: Turndown Detail

The rotational restraint provided by this semi-integral abutment tends to lessen the deflections due to the deck pour, see Section 4.2.1. It should be clear that if the approach slab were to be present during the deck pour of one of the phases and not present during the deck pour of the other phase the deflection from the two phases would not be equal.

8.1.2 Turndown Connectivity

Failure to properly account for turndown connectivity between the phases can lead to problems as well. During the construction of a phased construction project, typically half of the old bridge is removed and replaced while the remaining half of the old bridge continues to carry traffic. Traffic is then carried by half of the new bridge while the second half is replaced.

In the state of Nebraska, the standard order of operation for semi-integral abutments is to pour approximately ¾ of the turndowns at the ends and piers to lock the girder in place and eliminate the need for separators at these locations. In phased construction, it is important that the turndown on the second phase not be made continuous with the turndown from the first phase until after the deck has been cast on the second phase.

Consider the stiffness of the composite girder and slab system of the first phase compared with the stiffness of the steel only second phase which exists just prior to casting the deck of the second phase. Obviously the composite first phase is much stiffer. If the turndown is made continuous between the phases, the stiffness of the first phase will tend to restrain the ends of the girders from the second phase during the casting operation. This will result in a dissimilar restraint condition between the phases possibly resulting in several problems.

First, the additional restraint to the second phase will limit the deflection such that there will be a differential elevation at the time of closure.

Second, as the restraint to the second phase will be present towards the interior, there will also be a torsional deformation of the second phase.

A case study exhibiting this behavior is presented in Section 10.1

8.2 Differential Elevation Limits

Despite all the best efforts there will always be some amount of differential elevation at the time of closure. The next obvious question is how much is too much? There really is no one answer to this question since what is allowable is highly dependent upon the characteristics of the individual system. Consider, for example, a bridge geometry which has a dividing barrier such as commonly used on urban interstates. If this barrier occurs between phases, the amount of allowable differential would be virtually unlimited. However, if the closure should be required within a series of one way lanes, where vehicles will possibly be changing lanes over the closure region, the allowable differential would be quite low. Rather than developing a set of guidelines which would need to be violated as often as they would be followed, several items which need to be taken under consideration have be presented. Then, in Chapter 9, analysis tools are developed to help the designer evaluate the individual situation and determine the best solution.

8.2.1 Forming Requirements

Contractors have been known to be quite inventive when it comes to making form work fit despite misalignments. Therefore, the ability to place the formwork is usually not an issue. Generally, other factors would result in remediation of the differential elevation long before the forming requirements.

One consideration that falls under formwork requirements that can arise is clearance for transverse reinforcement from the first phase. For continuity, the transverse reinforcement is extended into the closure region

from the first phase. After the second phase is cast, these bars are lapped with the transverse reinforcement from the second phase. The elevation of the second phase prior to casting is above the first phase. As the concrete is placed, the second phase deflects to the elevation of the first. During the deflection, clearance must be provided so the formwork from the second phase does not collide with the reinforcement from the first phase. Figure 8-3 shows a typical solution to this problem. The transverse bars are bent out of the way and then bent back once the second phase has been cast. To prevent overstraining of the reinforcement, the closure region should be wide enough such that the required bend in the reinforcement is kept to a minimum.

Figure 8-3: Transverse Reinforcement Bent to Allow Clearance

8.2.2 Overlay Requirements

The wearing surface overlay is often charged with covering up an elevation differential at the time of closure. For small differentials, this is easily done without the need for much concern. However, when the magnitude of differential increases the additional amount of overlay on the low phase increases. Although some lateral distribution occurs between the phases the lower phase will carry a large portion of the load. In some cases, the effects can be great enough that the induced stresses can cause cracking within the closure region. Chapter 9 will introduce a method of analysis to determine if this is a potential problem. Of course there is also the basic issue of strength and whether the modified overlay would introduce an unacceptable level of additional load.

A second limitation to the magnitude of allowable differential elevation may be due to the change in profile due to the modifications of the overlay to accommodate the differential. Figure 8-4 shows several modifications which can be made to the overlay to accommodate the differential elevation. In the figures, the scales are grossly exaggerated for clarity. The overlay in Figure 8-4A ignores the differential and places the overlay such that the minimum overlay thickness and crown profile are maintained. This option is suitable when the differential is quite small. Figure 8-4B maintains the specified minimum thickness. However, the transverse profile is modified. Figure 8-4C modifies the transverse profile over a portion of the width then maintains the specified thickness. Finally, the modification in

Figure 8-4D decreases the overlay thickness over a portion of the bridge and modifies the transverse profile.

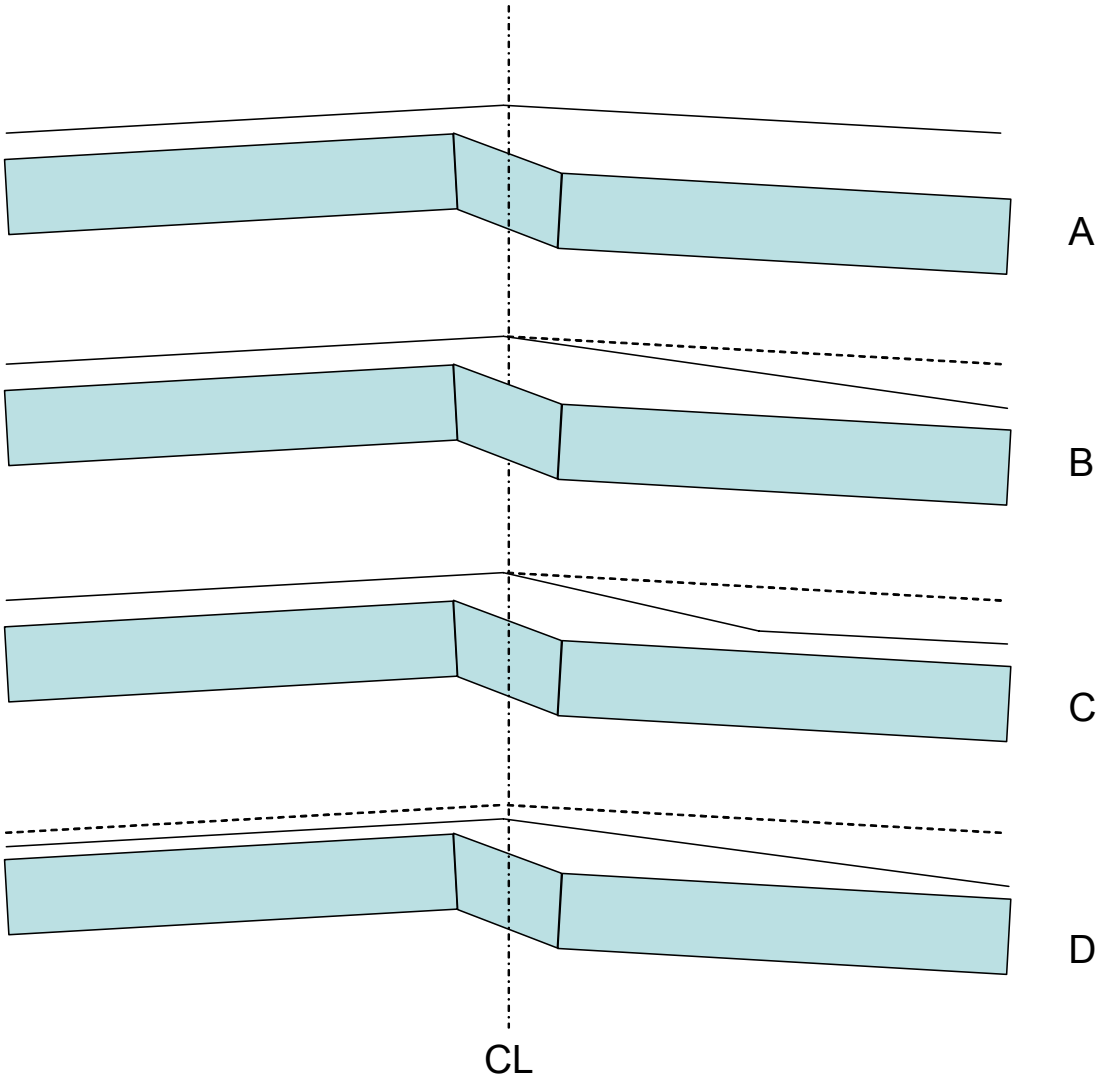

Figure 8-4: Differential Elevation at time of Closure

Each of these options assumed that the profile of each individual phase was correct. This is not necessarily the case. The phases may display some amount of rotation as well. The combinations in this case are too numerous to illustrate and it is not difficult to imagine the various solutions which can be devised to accommodate them.

As mentioned above, Chapter 9 will introduce an analysis method which will predict the impact the various overlay configurations will have on the structure.

8.3 REMEDIATION

In many instances, careful planning and attention to sequencing details will result in a structure where a minimal adjustment to the overlay can resolve any issue of differential elevation. However, as discussed in the previous section there are circumstances where the elevation difference is too great and the two phases must be brought into closer alignment prior to being joining together by the closure pour.

A disadvantage to remediation which is common to all techniques is the locked in stresses which arise as a result of the operation. All remediation techniques use force to bring the two phases closer to the same elevation to allow the closure region to be formed and cast. After the concrete has cured, the force is removed. The system is restrained from fully returning to its original position by the newly placed concrete closure region. Therefore, the locked in stresses are usually concentrated in or near the closure region which has just been cast. This can cause additional cracking problems which can lead to premature deterioration of the closure region.

8.3.1 TEMPORARY BALLAST

One of the simplest remediation techniques is adding temporary ballast to the phase that is too high. This method can be highly successful since the load can be placed near the closure region which will result in a beneficial rotation in addition to the dead load deflection. Suggested ballast items include temporary barriers and construction equipment. Figures 8-5 through 8-8 illustrate the process.

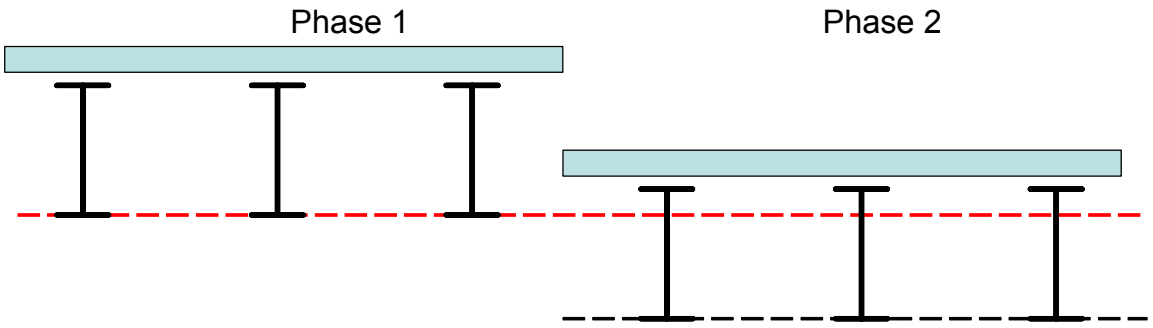

Figure 8-5: Differential Elevation at time of Closure

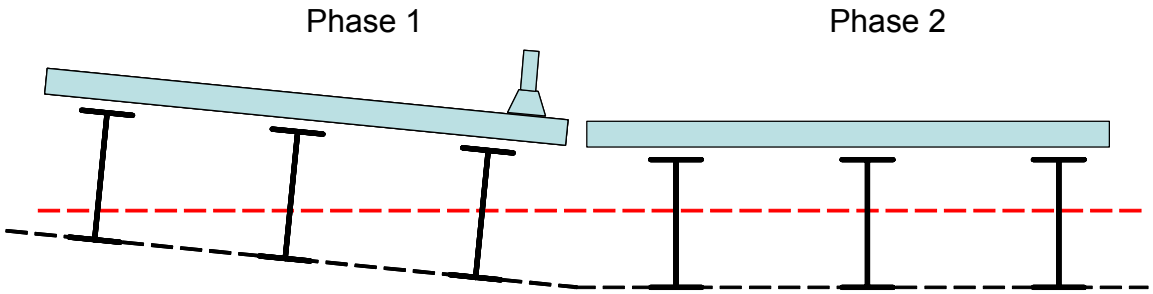

Figure 8-6: Additional Ballast Added

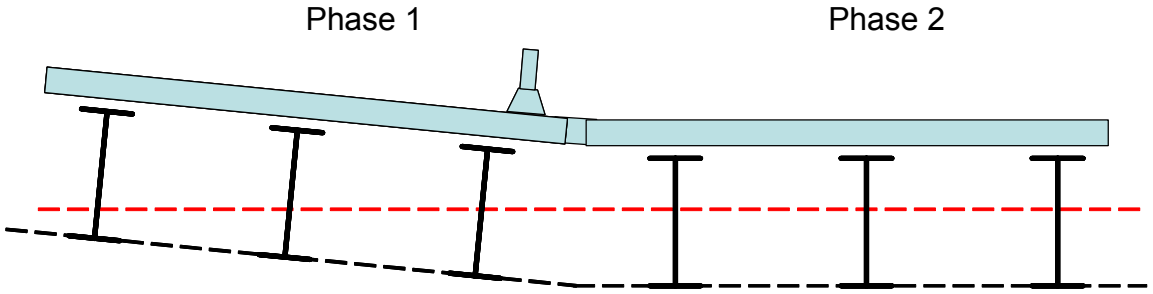

Figure 8-7: Closure Region Cast

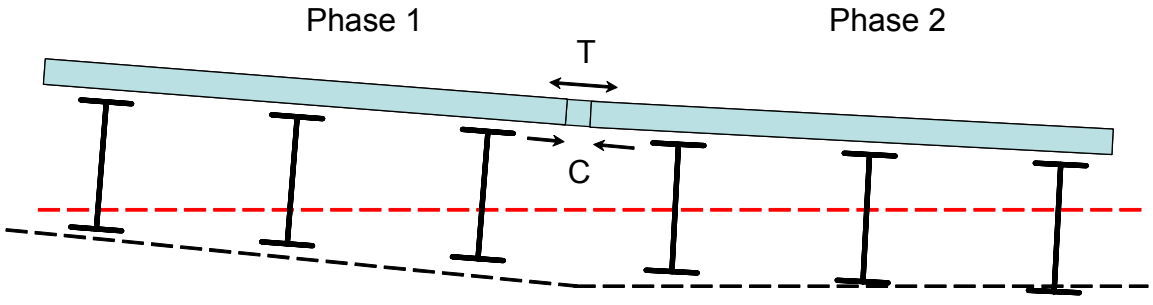

Figure 8-8: Ballast Removed

8.3.2 Temporary Support

The converse to temporary ballast would be a temporary support. This solution would probably not be very advantageous in most circumstances. The obvious drawback to this alternative is the need for the supporting structures to be erected below the bridge. These supporting structures would then get in the way of whatever the bridge was crossing. There may, however, be some circumstances where the temporary ballast solution falls just short of alleviating the problem and a single support on the other phase may be all that is required to pull the system into alignment in which case the alternative may be considered.

8.3.3 Inter-Phase jacking

The final force based remediation method is inter-phase jacking. Jacking beams are placed on the deck traversing the closure region while similar beams are placed below the supporting girders. When the two jacking beams are pulled towards each other the phases are brought into alignment. The method is illustrated in Figures 8-9 through 8-12.

This method is an option when the differential elevation is excessive such that the ballast option is insufficient. This situation can be encountered in bridges with horizontal curvature, grievous construction errors, or other extreme cases. The method makes use of the flexural and torsional flexibility from both phases which allow a large amount of corrective deformation to be obtained.

8.4 Temperature Considerations

Unfortuantely, as discovered in Chapter 7, vertical deflection may not necessarily be tied to the long term fluctuations in temperature, but may be more directly related to the time of year. Therefore, a method of correction, or adjustment based on temperature is not feasible.

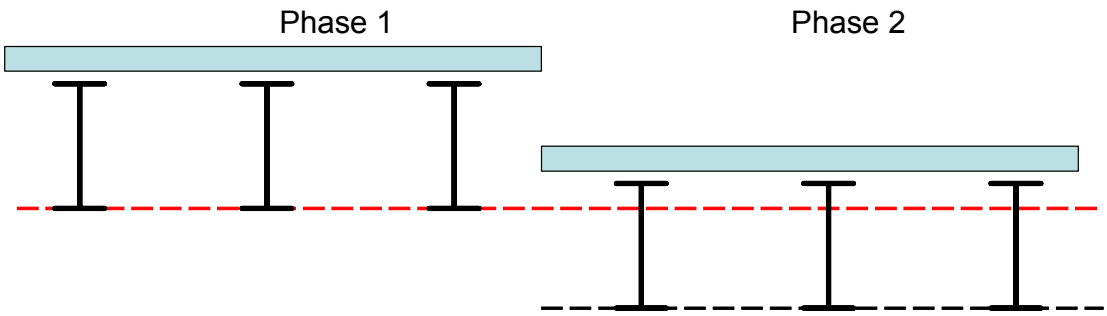

Figure 8-9: Differential Elevation at time of Closure

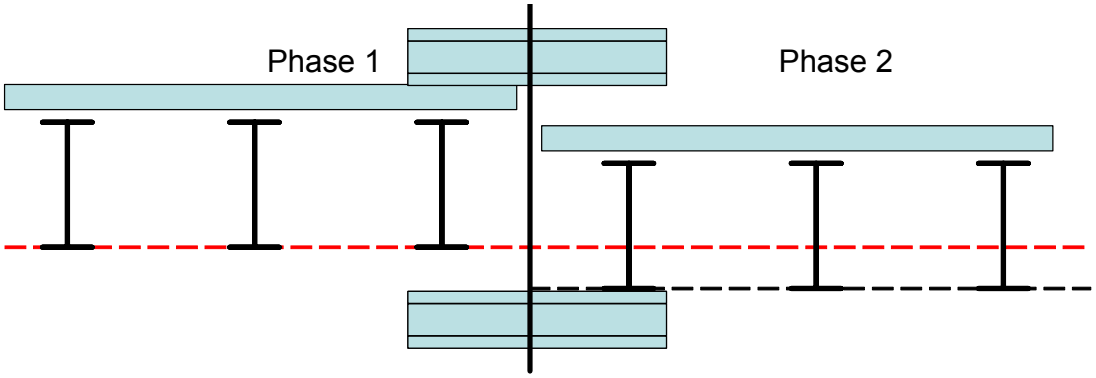

Figure 8-10: Jacking Beams in Place (Scale is Extremely Exaggerated)

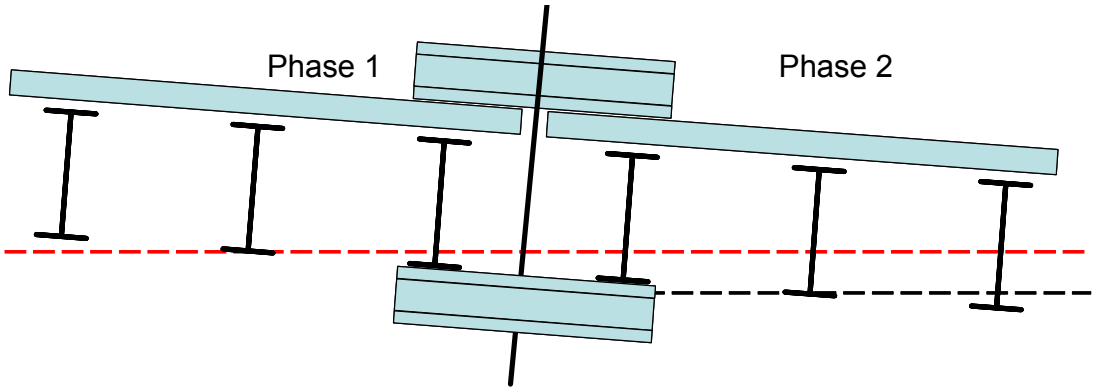

Figure 8-11: Phases after Jacking

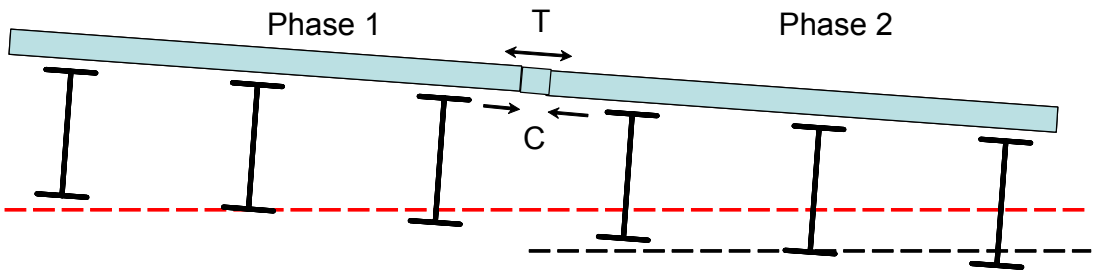

Figure 8-12: Jacks Removed

It was, however, seen that short term deflections can be greatly affected by temperature. This fact can be utilized to develop some very general common sense recommendations which ultimately come down to avoiding critical operations during periods of temperature extremes. These critical operations should not only refer to construction events but also surveying measurements.

8.5 Closure Region

The performance of the closure region is largely dependent on the greater aspects of the project including attainment of the correct elevation at time of closure so that remediation, which tends to lock in stresses, is not necessary and minimizing the additional relative deflection after closure. However, several items which have yet to be addressed are some specific details of performing the closure and the placement of the cross-frames.

8.5.1 Detailing Requirements

There are not a lot of specific details with respect to actually performing the closure except for basic recommendations germane to most quality concrete work. A couple of specific points to note are presented here.

Overlay lapping

To aid in sealing and protecting the longitudinal closure region joints any joints required in placing the overlay should be placed not less than six inches away from the closure region joints.

Shrinkage

An aggravating factor to the premature deterioration of the closure region is the formation of shrinkage cracks after casting. Due to the small dimensions of the closure region the area is sensitive to the bar size chosen for transverse reinforcement. Whenever practical, bar size should be kept to a minimum to reduce the potential for shrinkage cracking.

One suggested alternative which has not been investigated is the addition of some small gauge welded wire reinforcement to the closure region in an attempt to minimize the crack size. The welded wire reinforcement could be placed in lieu of or in addition to the required reinforcement.

8.5.2 Cross frames

There are a number of considerations with respect to the treatment of cross-frames in phased construction, both practical and theoretical. The biggest question about cross-frames is when they should be placed.

Prior to Second Phase Deck Pour

Should it become absolutely necessary to construct a phased construction bridge with an asymmetric second phase placement of cross frames prior to the second phase deck pour can help to reduce the torsional deformation experienced. This situation can also occur during widening projects

The amount of deflection expected from all but the shortest of bridges would require unacceptably long slotted holes should a fully rigid brace be in place during the second phase deck pour. However, several states are reportedly utilizing a partial bracing system whereby the horizontal struts are placed prior to the second phase pour. After the pour is completed the remaining diagonals of the braces are installed.

This option requires a careful analysis of the fit up conditions and tolerances since factors such as camber and dead load deflection can cause misalignment of holes requiring custom dimensioned frames per location. In general, placement of cross frames prior to the second phase deck pour should be avoided. Additional information can be found in, *Constructibility Issues with Widened and Stage Constructed Steel Plate Girder Bridges* (Swett, 1998).

Prior to Closure Region Pour

During the construction of the Dodge Street Bridge over I-480 only a small number of cross frames were placed after the second phase was finished and prior to the placement of the closure region. This was due to the fact that the differential elevation at time of clousure was so great that the pre-drilled holes in the stiffener assemblies did not align correctly. This is a scenario likely to repeat itself often in phased construction regardless of when the cross frames are placed. The only sure method around such a situation is to wait until both phases are completed prior to drilling the holes in the cross-frames. The simplest method of accomlishing this is to drill the holes on one side of the frame assembly and leave the other side blank to be field drilled.

After Closure

The performance of the closure pour is the trigger for a flurry of various tasks to finalize a project and it is therefore desirable to minimize the delays in its completion. For this reason, it is often desirable to perform the time consuming task of field drilling and final assembly of the cross frames after the closure has been made.

The main concern in this situation is that there will be a period of time when the bridge is open to traffic yet the cross frames will not be in place to aid in the transverse distribution of forces requiring the new concrete in the closure region to perform this task on its own. One suggestion to minimize the potential detriment this traffic may have on the is to limit the speedlimit on the bridge until the cross frames have been installed. This should not be much of problem since the speeds are often already reduced through construction zones.

Chapter

9 Transverse Analysis Programs

Development and Verification of Analysis Programs

Due to the nature of phased construction, the two phases will not behave the same over time. This can be attributed to both predictable and unpredictable mechanisms. Predictable mechanisms include creep and shrinkage effects and the fact that most of these effects in the first phase will be finished at the time of closure while they will be very active within the second phase at time of closure. Unpredictable mechanisms can include change in end restraint condition over time due to soil compaction, and difference in construction details between phases. Most often these changes are not necessarily done on purpose. However, differences due to changes in construction sequencing or work required on adjacent portions of the overall project can affect the relative performance of the phases.

To aid the engineer in dealing with these differential behaviors three programs were developed.

ADSTRESS
The differing behavior between the two phases will result in deformations which will be restrained to some degree by the interconnectivity between the two phases. It is the goal of this program to predict the magnitude of the stresses in the deck which will arise due to this restraint.

BALLAST
Despite the best efforts of both the engineers and contractors differential elevations at the time of closure can exist. As mentioned previously, one method for dealing with this situation is to place ballast on the phase that is too high. This program predicts the edge deflection due to a strip of ballast placed at any transverse location.

OVERLAY
To obtain the correct profile for both ride comfort and safety a non-uniform overlay may be required to cover up the differential elevations of the phases. This program predicts the stresses in the slab and the final profile of the bridge due to this loading condition.

9.1 PROGRAM DEVELOPMENT

Most of the problems encountered using phase construction occur near mid span where the deflections are the greatest. Elevation differential near the supports can usually be attributed to construction error and can be addressed through inspection and control. However, differential elevation near mid span can be difficult to predict.

Near mid span, concrete slab on steel girder bridges can be analyzed transversely on a strip wise basis as a beam on discrete elastic foundations. An example is shown in Figure 9-1. This is equivalent to saying that near mid span, the bridge responds to longitudinally distributed transverse loads as

though it were infinitely long. This approximation is suitable for long span bridges and a correction factor can be obtained for medium span bridges as well. Since the potential for problems due to phase construction increases as the span length increases, this approximation is justified. An important point to remember in evaluating these approximations is that the predicted value of the differential deflection and other input values are not very precise. For this reason, the approximations utilized provide sufficiently accurate results.

This concept has been implemented in a finite element code allowing for the quick and simple analysis of a number of situations..

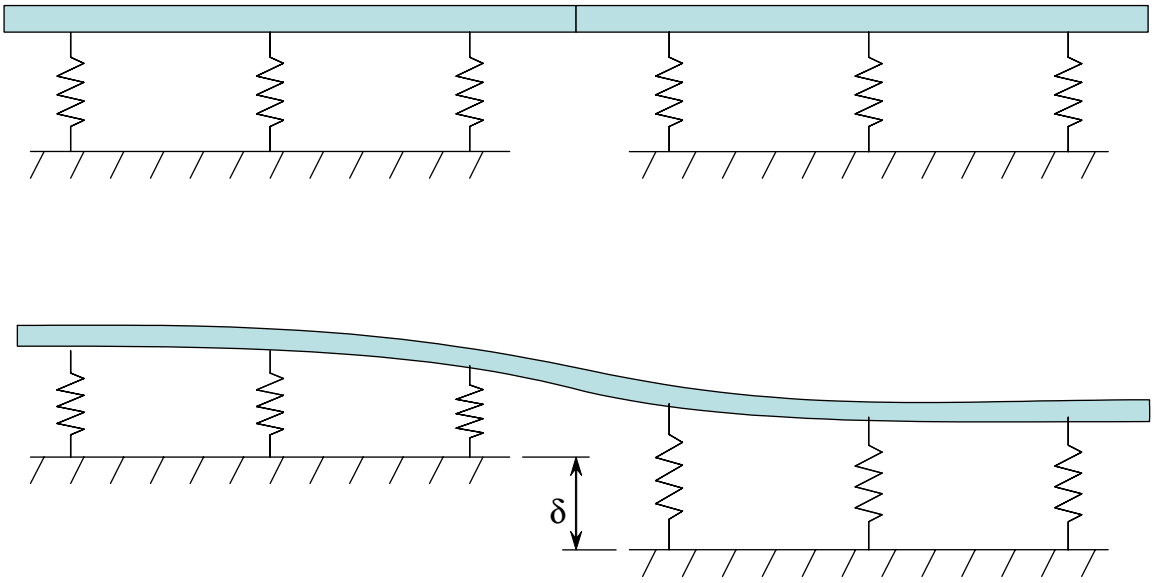

Figure 9-1: Support Settlement of Beam on Discrete Elastic Foundations

9.2 PROGRAM USAGE

This section details the use of each of the programs. The interface is similar for each as are the physical constants.

ADSTRESS

Figure 9-2 shows the input form for the program. Due to the presence of empirical factors within the program units of kips and inches are strictly required. Input of the geometry is straight forward. Concrete strength is

used both to evaluate the magnitude of stresses and to calculate the elastic modulus of the concrete using Equation 9-1. If it is desired to use a specific value for elastic modulus the appropriate strength can be back calculated and input for the analysis then comparing the resulting stress with the true strength. The spring constant for the girders may either be calculated from the dead load deflection due to the given applied dead load or input directly. When the spring constant is input directly, no correction is made with respect to span length as discussed in the conclusion section of this chapter. The final piece of information required is the anticipated relative displacement. This value can come from a long term deflection analysis such as the one presented in Chapter 6. Alternatively the value could come from past experience or even a simple monitoring of the deflection experienced by the first phase of the project. The use of values obtained from monitoring must be carefully considered due to the effects described in Chapter 7.

$$E_c = 57\sqrt{1000\, f_c'} \tag{9-1}$$

Where

E_c = Elastic modulus of concrete (ksi)

f'_c = Concrete Strength (ksi)

The resulting predicted maximum stress is calculated and displayed in the appropriate box. If the maximum stress is above 50 percent of the rupture strength of the concrete a message to that effect is displayed.

BALLAST

Figure 9-3 shows the input form for the program. Due to the presence of empirical factors within the program units of kips and inches are strictly required. Input of the geometry is straight forward and similar to the input for ADSTRESS. The overhang distance is the distance from the girder nearest the closure region to the edge of the slab. The load location is measured from the girder nearest the closure region with a positive value indicating

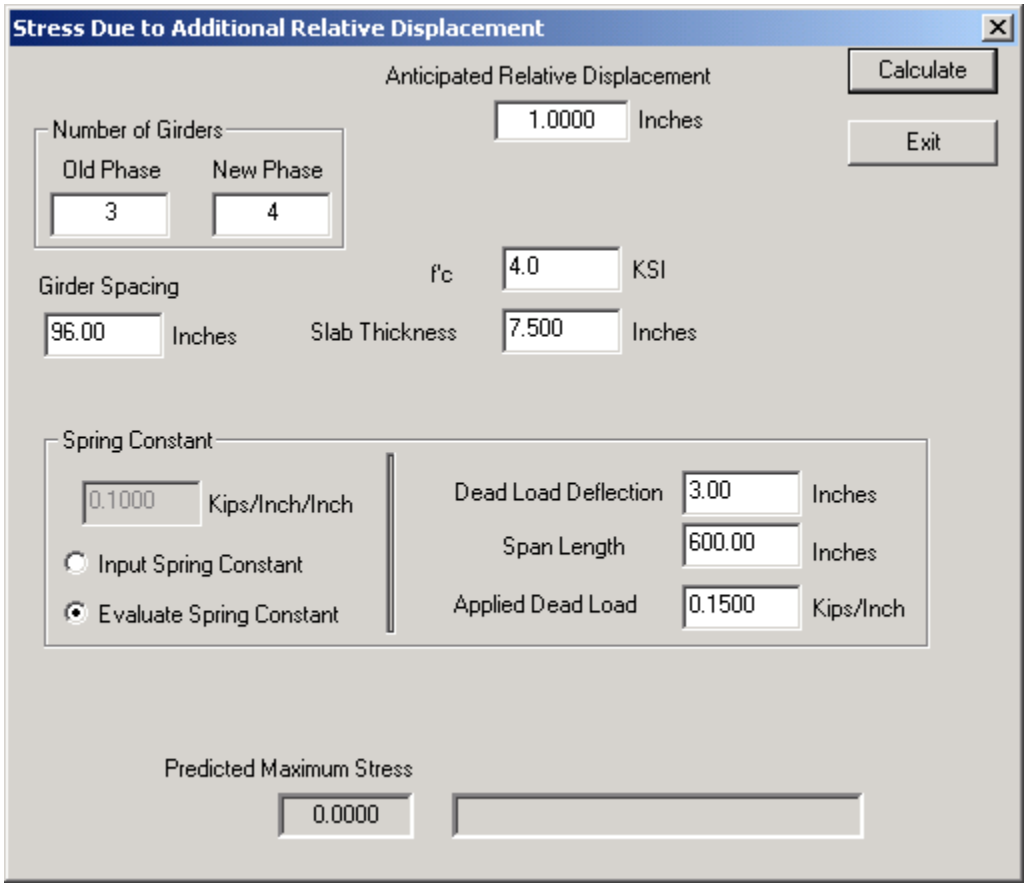

Figure 9-2: ADSTRESS Program Input Dialog

the load being placed between the girder and the edge of the slab. The spring constant for the girders may either be calculated from the dead load deflection due to the given applied dead load or input directly. When the spring constant is input directly, no correction is made to the resulting predicted deflections.

OVERLAY

Figure 9-4 shows the input form for the program. Due to the presence of empirical factors within the program units of kips and inches are strictly required. Input of the geometry is straight forward and similar to the input for ADSTRESS. The overhang distance is the distance from the exterior girder to the edge of the slab on each side. The overlay profile is given as a series of breakpoints with a linear profile assumed between points. The minimum number of points is therefore two, one for each edge of the slab.

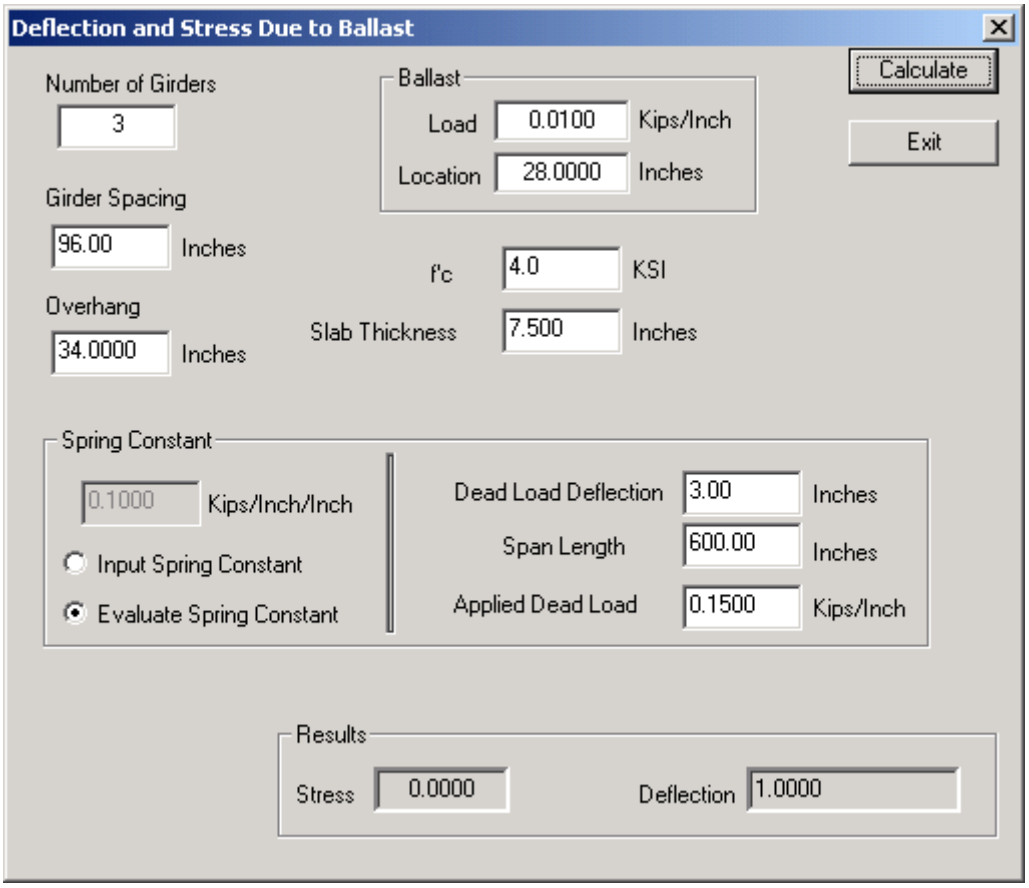

Figure 9-3: BALLAST Program Input Dialog

Location is measure from the left edge of the slab. The spring constant for the girders may either be calculated from the dead load deflection due to the given applied dead load or input directly. Upon calculating the results a profile box appears allowing one to copy the values to be placed into another application. Alternatively the user may plot the profile within the program, however, this feature is limited.

9.3 VERIFICATION

To verify the results obtained from the analysis program a finite element study was performed utilizing ANSYS. The analysis modeled a simply supported single span bridge constructed using phased construction. The girders were modeled using a seven degree of freedom per node offset beam element capable of modeling the warping torsion of open sections.

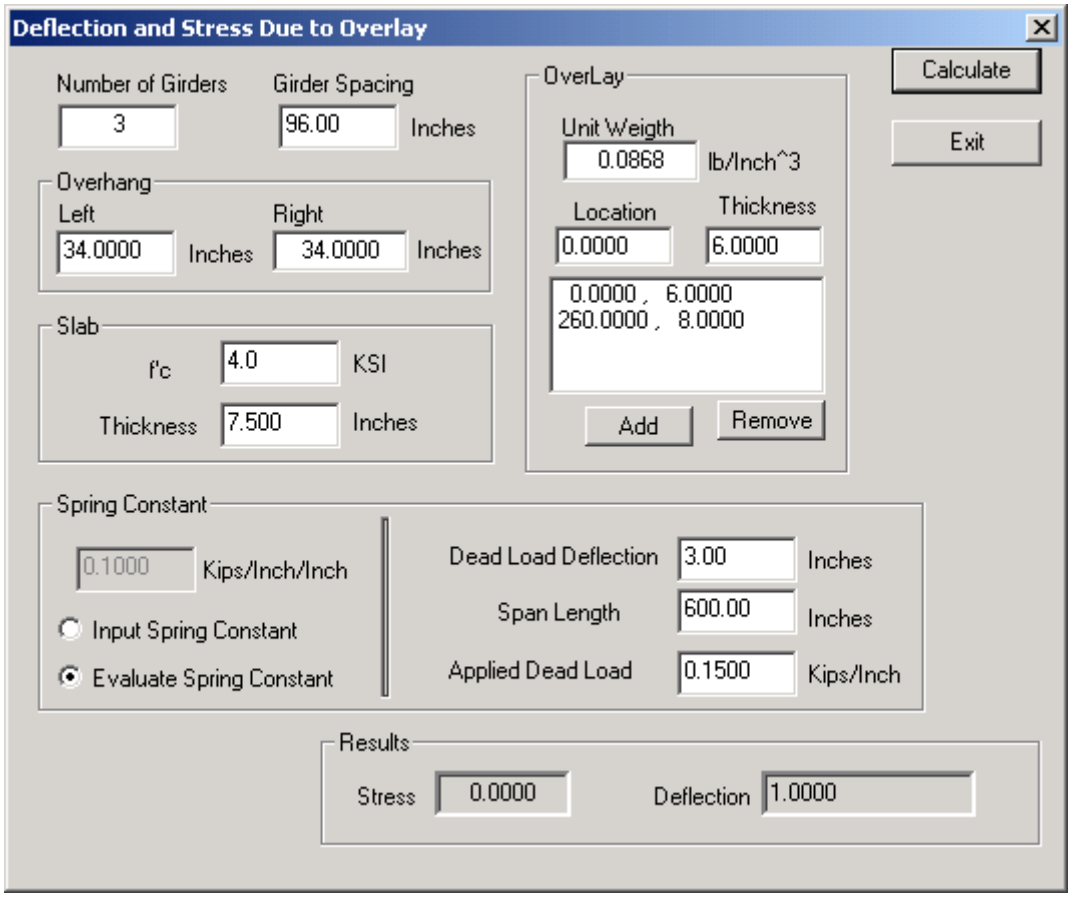

Figure 9-4: OVERLAY Program Input Dialog

The deck was modeled using four node shell elements. Linear elastic material properties were assumed throughout. Figure 9-5 shows a typical model. Note that the beam element used is actually a line element, however, section properties must be input to account for warping torsion and these section properties are used to generate the three dimensional figure shown.

The loading was applied as a line load of the girders in two stages. The first stage applies equal load over all girders of both phases to obtain the uniform bridge response. This is needed to determine the girder spring constant (k_s). The second stage applied loading to the girders of only one phase simulating the anticipated differential settlement. The magnitude of load applied is that magnitude as determined from the first loading stage

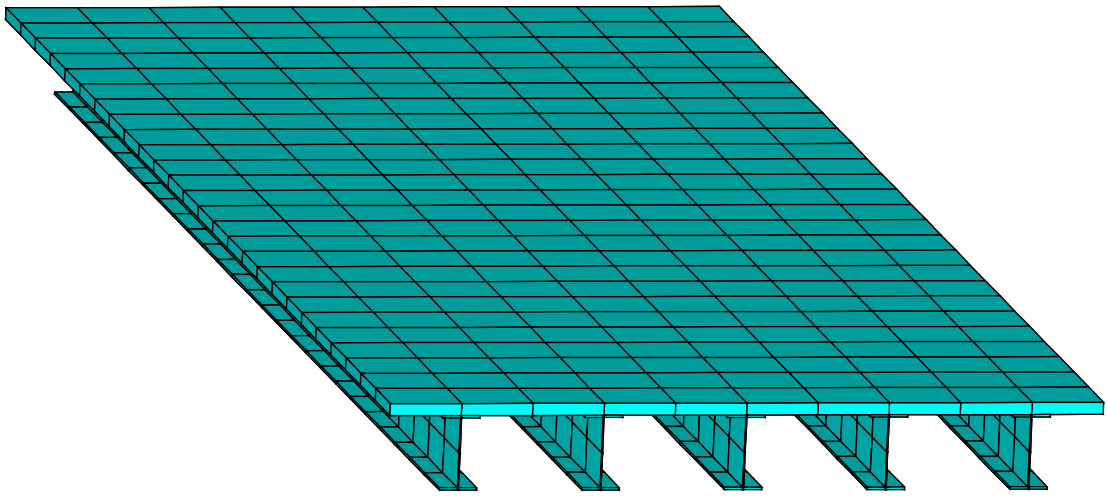

Figure 9-5: Typical Finite Element Model

which is required to obtain a unit deflection. From this loading the maximum observed stress was recorded.

Once these values were obtained the girder spring constant and bridge geometry were used as input to the program under development. The predicted stresses from the simplified analysis were compared with the results from the finite element results. As was expected, the simplified analysis did not compare well with the finite element results. However, it was observed that the discrepancy was predictable and dependent upon geometric considerations. Therefore, an equation was developed to produce very good results. The details of this calibration will be presented in Section 9.3.2.

9.3.1 Development of analysis suite

The basic suite of geometric factors are the same for all of the programs. The details of the selection process is provided in this section

The input parameters required for the simplified analysis are:

- Spring Constant
- Slab Thickness
- Girder Spacing
- Phasing Plan (# of Girders in each phase)
- Concrete Modulus of Elasticity

Note that the spring constant is a composite parameter representing the stiffness of a steel girder with accompanying slab, therefore, additional information is needed. These additional parameters for finite element model are:

- Girder Cross Section Dimensions
- Girder Length

Some very simple assumptions were utilized to develop the cross sections for analysis. The validity of these methods was largely proven by the results themselves. As will be discussed in later sections, the methods for choosing the additional parameters had no effect on the results.

The first three assumptions deal with the proportioning of the steel girder itself. First, the steel section is assumed to be symmetric. Second, the depth of the girder is assumed to two times the width of the flanges. And third, the area of the web is assumed to be 30 percent of the gross steel area. These three assumptions lead to Equation 9-2.

$$t_w = \frac{15 t_f}{35} \tag{9-2}$$

Where

t_w = Web thickness

t_f = Flange thickness

Ignoring bending of the flanges the moment of inertia is equal to:

$$I = \frac{t_w D^3}{12} + 2\left(\frac{D}{2}\right)^2 b_f t_f \tag{9-3}$$

Where

I = Moment of Inertia of steel girder

D = Depth of steel girder

b_f = Flange width

Using the previously defined relations and solving for t_f yields:

$$t_f = \frac{7I}{2D^3} \tag{9-4}$$

Due to various structural and economical considerations, the deflection observed during the placement of concrete deck will fall within certain limits which are closely related to the length of the beam. Therefore, this predictable deflection will be used to determine the moment of the inertia for the beam from. In order to account for variability in the stiffness of the girder, this predictable deflection was multiplied by a scale factor. This scale factor was one of the values varied in the parametric study. The deflection of a simple beam due to a uniform load is give by Equation 9-5.

$$\Delta_{dl} = \frac{5wL^4}{384EI} \tag{9-5}$$

Where

Δ_{dl} = Deflection due to Dead Load

w = applied load per unit length

E = Modulus of Elasticity

The weight due to the concrete placement is known to be:

$$w = \frac{0.150}{12^3} s\, t_s \tag{9-6}$$

Where

s = Girder Spacing

t_s = Slab Thickness

Therefore:

$$I = \frac{0.15}{12^3} \frac{5 s\, t_s\, L^4}{384 E\, \Delta_{dl}} \tag{9-7}$$

At this point, two values remain unknown. They are the girder depth and the dead load deflection due to the deck placement. For economically designed bridges, both of these variables tend to vary with span length. Therefore, to obtain this relation, typical values for several span lengths were obtained from existing bridge designs and a curve was fit through the them to obtain the remaining points. The resulting equations are 9-8 and 9-9 for girder depth and dead load deflection respectively. Table 9-1 shows the assumptions and the subsequent predicted values using the equations It should be noted that due to the origin and form of the equations they are valid only for the range under consideration.

$$D = \frac{L^{0.6}}{1.4} \tag{9-8}$$

$$\Delta_{dl} = 6.1\, Ln(L) - 34 \tag{9-9}$$

	Web Depth		Deflection	
Span	**Assumed**	**Calculated**	**Assumed**	**Calculated**
300	20	21.9	1	0.79
1200	48	50.3	9	9.25
2400	72	76.2	14	13.5

Table 9-1: Assumed Web Depth and Dead Load Deflections (inches)

The number of girders was allowed to vary from two to five in each phase. Note that a N1/N2 bridge gives the same result as a N2/N1 bridge. This duplication was therefore eliminated from the study. The length was allowed to vary from 25' to 250' in 25' increments. Three girder spacings were considered: 72", 96", and 120". The predicted dead load deflection used to determine girder stiffness was factored by the values 0.25, 0.65, 1.0, and 1.5. Finally, slab thicknesses of 6" and 8" were considered. The total number of cases analyzed therefore was 2400.

9.3.2 RESULTS

The results and calibration for each of the programs is provided in the following sections

ADSTRESS

Despite all of the variability considered, it was determined the following equation was adequate to correct the results obtained from the simplified analysis.

$$\frac{S_{Act}}{S_{Simp}} = 0.8 + \frac{1}{L}\left(180 + \frac{25}{S_{Simp}}\right) \tag{9-10}$$

Where

S_{Act} = Maximum Stress obtained from FEM analysis

S_{Simp} = Maximum Stress obtained from simplified analysis (program)

L = Span Length

Figures 9-6 and 9-7 show the predicted actual stress given the simplified stress before and after the correction factor respectively.

This correction has been coded into the ADSTRESS program.

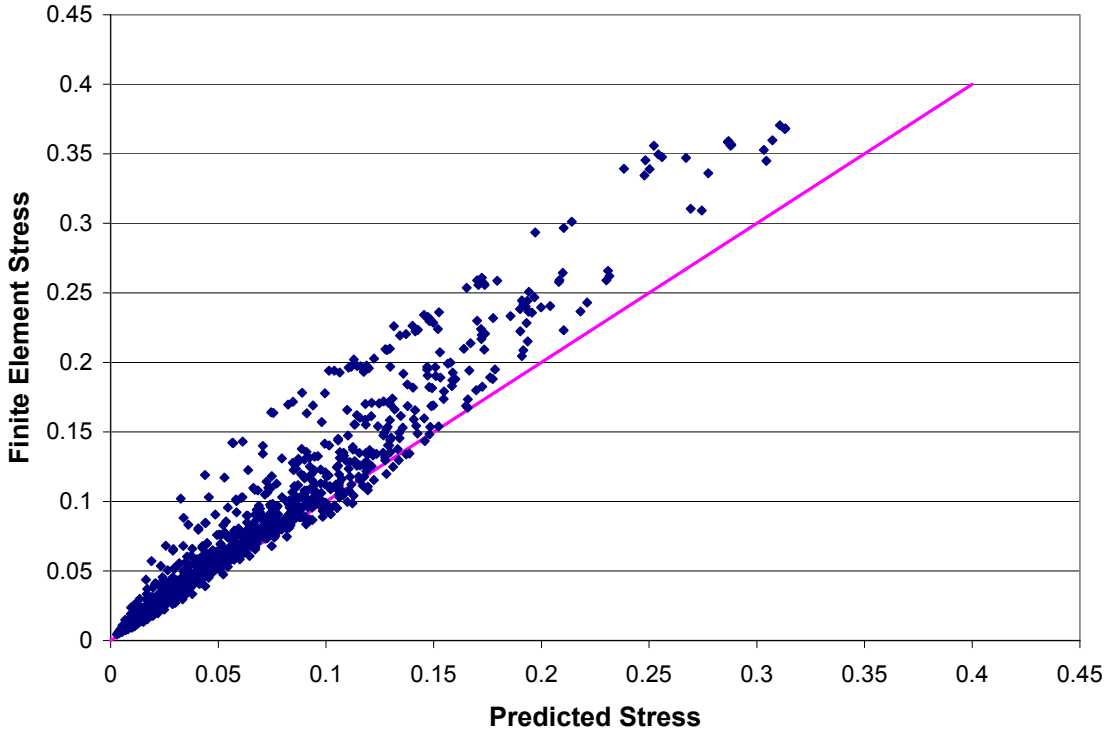

Figure 9-6: Resulting Finite Element Stress versus Predicted Stress

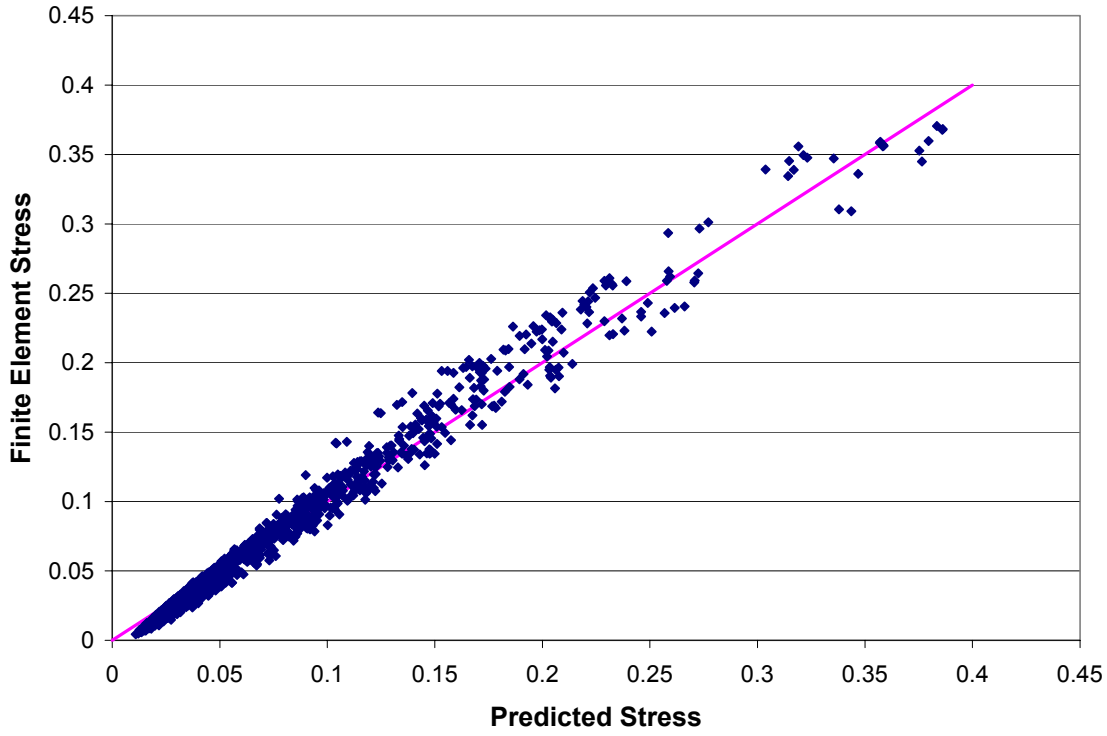

Figure 9-7: Finite Element Stress Versus Corrected Predicted Stress

BALLAST

Preliminary results showed that deck thickness appeared to have a greater impact of the results than in the ADSTRESS program. Therefore an additional thickness of 10" was included in the study.

Figure 9-8 is a plot showing the actual (FEM) deflection versus the predicted (BALLAST) deflection. Although the results appear quite poor Equation 9-11 provides a good correction to the results as is shown in Figure 9-9.

$$\frac{\delta_{Act}}{\delta_{Simp}} = 0.85 - \frac{t_s}{70}\left(8.35 - NG - \frac{S}{40} - \frac{L}{2000}\right) \qquad (9\text{-}11)$$

Where

δ_{Act} = Deflection obtained from FEM analysis

δ_{Simp} = Deflection obtained from simplified analysis (program)

t_s = Slab Thickness

S = Girder Spacing

NG = Number of Girders

L = Span Length

OVERLAY

The shortcomings of the simplified analysis method observed in the previous two sections were due in large part to the fact that the applied loadings were highly eccentric. The variability of the overlay condition, on the other hand, occurs towards the center of the bridge. In this case no modification is required as is shown in Figure 9-10 which plots the actual (FEM) deflection at both edges and center versus the predicted (OVERLAY) results.

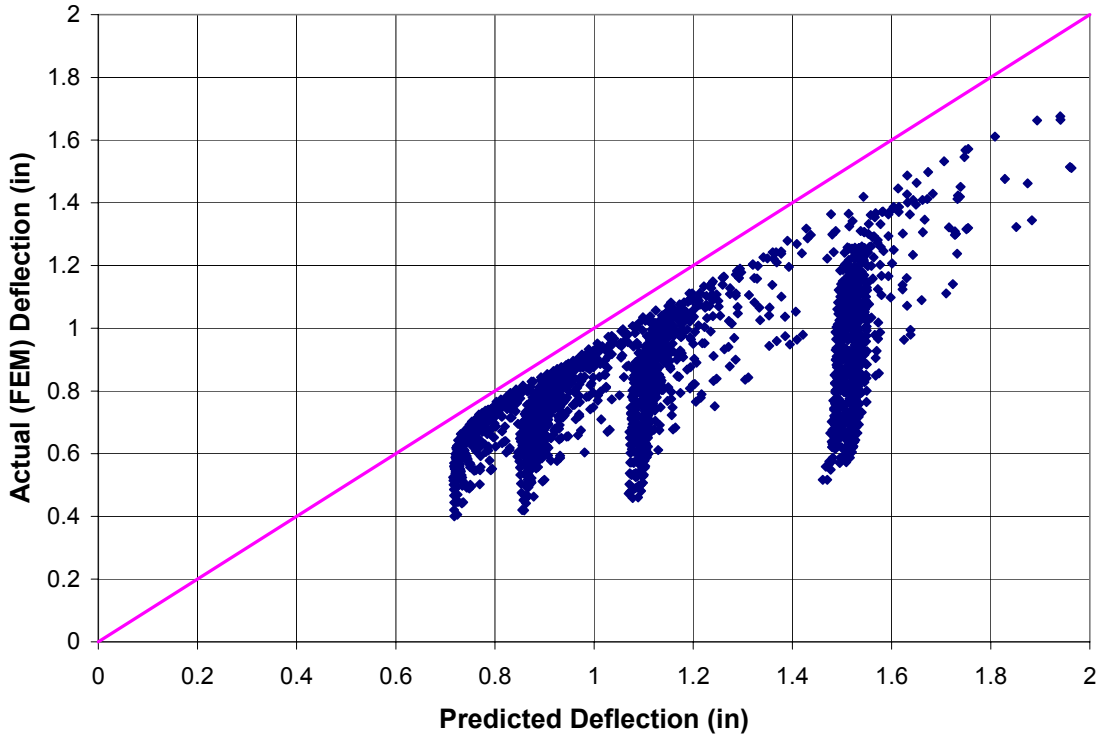

Figure 9-8: Resulting Finite Element Deflection versus Predicted Deflection

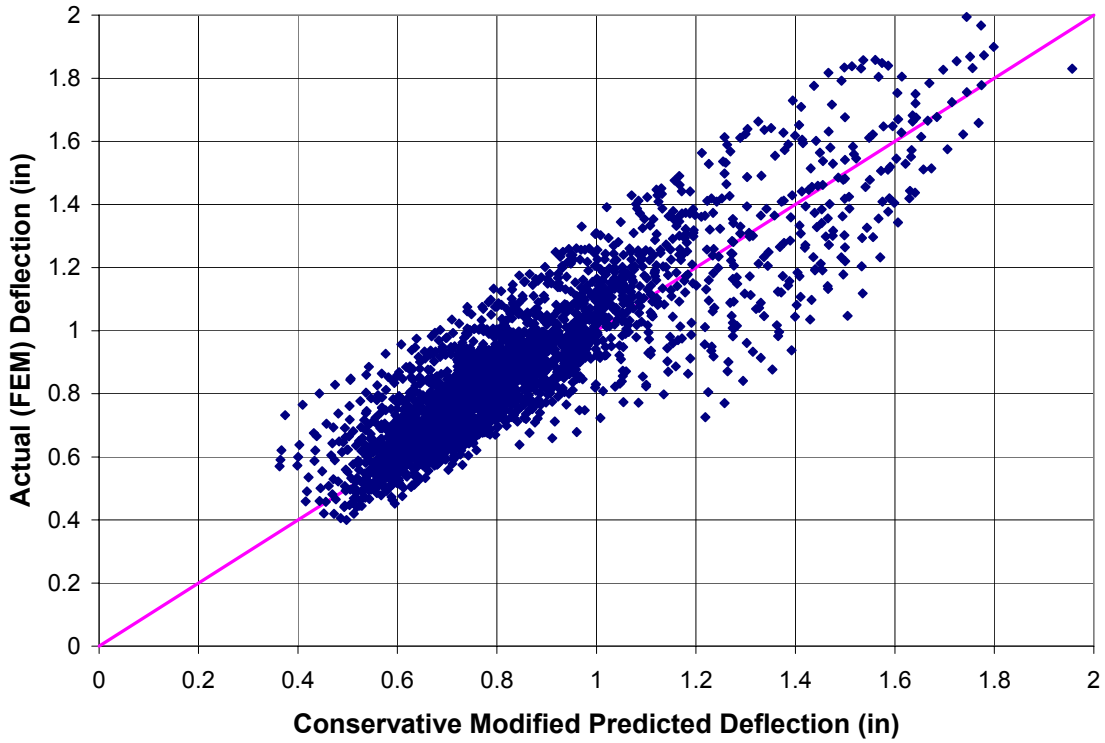

Figure 9-9: Resulting Finite Element Deflection versus Corrected Predicted Deflection

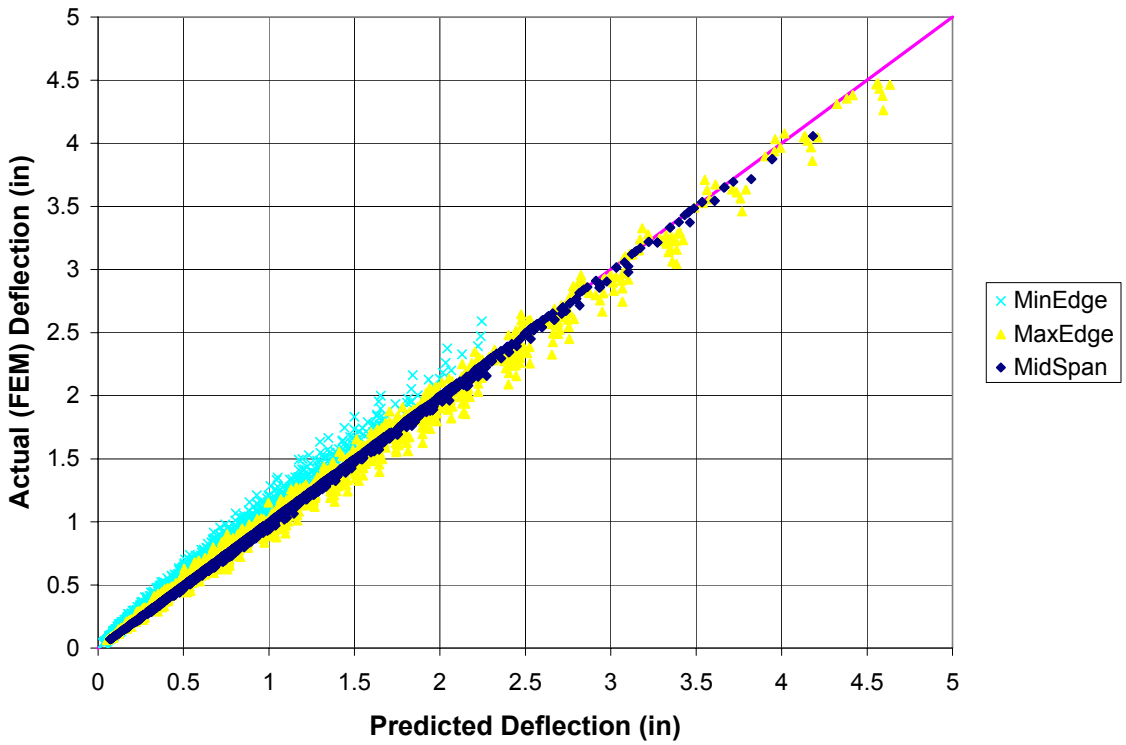

Figure 9-10: Resulting Finite Element Deflection versus Predicted Deflection

Chapter

10 Additional Case Studies

PREVIOUS PROBLEMS WITH PHASED CONSTRUCTION

The University of Nebraska-Lincoln has previously been consulted by the Nebraska Department of Roads on a couple of other projects involving phased construction. These are referred to as the Hay Spring to Rushville Bridge and the Snyder South Bridge. Each of these bridges had some particular problems during construction from which several lessons were learned. Therefore, a brief description and results are included here.

10.1 HAY SPRING TO RUSHVILLE BRIDGE

During the construction of a bridge using phased construction on Highway 20 between Hay Springs and Rushville a very large differential elevation at the time of closure was observed.

10.1.1 Bridge Description

The bridge was constructed using phased construction with two girders utilized in phase 1 and numbered from the exterior 1 and 2. The second phase contained three girders numbered 3, 4, and 5 continuing from the interior to the exterior.

10.1.2 Construction Stages

Different construction stages of the Hay Springs to Rushville Bridge, which are considered in the following numerical model, are explained below.

Stage #1 In this stage, the first two girders are installed and the dead weight of the girders is activated.

Stage #2 In this stage, the turndown and bent plates are installed first, and then the weight of the fresh concrete over the two girders is activated.

Stage #3 In this stage, the concrete is hardened and full composite action between steel and concrete is enforced.

Stage #4 In this stage, weight of the north curb and temporary jersey is applied.

Stage #5 In this stage, three additional girders are installed and the dead weight of the new girders is activated.

Stage #6 In this stage, the turndown and bent plates are installed first, and then the weight of the fresh concrete over the new three girders is activated.

Stage #7 In this stage, the concrete cast on three additional girders is hardened and full composite action between the steel and concrete is enforced.

Stage #8 In this stage, weight of the south curb is applied, and the location of the temporary Jersey is changed.

10.1.3 Analysis Overview

To investigate the deflection of different girders in different construction phases of the Hay Springs to Rushville Bridge, a numerical study using the finite element method is conducted. ADINA 6.1 finite element analysis program is used for conducting the analysis.

FINITE ELEMENT MESH

The finite element meshes, in different construction stages, are shown in Figures 10-1 to 10-6. Four-node isoparametric shell elements are used to model the concrete deck, the webs of girders, and bent plates. Flanges of girders are modeled using two-node three-dimensional Hermitian beam elements with six degrees of freedom per node. Turndowns are modeled using 8-node isoparametric solid finite elements. At all the nodes at which shell elements intersect at an angle, six degrees of freedom per node is considered. Since no stiffness is associated with the rotation normal to the shell mid surface, at all the nodes at which co-planar shell elements connect, the rotation normal to the shell mid surface has been restrained. The beam elements which represent the top flanges of the girders are connected to the shell elements which represent the deck using rigid link elements. This ensures that, for each pair of connected nodes, the nodal rotations are the same and the distance between the connected nodes does not change during the analysis. In constructing the finite element mesh, cambers are considered according to the design specifications.

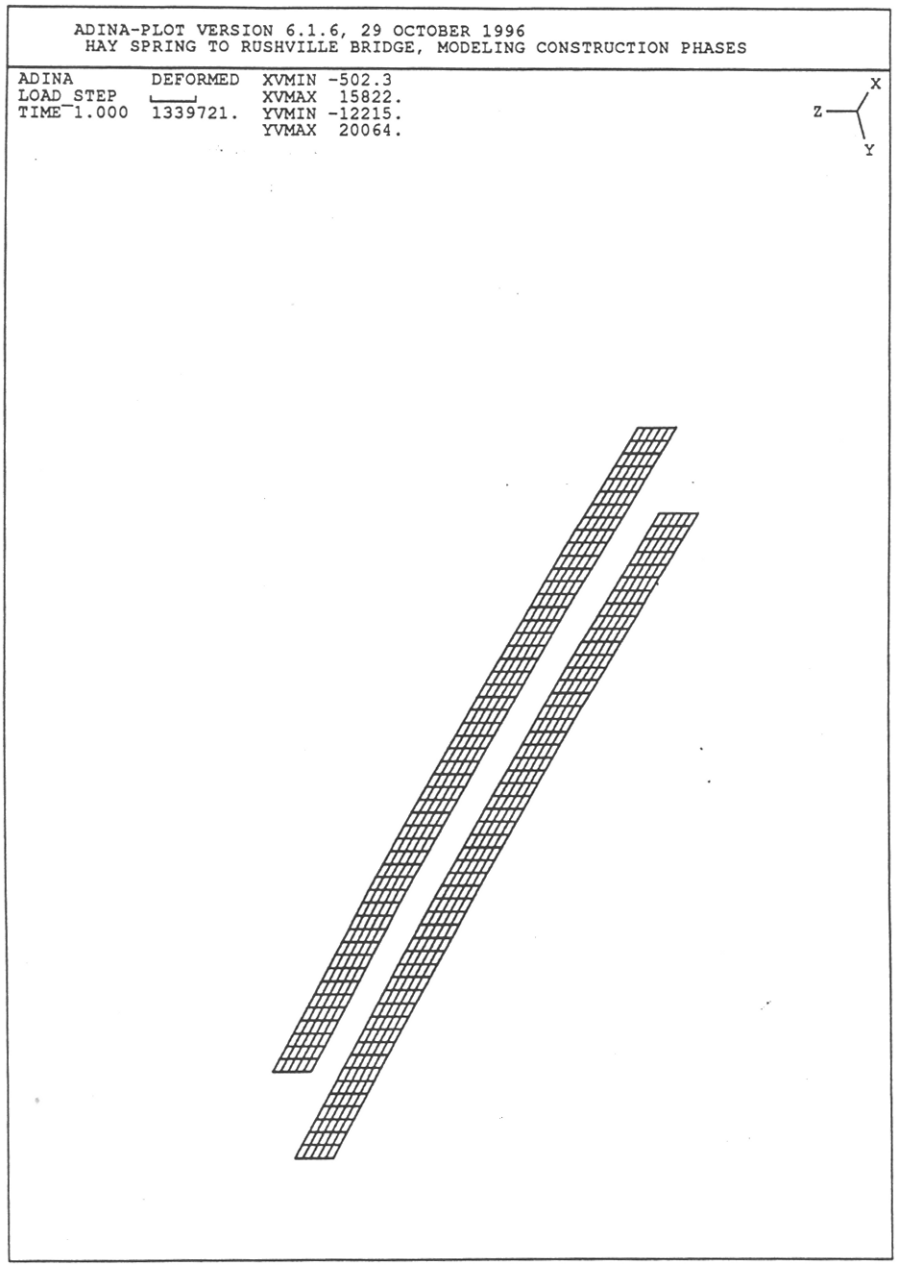

Figure 10-1: Phase 1 Girder Placement

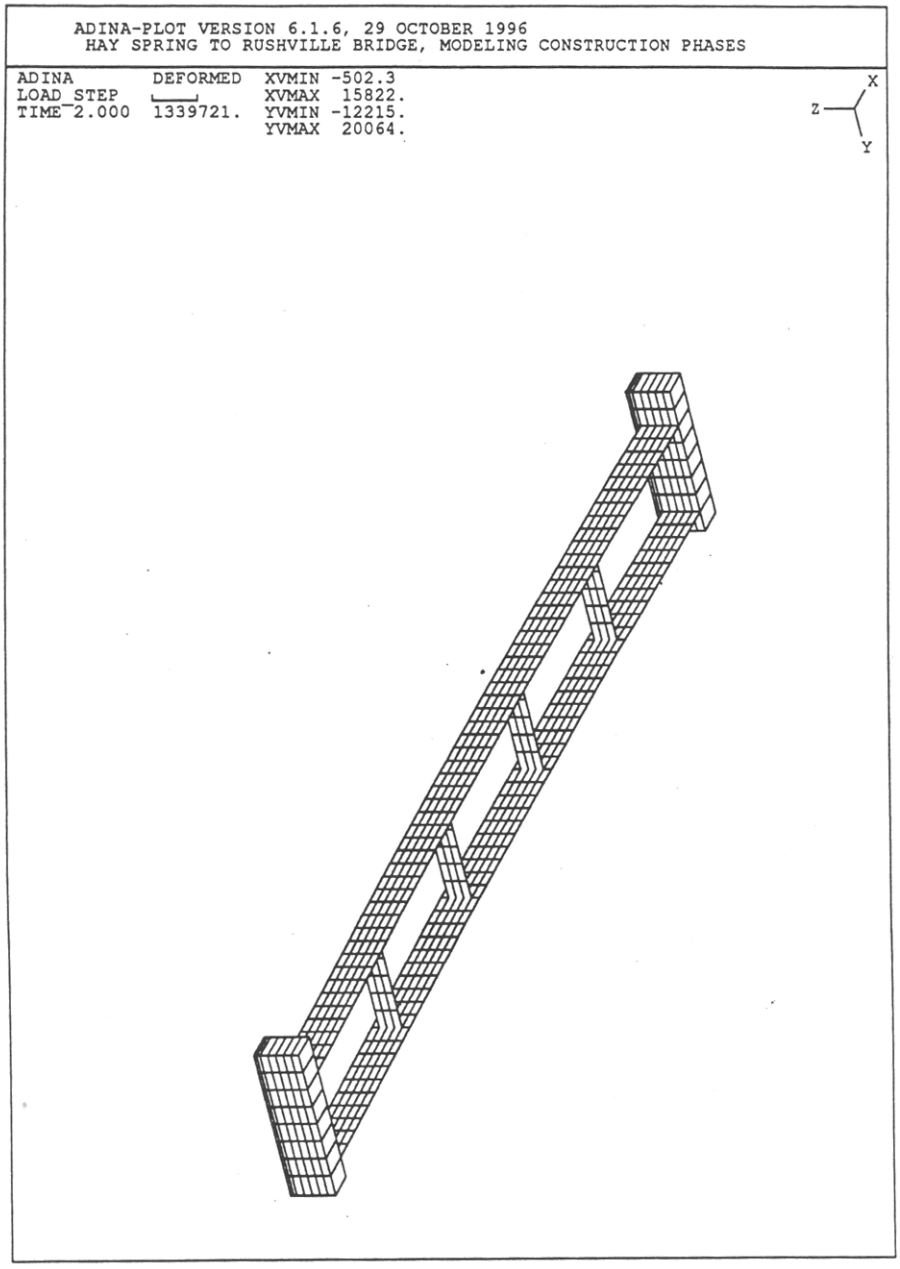

Figure 10-2: Turndown and Separator Plates Installed

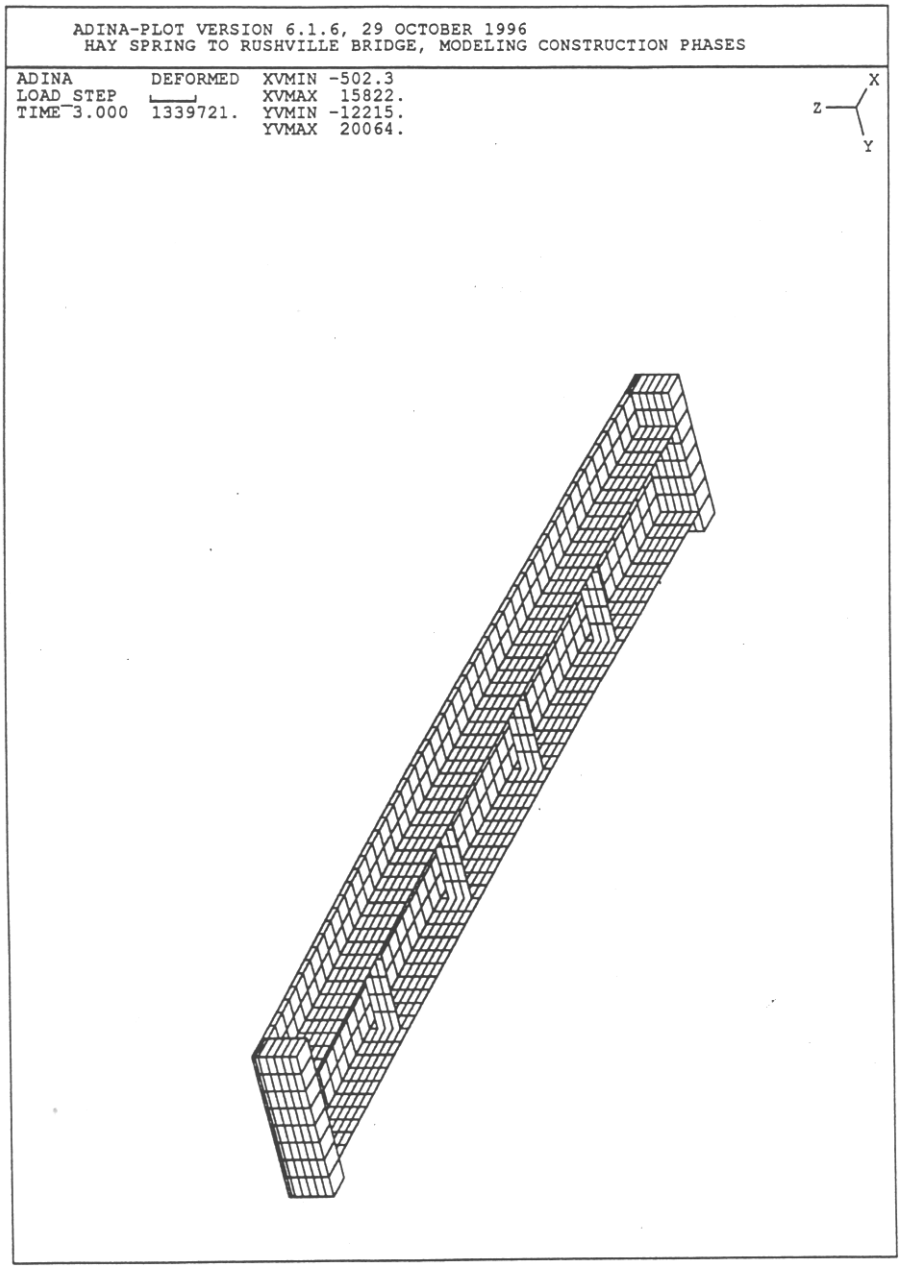

Figure 10-3: Phase 1 Concrete in Place

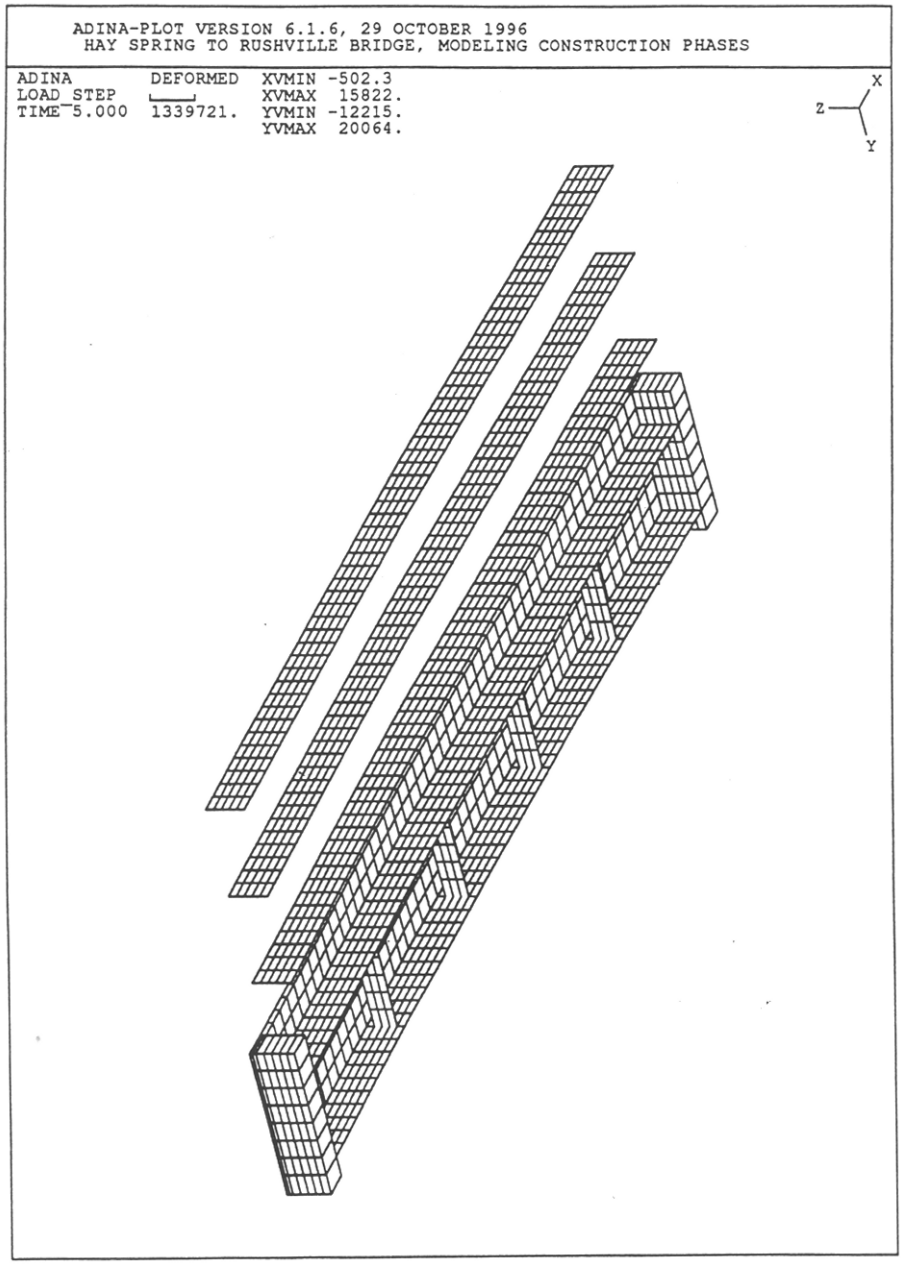

Figure 10-4: Second Phase Girders Placed

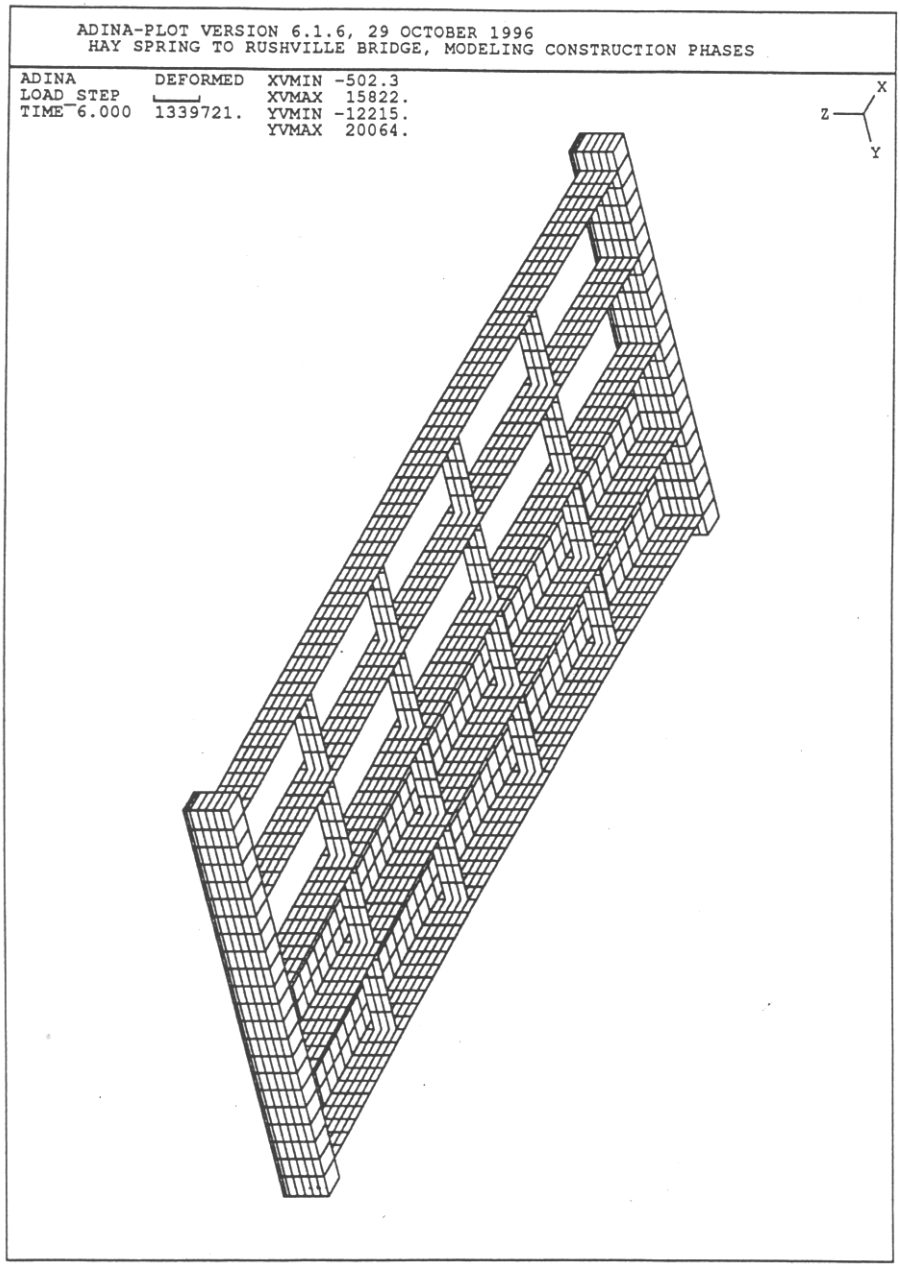

Figure 10-5: Second Phase Turndown and Separators Installed

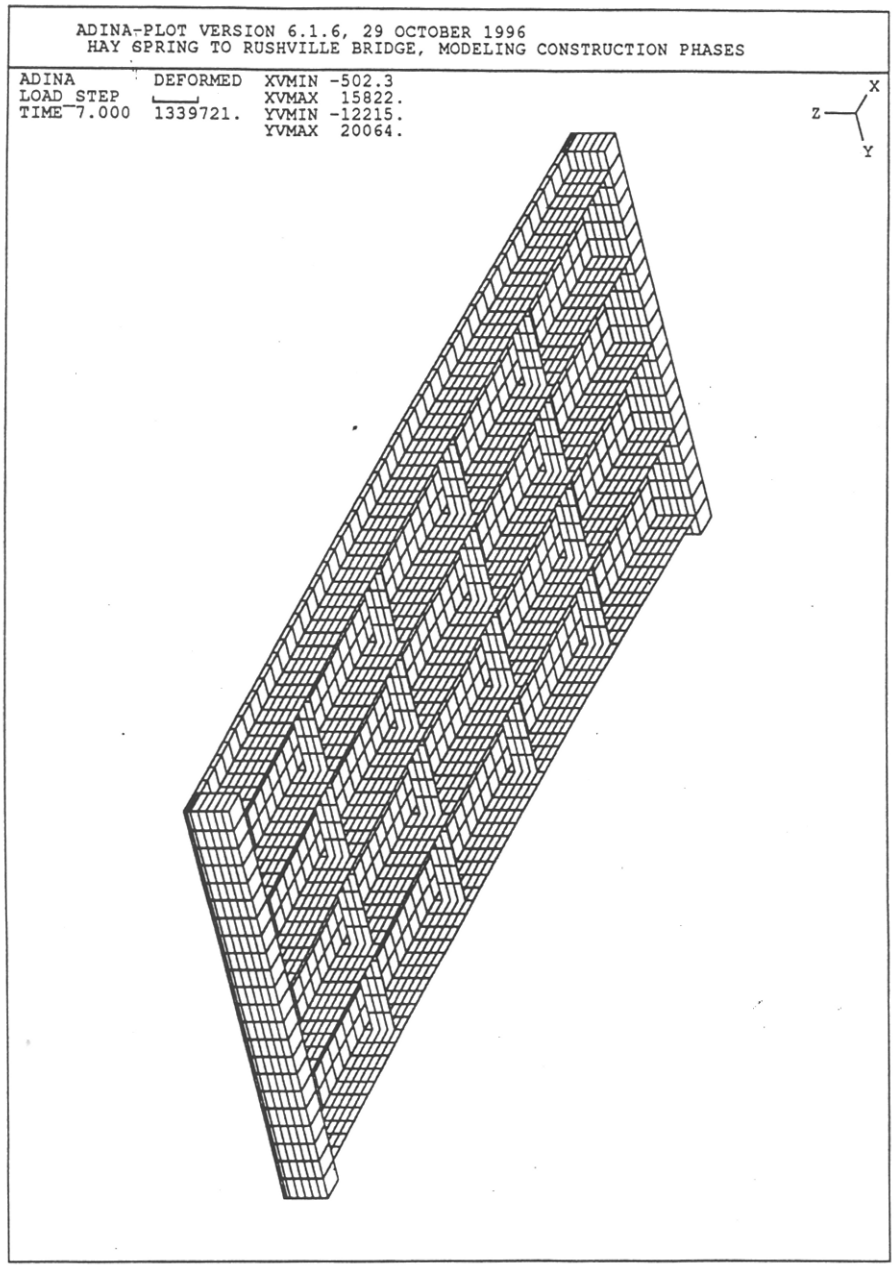

Figure 10-6: Remaining Deck Placed

LOADING AND BOUNDARY CONDITIONS

The boundary conditions of the model are chosen to closely simulate the boundary conditions of the bridge. The nodes located on each support are restrained in all directions but one, which is rotation about the turndown axes. Furthermore, the nodes located on west support are free to translate

in the direction of the bridge. The bridge is subjected to uniformly distributed dead loads, the location and magnitude of which is dependent on the construction stage as explained in Section 10.1.2.

Material Parameters

For the steel girders, an isotropic linearly elastic material model is used, with a modulus of elasticity of 200,000 MPa (29,000 ksi) and a Poisson's ratio of 0.3. For the concrete deck and the turndown, an isotropic linearly elastic material model is used, with a modulus of elasticity of 25,900 MPa (3,750 ksi) and a Poisson's ratio of 0. 175.

Solution Scheme

ADINA6.1 finite element analysis program is capable of simulating the construction stages in a single run. This is utilized for conducting the analysis. The member generation and load application is in accordance with different construction phases as explained in Section 10.1.2.

10.1.4 Numerical Results

For different girders, the girder deflection at mid span versus construction stage curves are shown in Figures 10-7 to 10-11. For different girders, the girder deflection at mid span versus construction stage is also tabulated in Table 10-1. For all girders, the girder deflection at mid span versus construction stage curve is compared in Figure 10-12. As shown in these figures, the deflection at mid span of the first two girders, which were installed in the first construction phase, is almost twice the deflection at mid span of the three girders which were installed in the second construction phase. The prime reason for this behavior is attributed to restraint provided by the turndown for the girders placed in phase II of construction. This problem could be eliminated by providing construction joints in the turndown, separating the end structure for the phase I and II portions of the bridge.

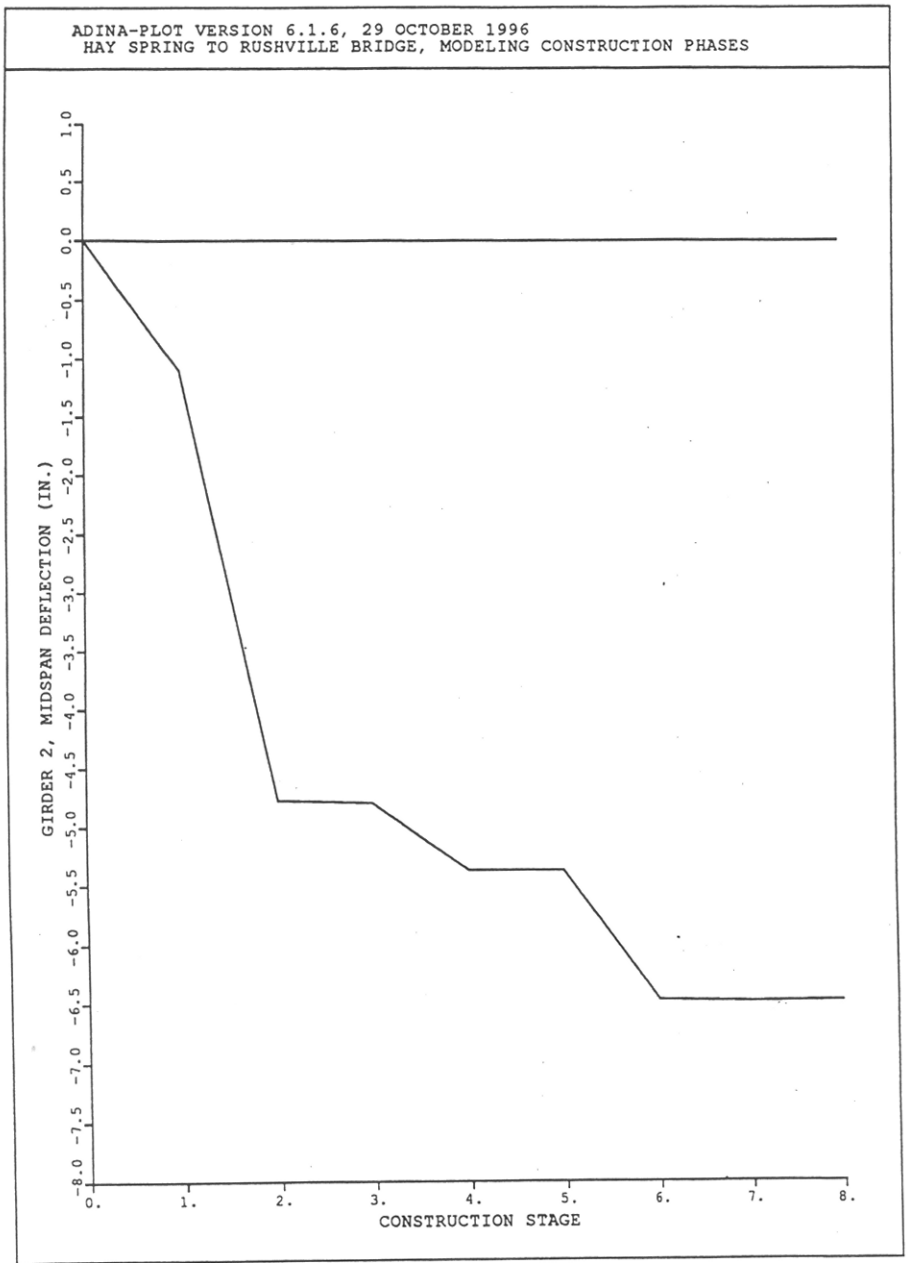

Figure 10-7: Girder #2 Mid span Deflection

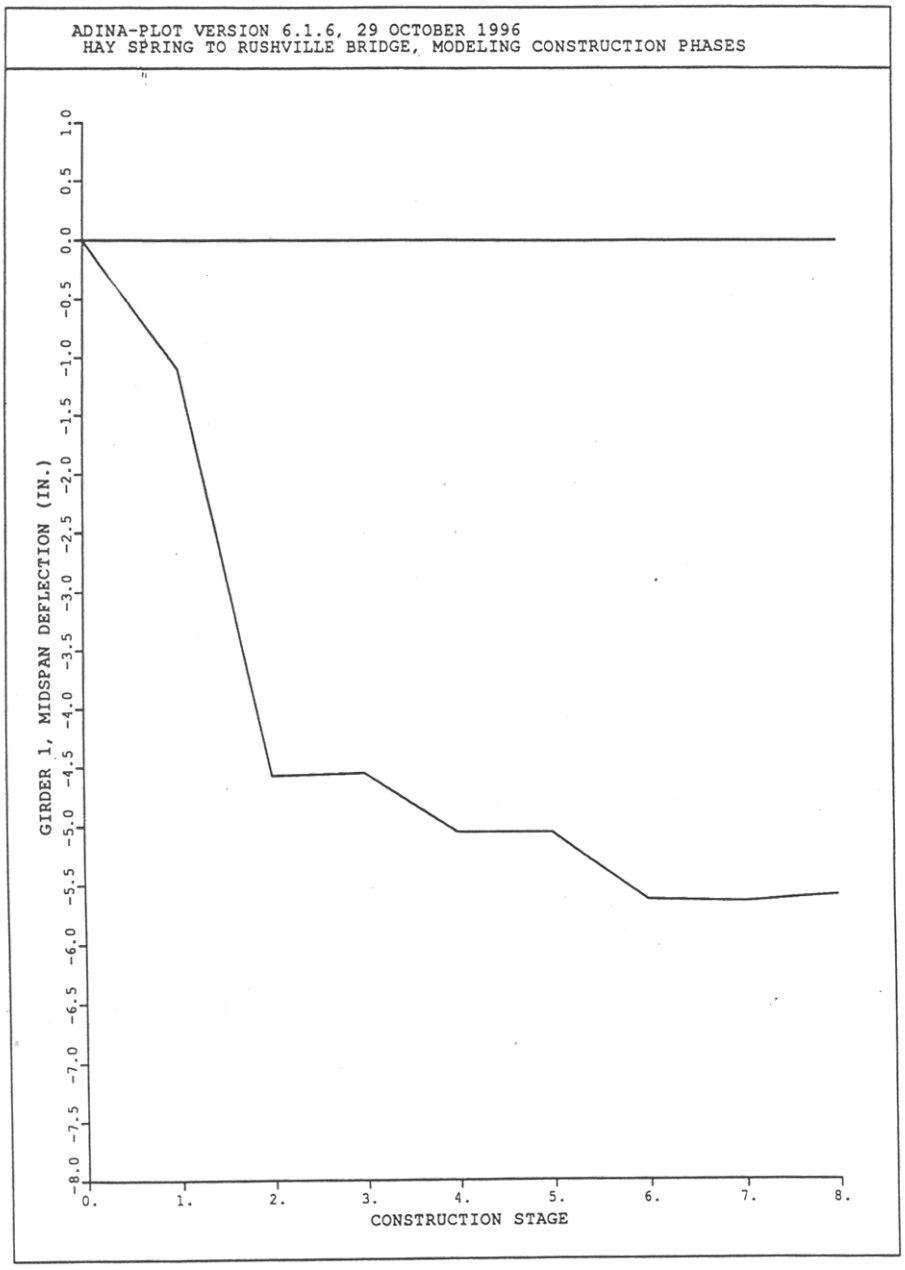

Figure 10-8: Girder #1 Mid span Deflection

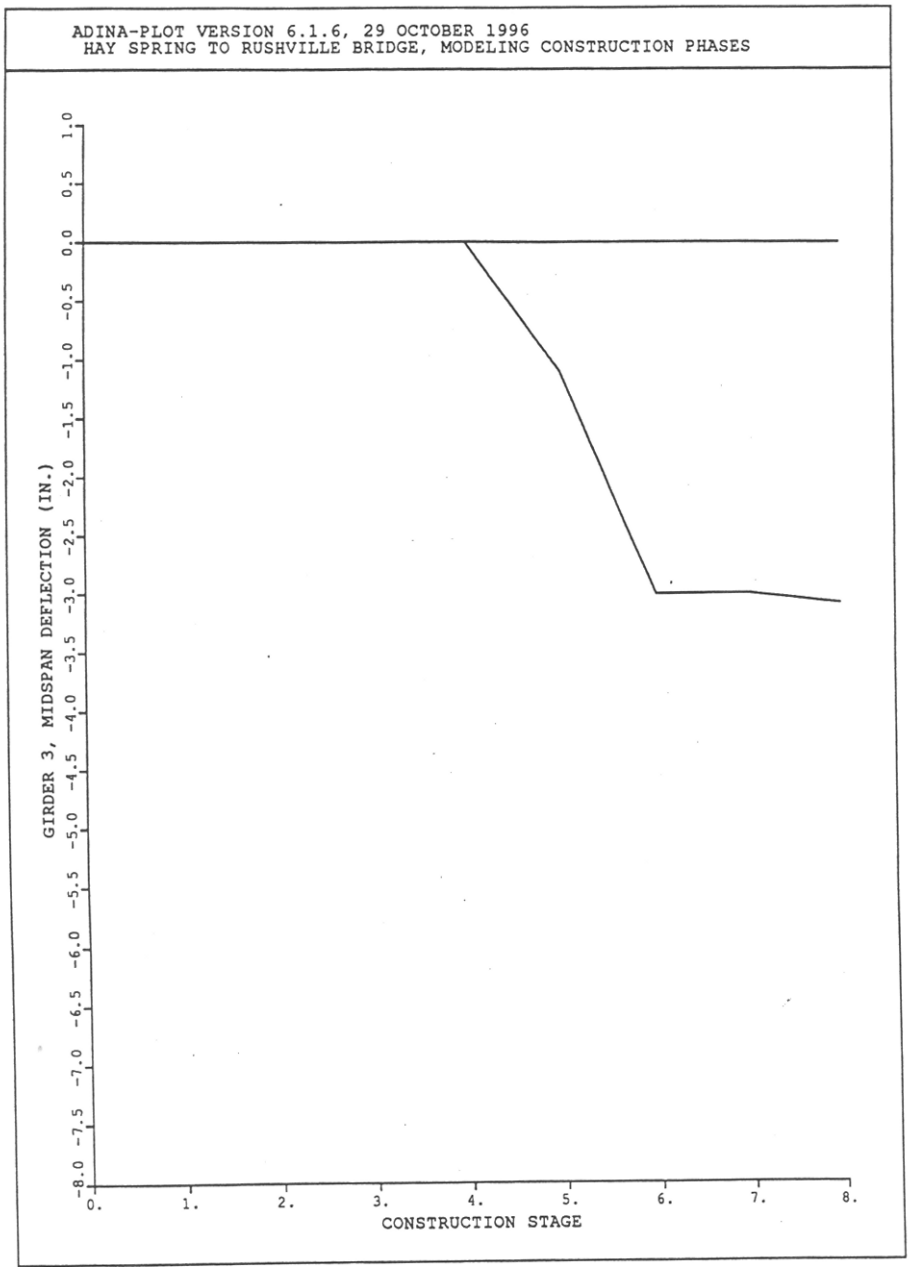

Figure 10-9: Girder #3 Mid span Deflection

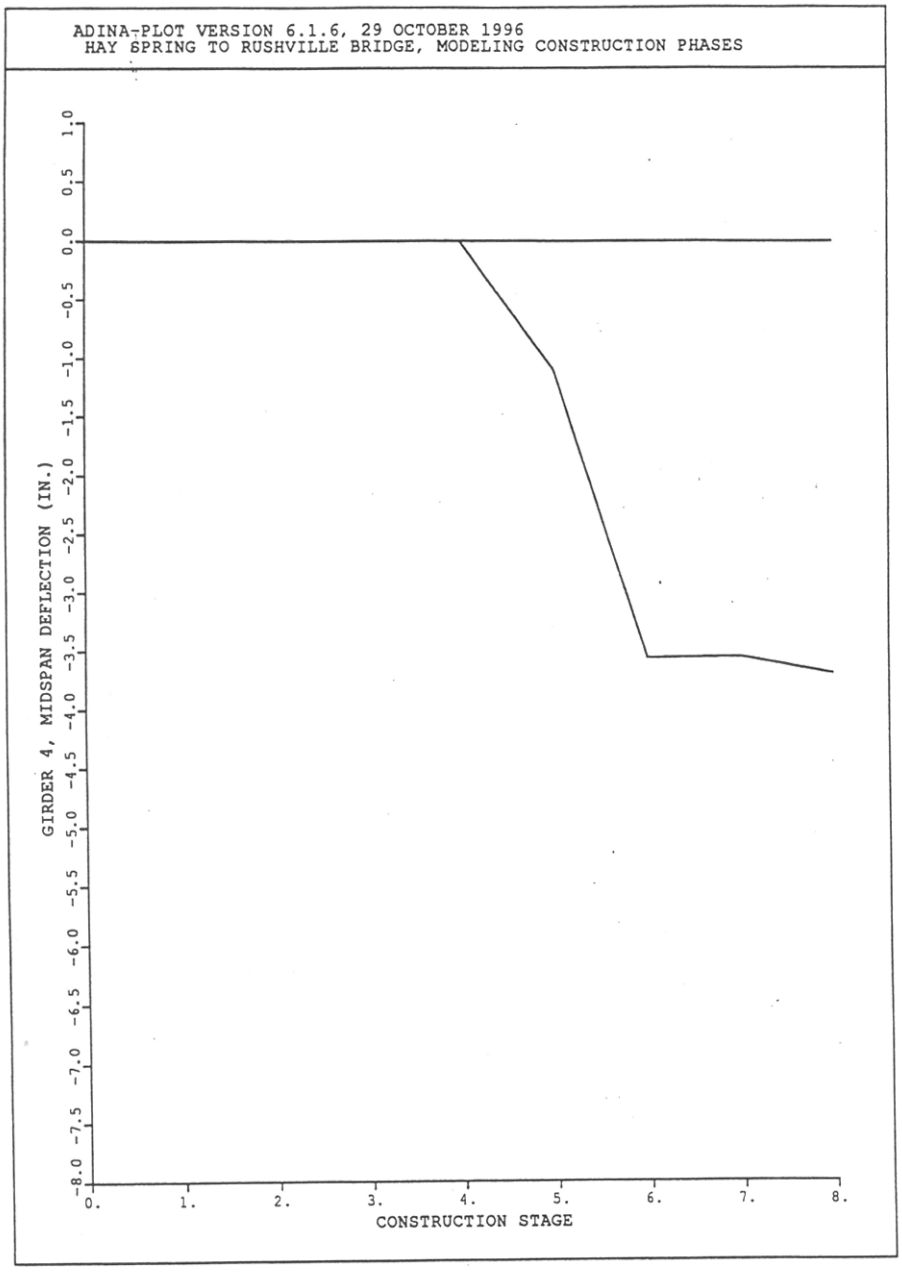

Figure 10-10: Girder #4 Mid span Deflection

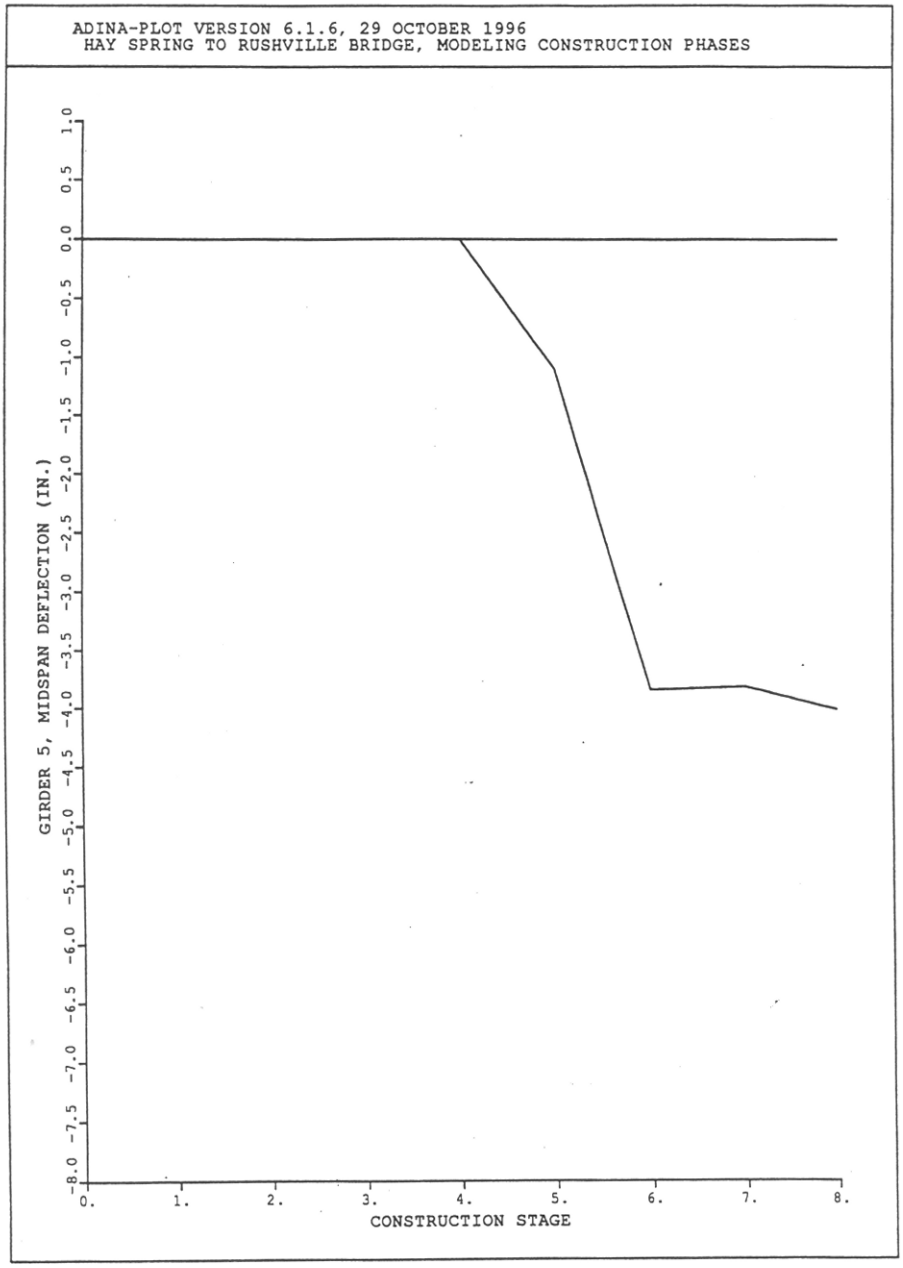

Figure 10-11: Girder #5 Mid span Deflection

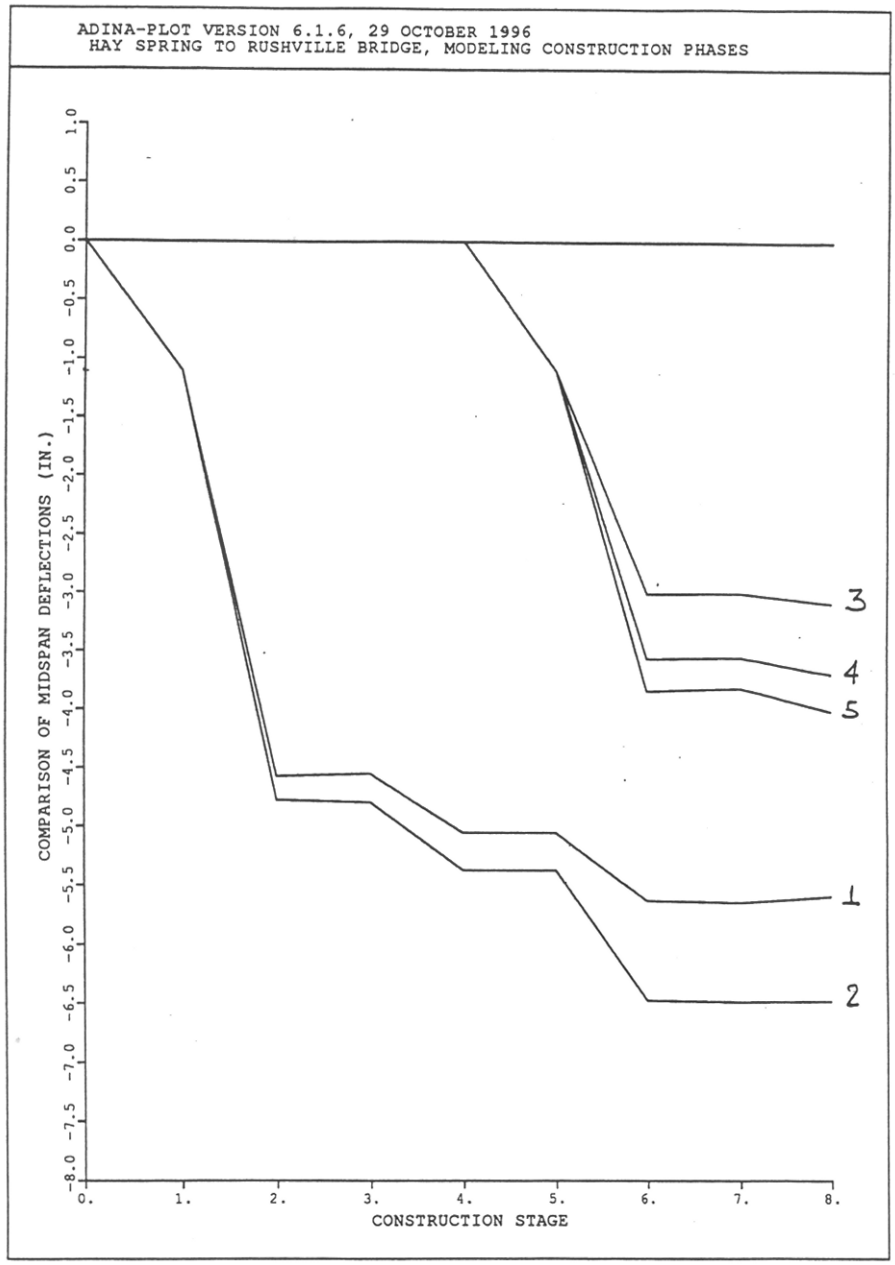

Figure 10-12: Mid span Deflection of All Girders

	Girder				
Stage	#1	#2	#3	#4	#5
1	-1.10	-1.10			
2	-4.57	-4.77			
3	-4.55	-4.79			
4	-5.05	-5.37			
5	-5.05	-5.37	-1.10	-1.10	-1.10
6	-5.63	-6.47	-3.06	-3.57	-3.84
7	-5.64	-6.49	-3.03	-3.56	-3.82
8	-5.59	-6.48	-3.09	-3.70	-4.01

Table 10-1: Girder Deflection Summary

10.1.5 Resulting Recommendations

It was concluded from the finite element analysis performed that the continuity of the turndown between the two phases restrained the ends of the second phase girders. This restraint stiffened the system such that the additional loading from the deck pour and barrier placement did not result in as much deflection as experienced by the first phase.

Therefore, the recommendation is that the turndown should not be made continuous between the phases. The recommended alternative is the use of a closure region within the turndown itself similar to the closure region used in the deck. Turndown reinforcement can extend through the forms into the closure region the reinforcement from both phases lapped together. After both phases have been completed, casting of concrete within the closure region will lock the reinforcement resulting in a continuous turndown.

10.2 Snyder South Bridge

During the construction of a bridge on Highway 77, 8 miles south of Snyder, Nebraska, using phased construction, it was observed that the first phase had rotated an appreciable amount. During the deck casting, at mid span the interior girder deflected 8.27 inches while the exterior girder only deflected 5.15 inches. In addition, the bottom flanges of both girders swept

towards the interior 0.75 inches at mid span while the top flanges swept towards the interior by approximately 1.9 inches.

10.2.1 DESCRIPTION

The Snyder South Bridge utilized two girders in the first phase and three girders in the second phase as shown in Figure 10-13. As can be seen in Figure 10-13, the first phase was designed to be asymmetric. As will be shown, the asymmetry attributed much to the rotation. However, in addition to the asymmetry, the ends of the girders were not prevented from overturning. At the request of the contractor and with the approval of the inspector, the slab and turndown were cast monolithically. While this practice is generally acceptable, when combined with the asymmetric deck this produced large torsional deformations within the system.

10.2.2 ANALYSIS

A full 3-D finite analysis was carried out on the structure. Many different scenarios were analyzed to determine what caused the difficulties and how the system would have responded to various options.

The as built model has been verified against the measured deflections and been found capable of predicting the bridge response. In general, the model was slightly stiffer. This is expected since P-Δ effects were neglected and no slipping of any sort was modeled. Model results were compared with measured results although these comparisons were difficult since each required some type of an assumption. Take for example one of the most critical values, relative girder displacement. This value came from a survey of the bridge deck after the pour and is therefore sensitive to a uniform deck thickness over the girders. Therefore, to provide consistency, for the purpose of comparison among alternatives, the as built model will be used as a base line as opposed to the measured results.

Finite element analysis shows that if the turndowns had been poured and allowed to harden prior to the addition of the deck the differential settle-

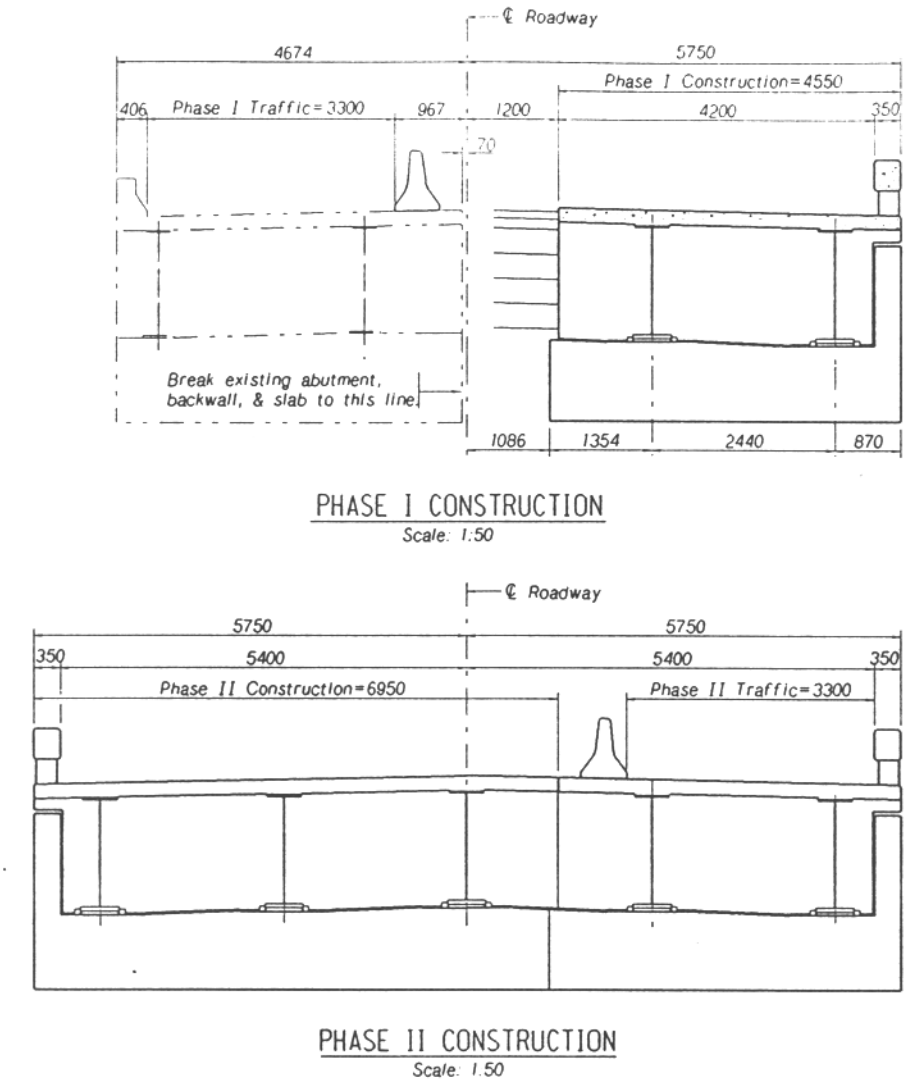

Figure 10-13: Snyder Bridge South

ment between the two girders would have been limited to 13 mm. This value should be compared to the baseline differential settlement value of 50 mm.

LATERAL BRACING

Due to the circumstances at the time of construction there was an interest in evaluating an alternative whereby an external bracing system would provide restraint to minimize the unwanted deformation. The result of the investigations into the feasibility of an external bracing system is therefore presented here.

While a finite element analysis has shown that if adequate external lateral bracing would have been provided the differential settlement would not have occurred, where this bracing would come from is in question. An independent bracing structure has been ruled out, as it would have required actual construction within the stream channel. The only feasible option would therefore be to brace the new girders to the remaining portion of the existing bridge. This option is difficult at best. Analysis could be done to determine the response of the old bridge to the loads and the bracing system could then be pre-loaded to overcome the expected deflections. However, the connection in itself is what is most troubling.

Connecting the new girders to the old bridge presents a number of challenges. During the deck pour, the new girders will deflect approximately six inches while the old bridge elevation remains fixed. Therefore, any connection between the two systems must not provide vertical restraint, only horizontal. Vertically slotted holes have been suggested to accomplish this. While these would certainly reduce the reliable vertical load carrying capacity of the connection, it would be a mistake to believe no vertical force would be transmitted. For one, the horizontal loads will create a contact force, which will then provide some shear resistance. Also, any imperfections in the slots would tend to "catch" and prevent free translation. Finally, movement out of the plane of the connection would bind all but the sloppiest of connections, again, transferring vertical forces.

The last point alludes to another difficulty. Since a couple is actually required for bracing, not just lateral support, the connecting member must be capable of supporting compression. The column condition, being pinned-pinned with an unbraced length of approximately 15 feet, requires a substantial member. The finite element analysis gives a maximum required support load at the middle of the span of 24 kN if it is assumed that a brace point has been located at each existing cross-frame. Again it should be pointed out that the resistance needed is actually a couple and

the model assumes the attachment points to be at the flanges. In reality these are quite a bit closer together. After allowing 3" top and bottom for connections and another 8" at the bottom to allow for the connection and also the required deflection moves the connecting points together another 14". Considering an original web depth of 54" means the calculated load must be increased by 35% to 32.4 kN, or 7.3 kips. Considering a safety factor of 2.0 yields a 15 kip couple at a 40" offset as the final loading a connecting system must withstand.

10.2.3 Resulting Recommendations

The primary result to be drawn from the analysis of the Snyder South Bridge is that an asymmetric phase can have a detrimental impact on the deformations. While the deformations were exacerbated by the absence of restraint at the girder ends, the predicted differential had the turndowns been cast prior to deck placement was still 13 mm.

Further, it has been conclude that had end cross-frames been provided or the turndown been cast prior to casting the slab the amount of rotation would have greatly reduced. Therefore, in circumstances such as in short spans where an asymmetric phase has been deemed acceptable, it is recommended that overturning restraint be provided to the girders at the time of deck placement.

Chapter

11 Conclusion

Recommended Design and Construction Procedures for Phased Construction

The main objective of this project was to develop recommendations for constructing bridges using the Phase Construction method. The two major facets of bridge design and construction to be impacted by the phase construction are analysis, or design issues, and constructability. Although deflection prediction is typically considered a part of analysis, it will be considered separately due to the large impact deflection prediction has on the success of a phase construction project. The conclusions drawn with respect to each of these is presented in the following sections.

As the flexibility of the structure and predicted deflections increase, so too does the potential magnitude of error as well as corresponding need for additional provisions to assure a minimization of these errors. Therefore, the magnitude of dead load deflections appears to be a good, readily available parameter to use in specifying the applicability of restrictions and

advanced analysis requirements. Determination of limiting values beyond which a particular recommendation should apply was beyond the scope of this project as it will require field experience to develop reasonable limits. However, when appropriate, a qualitative assessment as to the sensitivity with respect to flexibility of a particular recommendation is provided.

11.1 Analysis

11.1.1 Symmetry Considerations

Two cases of symmetry must be addressed. The first is symmetry within each individual phase; an example of non-symmetry with this respect is an uneven amount of overhang on a phase. The Snyder South Bridge discussed in Section 10.2 is an example of this type. The non-symmetry can give rise to torsional distortion of the individual phase due to the loading pattern. This can lead to a potential differential elevation at the time of closure. This type of non-symmetry should be avoided on all but the shortest and simplest of projects. As the length of the span increases, so do the torsional flexibility and the associated deformations.

The second type of symmetry that must be considered is symmetry within the system. When the two phases have a dissimilar number of girders, there is the potential for one phase to carry a larger load per girder than the other despite the presence of symmetry within each individual phase. This situation is simple to account for in the design process so long as it is recognized.

11.1.2 Distribution Factors

As was discussed in Section 5.2, the problem with distribution factors for bridges with a small number of girders, which was a large issue at the outset of this research, has largely become moot since the AASHTO LRFD Specifications have been modified to incorporate as few as two girders in a bridge.

On a more general note, the distribution factors obtained from live load testing indicate that the values obtained from the lever rule and commentary methods are highly conservative and unnecessarily control the design.

11.1.3 End Restraint

A common construction detail is that of a semi-integral abutment whereby the girders are embedded in the abutment, but additional detailing is not provided to ensure moment transfer. Despite the absence of these additional details, some amount of moment is indeed transferred thereby reducing the observed deflections. The greatest challenge of a phased construction is the prediction of deflections during the construction process, and an accurate accounting for the effects of end restraint will aid in this endeavor.

An analysis technique is presented in Section 5.3 which is dependent on the percentage of fixity provided by the abutment as determined by the observed deflections compared with the deflections assuming simple supports and full fixity.

A small program was developed to aid in the implementation. Many of the software packages currently utilized for design are not capable of accepting a specified torsional restraint. However, the torsional restraint provided by the abutment can be modeled as an additional span continuous with the structure. The program determines the required properties of the additional spans to allow for the design to be carried out utilizing the current software packages.

11.1.4 Pour Sequencing

Given the available data, two additional questions were posed by the Nebraska Department of Roads concerning several items which are routinely ignored in the analysis of continuous bridges and assumed to have minimal impact on the results. These are the pour sequencing, the fact that

the positive region pour is often completed prior to completion of the negative region, and the vertical profile of the bridge.

The Dodge Street Bridge was constructed using separate positive and negative region pours. Finite element analysis performed on the system indicates that the error introduced due to neglecting the separate pours is on the order of two percent.

The Dodge Street Bridge also had a considerable amount of vertical curve. However, the difference in results assuming a straight girder versus the curved girder was negligible.

It was therefore concluded that the practice of ignoring pour sequencing and girder profile are justified.

11.1.5 Skew

The effects which skew angle has on the deflection profile of a bridge are most pronounced near the ends of the bridge. Near the ends of a bridge the elevation differentials experienced in phase construction would most often be due to construction tolerances and errors, the source of which has nothing to do with the use of phase construction.

Further, for medium to long bridges the impact of skew near midspan is nonexistent. However, most of the concerns associated with phased construction increase with span length. Therefore, skew is not considered a factor which impacts the use of phased construction. Should a concern arise in a particular instance a simple three-dimensional grillage analysis should suffice in determining the effects.

11.1.6 Horizontal Curvature

A bridge with horizontal curvature that is to be constructed using phased construction requires a detailed three dimensional analysis. Horizontally curved bridges using phase construction have experienced differential elevations of six to eight inches. The main cause of this is that the torsional

properties of each individual phase are significantly different from the torsional properties of the entire system.

11.2 Deflections

11.2.1 Long Term Creep and Shrinkage

After the construction of the first phase and prior to the completion of the second, the first phase of the bridge experiences long term deflections due to creep and shrinkage causing challenging problems trying to match the elevations of the second half to the first half.

A theoretical discussion of these deflections was presented and a program capable of predicting these movements was developed in Chapter 6. It is certainly not recommended that such an analysis be performed on each and every project as this can be time consuming and the results are highly dependent on the long term properties of the concrete which must be estimated at design time and whose actual values can only be known after the project's completion.

Despite these limitations, the method can still be useful in obtaining estimated values which can serve to augment the decision making process.

11.2.2 Stress Prediction

Near midspan, concrete slab on steel girder bridges can be analyzed transversely on a strip-wise basis as a beam on discrete elastic foundations. This is equivalent to saying that near midspan, the bridge responds to longitudinally distributed transverse loads as though it were infinitely long. This approximation is suitable for long span bridges and a correction factor can be obtained for medium span bridges as well. Since the potential for problems due to phase construction increases as the span length increases, this approximation is justified.

This concept has been implemented in a finite element code allowing for the quick and simple prediction of stresses due to the additional differen-

tial deflection which occurs after closure. The details of this procedure are presented in Chapter 9.

11.2.3 Implementation

Given the knowledge of the potential for large stresses coupled with the experience and judgment of the engineer, a decision could be made to alter the timetable to allow the second phase to experience an additional portion of the predicted deflection prior to placement of the closure region. While it is certainly understood that such a delay is extremely undesirable the rate of deflection due to time effects in the concrete is greatest at the outset so that a short delay may yield great benefits.

Conversely, this predictive tool may allow the engineer to determine that a delay will not help alleviate the differential elevation between phases and that an alternative remediation method be sought. Currently, when a large differential is observed, it is often conjectured that should the completion of the closure region be postponed the differential elevation will be reduced. Given the predictive tools presented, this option can be investigated and potentially eliminated.

11.2.4 Temperature and Other Meteorological Effects

Chapter 7 describes the methods used to deal with the movements due to temperature in the reduction of data. An observation made was that vertical deflection is not directly correlated to temperature on a seasonal basis. Although there is a definite deflection trend from summer to winter, the deflection peak occurs about one month after the temperature peak. It does not appear as though the vertical deflection due to temperature effects is large enough to require special consideration. This is reinforced by the fact that, except in extremely rare instances, concrete is not placed during days of utmost extreme temperatures. Therefore, the temperature difference at time of pour between the phases will not be extreme nor will the the associated deflections.

Also examined was the longitudinal movement due to temperature and the impact the semi-integral abutments had on this movement. It was determined that the actual longitudinal deformation is 88% of the predicted value ignoring the effects of the abutments. The lower expected longitudinal movement reduces the required size of the expansion joint

11.3 CONSTRUCTABILITY

11.3.1 DIFFERENTIAL ELEVATION LIMITS

Despite all the best efforts there will always be some amount of differential elevation at the time of closure. Analysis tools are developed in Chapter 9 to help the designer evaluate the individual situation and determine the best solution.

11.3.2 REMEDIATION

When the differential elevation at the time of closure is too great to be handled by a modified overlay then a plan for remediation must be devised to bring the two phases closer to the correct elevation. Several remediation techniques are discussed in Section 8.3 including temporary ballast or support, and inter-phase jacking. The great disadvantage to any remediation technique in addition to the obvious time and cost is the fact that stress will be locked into the closure region as a result of the operation. To evaluate the magnitude of these stresses, analysis tools have been developed in Chapter 9.

11.3.3 CLOSURE REGION

The performance of the closure region largely depends on the successful fulfillment of the other aspects of the construction. For example, if some sort of remediation technique is required due to an unacceptable difference in elevation, the induced stress may lead to cracking of the closure region and a subsequent premature deterioration.

The program ADStress presented in Chapter 9 can be used to predict the stress level within the closure pour due to additional relative deflections of the phases.

11.3.4 Cross Frames

The cross frames within the closure region should be placed prior to joining the phases. After the closure region has been joined, a crane can no longer be used to place the cross frames requiring the frames to be placed by hand from below.

The cross frames joining the two phases is a potential topic for future research. There has been some speculation that these frames in this region may not be required at all or at least be of a minimal design. However, cross frames between the two phases may also help to protect the green concrete since one phase of the bridge is typically open to traffic during or immediately after the closure operation. Although not investigated within the scope of the project, consideration could be given to restricting traffic, either weight or speed, during the period of time that the closure region is in place without the presence of cross frames.

11.3.5 End Restraint

Care must be taken to ensure that the end restraint conditions are the same for each phase. Explicitly specify the construction sequence to ensure the order of operation is the same for both phases. If provisions for optional joints or details are provided, ensure the same option is exercised on both phases. In addition, the construction of the first phase should not restrain the ends of the girders for the second phase and demolition of existing structures should not release restraint which was present during construction of the first phase. One particular recommendation is that a concrete end diaphragm encasing the girder ends should not be made continuous between the phases.

Bibliography

[1] AASHTO (1998). *AASHTO LRFD Bridge Design Specifications* - 1994, American Association of State Highway and Transportation Officials, Inc., Washington D.C.

[2] Meyers, B.L., Branson, D.E., Schumann, C.G. and Christiason, M.L., "The Prediction of Creep and Shrinkage Properties of Concrete", *Final Report No 70-5*, Iowa Highway Commission, August 1970, 140 pp.

[3] ACI Committee 209, Subcommittee II, "Prediction of Creep, Shrinkage and Temperature Effect, 2", *Draft Report*, Detroit, October 1978, 98 pp.

[4] Faber, O., "Plastic Yield, Shrinkage and Other Problems of Concrete and their Effects on Design", *Minutes of Proc. of the Inst. of Civil Engineers, 225*, Part I, London, 1927, pp 27-73.

[5] Bresler, B., and Selna, L., "Analysis of Time Dependent Behavior of Reinforced Concrete Structures", Symposium on Creep of Concrete, *ACI Special Publication SP-9*, No. 5, Mar 1964, pp 115-128.

[6] Stallings, J.M. and Yoo, C.H. (1993), "Tests and Ratings of Short-Span Steel Bridges," *Journal of the Structural Division*, ASCE, 119, ST7 (July 1993).

[7] Swett, G.D. (1998), *Constructability issues with widened and stage constructed steel plate Girder Bridges,* M.S. thesis, University of Washington, 124 pp.

[8] Swendroski, J.P. (2001), *Field Monitoring of a Staged Construction Bridge Project,* M.S. thesis, University of Nebraska, Lincoln, NE, 626 pp.

Appendix

A Gaging Locations

MONITORING PLAN DETAILS FOR DODGE STREET OVER I-480

A.1 GAGE LOCATIONS

Redundant instrumentation to obtain the desired data adds to the project cost and produces massive data files. Therefore, a cost effective instrumentation strategy was devised by judiciously selecting the location of gages.

Using the 1997 AASHTO LRFD Bridge Design Manual, the bridge as designed by the Nebraska Department of Roads (NDoR) was analyzed. From the dead and live load analyses the gaging locations were chosen as described below. It was desirable to place gages on the East span because the distance to the ground is only 20' versus nearly 50' on the West span.

A.1.1 Spot-Weldable Gage Locations

The location of maximum positive bending moment from the Strength I combination was chosen as a gaging location. These strain readings will relate to the bending moment experienced by the girders. To obtain the amount of negative moment carried by girders, strain gages were also placed 2' East of the pier centerline. The gages could not be placed directly at the pier because of the bearing stiffeners there. Finally, spot-weldable gages were placed near the abutments so the amount of end restraint could later be determined and compared to the simple support assumed for design. Figures A-1 and A-2 show the bridge sections where spot-weldable gages were placed on girders for Phase I and Phase II respectively.

Looking at Figures A-1 and A-2 a few differences are evident in the gaging plans of Phase I and Phase II. For Phase I only the two girders closest to the closure pour were gaged at Section 3 versus all four girders for Phase II. Also, at Section 1 for Phase I, Girder J was not gaged. All gages were placed prior to girder erection.

Figures A-3 through A-6 show the gage placement on the girder at each section. The gages were centered on the flange at their respective position. To name the gages, the following convention was used: Vxy,1t or Vxy,2b. The V indicates it is a spot-weldable vibrating wire gage while x is the girder the gage is located on and the y is the section the gage is on. The 1t or 2b designates if the gage is located on the top or bottom flange, respectively. For example VG2,1t is the vibrating wire gage on Girder G of Section 2 on the top flange.

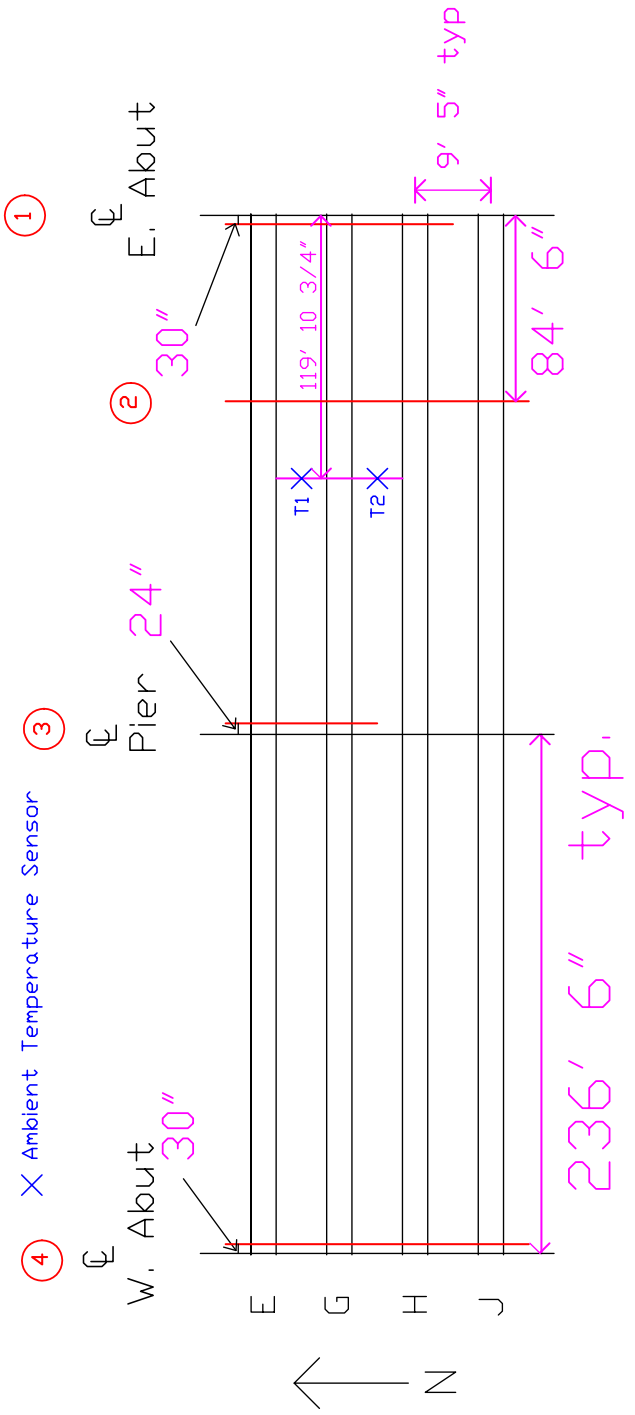

Figure A-1: Sections for spot-weldable steel strain gages for Phase I. Sections 1 and 4 are at the abutments, section 2 is at the maximum positive moment, and section 3 is at the pier

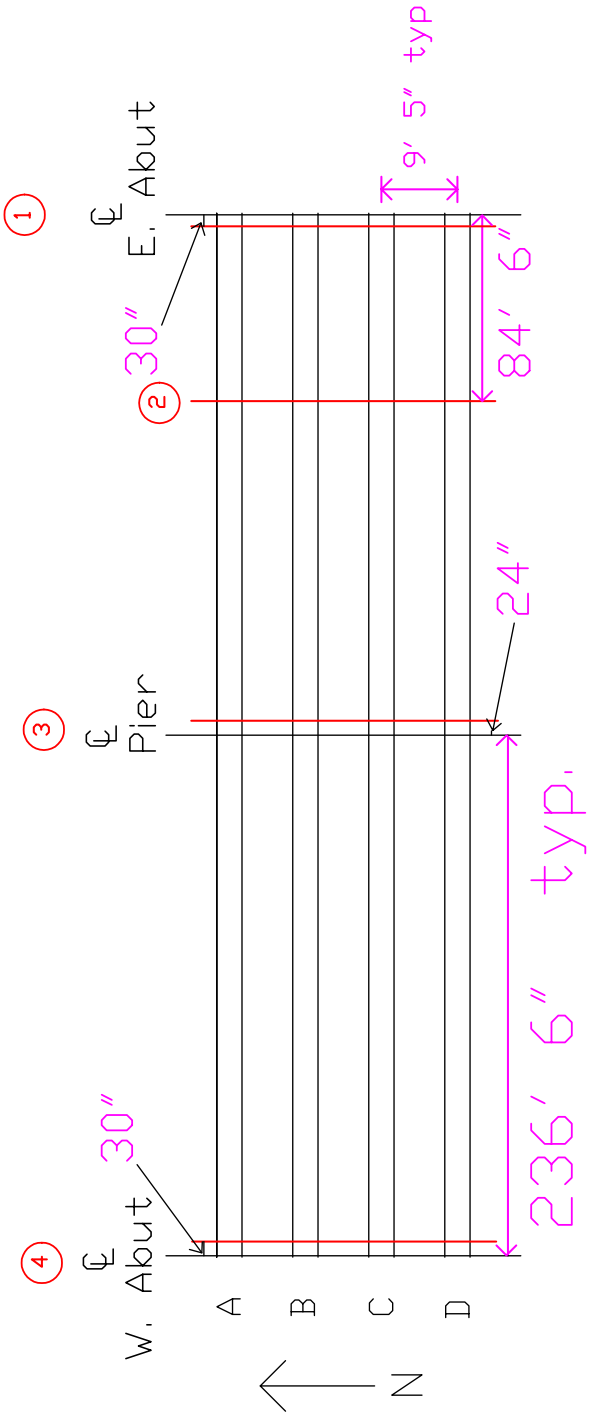

Figure A-2: Sections for spot-weldable steel strain gages for Phase II. Sections 1 and 4 are at the abutments, section 2 is at the maximum positive moment, and section 3 is at the pier

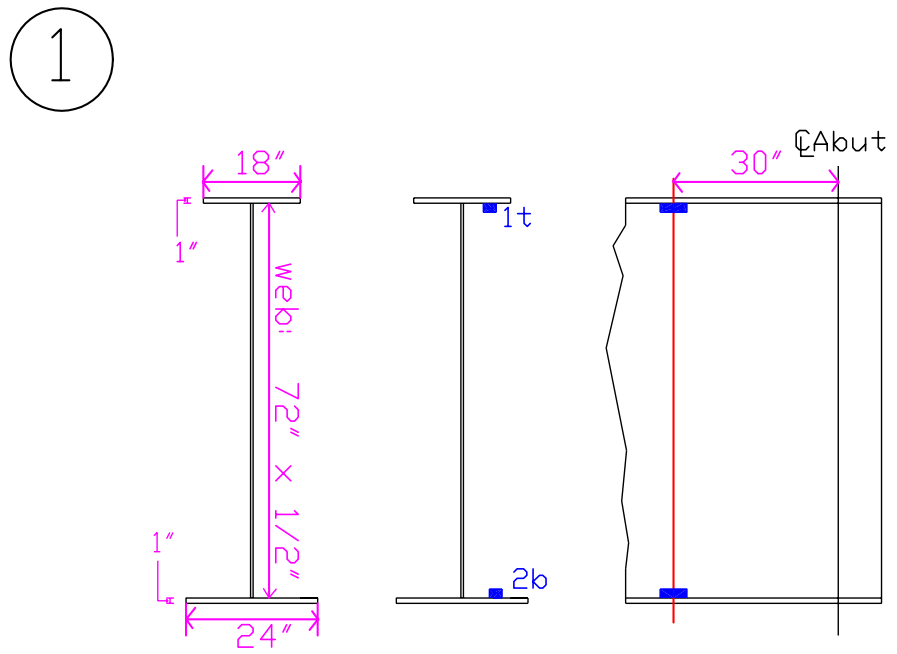

Figure A-3: Gaging Section 1 - East abutment

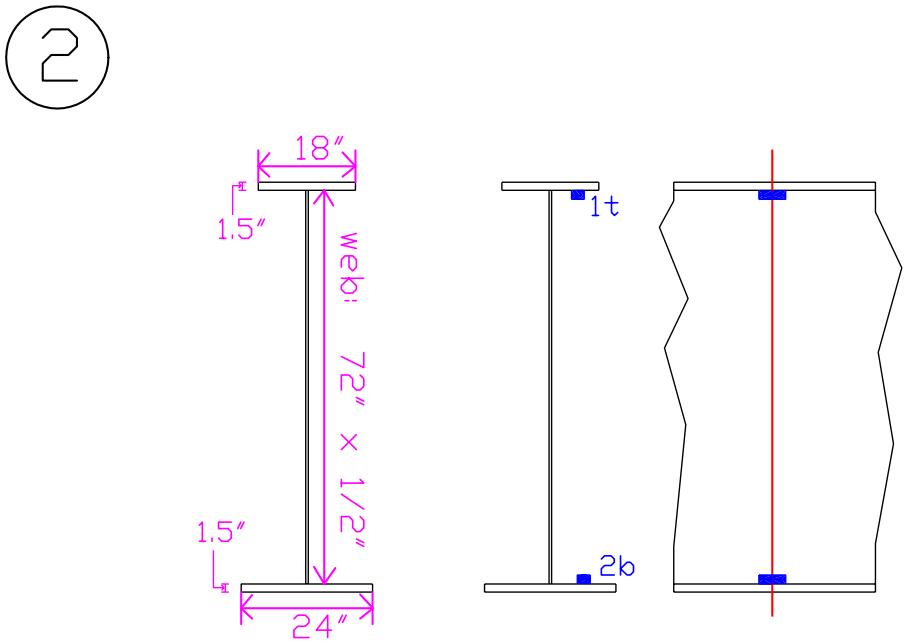

Figure A-4: Gaging Section 2 - maximum positive bending moment

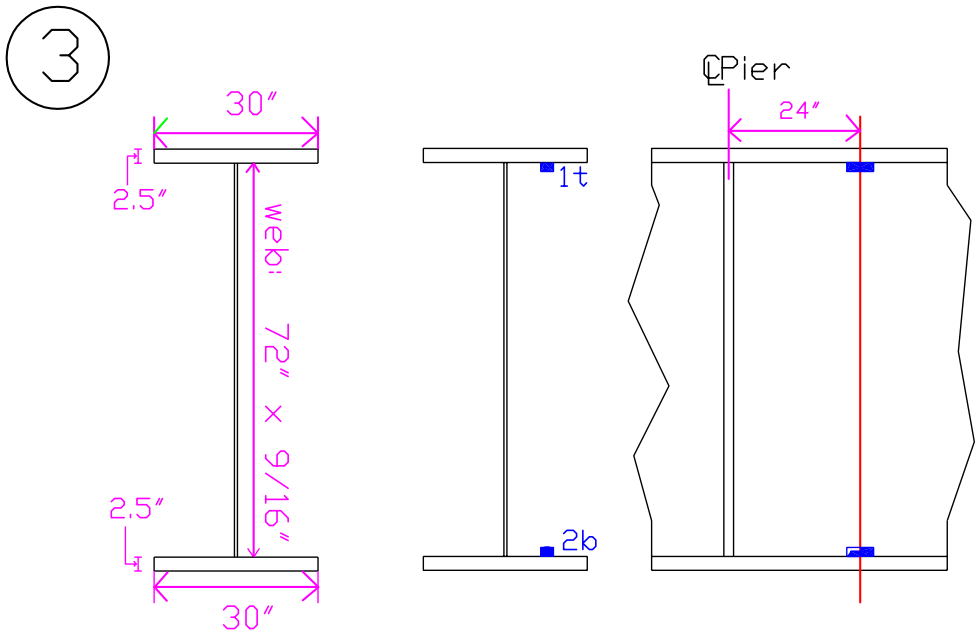

Figure A-5: Gaging Section 3 - maximum negative bending moment

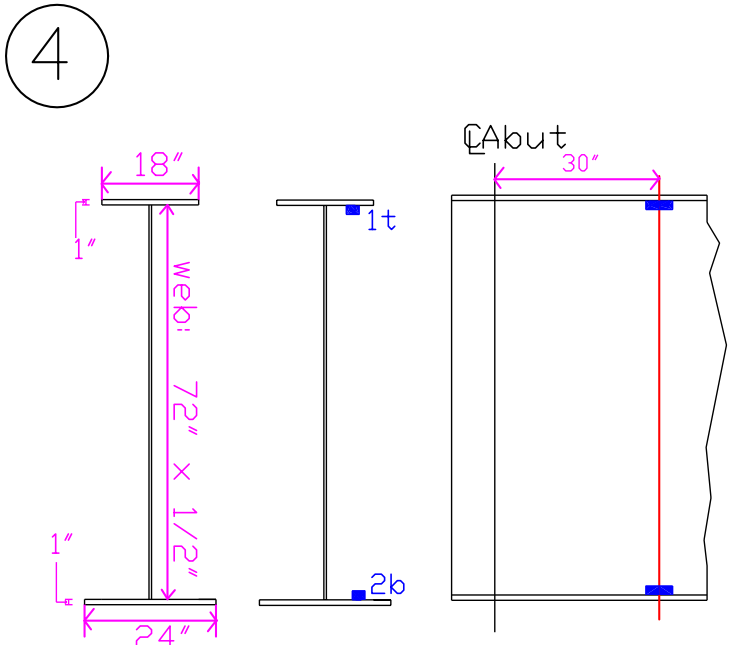

Figure A-6: Gaging Section 4 - West abutment

Two cross frames for Phase II and were also gaged. These strain readings will indicate how effective cross frames are in transmitting load in the transverse direction as the phases deflect relative to each other. The cross

frames chosen to be gaged were the ones closest to the maximum positive moment section (Section 2). How these cross frames were gaged and their locations can be seen in Figures A-7 and A-8. The naming convention is as follows: XCD-1 to XCD-5 and XDE-1 to XDE-5. X indicates it is a cross frame gage, the two letters following that indicate what girders the cross frames connect, and the number is a location. As can be seen there was one cross frame gaged in Phase II and one cross frame that connects the two phases.

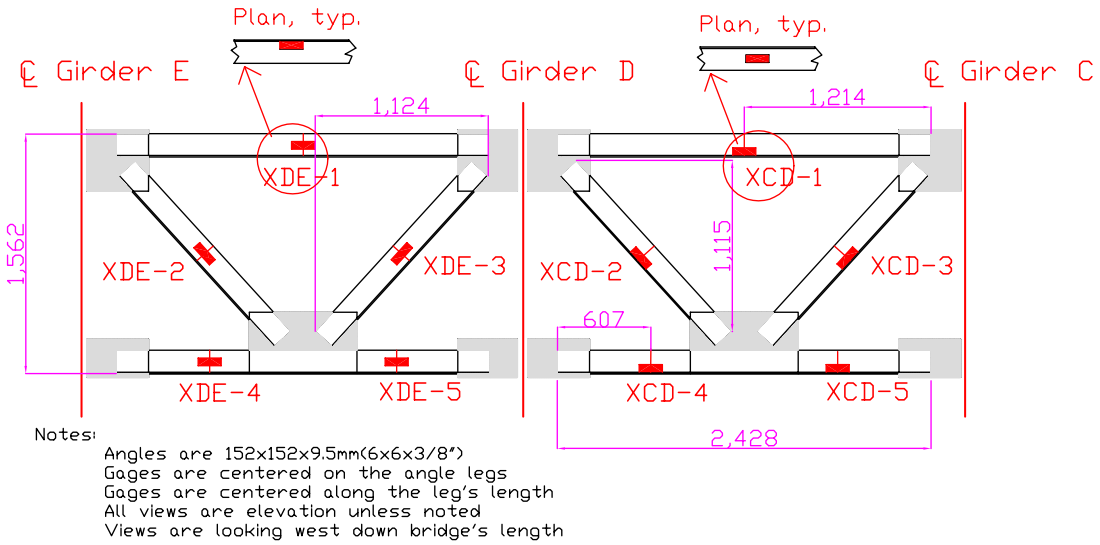

Figure A-7: Cross frame gage placement

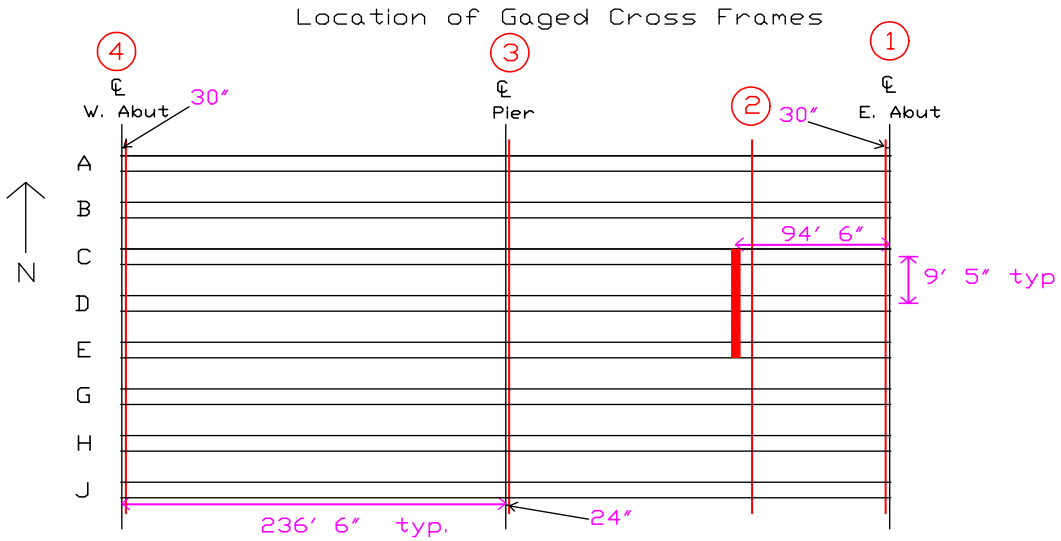

Figure A-8: Location of gaged cross frames

A.1.2 EMBEDMENT GAGE LOCATIONS

To obtain concrete strain data, gages were placed at several locations and orientations in the deck. On Phase I, gages were placed directly above Girders E, G, H, and J at Sections 2 and 3 and orientated parallel to the girders. Several other gages were placed orientated perpendicular to girders at Section 2. Another gage was placed at Section 2, 3" from the pour edge nearest the closure, orientated parallel to the girders. Finally, one gage was placed in a control specimen 7" deep x 6" wide x 18" long that was placed near the DAS to obtain the concrete's free shrinkage behavior. Figure A-9 shows the locations of Phase I embedment gages. Table A-1 indicates the distance from the bottom of the deck to the center of the gage for Phase I embedment gages.

Gage	Distance above deck	Section	Orientation
E1	4.25”	2	3” from N face of pour edge
E2	5.625”	2	Above CL Girder E parallel to girder
E3	3.875”	2	Between E&G perpendicular to girders
E4	5.25”	2	Above CL Girder G parallel to girder
E5	4.00”	2	Between G&H perpendicular to girders
E6	4.75”	2	Above CL Girder H parallel to girder
E7	4.25”	2	Above CL Girder J parallel to girder
E8	4.625”	3	Above CL Girder E parallel to girder
E9	5.25”	3	Above CL Girder G parallel to girder
E10	4.375”	3	Above CL Girder H parallel to girder
E11	4.125”	3	Above CL Girder J parallel to girder
E12	4.00”		In a 7” x 6” x 18” control specimen

Table A-1: Information on embedment gage location for Phase I

Phase II has different embedment gage locations than Phase I as can be seen in Figure A-10. For this phase only two gages were placed in the bridge deck to preserve system resources so embedment gages could be placed in the closure pour region as seen in Figure A-11. Gages were placed in the closure pour because it joins the two phases and can carry high strains and crack if differential settlement between the phases occurs. The gages will also provide long-term data on the closure region concrete behavior as it

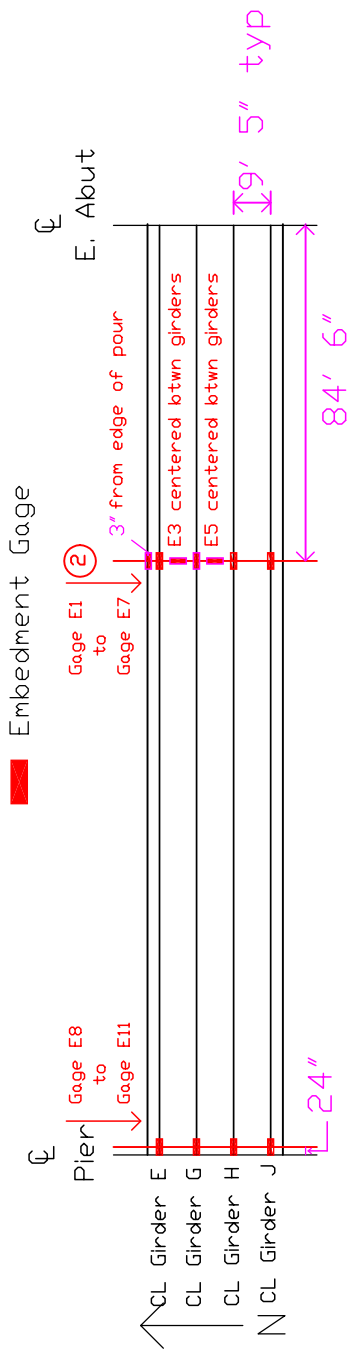

Figure A-9: Location of embedment gages for Phase I

creep and shrinks. The gages in Phase II and the closure pour were all placed 4 inches above bottom of the deck. These gages are named with the prefix E and a number indicating their location.

Embedment gages were also placed in the Pier, East abutment, and West abutment for Phase I. The locations of these gages are in Figures A-12, A-

13, and A-14 for the Pier, East abutment, and West abutment, respectively. On the East abutment the gages were placed over the second set of piles, which is behind the girder seat centerline. On the West abutment, gages were centered along the width of the pile cap. This locates the gages directly below girder seats.

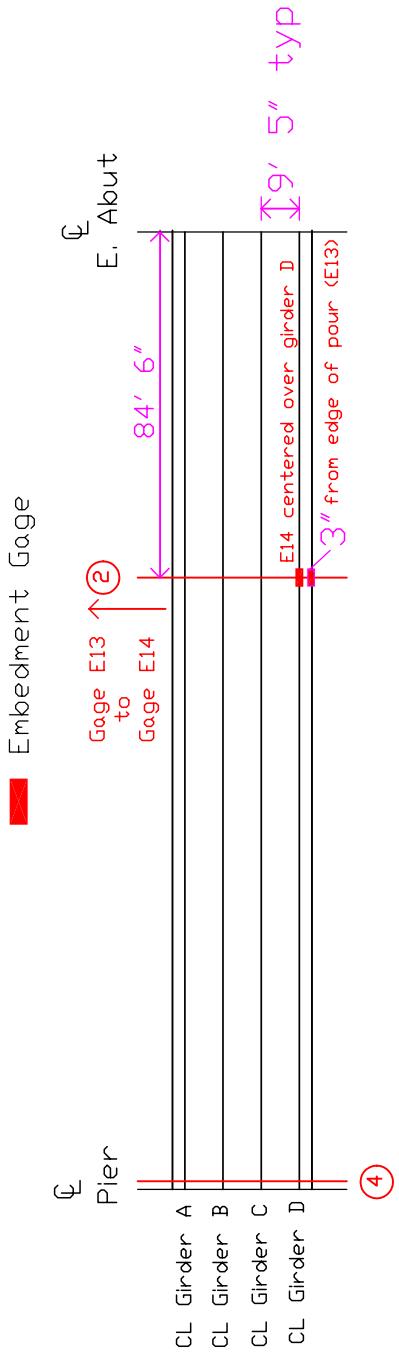

Figure A-10: Location of Embedment gages for Phase II

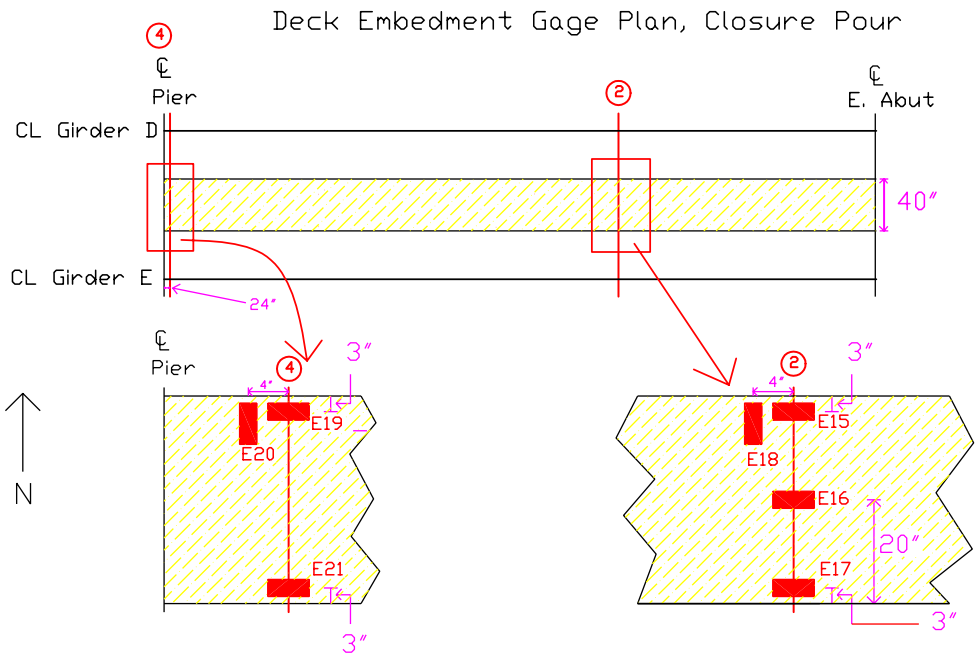

Figure A-11: Location of Embedment gages in the closure region

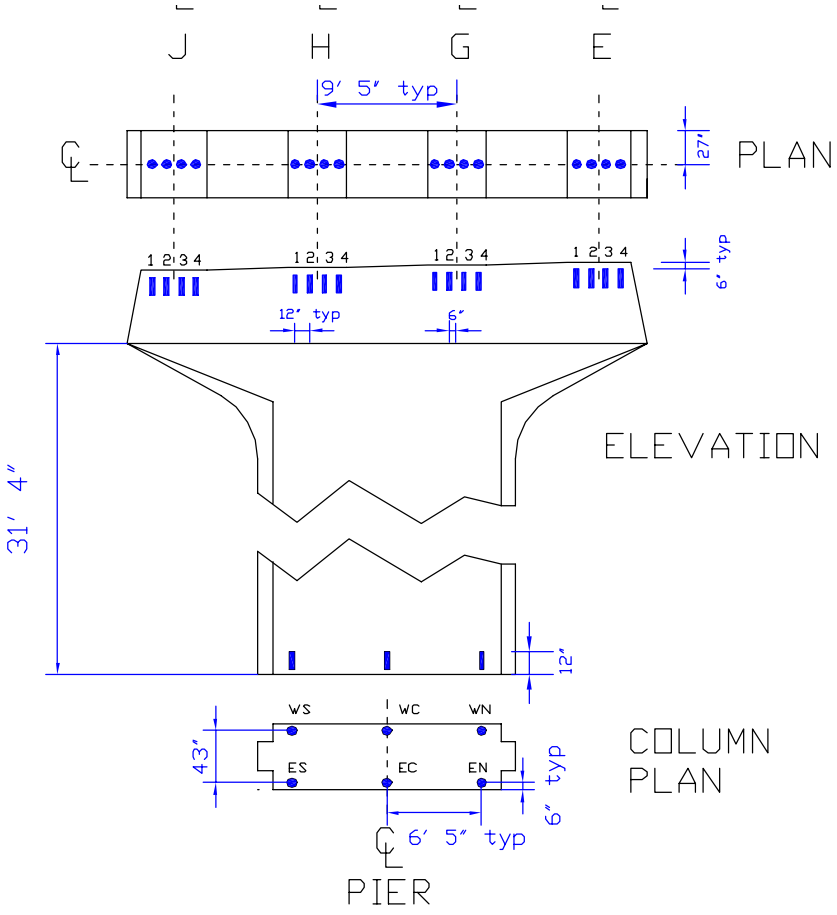

Figure A-12: Embedment gage locations in the Pier

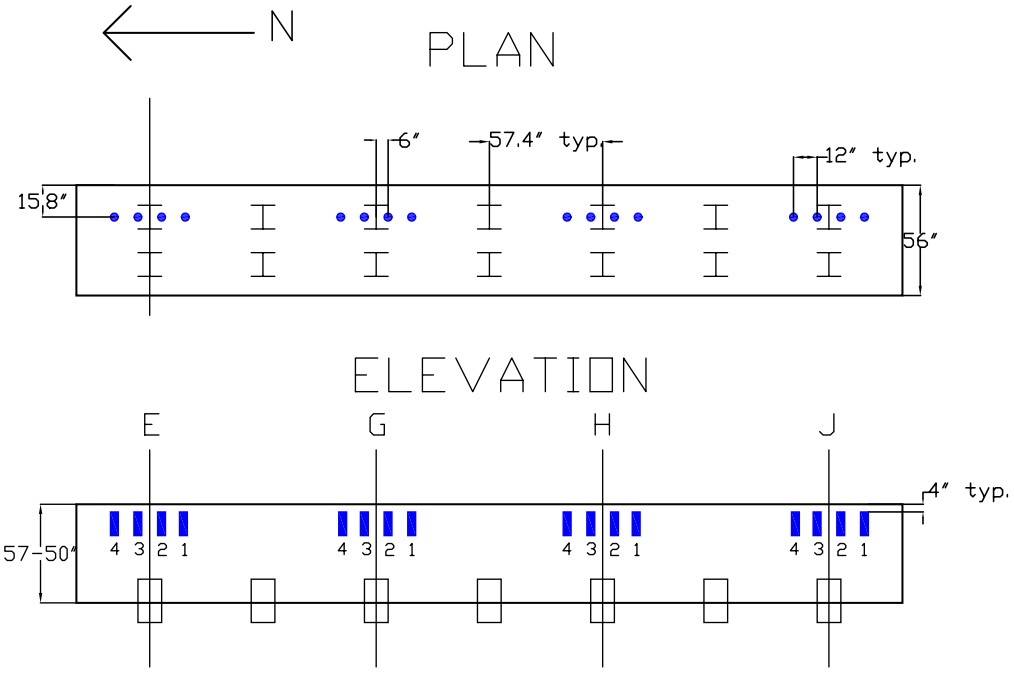

Figure A-13: Embedment gage locations in the East abutment

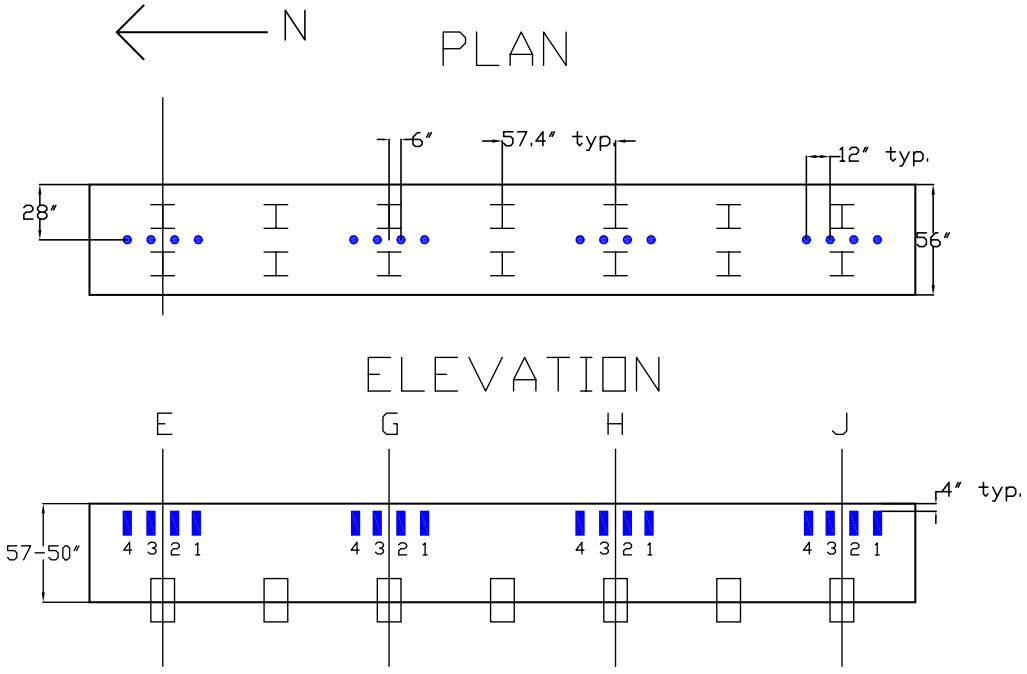

Figure A-14: Embedment gages in the West abutment

A.1.3 Displacement Measurement Locations

To obtain meaningful vertical displacement data it is desirable to measure deflection at the predicted location of maximum deflection, 0.4L. Potentiometers (pots) could not be placed exactly at this location because there is a roadway underneath the bridge. Therefore they were placed as close to the roadway as possible while still in a location that would not interfere with construction. The pots are tightly clamped to the underside of the girders while the other end is connected to a rigid test frame, which has its base cemented in the ground below the frost line. It is assumed the test frame does not move. This test frame can be seen in Figure A-15. At this location one pot is mounted on each girder of Phase I and II as seen in Figures A-16 and A-17. The pots monitor deflection during significant construction events and also long-term behavior. This data will indicate the amount of differential deflection occurring between the phases. The pots are named with the convention pot x, where x is the girder letter the pot is monitoring.

Girders D and E were instrumented at each abutment as seen in Figures A-16 and A-17 to measure the longitudinal displacement of each phase. These girders were chosen because they are adjacent to the closure pour and should have the most effect on the closure region behavior. This data allows comparisons between the behaviors of the two phases.

Figure A-15: Test frame used to measure deflection. Note pots mounted on the underside of girders

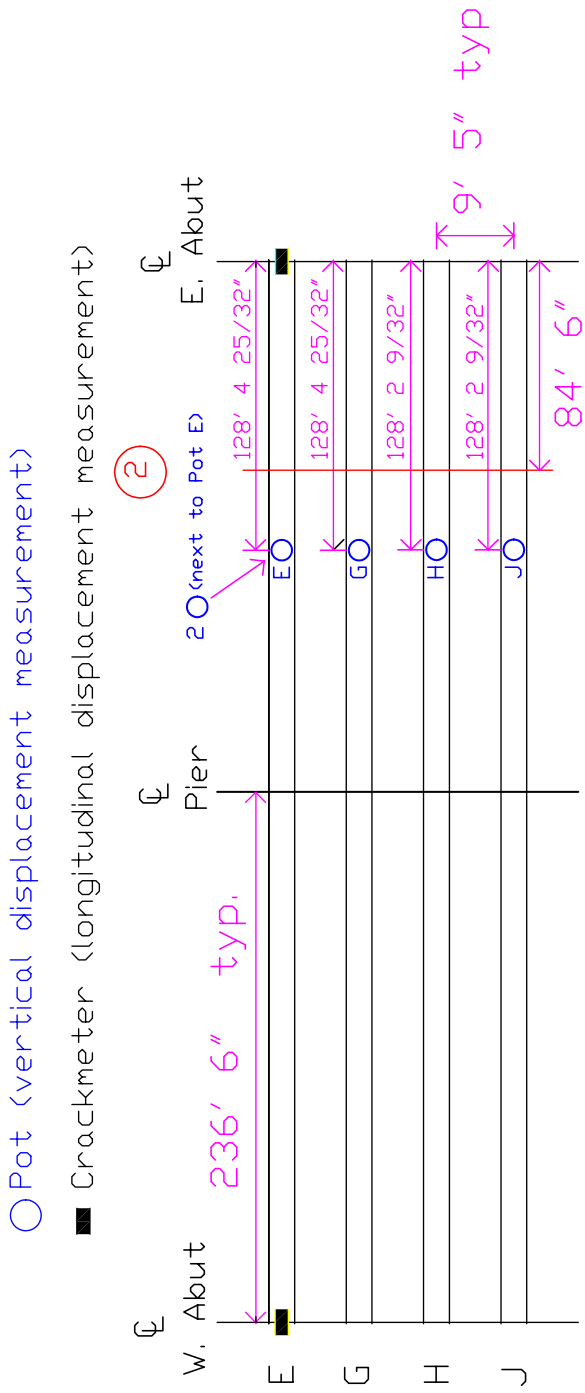

Figure A-16: Location of Displacement measurement for Phase I

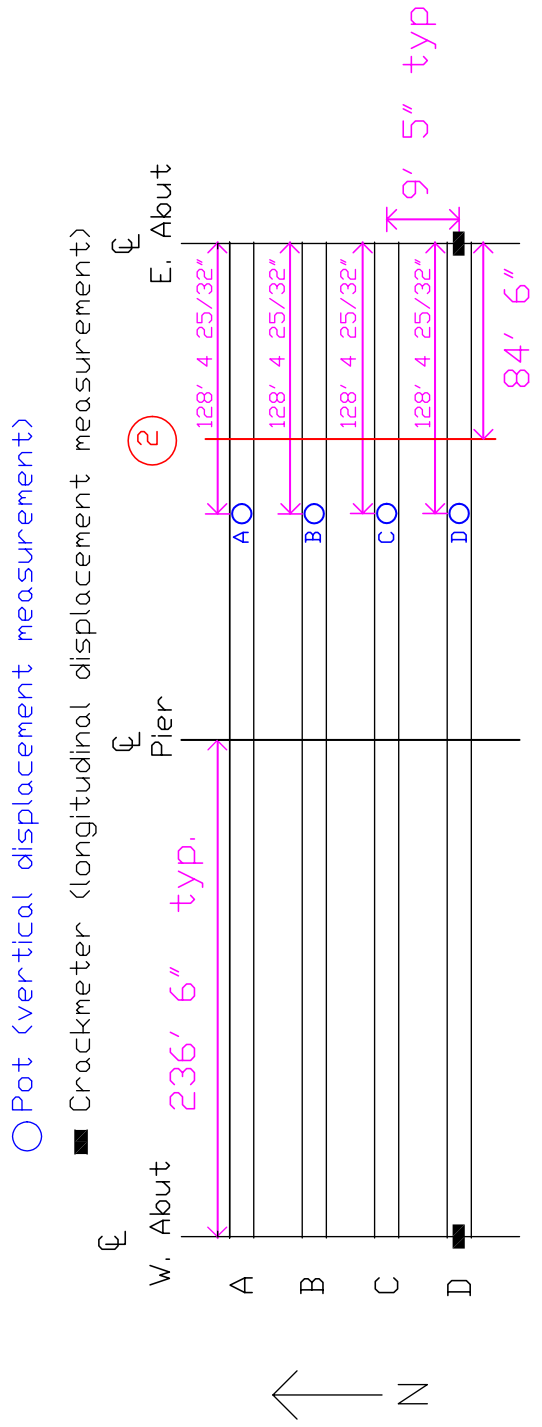

Figure A-17: Location of Displacement measurement for Phase II

Appendix

B Construction Deflection

Detailed Analysis of Deflections
Experienced During Construction

B.1 General

In phase construction the differential elevation between the phases is important when the closure pour is performed. Deflection occurs from applied loads and time dependent effects. Applied loads include concrete from concrete pours and temporary barriers. Time dependent effects include concrete creep/shrinkage deflections and temperature changes. If the phases have deflected different amounts, a differential elevation will be present. This differential elevation arises from the phases having different deflection histories. Large differential elevations make performing the closure pour difficult. Figure B-1 depicts a differential elevation between phases at the time of the closure pour.

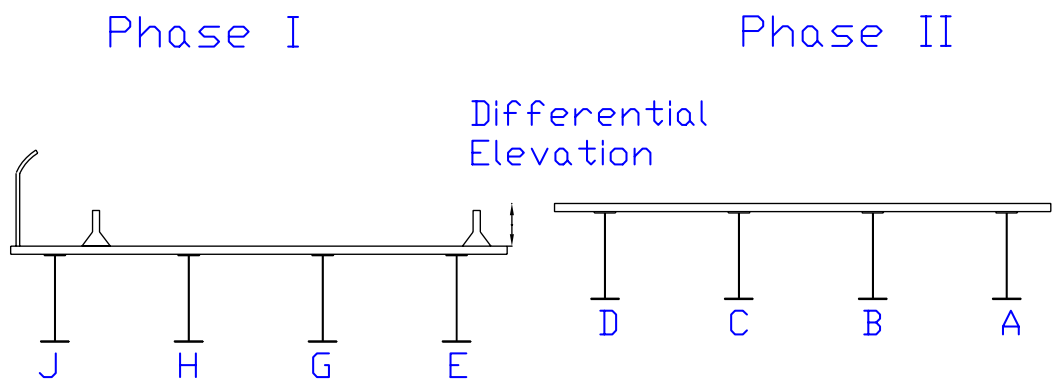

Figure B-1: Differential Elevation of Phase I and II at the time of closure

Phases I and II of Dodge Street over I-480 were constructed symmetrically. Similar deflections from positive region and negative region pours are expected from both Phases. Differential elevations can arise due to Phase I experiencing more time dependant deflections, as it is 6 months older than Phase II. The differential elevation can be determined by summarizing deflections of each phase until the closure pour.

Deflection histories can also be used after the closure pour to investigate girder deflections after the phases are joined. After closure each phase no longer deflects independently of the other. The closure pour and cross frames joining the phases cause loads placed on one phase to affect deflections of the other.

Beginning at the Phase I positive region pour, the deflections Phase I experiences will be reported until the closure pour. Phase II's deflections will be reported from its positive region pour until closure time. This data will yield the differential elevation at closure and behavior comparisons between Phase I and II can be made. System deflections after closure will be analyzed during overlay and permanent rail pours. Long-term system deflections will be reported showing time dependant deflections. Finally the pouring sequence will be studied and predicted deflections will be compared to actual values.

B.2 PHASE I DEFLECTION HISTORY UNTIL CLOSURE

B.2.1 DECK CASTING DEFLECTIONS

On October 20, 1999 the Phase I positive region pour occurred. Prior to the pour beginning, readings were taken to establish a datum elevation. This datum will be used to determine the total deflection at any time. By subtracting successive elevation readings from the datum elevation, deflection at any time can be determined according to:

$\Delta(t)$ = elevation reading(t) - datum elevation

During the pour additional readings were taken at 15 minute intervals to capture the deflection behavior during the operation. Table B-1 contains girder deflection information for the Phase I positive region pour. Average system temperature is also included as it has been shown that this affects deflection.

	Girder J	Girder H	Girder G	Girder E	Temp, F
Initial	0.000”	0.000”	0.000”	0.000”	32.94
Final	-4.932”	-4.855”	-4.615”	-4.593”	63.53
Change	-4.932”	-4.855”	-4.615”	-4.593”	30.59

Table B-1: Girder Deflections for Phase I positive region pour

During this pour Girder E, which is closest to the closure region, deflected the least while Girder J deflected the most at 0.339" more. Girders G and H are expected to deflect more than E and J because interior girders (G and H) have more tributary area of concrete to support than exterior girders (E and J). There is no current explanation why this occurred. This gives a transverse deflection profile to the system as seen in Figure B-2.

Before the negative region pour could occur, positive region concrete had to attain its design 28 day compressive strength. During this time shrinkage induced deflections occurred. Readings taken before the negative region pour began allow measurement of this deflection. Table B-2 con-

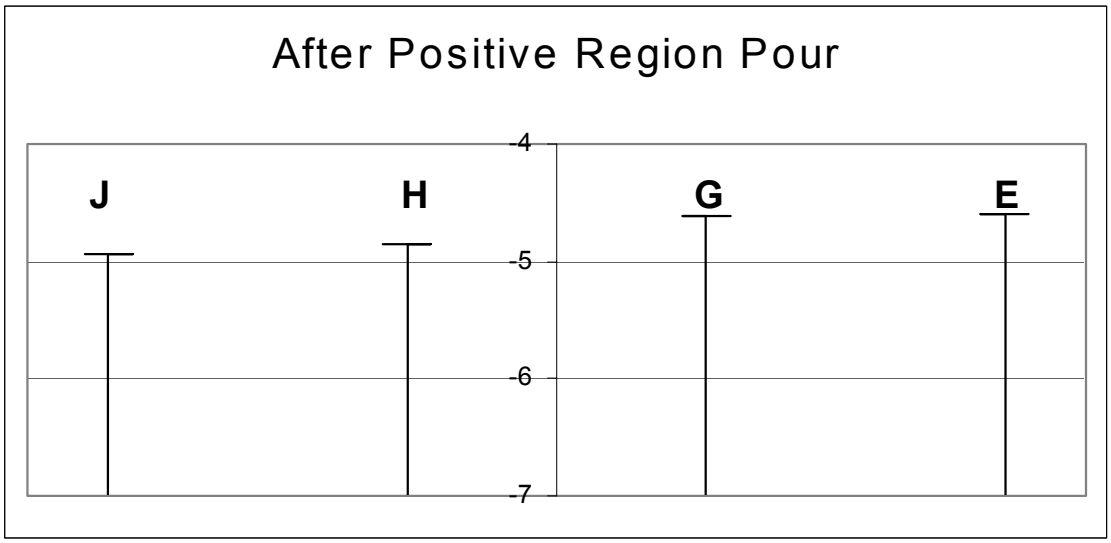

Figure B-2: Transverse deflection profile after positive region pour

tains data from the end of the positive pour to the beginning of the negative pour.

	Girder J	Girder H	Girder G	Girder E	Temp, F
Initial	-4.932"	-4.855"	-4.615"	-4.593"	63.53
Final	-5.002	-4.823	-4.706	-4.677	48.73
Change	-0.070"	0.032"	-0.091"	-0.084"	-14.8

Table B-2: Deflection of Phase I girders between positive and negative region pours

This data shows very little deflection occurring between pours. Girder H lost some deflection, moving upwards, while the other three girders experienced a small additional downward deflection. One would expect concrete shrinkage between these pours to cause additional deflection; however, this is not evident. A possible explanation is that between the sets of readings movement due to the temperature difference masked the expected deflection. System temperature between pours is shown in Figure B-3.

Girder deflections for the negative region pour can be see in Table B-3. The negative region pour occurred On October 28, 1999.

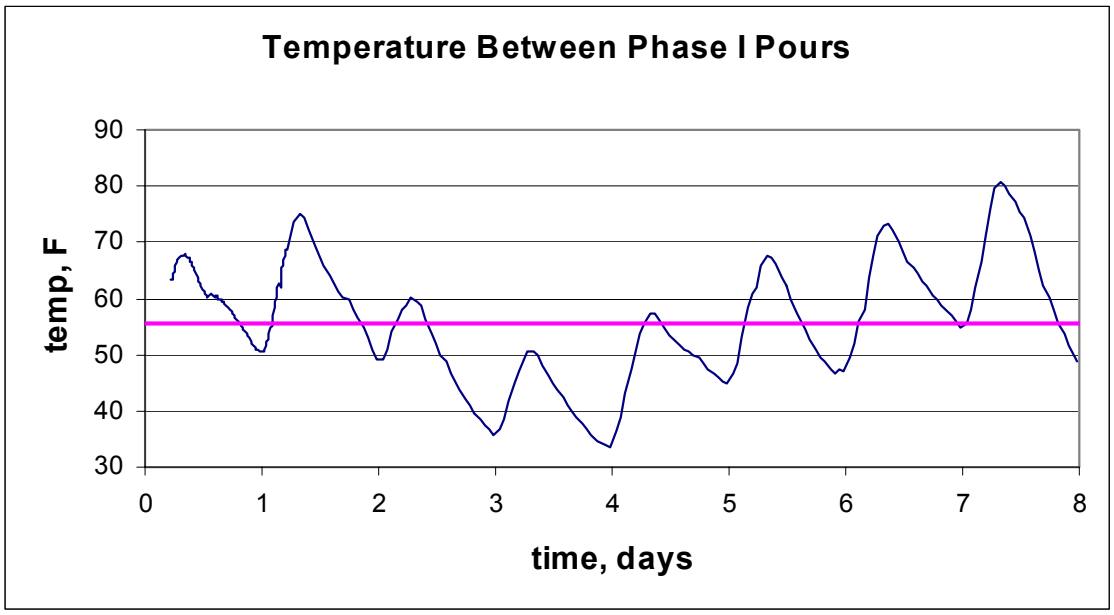

Figure B-3: Average system temperature between Phase I and II concrete pours. Average temperature between pours is the horizontal line. Time is measured in days since the beginning of the positive region pour.

	Girder J	Girder H	Girder G	Girder E	Temp, F
Initial	-5.002	-4.823	-4.706	-4.677	48.73
Final	-5.455	-5.343	-5.130	-5.010	54.41
Change	-0.453”	-0.520”	-0.424”	-0.333”	5.68

Table B-3: Deflection of Phase I Girders during negative region pour

Looking at the final readings, girder deflections are greater farther from the closure pour, as was the case in the positive region pour. Girder H shows the largest deflection during the pour but the final elevation is between that of Girders G and J. The transverse profile after this pour is shown in Figure B-4.

Table B-4 compares transverse girder deflections after and between the pours. Numbers in Table B-4 represent how much more a girder is deflected compared to Girder E. Each girder's deflection has been subtracted from that of Girder E. Negative numbers indicate a girder deflected more than Girder E. The row (change between + and - pours) is computed by subtracting the value in row (after negative pour) from the (after posi-

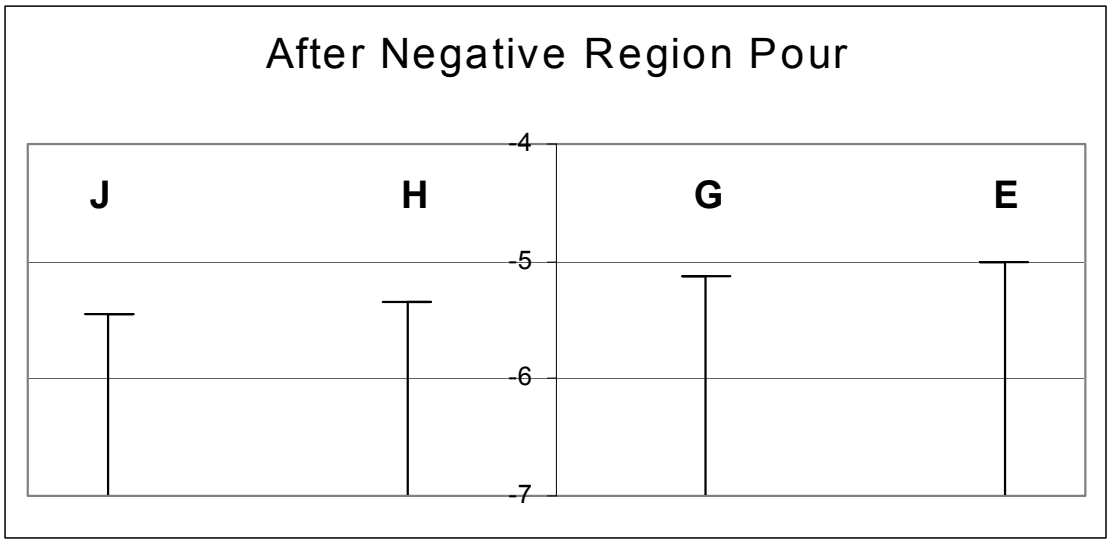

Figure B-4: Transverse deflection profile after negative region pour ended

tive pour) row value. A negative value here indicates a girder is lower than Girder E than before.

	J-E	H-E	G-E	E-E
After Positive pour	-0.339	-0.262	-0.022	0.000
Between pours	-0.325	-0.146	-0.029	0.000
After Negative pour	-0.445	-0.333	-0.120	0.000
Change between (+) and (-) pours	-0.106	-0.071	-0.098	0.000

Table B-4: Girder deflections in relation to Girder E at the end of positive and negative region pours

Looking at Table B-4, after the positive pour Girders G and E have nearly the same elevation (G is 0.022" lower than E) while H and J have substantially more deflection. Between pours Girders G and J are almost the same amount lower than E as after the positive pour while the elevation of Girder H has become closer to Girder E's elevation (Girder H was 0.262" lower than Girder E after the positive region pour while between pours it was only 0.146" lower than Girder E). After the negative pour Girders G, H and J are all lower than Girder E.

The (change between + and - pours) row indicates that G and J have deflected almost the same amount more than Girder E since the positive pour (0.106" and 0.098" for Girders J and G respectfully). A change value of zero would mean the girders deflected equally, keeping the same transverse profile. Each girder deflected almost an additional 0.1 in. more than Girder E.

B.2.2 Temporary Barrier Placement

Temporary barriers were placed on Phase I to carry traffic while Phase II was constructed. On November 5, 1999, temporary barriers were placed on the South side of Phase I. North side barriers were placed on November 12, 1999. Barrier locations can be seen in Figure B-5.

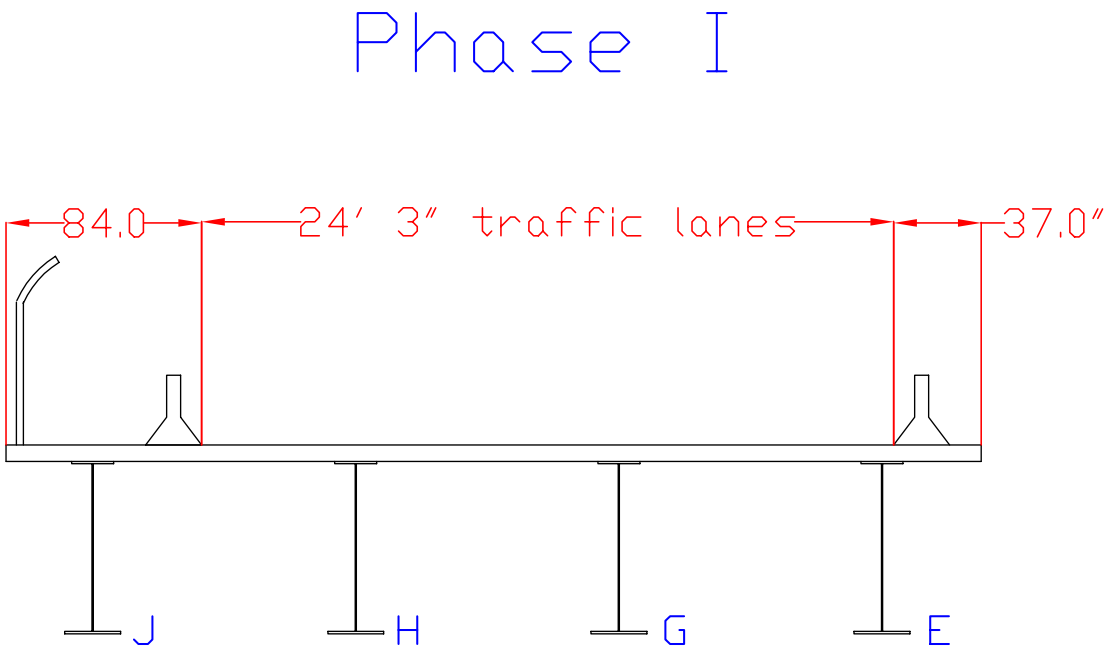

Figure B-5: Location of Temporary Barriers. South side barriers are on the left. North side barriers are on the right

Temporary barriers weigh approximately 360 lbs/ft and their location should affect the deflection profile. South side barriers are between Girders J and H so those girders should deflect more. Similarly, North side barriers should cause Girder E to deflect more than the others. Once again, because time elapsed between the negative region pour and barrier addi-

tion time dependant deflections can occur. Table B-5 summarizes deflection data from the negative region pour's end to before adding South side barriers. The interior girders deflect more than the others but Girder J still deflects a substantial amount. The average system temperature before barriers were added is close to the temperature at the negative pour's end. Between those events the temperature can vary although initial and final temperatures were nearly equal. The transverse deflection profile can be seen in Figure B-6.

	Girder J	Girder H	Girder G	Girder E	Temp, F
Initial	-5.455	-5.343	-5.130	-5.010	54.41
Final	-5.626	-5.641	-5.350	-5.103	51.48
Change	-0.171”	-0.298”	-0.220”	-0.093”	-2.97

Table B-5: Change in girder deflections between negative region pour and addition of South side temporary barriers

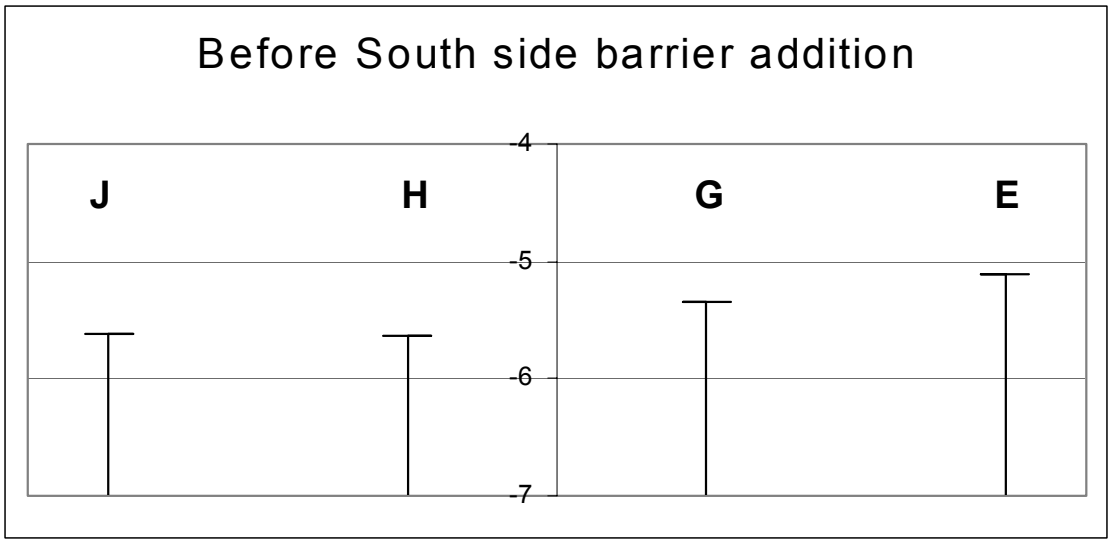

Figure B-6: Transverse deflection profile before South side temporary barrier placement

South side temporary barrier deflections can be seen in Table B-6. Clearly, Girder J and H deflect more than other girders as expected. Girder E actually loses deflection from this addition. System temperature also rose 10.52 degrees Fahrenheit during barrier addition. This change in tempera-

ture can cause downward deflection and skew results as outlined in Chapter 9. The transverse deflection profile after the South side barrier addition can be seen in Figure B-7.

	Girder J	Girder H	Girder G	Girder E	Temp, F
Initial	-5.626	-5.641	-5.350	-5.103	51.48
Final	-6.221	-6.023	-5.519	-5.083	62.00
Change	-0.595”	-0.382”	-0.169”	0.020”	10.52

Table B-6: Girder deflections caused by South side temporary barriers

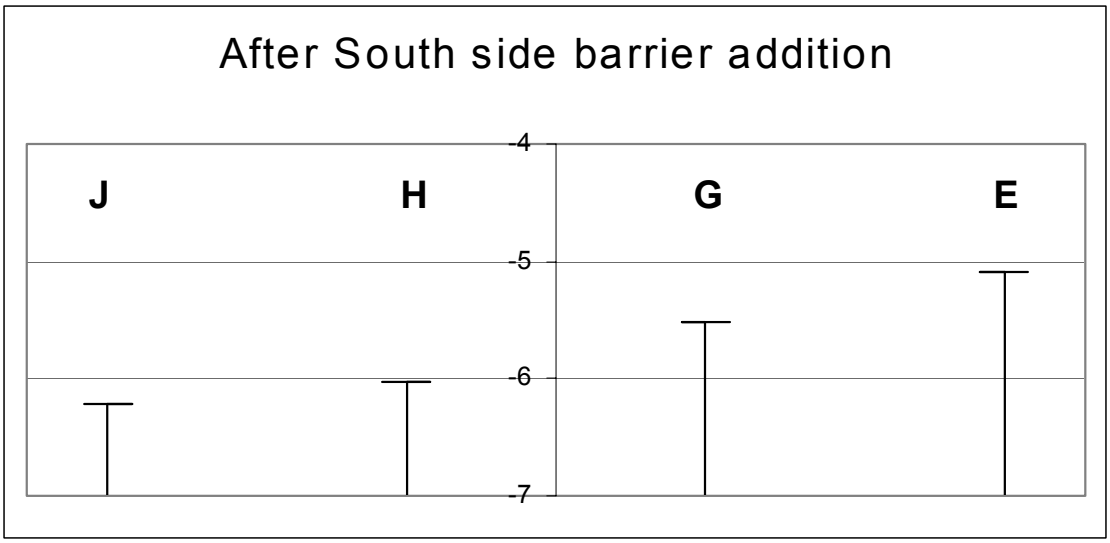

Figure B-7: Transverse deflection profile after the addition of South side temporary barriers

Table B-7 contains girder deflections between the South side barrier addition and the North side barrier placement. Temperature change between the operations was -16.51 degrees Fahrenheit. A negative temperature change causes the bridge to lose deflection, as has been shown. Time effects (the combination of creep, shrinkage and temperature changes) caused girders near the South barriers to deflect additional amounts while Girder E rebounded. Figure B-8 shows system temperature variation between barrier additions and Figure B-9 shows the transverse deflection profile before the North Side barrier placement.

	Girder J	Girder H	Girder G	Girder E	Temp, F
Initial	-6.221	-6.023	-5.519	-5.083	62.00
Final	-6.465	-6.176	-5.594	-5.072	45.49
Change	-0.244”	-0.153”	-0.075”	0.011”	-16.51

Table B-7: Deflection between South side barrier placement and beginning of North side barrier placement. 7 days passed between additions

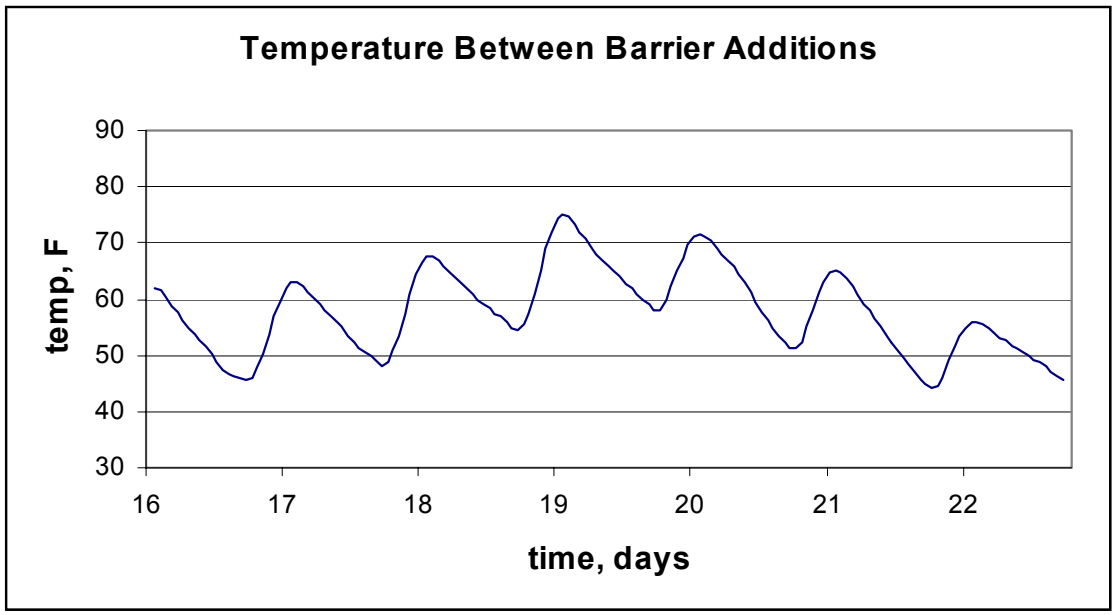

Figure B-8: System temperature variation between barrier additions

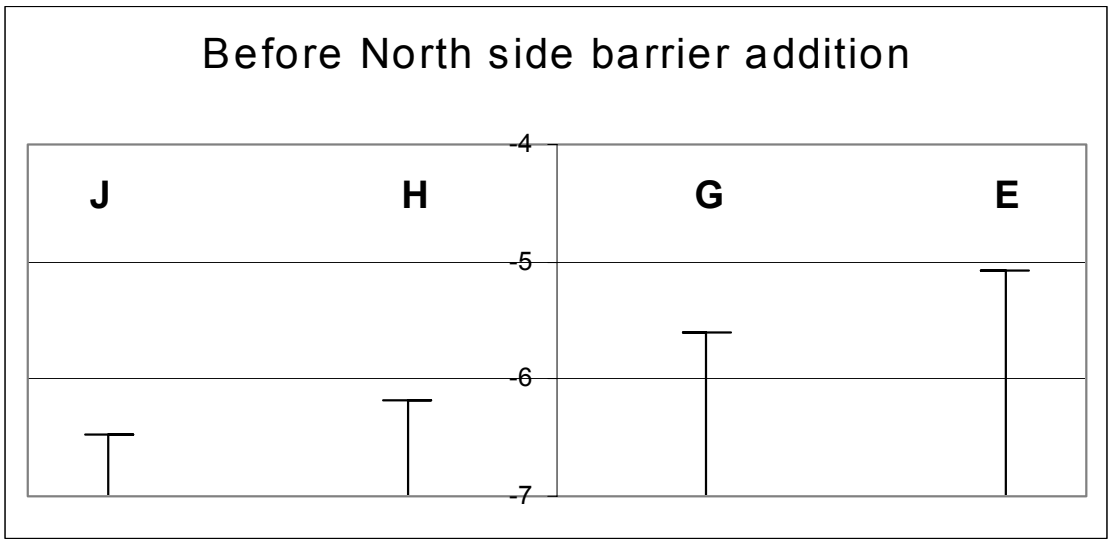

Figure B-9: Transverse deflection profile before North side temporary barrier placement

Girder deflections from placing North side temporary barriers are reported in Table B-8. Girder E, which is directly below the barriers, deflects more than the others but Girders H and J do deflect significant amounts. Girder J rebounds from this addition. The transverse deflection profile after the North side barrier addition is depicted in Figure B-10.

	Girder J	Girder H	Girder G	Girder E	Temp, F
Initial	-6.465	-6.176	-5.594	-5.072	45.49
Final	-6.457	-6.474	-6.183	-6.030	56.25
Change	0.008”	-0.298”	-0.589”	-0.958”	10.76

Table B-8: Girder deflections due to North side temporary barriers

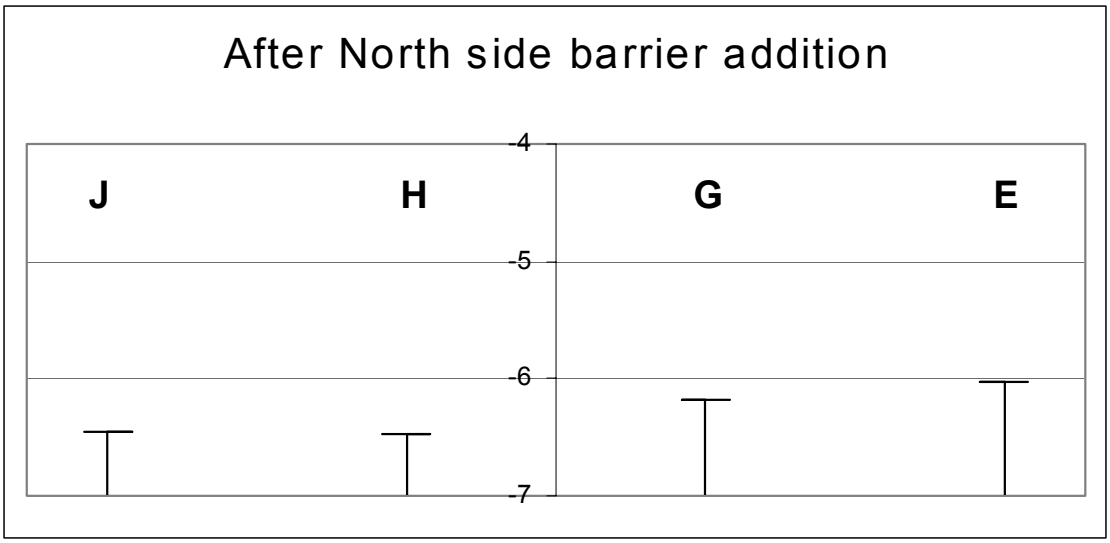

Figure B-10: Transverse deflection profile after North side temporary barrier placement

As seen in Figure B-10, after the North barriers were placed, Girders H and J are still at a lower elevation than Girders E and G. Table B-9, which is similar to Table B-4, contains transverse deflection profile information with respect to Girder E during barrier placement stages. Before South side barriers are added G, H, and J are already lower in elevation than E. Adding South side barriers causes Girders H and J to deflect much more than E. Time effects between the South side and North side barrier placement increase the elevation differences. Finally, the North side barriers bring the

transverse deflection profile closer to what was present before any additions. This is seen in the final row of Table B-9.

	J-E	H-E	G-E	E-E
Before S side added	-0.523	-0.538	-0.247	0.000
After S side added	-1.138	-0.940	-0.437	0.000
Before N side added	-1.393	-1.104	-0.522	0.000
After N side added	-0.427	-0.444	-0.153	0.000
Change during additions	0.096	0.094	0.094	0.000

Table B-9: Transverse girder deflection profile during various stages of temporary barrier placement

Superposition of loads was shown to be valid in the Live Load tests Section C.5.2. Superposition can also be used to determine girder deflections from barrier addition. If a girder deflect X in. from North side barriers and Y in. from South side barriers, the total deflection is X + Y in.

As barriers were not placed at the same time, instantaneous and time dependant deflections both occur. Instantaneous deflections during placements can be added to obtain the superposition of barrier displacements. Also the final elevation after all barriers were in place can be subtracted from the elevation before any barriers were in place to obtain the actual displacement that includes time effects. Table B-10 summarizes the superposition and actual displacements. The time effects are the differences between actual displacements and the superposition values. These values are seen in the final row of Table B-10 and are the same as those shown previously in Table B-7.

	Girder J	Girder H	Girder G	Girder E
Superposition	-0.587	-0.680	-0.758	-0.938
Actual	-0.831	-0.833	-0.833	-0.927
Difference	-0.244”	-0.153”	-0.075”	0.011”

Table B-10: Total deflection due to barrier addition

While Girder E has lost deflection from time effects the others have deflected more. It is interesting that the time effect has nearly equalized

the actual deflections experienced by Girders G, H, and J in Table B-10. Girder E is deflected more as it had a large deflection from the North side barrier.

Before the closure pour is performed these barriers are removed from Phase I. Deflections from removal should be much closer to values one would expect in a laboratory. This is because additions occurred during the day when temperature effects can induce deflection. It will be shown that during removal, temperature change is minimal. The removal deflections will be summarized later and compared to barrier addition deflections.

B.2.3 Phase I Long-Term Deflections up to the Closure Pour.

Phase I was opened to traffic on November 15, 1999. The closure pour occurred on May 6, 2000. During this 6 month period deck formwork was removed from Phase I and Phase II was constructed. Table B-11 summarizes the deflection which occurred between the time when North side barriers were placed and opening to traffic. Any change in deflection from time effects was small.

	Girder J	Girder H	Girder G	Girder E	Temp, F
N side barriers placed	-6.457	-6.474	-6.183	-6.030	56.25
Open to traffic	-6.417	-6.474	-6.224	-6.077	46.14
Change	0.040”	0.000”	-0.041”	-0.047”	-10.11

Table B-11: Deflection summary between North Side barrier placement and opening to traffic

Table B-12 summarizes deflections between Phase I opening to traffic and the closure pour. Girders E and G show more time dependant deflection than H and J. Table B-13 contains the transverse girder deflection profile at this time. The time effects have brought girder elevations to nearly the same amount. This is especially true for Girder J, which had always been deflected significantly more than E. Figure B-11 is a plot of the transverse girder deflection profile at the time before the closure operation began.

	Girder J	Girder H	Girder G	Girder E	Temp, F
Open to traffic	-6.417	-6.474	-6.224	-6.077	46.14
Closure Pour	-6.532	-6.622	-6.530	-6.507	78.56
Change	-0.115"	-0.148"	-0.306"	-0.430"	32.42

Table B-12: Girder deflections between Phase I being opened to traffic and the closure pour

	J-E	H-E	G-E	E-E
When opened to traffic	-0.340	-0.397	-0.147	0.000
Before closure operation	-0.025	-0.115	-0.023	0.000
Change	0.315	0.282	0.124	0.000

Table B-13: Transverse girder deflection profile when opened to traffic and before closure

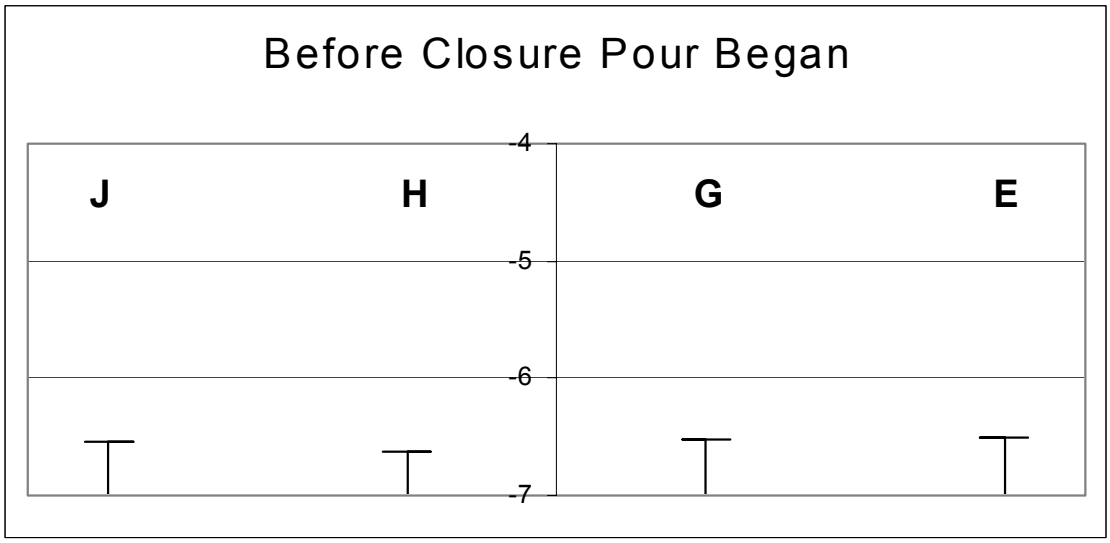

Figure B-11: Transverse deflection profile immediately before closure operation began

Figures B-12 through B-15 show the deflection history for each Phase I girder from the time traffic opened until the closure pour. Temperature is also plotted as it has an effect on deflections, as shown previously.

On each figure time effects can be seen. Deflection increases although no permanent loads are applied to Phase I. The deflections are caused by a combination of shrinkage induced deflection and temperature change. The straight-line portion near day 60 is where data for those times were lost. In

a laboratory setting temperature changes would not occur and only shrinkage deflections would occur in this time.

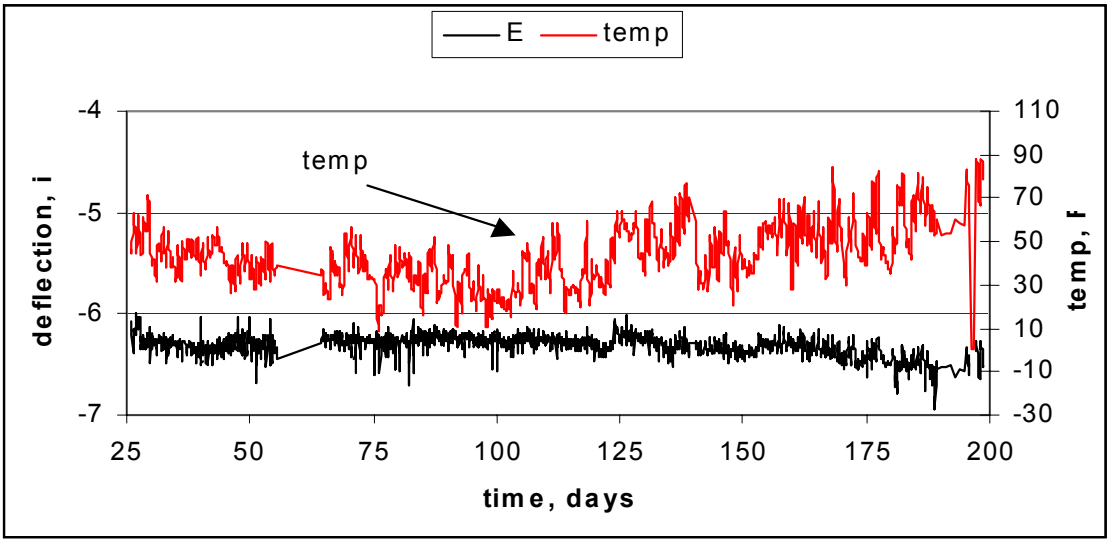

Figure B-12: Long term deflection of Girder E between opening to traffic and closure pour

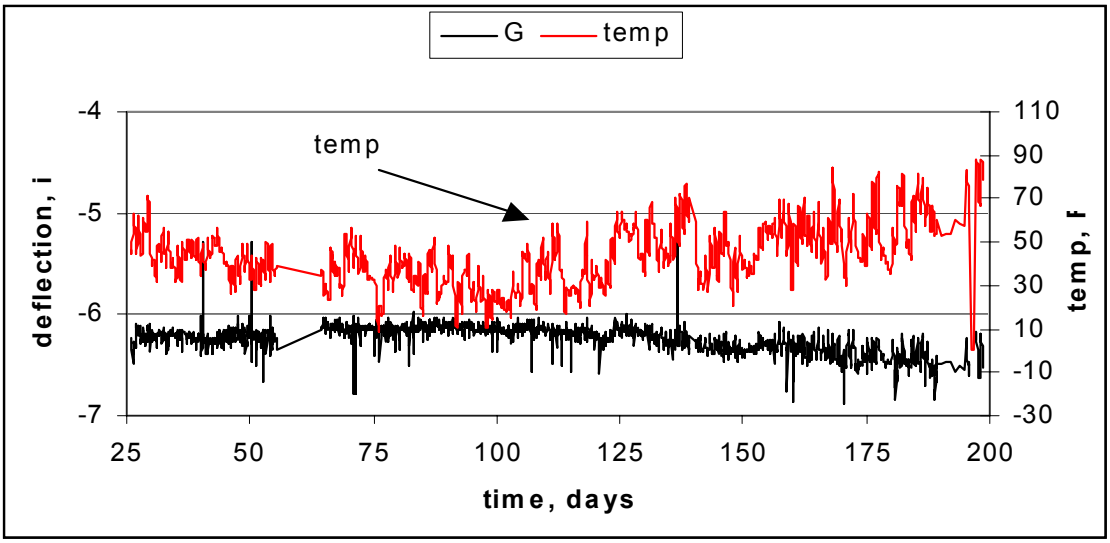

Figure B-13: Long term deflection of Girder G between opening to traffic and closure pour

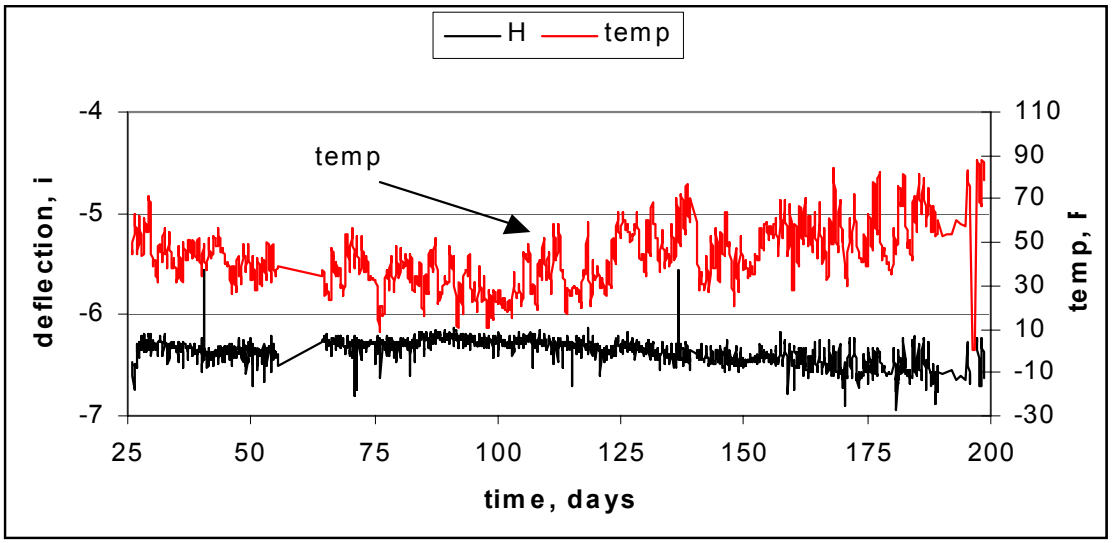

Figure B-14: Long term deflection of Girder H between opening to traffic and closure pour

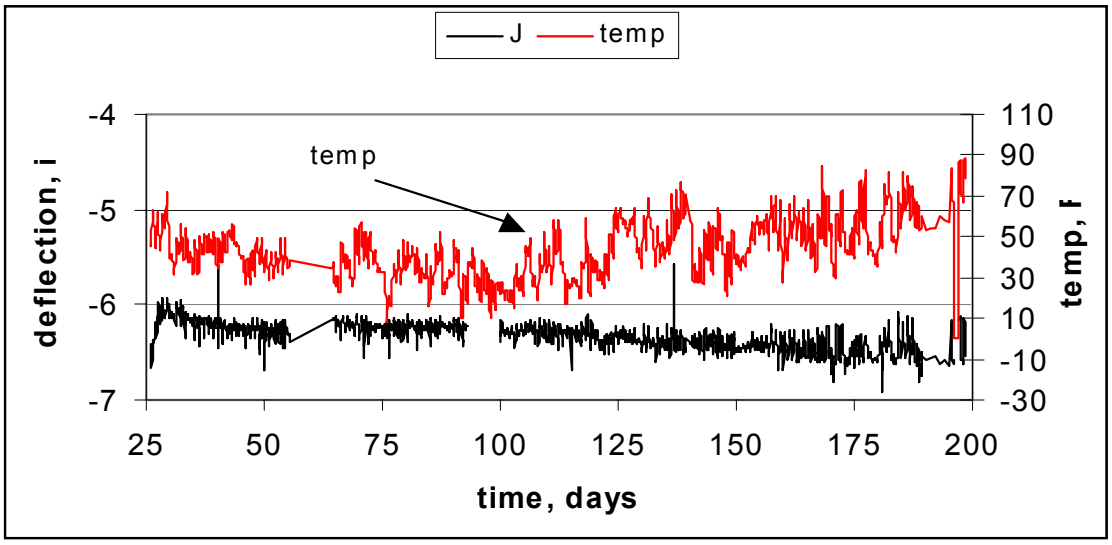

Figure B-15: Long term deflection of Girder J between opening to traffic and closure pour

B.3 Phase II Deflection History Until Closure

Phase II was constructed while Phase I carried traffic. The Phase II positive region pour occurred on April 18, 2000. Prior to this pour beginning, readings for Phase II were obtained to use as a datum elevation for Phase II. Girder deflections for this Phase will be relative to this datum. It is

assumed that each phase was at the same elevation prior to positive region pours. Table B-14 contains girder deflection data for the Phase II positive region pour.

	Girder D	Girder C	Girder B	Girder A	Temp, F
Initial	0.000”	0.000”	0.000”	0.000”	44.65
Final	-4.432”	-4.623”	-4.714”	-4.936”	65.42
Change	-4.432”	-4.623”	-4.714”	-4.936”	20.77

Table B-14: Girder Deflections for Phase II positive region pour

During this pour Girder D, which is closest to the closure pour, deflected the least while Girder A deflected 0.504" more. This is the same phenomenon as observed for the Phase I positive pour as deflection increases away from the closure. Currently there is no explanation for this behavior. Figure B-16 shows girder deflections after the positive region pour.

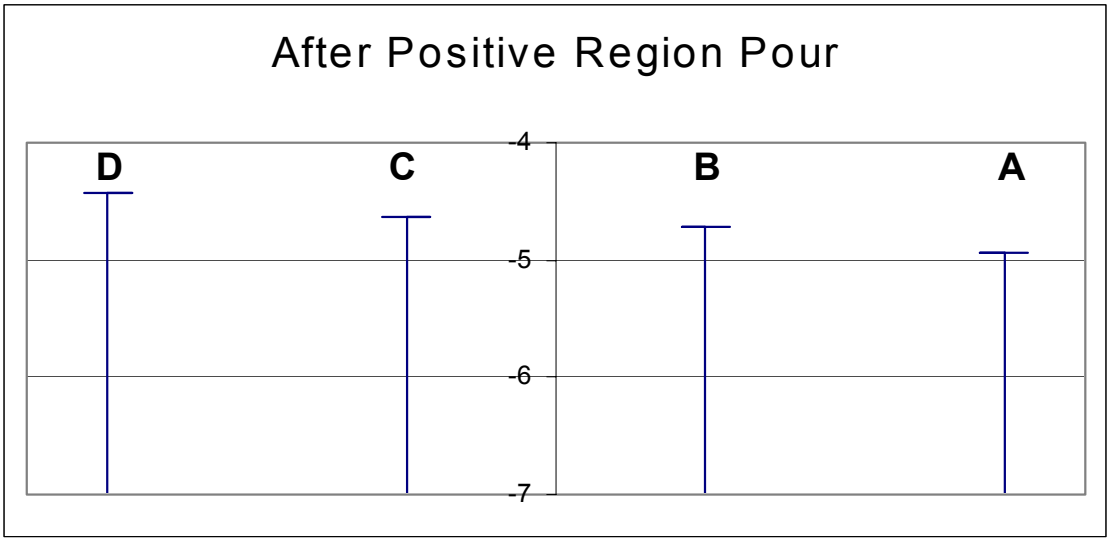

Figure B-16: Phase II transverse girder deflection profile after positive region pour completion

Before the negative region pour could occur the positive region concrete had to reach its design 28 day compressive strength. During this time shrinkage induced deflections occurred. Readings taken before the negative region pour allow measurement of this deflection. Table B-15 contains

data from the end of the positive region pour to the beginning of the negative region pour.

	Girder D	Girder C	Girder B	Girder A	Temp, F
Initial	-4.432"	-4.623"	-4.714"	-4.936"	65.42
Final	-4.864	-5.079	-5.155	-5.357	53.46
Change	-0.432"	-0.456"	-0.441"	-0.421"	-11.96

Table B-15: Girder Deflections between Phase II positive and negative region pours

This data shows a significant deflection increase between pours. Every girder deflects nearly the same amount which will preserve the transverse profile. The profile before the negative region pour is shown in Figure B-17. Average system temperature between pours is shown in Figure B-18.

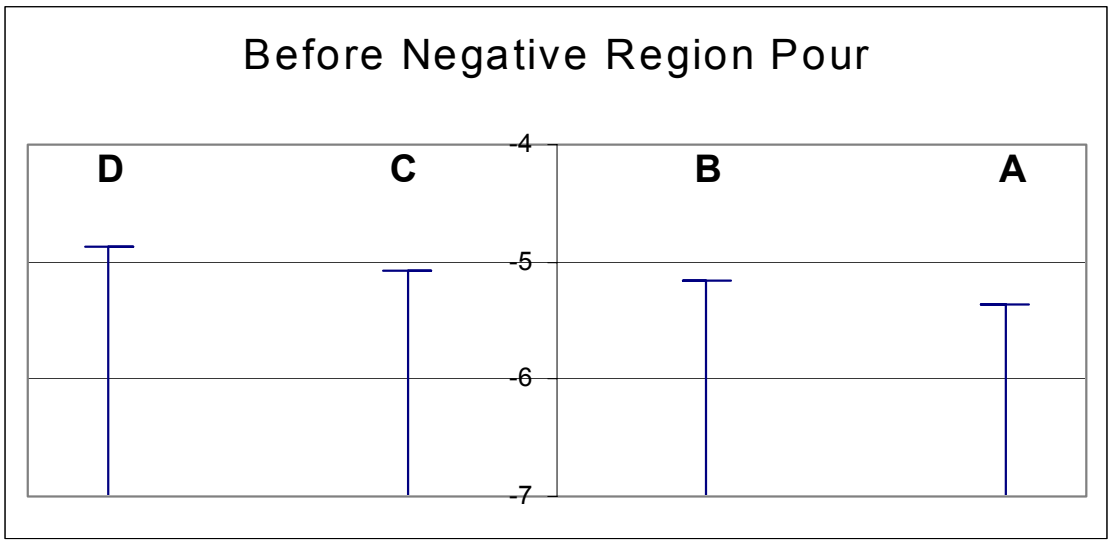

Figure B-17: Phase II transverse girder deflection profile before negative region pour began

Girder deflections during the negative region pour that occurred on April 26, 2000 are contained in Table B-16. Girder deflections during this pour are nearly equal. Once again this will preserve the transverse profile introduced by the positive region pour. The deflection profile of Phase II after this operation is seen in Figure B-19.

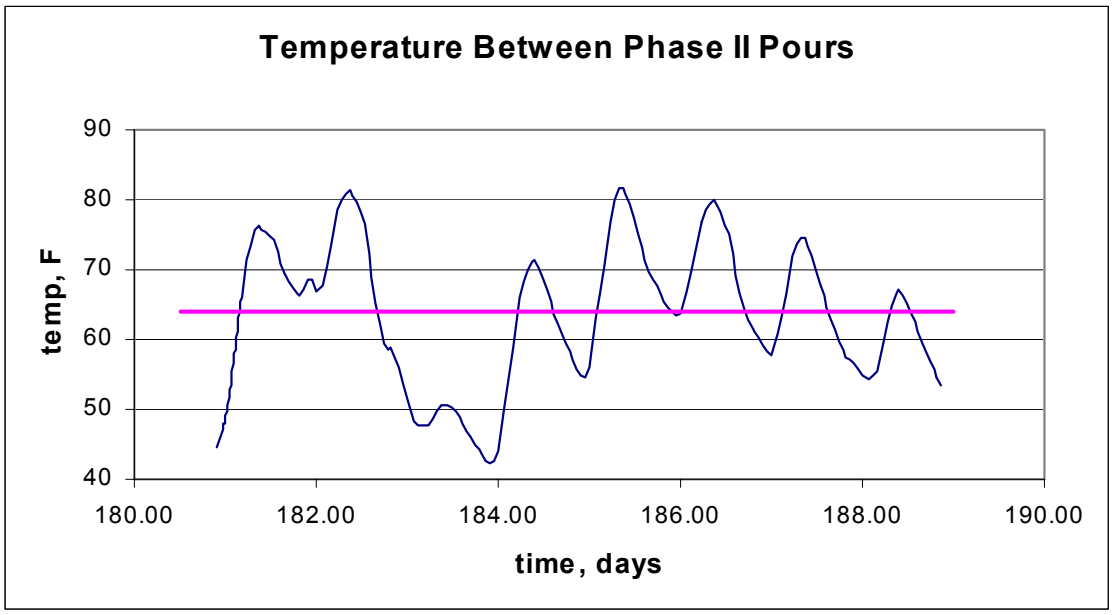

Figure B-18: Average system temperature between Phase II positive and negative region pours. The straight line is the average temperature during this time

	Girder D	Girder C	Girder B	Girder A	Temp, F
Initial	-4.864	-5.079	-5.155	-5.357	53.46
Final	-5.299	-5.502	-5.581	-5.799	57.01
Change	-0.435”	-0.423”	-0.426”	-0.442”	3.55

Table B-16: Girder Deflections during Phase II negative region pour

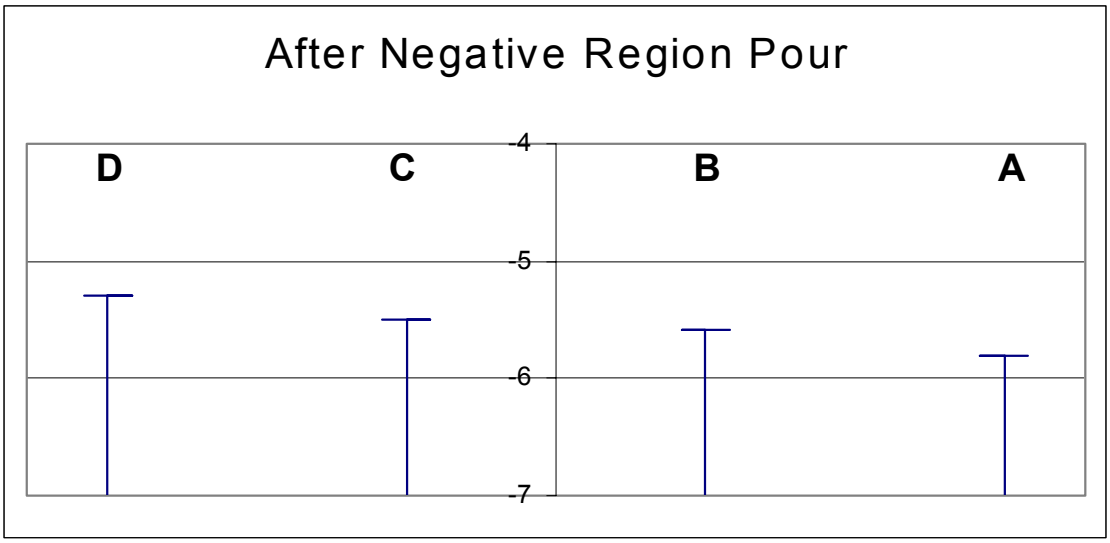

Figure B-19: Phase II transverse girder deflection profile after negative region pour completion

Once the negative pour concrete reached its 28 day design compressive strength, the closure operation could take place. The closure pour occurred on May 6, 2000. Time effects took place while preparations for the closure operation were made. Table B-17 contains deflection information from the end of the negative pour to the closure operation beginning. The positive change values show that the girders actually lost deflection during this time. This could be due to formwork removal but is unlikely with the composite section's stiffness. Figure B-20 shows the deflection profile before closure operations began.

	Girder D	Girder C	Girder B	Girder A	Temp, F
Initial	-5.299	-5.502	-5.581	-5.799	57.00
Final	-4.910	-5.176	-5.277	-5.454	78.57
Change	0.389”	0.326”	0.304”	0.345”	21.57

Table B-17: Girder Deflections between the Phase II negative region pour and the closure operation

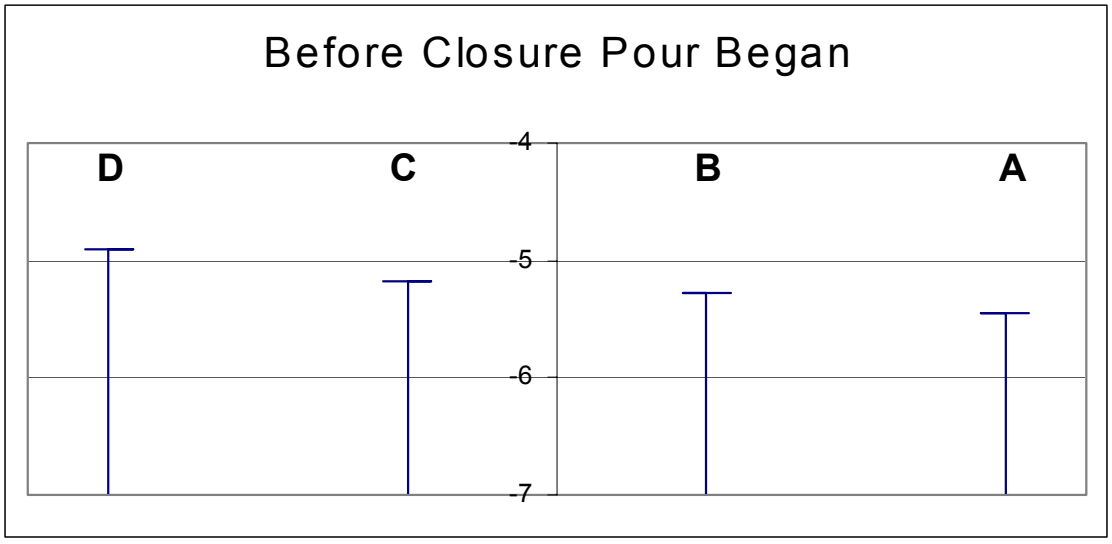

Figure B-20: Phase II transverse girder deflection profile before beginning of closure operation

Table B-18 summarizes deflection profiles for Phase II until closure. Data is shown in relation to Girder A with negative values representing a girder being deflected more than A. Time effects between the negative pour and

closure cause most of the change. The transverse profile change is computed by subtracting the value after the positive pour from the value at closure pour.

	D-D	C-D	B-D	A-D
Positive pour	0.000	-0.191	-0.282	-0.504
Between pours	0.000	-0.215	-0.291	-0.493
Negative pour	0.000	-0.203	-0.282	-0.500
At closure pour	0.000	-0.266	-0.367	-0.544
Change	0.000	-0.075	-0.086	-0.045

Table B-18: Phase II relative deflections with respect to Girder A

B.4 Comparison of Phase I and II Deflections until the Closure Pour

Deflection comparisons of Phase I and II can be made to determine girder elevations at closure time. As the system is symmetric about the project centerline, girders equal distance from the closure region should be compared. This leads to Girder E compared to D, G to C, H to B, and J to A. Table B-19 shows girder deflections due to the positive region pours. The final row is computed by subtracting Phase II girder deflections from Phase I girder deflections. A negative value represents a Phase I girder deflecting more than the similar girder on Phase II.

J	H	G	E	Temp Change
-4.932”	-4.855”	-4.615”	-4.593”	30.59
A	**B**	**C**	**D**	**Temp Change**
-4.936”	-4.714”	-4.623”	-4.432”	20.77
J-A	**H-B**	**G-C**	**E-D**	**Temp Difference**
0.004	-0.141	0.008	-0.161	-9.9

Table B-19: Comparison of Phase I and Phase II girder deflections due to the positive region pour

Both phases deflected similarly during positive region pours as expected. Although E-D shows what looks like a significant difference it is only a 4%

difference. Table B-20 compares Phase I and II transverse profiles after positive pours. Measurements are relative to Girder E for Phase I and D for Phase II. As the table shows transverse comparisons for Girders G and C as well as J and A have different magnitudes. Phase II shows a more linear variation moving away from the closure than Phase I.

J-E	H-E	G-E	E-E
-0.339	-0.262	-0.022	0.000
A-D	**B-D**	**C-D**	**D-D**
-0.504	-0.282	-0.191	0.000

Table B-20: Comparison of Phase I and Phase II transverse girder deflection profiles due to positive region pours

Time between the positive and negative pours allowed shrinkage deflections to occur for both phases. The amount of time dependant deflection for both phases is summarized in Table B-21. Phase II experienced a significant time dependant deflection while Phase I did not. The time dependant deflections are a combination of temperature and shrinkage effects. For Phase I these effects negated each other resulting in small net deflection changes. Although Table B-21 shows a similar net temperature change for both phases between pours Figures B-3 and B-18 show very different temperature histories for each phase between pours

J	H	G	E	Temp Change
-0.070”	0.032”	-0.091”	-0.084”	-14.80
A	**B**	**C**	**D**	**Temp Change**
-0.432”	-0.456”	-0.441”	-0.421”	-11.60
J-A	**H-E**	**G-C**	**E-D**	**Temp Difference**
0.362	0.424	0.350	0.337	-3.20

Table B-21: Comparison of deflection changes between positive and negative region pours for Phases I and II

Phase I pours occurred during fall while Phase II's occurred during spring. Temperatures during these seasons can be different. Table B-22 summa-

rizes Phase I and II temperature data between positive and negative region pours. Average temperature between pours for Phase II was 8.5 degrees Fahrenheit higher than Phase I. Although maximum temperatures are nearly equal minimum temperatures are not. Temperature range was also smaller for Phase II.

Temp, F	Phase I	Phase II
Average Temperature	55.4	63.9
Minimum Temperature	33.4	44.2
Maximum Temperature	80.7	81.7
Temperature Range	47.3	37.5

Table B-22: Summary of temperature data between positive and negative region pours

Deflection comparisons during negative region pours are also important. Table B-23 contains these comparisons. Temperature when the Phase I operation ended was 54.41 degrees Fahrenheit and Phase II was 57.01 degrees Fahrenheit when the operation ended. Phase II girders deflected more evenly than Phase I. This will maintain the initial transverse profile of Phase II as already shown. The G-C and J-A values show these girders deflect very similarly for this operation. This is expected as the pour regions are the same and phases are symmetric. Table B-24 contains transverse deflection profile information after the negative region pour.

J	H	G	E	Temp Change
-0.453”	-0.520”	-0.424”	-0.333	5.68
A	**B**	**C**	**D**	**Temp Change**
-0.442”	-0.426”	-0.423”	-0.435”	3.55
J-A	**H-E**	**G-C**	**E-D**	**Temp Difference**
-0.011	-0.094	-0.001	0.102	-2.13

Table B-23: Comparison of Phase I and Phase II girder deflections due to the negative region pour

Although Table B-24 shows different transverse profiles for each phase the difference increases for girders farther from the closure in both cases.

J-E	H-E	G-E	E-E
-0.445	-0.333	-0.120	0.000
A-D	**B-D**	**C-D**	**D-D**
-0.493	-0.291	-0.215	0.000

Table B-24: Comparison of Phase I and Phase II transverse girder deflection profiles after negative region pours

After negative region deck casting the phases have different deflection histories. Phase I has barriers placed and carries traffic. Phase II undergoes no additional construction operations until the closure pour begins. Table B-25 contains final girder deflections prior to closure operation commencement.

J	H	G	E
-6.532	-6.622	-6.530	-6.507
A	**B**	**C**	**D**
-5.454”	-5.277”	-5.176”	-4.910”

Table B-25: Comparison of Phase I and Phase II girder deflections before closure operation

It is not appropriate to compare these deflections. Phase I still has barriers on it so conditions are not similar, as they were for other comparisons. Both systems now have equal system temperatures and temperature effects should be equal. Many events occurred during closure such as moving and placing barriers. This will be studied in detail in the following section.

B.5 System Deflections During Closure

Closure operations began on May 5, 2000 at 11pm with closing traffic on Phase I. During closure was the only time traffic was completely closed. As seen previously in Table B-25 the phases were at significantly different elevations due to the presence of barriers on Phase I. This can also be seen in

Figure B-21. Several steps were taken to relieve the elevation difference. First, barriers were completely removed from Phase I.

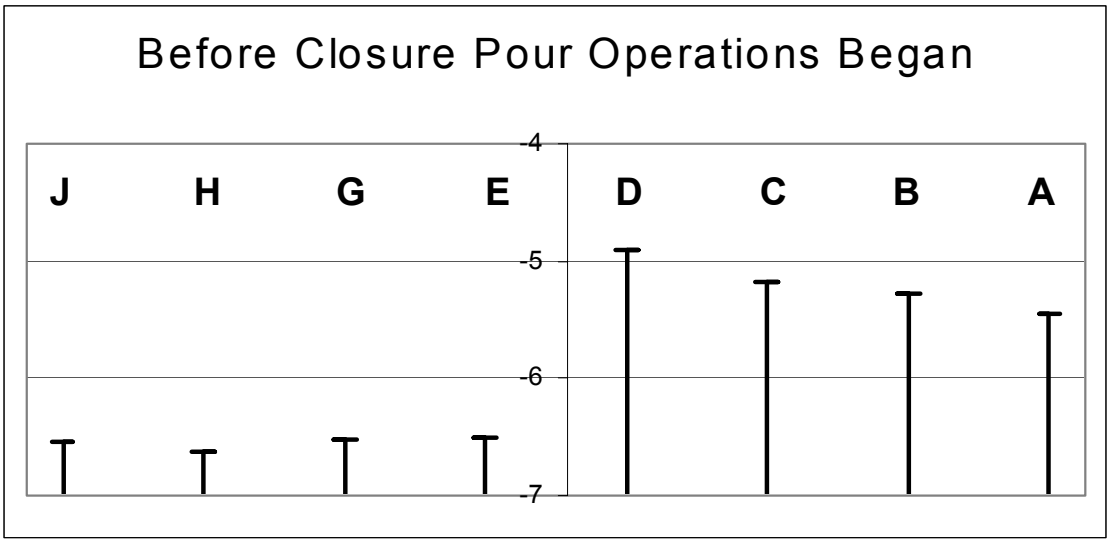

Figure B-21: Transverse girder deflection profile before closure operations began

Barriers on the closure side (North side of Phase I) were removed first. These were also the last barriers placed before Phase I was opened to traffic. Table B-26 compares deflections from adding and removing barriers. Positive numbers represent girders losing deflection. Removal deflections were all opposite to addition deflections as expected. Deflections from removal were smaller than from addition. Temperature change was much smaller when barriers were removed than added. Figure B-22 shows the transverse girder deflection profile after these barriers were removed.

Next, sidewalk barriers (South side of Phase I) were removed. Removal deflections can once again be compared to addition deflections as seen in Table B-27. Deflections from removing these barriers are actually greater than deflections from addition. Once again temperature change when adding and removing is quite different.

Total addition and removal deflections can be found using superposition. These results are shown in Table B-28. Time dependant deflections between additions are included as they have a significant affect. The differ-

	J	H	G	E	Temp
Beginning of closure barrier removal	-6.532	-6.622	-6.530	-6.507	78.57
After Closure barriers removed	-6.575	-6.429	-6.091	-5.804	77.61
Removal Change	-0.043	0.193	0.439	0.703	-0.96
Addition Change (Table 10.7)	0.008”	-0.298”	-0.589”	-0.958”	10.76
Difference in adding and removing deflections	-0.035	-0.105	-0.150	-0.255	11.72

Table B-26: Comparison of Phase I deflections from removing and adding barriers near sidewalk (North side Phase I)

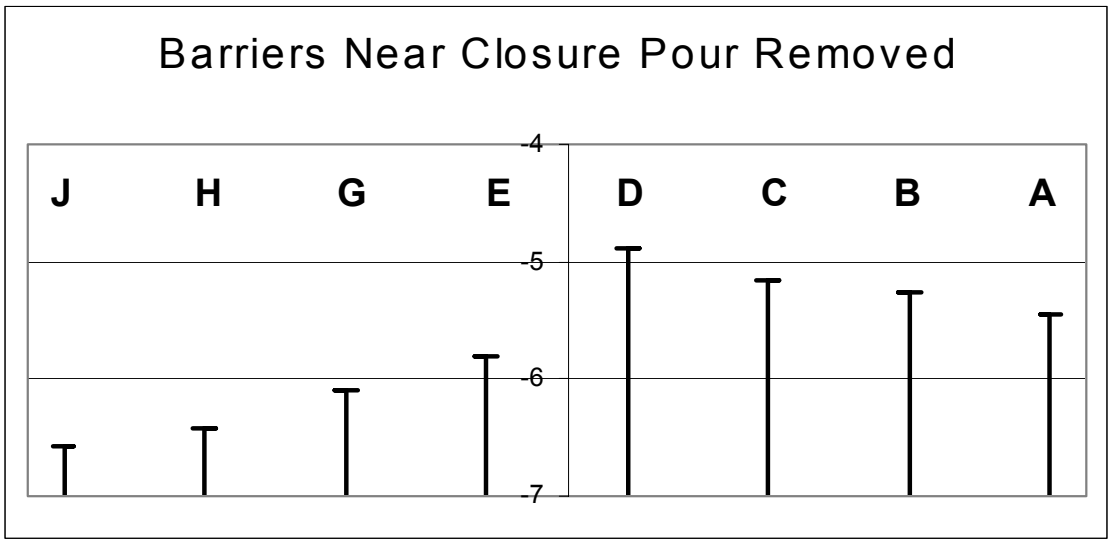

Figure B-22: Transverse girder deflection profile after barriers near closure were removed

ence is computed by the difference in addition and removal deflections. There is a significant difference in addition and removal deflections. During addition temperature changes were much larger and affected results. This illustrates the problem of temperature change during construction events and acquiring reliable data. Removal deflections should be more accurate.

	J	H	G	E	Temp
Beginning of sidewalk barrier removal	-6.591	-6.442	-6.099	-5.811	76.28
After sidewalk barriers removed	-5.889	-5.991	-5.886	-5.810	74.39
Removal Change	0.702	0.451	0.213	0.001	-1.89
Addition Change (Table 10.6)	-0.595	-0.382	-0.169	0.020	10.76
Difference in adding and removing deflections	0.107	0.069	0.044	-0.019	12.65

Table B-27: Comparison of Phase I deflections from removing and adding barriers near sidewalk (South side Phase I)

	J	H	G	E
Addition Superposition	-0.587	-0.680	-0.758	-0.938
Addition Time Dependent Deflections (Table 10.7)	-0.244	-0.153	-0.075	0.011
Deflection from barrier addition	-0.831	-0.833	-0.833	-0.927
Deflection from barrier removal	0.643	0.630	0.644	0.697
Difference	-0.188	-0.203	-0.189	-0.230

Table B-28: Comparison of total girder deflection from barrier addition and removal

Girders do not rebound equal amounts as barriers are removed from each side but the net effect is such that each girder loses nearly the same amount of deflection after superposition. As each girder rebounds nearly equally, the transverse profile should not change significantly. Table B-29 compares the Phase I transverse profile before any barriers were removed during closure operations to the profile after both barriers were removed. The transverse profile is slightly higher than before but the changes were small. Figure B-23 shows the transverse girder profile after all barriers were removed from Phase I.

	J-E	H-E	G-E	E-E
Before closure operation	-0.025	-0.115	-0.023	0.000
After barriers removed	-0.079	-0.181	-0.076	0.000
Change	-0.054	-0.066	-0.053	0.000

Table B-29: Transverse girder deflection profile as barriers were removed from Phase I for closure

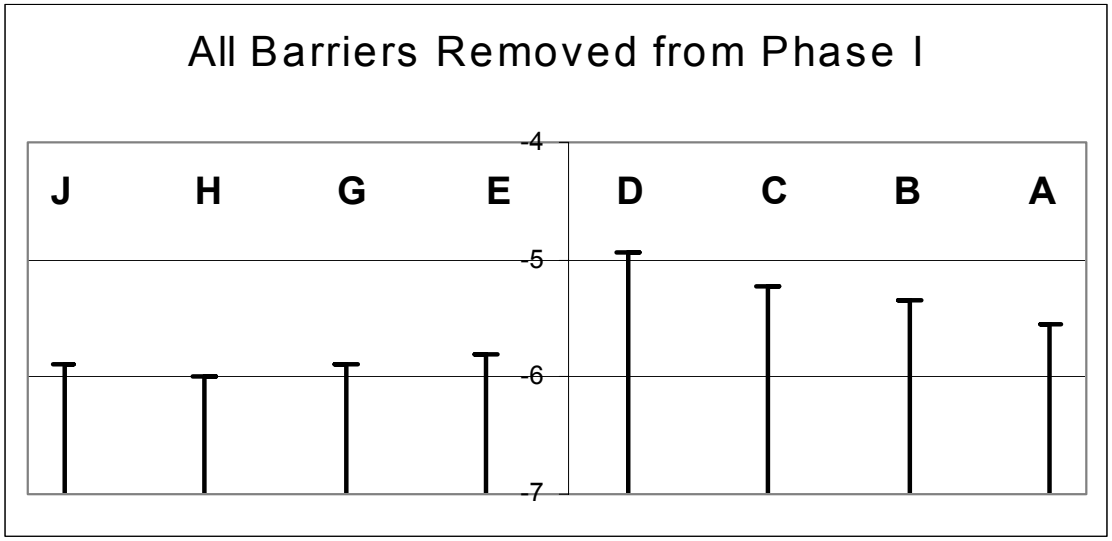

Figure B-23: Transverse Girder profile after all barriers on Phase I were removed

Once barriers are removed from Phase I long-term deflections can be determined. To determine long-term deflections, instantaneous deflections are removed from readings. The complete deflection history for Girder E is shown in Figure B-24 and the long-term deflection history appears in Figure B-25. Instantaneous deflections can be in error due to short term temperature changes during events but this is the best that can be expected in the field.

From data similar to that in Figure B-25 the time dependant deflections after barrier removal can be determined. This data appears in Table B-30. Phase I Girders deflected a significant amount from time effects. Phase II girders also show time dependant deflections but they are not as large.

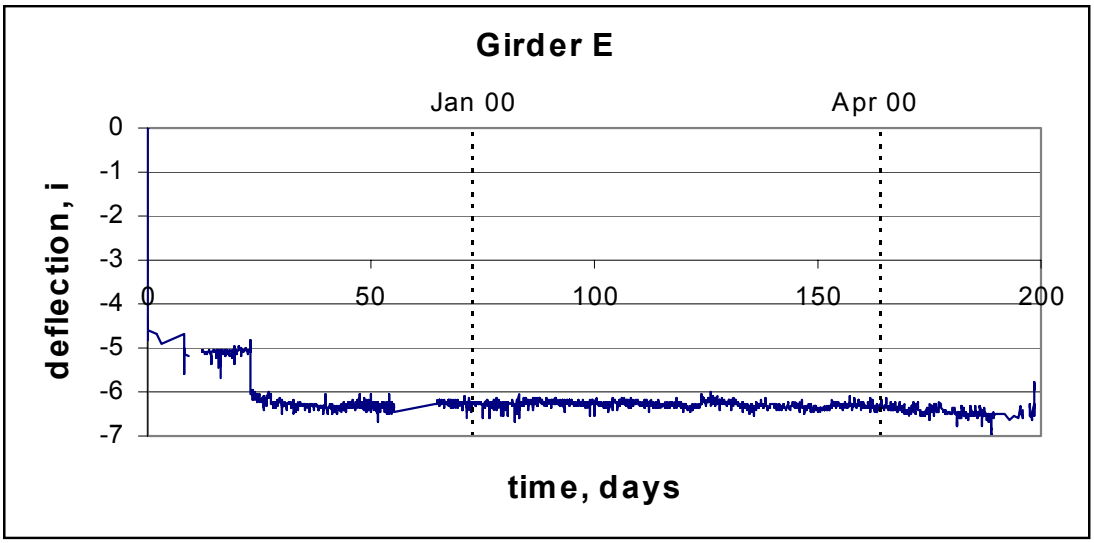

Figure B-24: Deflection History of Girder E

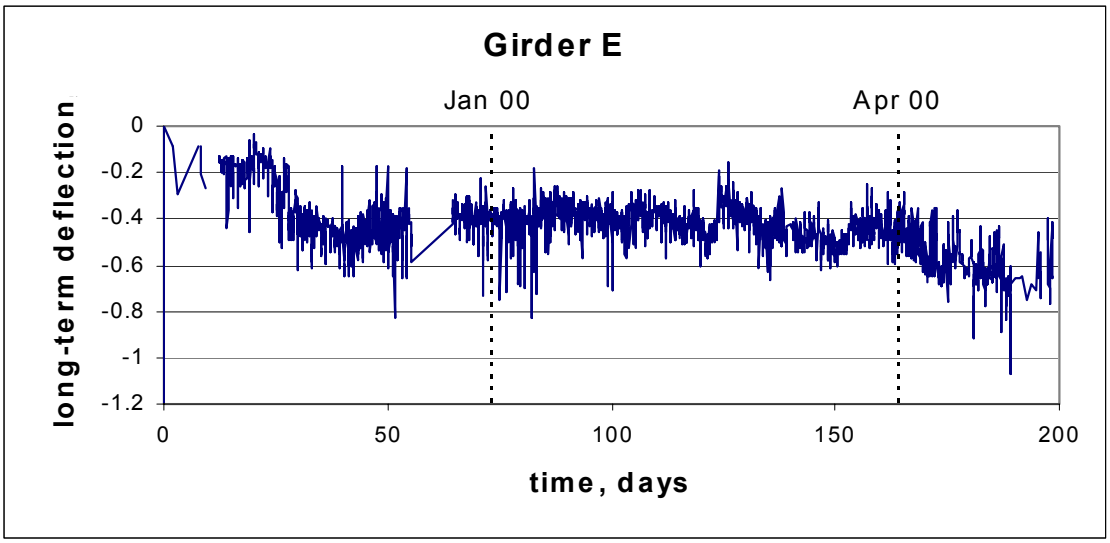

Figure B-25: Long-term deflection of Girder E. Instantaneous deflections have been removed from data

J	H	G	E	D	C	B	A
-0.577	-0.580	-0.741	-0.650	-0.063	-0.173	-0.205	-0.170

Comparison of Phase I and Phase II Deflections

J-A	H-B	G-C	E-D
-0.407	-0.375	-0.568	-0.587

Table B-30: Time dependent deflections of both Phases

At closure time 200 days have passed since the Phase I positive region pour. Only 17 days have passed since Phase II positive region pour. Phase I has had much more time to undergo shrinkage deflections. Free shrinkage strains from specimens made at the time of each Phase's positive region pour appear in Figure B-26. Embedment gage E12, in the free shrinkage specimen from Phase I, shows -400με of shrinkage for Phase I while embedment gage E22, in the free shrinkage specimen from Phase II, shows only -250με of shrinkage. This difference in shrinkage accounts for some of the difference in Table B-30. Temperature affects also account for some of the difference

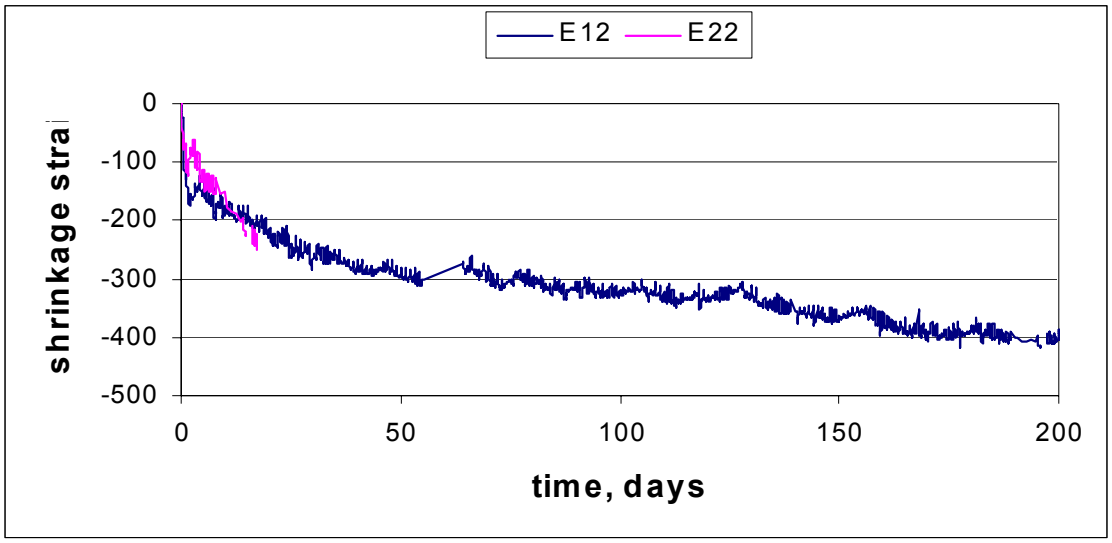

Figure B-26: Free shrinkage strains for Phase I (E12) and Phase II (E22)

As temporary barriers were removed from Phase I both phases were under similar conditions and differential elevations can be determined. The differential elevation is a combination of differences in time dependant deflections and construction deflections. Table B-31 compares elevations of Phase I and II. Negative numbers represent Phase I girders which are lower than the corresponding Phase II girder. At this stage, all Phase I girders are significantly lower than Phase II girders.

J	H	G	E	D	C	B	A
-5.889	-5.991	-5.886	-5.810	-4.942	-5.230	-5.350	-5.551

Comparison of Phase I and Phase II elevations

J-A	H-B	G-C	E-D
-0.338	-0.641	-0.656	-0.868

Table B-31: Phase I and II elevation comparison after barriers removed from Phase I

Time dependant deflections of similar girders can also be compared. These values from Table B-30 and values from Table B-31 allow determination of the amount of elevation difference due to construction. To do this, time dependant deflections are subtracted from the elevation difference. This is done in Table B-32. Construction difference accounts for 32% of the total elevation difference for Girders E and D.

	J-A	H-B	G-C	E-D
Time dependant deflections (Table 10.30)	-0.407	-0.375	-0.568	-0.587
Elevation differences (Table 10.31)	-0.338	-0.641	-0.656	-0.868
Construction Difference	0.019	-0.366	-0.072	-0.279

Table B-32: Contributions to the elevation difference

As the differential elevation between the phases, especially near the closure, was very high as shown in Table B-31, steps were taken to reduce the differential. Temporary barriers were placed on Phase II near the closure on the East span as seen in Figure B-27. This caused Phase II girders to deflect, especially those near the closure region. Deflections before and after these barriers were placed appear in Table B-33.

The measure to reduce differential deflections also influences the transverse profile. Figure B-28 shows the transverse profile after these barriers were placed. The barrier addition not only reduced the differential deflection but it also created a more even transverse profile.

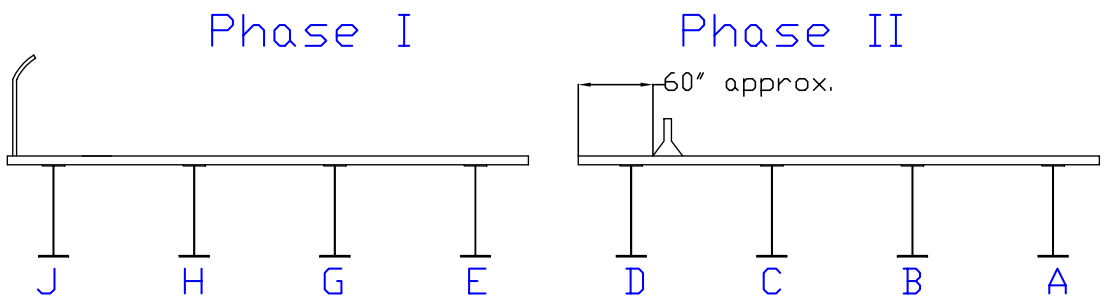

Figure B-27: Barrier placement on Phase II near closure. Exact location is unknown

	D	C	B	A
Before barriers placed on Phase II East span	-4.942	-5.230	-5.350	-5.551
After barriers placed on Phase II East Span	-5.966	-6.016	-5.879	-5.844
Deflection	-1.024	-0.786	-0.529	-0.293

Table B-33: Deflection due to barriers placed on Phase II East span

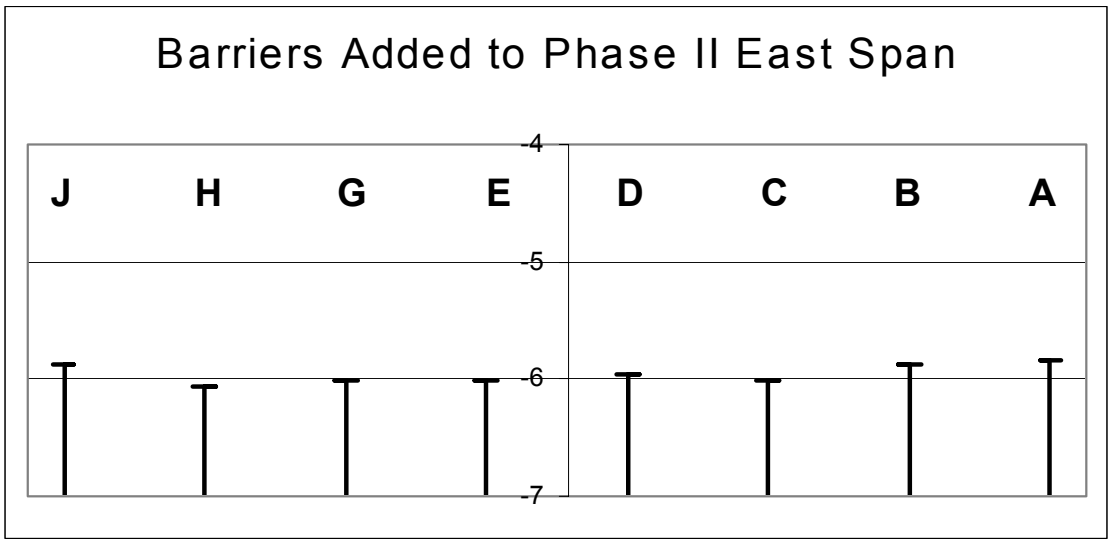

Figure B-28: Transverse profile after barriers added to Phase II East span

Deflections of the two phases can now be compared to determine differential deflections after barriers were placed on the Phase I East span as seen in Table B-34. The large differential elevation between E-D has been reduced greatly. This is more favorable than a large difference. Large differences make performing the closure pour difficult with respect to finish-

ing the concrete and the deck surface would not be smooth across the width.

J	H	G	E	D	C	B	A
-5.883	-6.056	-6.017	-6.012	-5.966	-6.016	-5.879	-5.844

Comparison of Phase I and Phase II elevations

J-A	H-B	G-C	E-D
0.001	-0.177	-0.001	-0.046

Table B-34: Girder deflections after barriers placed on Phase II East Span

The closure pour concrete placement began May 6, 2000 at 5:15am once closure region formwork was adjusted. Small gaps were present in the closure region formwork and screws were used to remove the gap. Table B-35 contains girder elevations of each phase just before concrete placement commenced.

J	H	G	E	D	C	B	A
-5.898	-6.052	-5.992	-5.969	-5.884	-5.916	-5.774	-5.731

Comparison of Phase I and Phase II elevations

J-A	H-B	G-C	E-D
-0.167	-0.308	-0.076	-0.085

Table B-35: Girder elevations prior to closure pour beginning

Closure region concrete is only 40 in wide by 7 in deep running the bridge length. This is a small load that is mainly carried by Girders D and E but deck stiffness will cause other girders to deflect. If girders deflected equally there would only be bending moment in each phase. The unequal deflections suggest a torsional effect. This has been seen previously also when barriers were placed and removed. Girder deflections caused by the closure pour can be seen in Table B-36. The final row in the table is computed by subtracting the Phase II girder deflection from the similar girder deflection of Phase I. Negative values indicate the Phase II girder deflected more than the Phase I girder. Both phases show similar deflections as values are close to zero. This is expected from symmetry.

	J	H	G	E	D	C	B	A
Beginning elevation	-5.898	-6.052	-5.992	-5.969	-5.884	-5.916	-5.774	-5.731
Final elevation	-5.900	-6.187	-6.262	-6.401	-6.298	-6.183	-5.897	-5.733
deflection	-0.002	-0.135	-0.270	-0.432	-0.414	-0.267	-0.123	-0.002

Comparison of Phase I and Phase II final elevations

J-A	H-B	G-C	E-D
0.000	-0.012	-0.003	-0.018

Table B-36: Deflection readings before and after closure completion

Figures B-29 and B-30 show the transverse profile for both phases before and after closure concrete placement. As can be clearly seen a new transverse deflection profile is present. Girders near the closure are at a lower elevation than exterior girders and Phase I girders are still lower than Phase I girders.

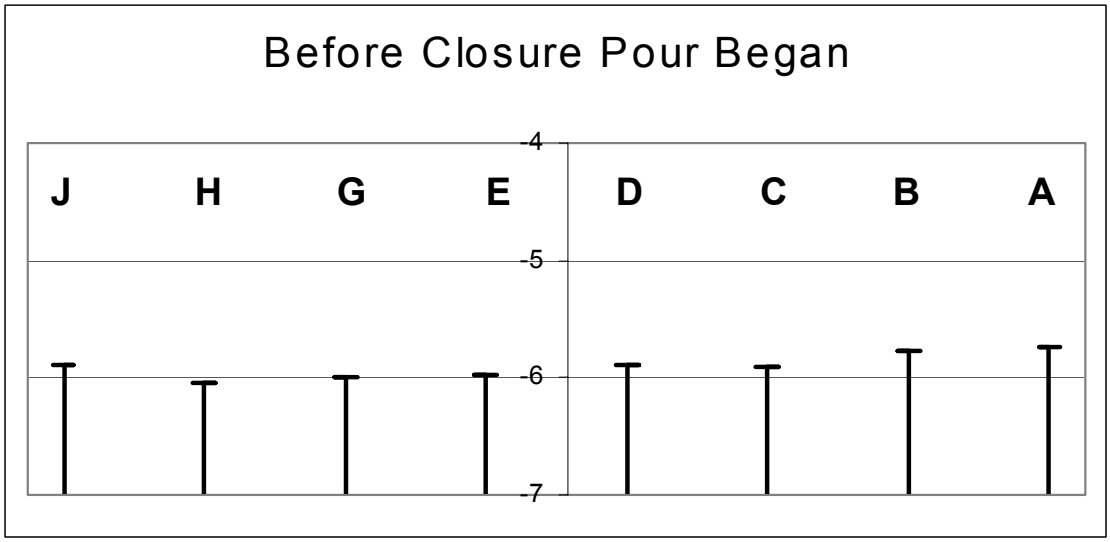

Figure B-29: Girder elevations prior to closure pour concrete placement

Phase I was re-opened to traffic on May 7, 2000 at 3pm. Phase II East span barriers were removed and barriers were repositioned on Phase I as seen in Figure B-31.

Any barrier additions or removals induce deflection. Time effects can also occur as concrete cures and temperature changes. Temperature change

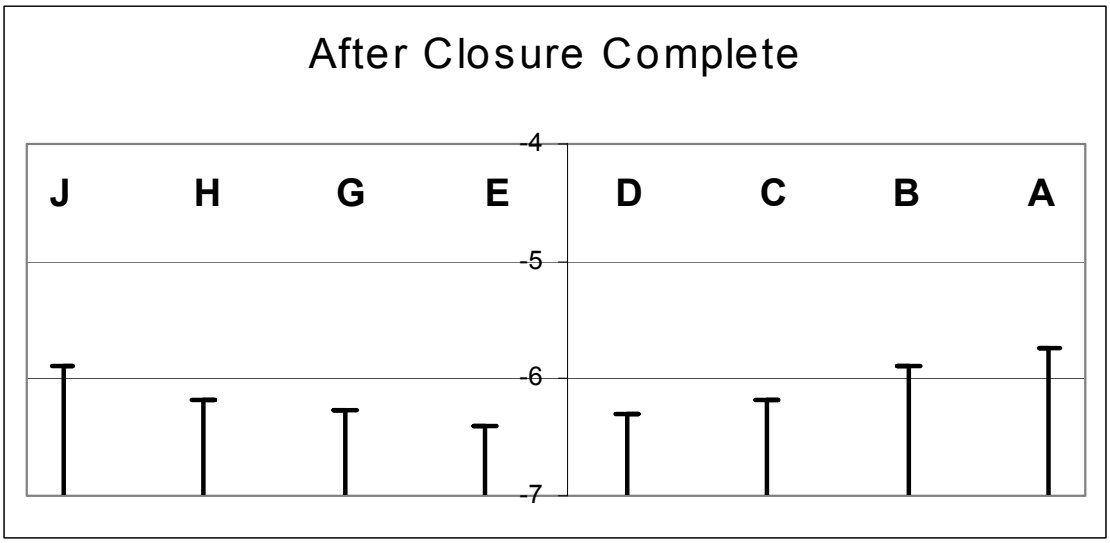

Figure B-30: Girder deflections after closure pour concrete placement

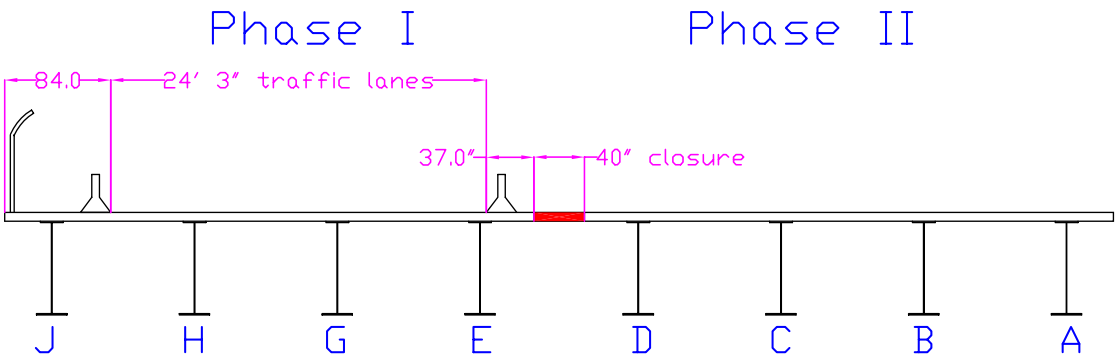

Figure B-31: Barrier relocation on Phase I. Note barriers on Phase II have been removed

was not considered above as both phases are at equal temperature and changes should affect both equally during events. Table B-37 contains data from closure pour concrete placement completion and beginning of preparations to re-open Phase I. Time effects were small during these 26 hours.

Relocating barriers on Phase I causes deflection changes. Table B-38 contains data from before barriers were relocated to after barriers were relocated.

Although barriers were placed nearly directly over Girder E, moving the barriers caused a net deflection loss, shown by the positive number. Once

	J	H	G	E	D	C	B	A
Beginning elevation	-5.900	-6.187	-6.262	-6.401	-6.298	-6.183	-5.897	-5.733
Final elevation	-5.888	-6.130	-6.196	-6.366	-6.254	-6.133	-5.867	-5.742
deflection	0.012	0.057	0.066	0.035	0.044	0.050	0.030	-0.009

Temp at end of closure	67.74
Temp before barriers relocated	68.77

Table B-37: Girder deflections between end closure concrete placement and before preparations to re-open to traffic

	J	H	G	E	D	C	B	A
Beginning elevation	-5.888	-6.130	-6.196	-6.366	-6.254	-6.133	-5.867	-5.742
Final elevation	-6.437	-6.395	-6.230	-6.195	-5.901	-5.670	-5.367	-5.216
deflection	-0.549	-0.265	-0.034	0.171	0.353	0.463	0.500	0.526

Beginning of barrier relocation	68.77
After barriers relocated	79.58

Table B-38: Girder deflections between before and after moving barriers to re-open Phase I

the closure region concrete has hardened the phases are joined and transverse stiffness exists. Removing barriers which were placed on Phase II to reduce differential defection causes Girder E to lose deflection because of continuity and deck stiffness. Girder E lost more deflection from barrier removal from Phase II than it gained from barriers being placed back on Phase I. For Phase II girders, relocating barriers caused a deflection loss. Addition of Phase I barriers causes a small downward deflection for Phase II girders which is counteracted by system rotation, yielding a net upward movement. The transverse profile as Phase I was re-opened to traffic can be seen in Figure B-32. Closure pour strains due to this barrier removal will be studied later.

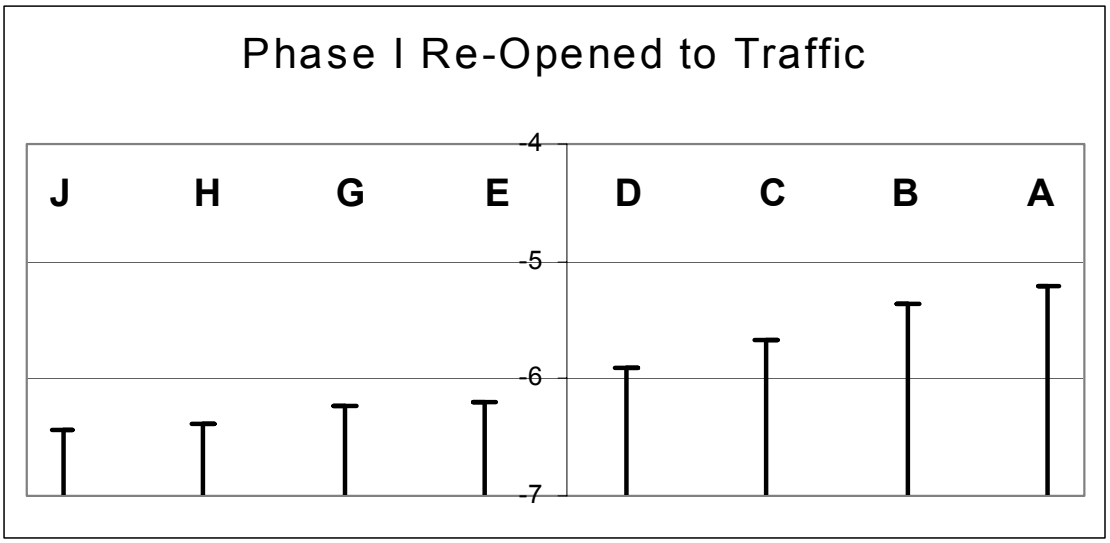

Figure B-32: Transverse profile when Phase I was re-opened to traffic

B.6 System Deflections From Overlays and Permanent Railings

Once Phase I and II were joined overlays and permanent railings were placed. On May 22, 2000 Phase II was overlaid. Time between Phase I reopening and overlay (15 days) allows time dependant deflections to occur. Table B-39 summarizes deflections between Phase I re-opening and before the overlay operation began. Figure B-33 shows the transverse profile before the overlay operation commenced. It is very similar to the profile when Phase I was re-opened shown previously in Figure B-32. Phase I girders are at a more even elevation than Phase II girders.

	J	H	G	E	D	C	B	A
Beginning elevation	-6.437	-6.395	-6.230	-6.195	-5.901	-5.670	-5.367	-5.216
Final elevation	-6.638	-6.663	-6.525	-6.480	-6.116	-5.905	-5.591	-5.422
deflection	-0.201	-0.268	-0.295	-0.285	-0.215	-0.235	-0.224	-0.206

Temp when opened to traffic	79.58
Temp before overlay	71.98

Table B-39: Girder deflections between Phase I re-opening and Phase II overlay

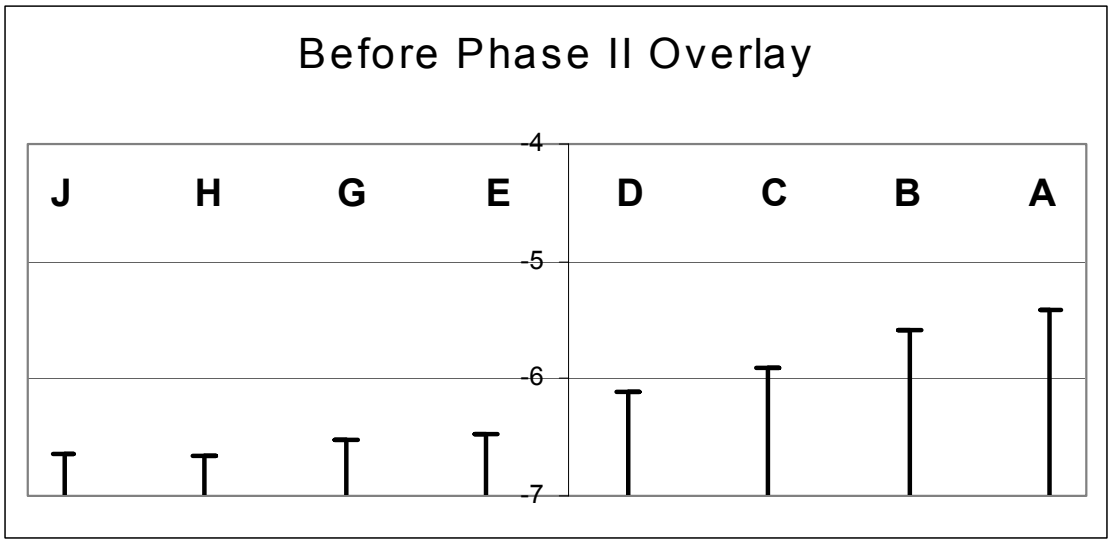

Figure B-33: Transverse profile before Phase II overlay

Phase I carried traffic as Phase II was overlain. The operation was performed at night and the overlay was covered with wet burlap for one week. Figure B-34 shows the overlay area being half the total deck width.

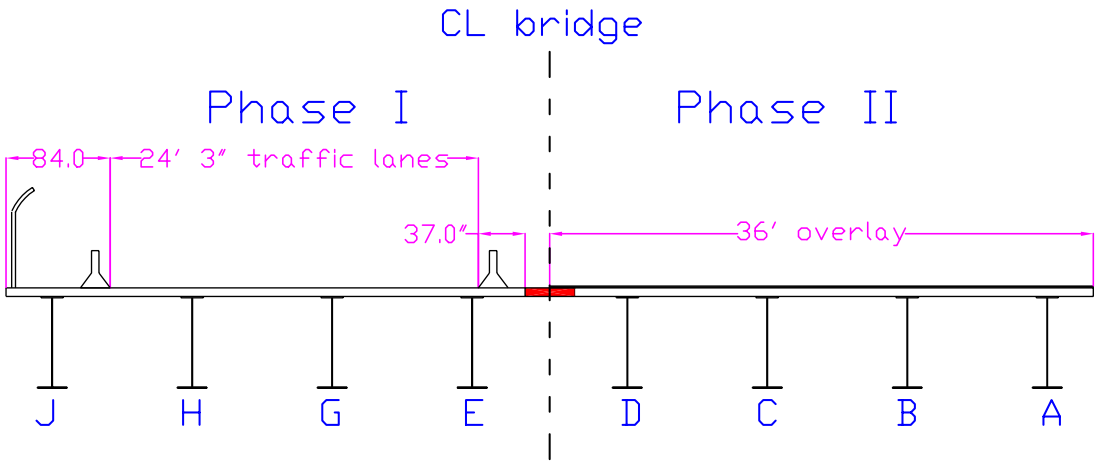

Figure B-34: Phase II overlay region

Table B-40 shows deflections that occurred during the operation. During this pour, girders that had been deflected the least, A and B, deflected more than others. Transverse stiffness also caused Phase I girders to deflect. The overly took 6 hours to complete and the system cooled 10 degrees Fahren-

heit during this time. The transverse profile after Phase II overlay can be seen in Figure B-35.

	J	H	G	E	D	C	B	A
Beginning elevation	-6.638	-6.663	-6.525	-6.480	-6.116	-5.905	-5.591	-5.422
Final elevation	-6.641	-6.784	-6.763	-6.862	-6.655	-6.586	-6.377	-6.324
deflection	-0.003	-0.121	-0.238	-0.382	-0.539	-0.681	-0.786	-0.902
Temp at beginning						79.58		
Temp when finished						69.03		

Table B-40: Girder deflections due to Phase II overlay

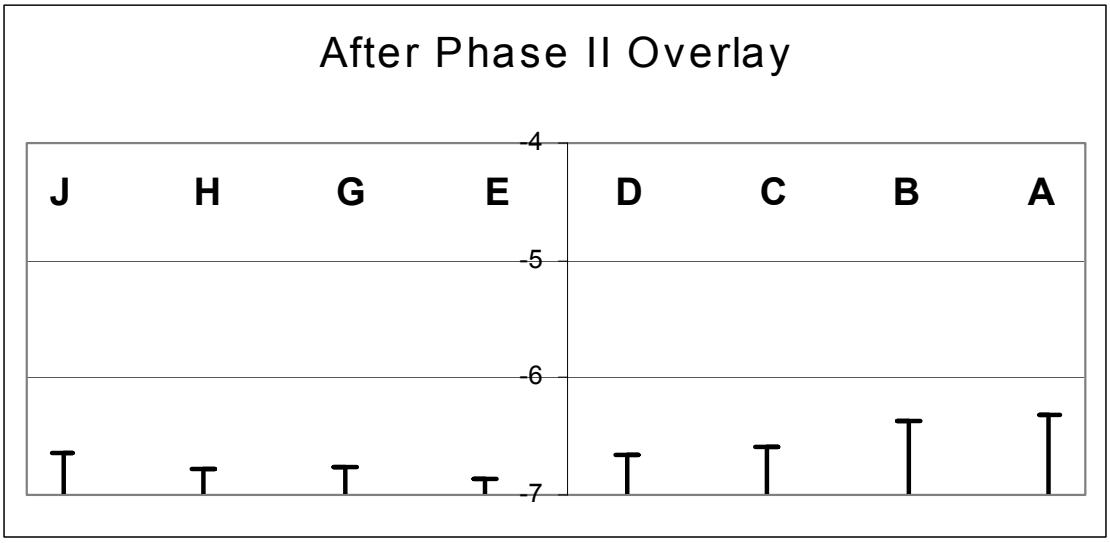

Figure B-35: Transverse profile after Phase II overlay

Slipforming the Phase II permanent rail was the next construction event. This occurred on June 2, 2000. Time effects can occur between overlay and rail casting (11 days). Table B-41 summarizes data between Phase II overlay ending to Phase II barrier casting. Between operations Girders A and B deflected additionally while the other girders lost deflection. The transverse deflection profile before rail pouring can be seen in Figure B-36.

Figure B-37 shows the Phase II permanent rail location. Deflections that occurred during this addition are shown in Table B-42.

	J	H	G	E	D	C	B	A
Beginning elevation	-6.641	-6.784	-6.763	-6.862	-6.655	-6.586	-6.377	-6.324
Final elevation	-6.418	-6.509	-6.541	-6.693	-6.585	-6.616	-6.514	-6.599
deflection	0.223	0.275	0.222	0.169	0.070	-0.030	-0.137	-0.275

Temp at beginning	69.03
Temp when finished	70.60

Table B-41: Girder deflections between Phase II overlay and Phase II permanent rail

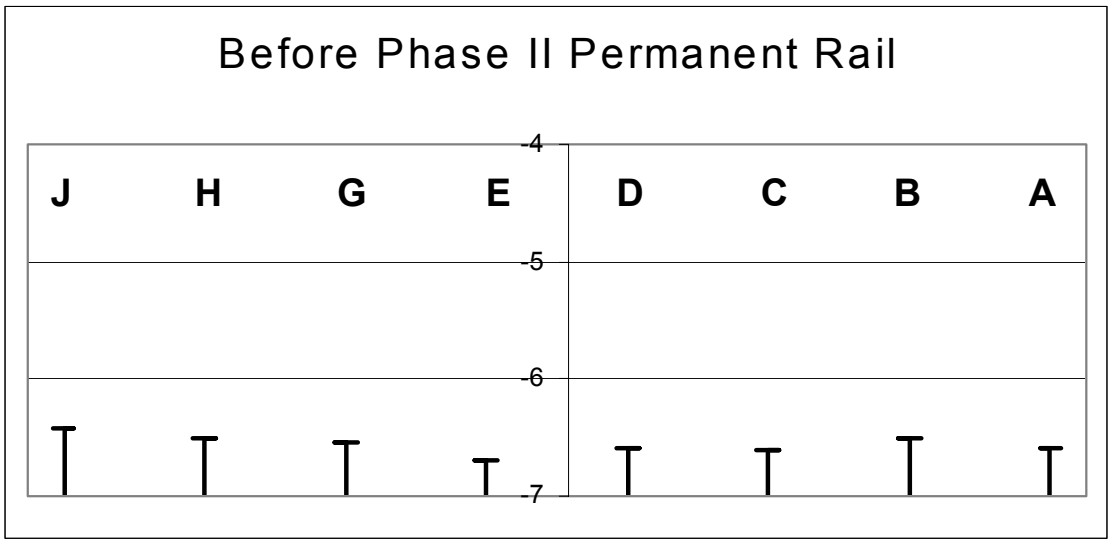

Figure B-36: Transverse deflection profile prior to Phase II permanent rail placement

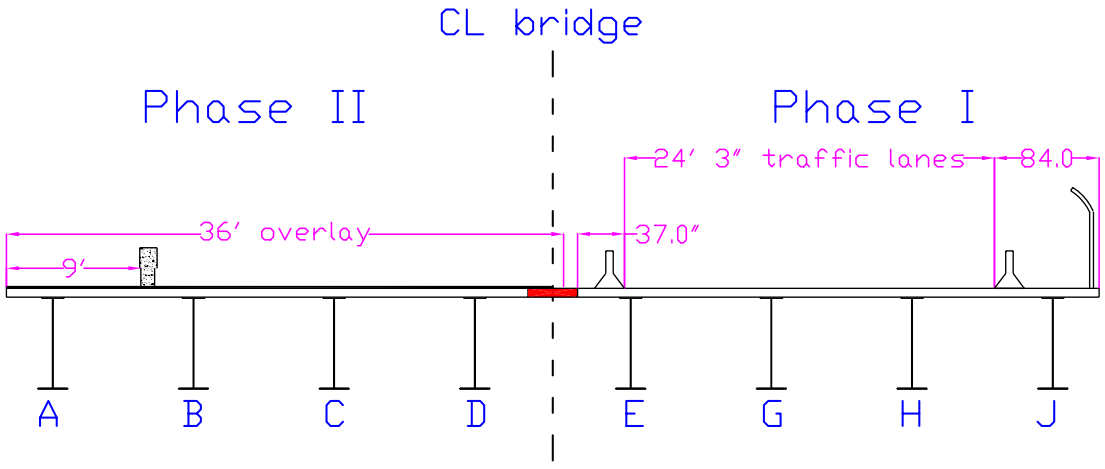

Figure B-37: Location of Phase II permanent railing. Overlay area is also shown

	J	H	G	E	D	C	B	A
Beginning elevation	-6.418	-6.509	-6.541	-6.693	-6.585	-6.616	-6.514	-6.599
Final elevation	-6.223	-6.468	-6.591	-6.827	-6.833	-6.957	-6.903	-7.045
deflection	0.195	0.041	-0.050	-0.134	-0.248	-0.341	-0.389	-0.486

Temp at beginning	70.60
Temp when finished	81.09

Table B-42: Girder deflections due to Phase II permanent rail casting

Clearly Phase II girders deflected more than Phase I girders but transverse stiffness did cause Phase I girders to deflect some. Once again the deflections are a combination of downward deflection and rotation, or twisting. Figure B-38 depicts the transverse deflection profile after the railing was poured. Phase II girders are at nearly the same elevation now while Phase I girders show a significant transverse profile.

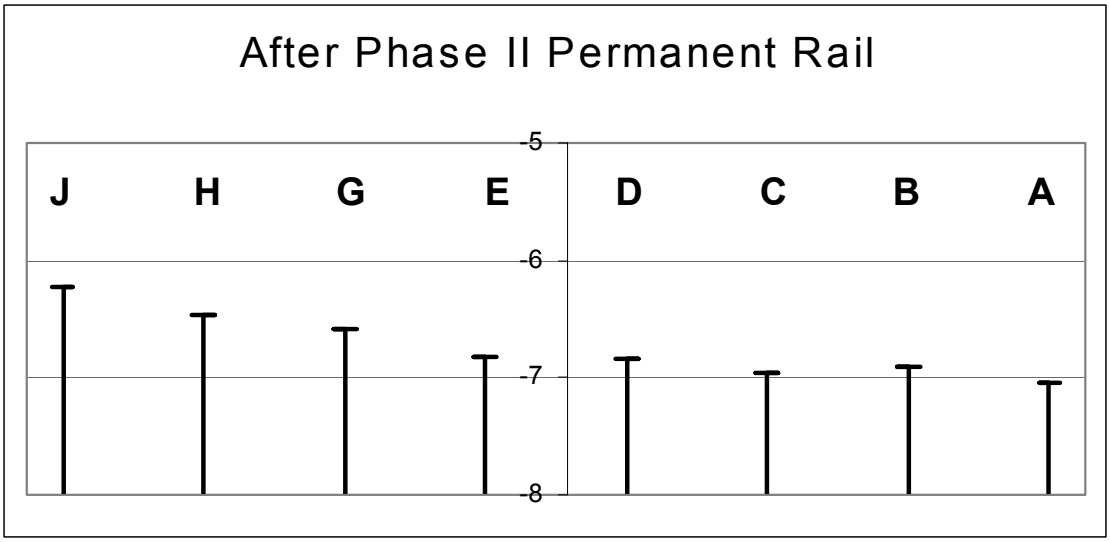

Figure B-38: Transverse deflection profile after Phase II permanent railing placement. Note girders of Phase II are deflected similarly while Phase I girders are not

With Phase II permanent railing in place temporary barriers could be moved to prepare Phase I for overlay. Barriers were removed completely from Phase I and placed on Phase II as seen in Figure B-39. This allows

Phase II to carry traffic. Barrier movement occurred on June 13, 2000, 11 days after Phase II overlay.

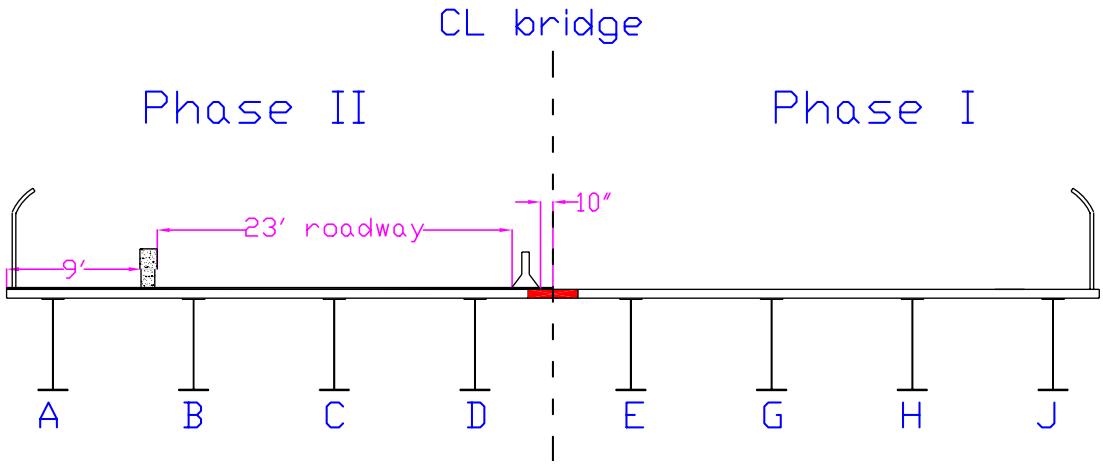

Figure B-39: Location of barriers during overlay preparations, overlay, and permanent rail placement on Phase I

Time dependent deflection can occur between Phase II permanent rail pour and moving temporary barriers. This deflection information is summarized in Table B-43.

	J	H	G	E	D	C	B	A
Beginning elevation	-6.223	-6.468	-6.591	-6.827	-6.833	-6.957	-6.903	-7.045
Final elevation	-6.613	-6.860	-6.993	-7.230	-7.234	-7.327	-7.270	-7.368
deflection	-0.390	-0.392	-0.402	-0.403	-0.401	-0.370	-0.367	-0.323

Temp at beginning	81.09
Temp when finished	77.49

Table B-43: Girder deflections between Phase II permanent rail placement and barrier movement

Girders show similar time deflections and the differential E-D is small. Deflection data between the operations is seen in Figures B-40 and B-41. A girder from each phase was chosen to show the similar time behavior as seen in Table B-43. Although the total temperature change appears at first glance to be small, average temperature fluctuated greatly. Daily tempera-

ture changes of 27 degrees Fahrenheit cause about 0.4" deflection during this time. Similar girder movements show both phases acting as one system.

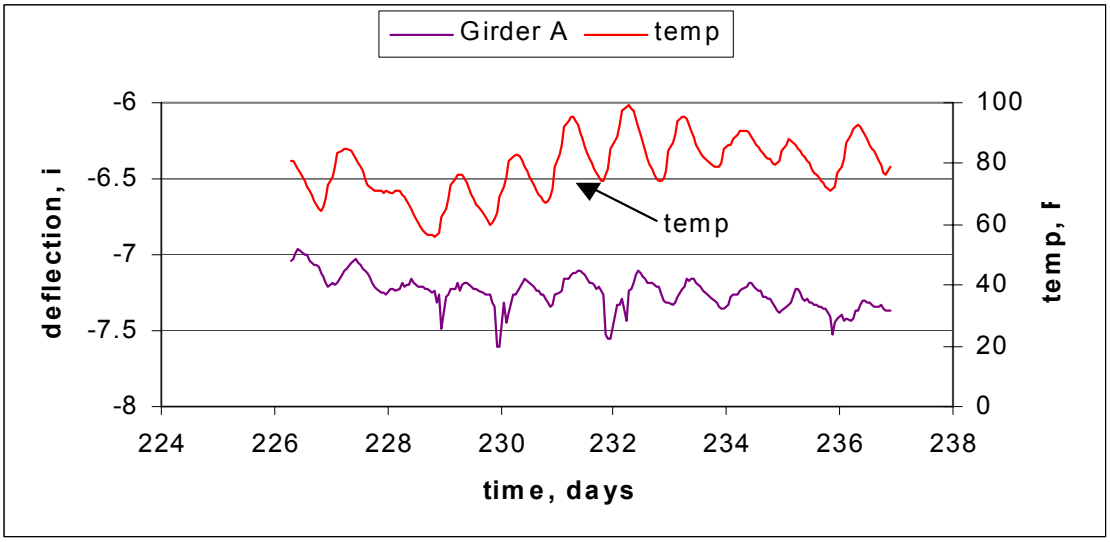

Figure B-40: Girder A deflection between Phase II permanent rail pour and barrier movement

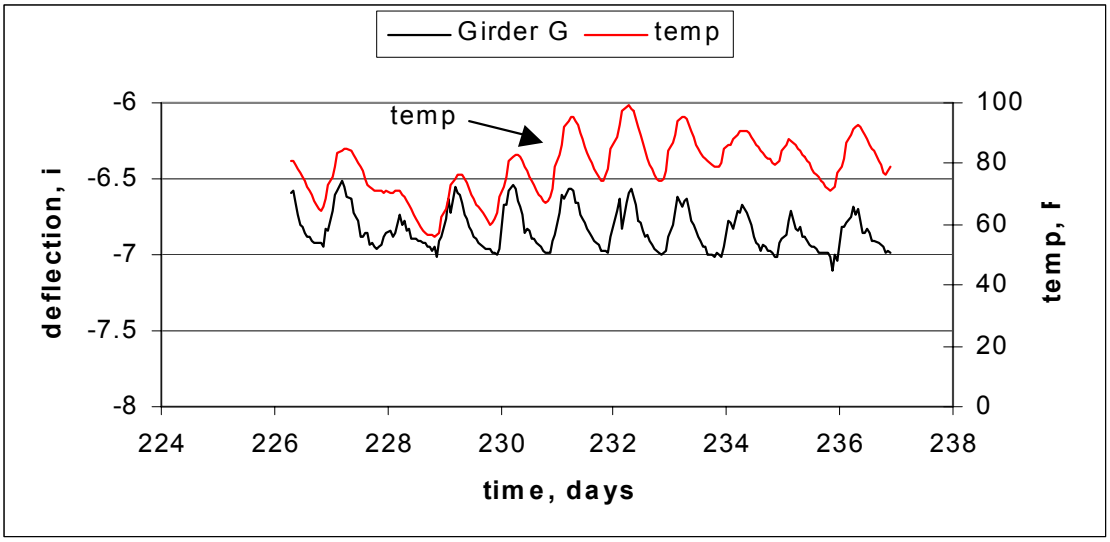

Figure B-41: Girder G deflection between Phase II permanent rail pour and barrier movement

Deflection caused by moving temporary barriers from Phase I is summarized in Table B-44. Clearly, moving the barriers had a large impact. Phase I girders rebounded significantly creating larger differential elevations.

Also, Phase II near the temporary barrier location rebounded more from removing barriers from Phase I than the girders deflected from placement on Phase II. The result was a net uplift of Girders D and C. The transverse profile after barrier movement is shown in Figure B-42.

	J	H	G	E	D	C	B	A
Beginning elevation	-6.613	-6.860	-6.993	-7.230	-7.234	-7.327	-7.270	-7.368
Final elevation	-5.640	-6.164	-6.484	-6.890	-7.072	-7.300	-7.349	-7.567
deflection	0.973	0.696	0.509	0.340	0.162	0.027	-0.079	-0.199
Temp at beginning						77.49		
Temp when finished						74.52		

Table B-44: Girder deflections during barrier movement

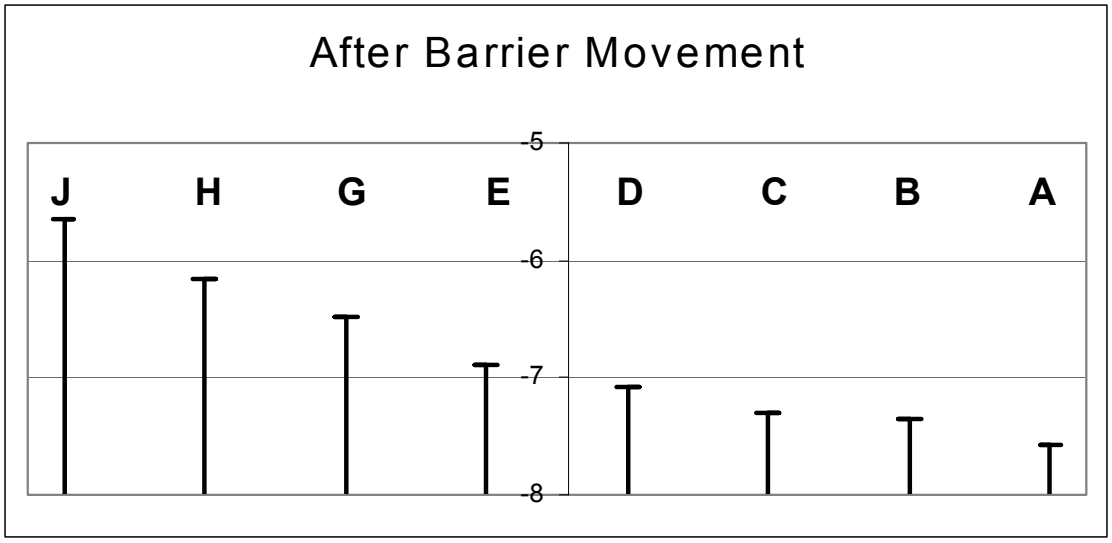

Figure B-42: Transverse girder deflections after barriers were moved so Phase II could carry traffic. Note, not to scale, distance between girders is 113"

Phase I was overlaid in two steps. Permanent fencing prevented finishing machines to do the entire width. The overlay on the majority was performed on June 30, 2000 in early morning. Table B-45 summarizes time dependant deflections occurring while preparations for Phase I overlay were made (17 days). Time dependant deflections were minimal.

	J	H	G	E	D	C	B	A
Beginning elevation	-5.640	-6.164	-6.484	-6.890	-7.072	-7.300	-7.349	-7.567
Final elevation	-5.724	-6.223	-6.537	-6.928	-7.078	-7.297	-7.341	-7.553
deflection	-0.084	-0.059	-0.053	-0.038	-0.006	0.003	0.008	0.014

Temp at beginning	74.52
Temp when finished	72.63

Table B-45: Girder deflections between barrier movement and Phase I overlay (17 days)

Table B-46 summarizes Phase I overlay deflections, for the majority of the pour. Phase I girders deflected more than Phase II girders. This makes sense, as the load was over Phase I. It is interesting that Girder J deflected 0.136" more than Girder E. This is consistent with Phase I where Girder A deflected more than D. Transverse stiffness caused Phase II girders to deflect downward as well.

	J	H	G	E	D	C	B	A
Beginning elevation	-5.724	-6.223	-6.537	-6.928	-7.078	-7.297	-7.341	-7.553
Final elevation	-6.163	-6.619	-6.898	-7.234	-7.300	-7.469	**	**
deflection	-0.439	-0.396	-0.361	-0.306	-0.222	-0.172	**	**

Temp at beginning	72.63
Temp when finished	76.19

Table B-46: Girder deflections during Phase I overlay. ** see text

Unfortunately, Girders A and B deflected enough to cause potentiometers on Girders A and B to lose their entire stroke. Maximum measurable deflection on Girders A and B was -7.603" and -7.362" respectfully. Looking at data, readings are valid for cooler temperatures when the bridge rebounds. Thus Girders A and B must be close to their maximum deflection.

July 6, 2000 the temporary concrete rail on Phase II was replaced with orange plastic barrels. The barrels were placed at the same location to

maintain traffic on Phase II. Figure B-43 shows the barrel location. The barrel weight is very small and their spacing is large. Therefore, barrels produce no notable deflection. Time dependent deflections from the completed portion of Phase I overlay to barrier replacement are shown in Table B-47 (6 days). Girders A and B were still deflected too far to obtain reliable readings. All girders deflected additionally and it is reasonable to say Girders A and B did also.

	J	H	G	E	D	C	B	A
Beginning elevation	-6.163	-6.619	-6.898	-7.234	-7.300	-7.469	**	**
Final elevation	-6.253	-6.700	-6.985	-7.337	-7.417	-7.605	**	**
deflection	-0.090	-0.081	-0.087	-0.103	-0.117	-0.136	**	**

Temp at beginning	76.19
Temp when finished	74.71

Table B-47: Time dependant deflections between the majority of Phase I overlay completed to concrete temporary barrier replacement with barrels. ** see text

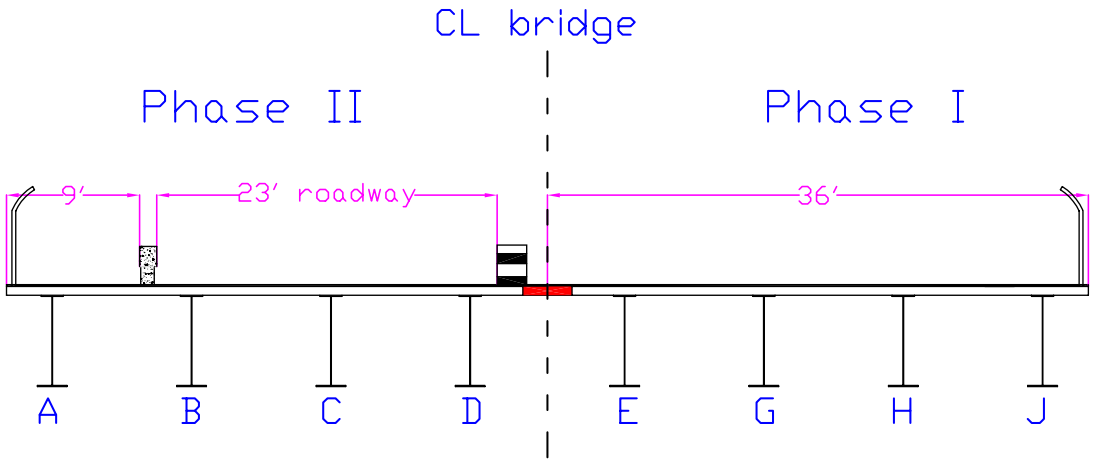

Figure B-43: Location of barrels after concrete temporary rail was removed. Note completed overlay shown on Phase I

Table B-48 shows deflections from replacing concrete temporary barriers with plastic barrels. Girders A and B rebounded enough to obtain valid elevation readings at the end although the total amount of rebound is

unknown. Transverse stiffness caused all girders to lose deflection but the greatest loss was for girders near the barrier's location. Figure B-44 shows the transverse profile after barrier replacement.

	J	H	G	E	D	C	B	A
Beginning elevation	-6.253	-6.700	-6.985	-7.337	-7.417	-7.605	**	**
Final elevation	-6.020	-6.474	-6.728	-7.024	-7.040	-7.216	-7.251	-7.487
deflection	0.233	0.226	0.257	0.353	0.377	0.389	**	**
Temp at beginning						74.71		
Temp when finished						86.25		

Table B-48: Deflections from replacing concrete temporary barriers with plastic barrels. ** see text

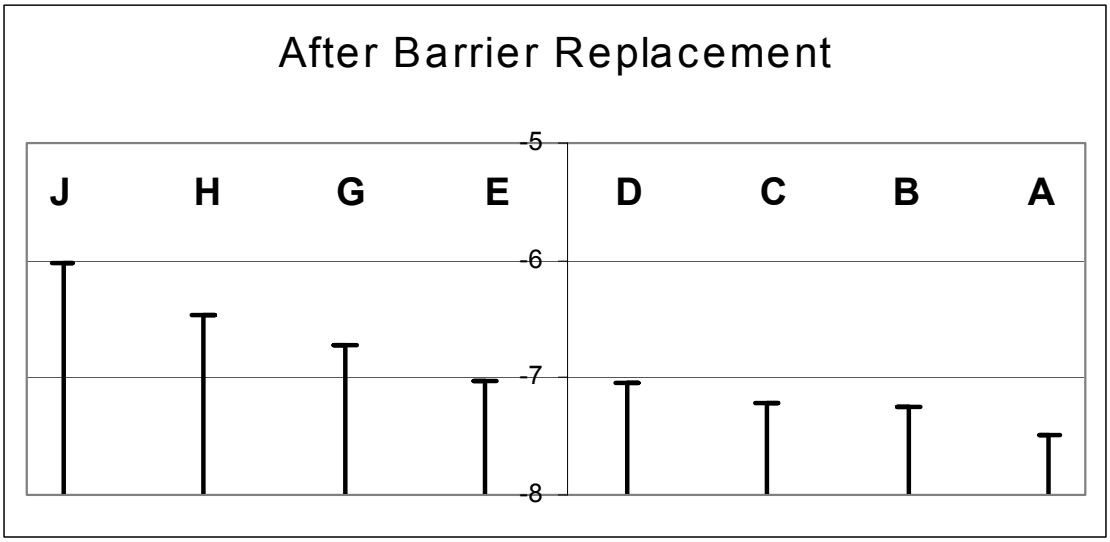

Figure B-44: Transverse profile after concrete temporary barriers were replaced with plastic barrels

Phase I overlay was completed on July 8, 2000 with the sidewalk region being overlain. Table B-49 shows deflection between replacing barriers and before completing Phase I overlay (2 days). Most girders deflected additionally while Girder A lost deflection.

	J	H	G	E	D	C	B	A
Beginning elevation	-6.020	-6.474	-6.728	-7.024	-7.040	-7.216	-7.251	-7.487
Final elevation	-6.208	-6.644	-6.879	-7.146	-7.146	-7.295	-7.285	-7.441
deflection	-0.188	0.170	-0.151	-0.122	-0.106	-0.079	-0.034	0.046

Comparison of Phase I and Phase II final elevations

J-A	H-B	G-C	E-D
1.233	0.641	0.416	0.000

Temp at beginning	86.25
Temp when finished	81.37

Table B-49: Girder deflections between barrier change and sidewalk overlay

Finishing Phase I overlay adds additional load. Girders H and J should deflect more than others as they are closest to the loading. Table B-50 contains deflection data for completing the Phase I overlay.

	J	H	G	E	D	C	B	A
Beginning elevation	-6.208	-6.644	-6.879	-7.146	-7.146	-7.295	-7.285	-7.441
Final elevation	-6.441	-6.801	-6.977	-7.215	-7.187	-7.319	-7.308	-7.484
deflection	-0.233	-0.157	-0.098	-0.069	-0.041	-0.024	-0.023	-0.043

Temp at beginning	81.37
Temp when finished	81.36

Table B-50: Girder deflections during Phase I overlay completion

Girders E-A deflect minimally while G-H deflect more. Figure B-45 shows the transverse profile after Phase I overlay completion.

The final operation before the entire bridge can carry traffic is slipforming the Phase I permanent rail. The rail was cast July 14, 2000 after preparations were made. Deflections occurring between Phase I overlay completion and Phase I permanent rail are shown in Table B-51 (6 days). Deflection and temperature changes were minimal.

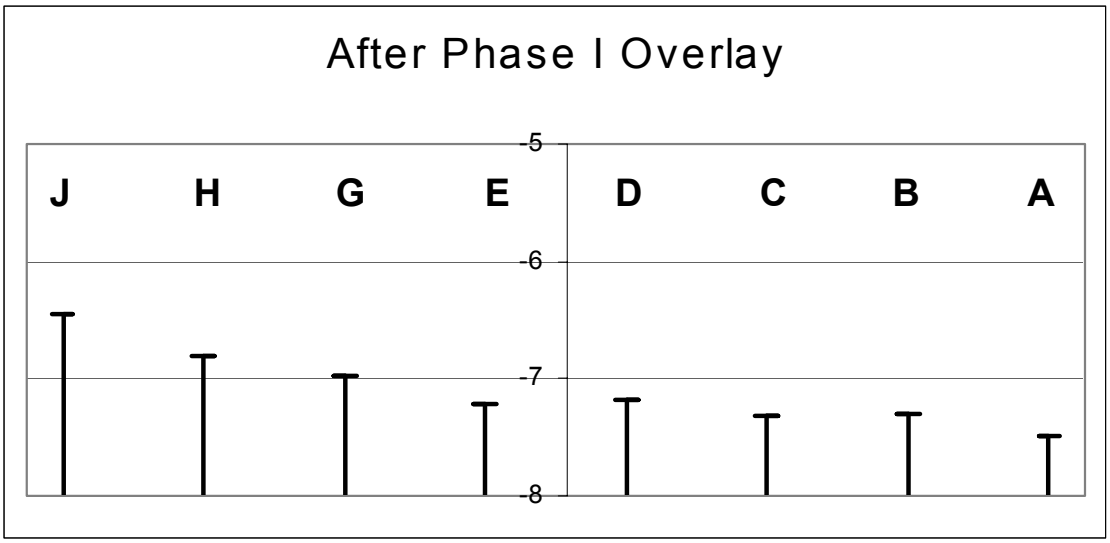

Figure B-45: Transverse deflection profile after Phase I overlay

	J	H	G	E	D	C	B	A
Beginning elevation	-6.441	-6.801	-6.977	-7.215	-7.187	-7.319	-7.308	-7.484
Final elevation	-6.449	-6.856	-7.043	-7.286	-7.260	-7.395	-7.352	-7.481
deflection	-0.008	--0.055	-0.066	-0.071	-0.073	-0.076	-0.044	0.003

Temp at beginning	81.36
Temp when finished	83.46

Table B-51: Girder deflections between Phase I overlay completion and Phase I permanent rail

Figure B-46 shows the Phase II permanent rail location. Deflections from adding this rail can be seen in Table B-52. Girders near the rail deflected additionally while the Phase I girders lost deflection.

At this time both phases have equal dead loads. Comparable girders should show equal deflections. The transverse profile after rail placement is shown in Figure B-47. Girders B-H show close elevations while Girders A and J are substantially different.

Phases I and II were both opened to traffic on August 10, 2000. Time deflections between Phase I barrier placement and opening to traffic are summa-

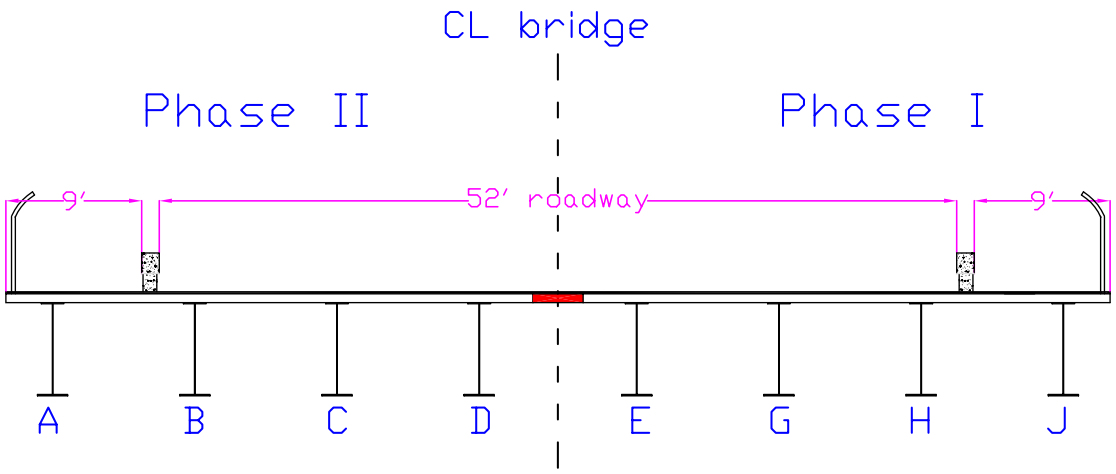

Figure B-46: Phase I permanent barrier location. Note symmetry. Bridge cross section is shown in its final configuration

	J	H	G	E	D	C	B	A
Beginning elevation	-6.449	-6.856	-7.043	-7.286	-7.260	-7.395	-7.352	-7.481
Final elevation	-6.762	-6.987	-7.011	-7.131	-7.029	-7.132	-7.101	-7.283
deflection	-0.313	-0.131	0.032	0.155	0.231	0.263	0.251	0.198

Temp at beginning	83.46
Temp when finished	95.32

Table B-52: Girder deflections from Phase I permanent rail

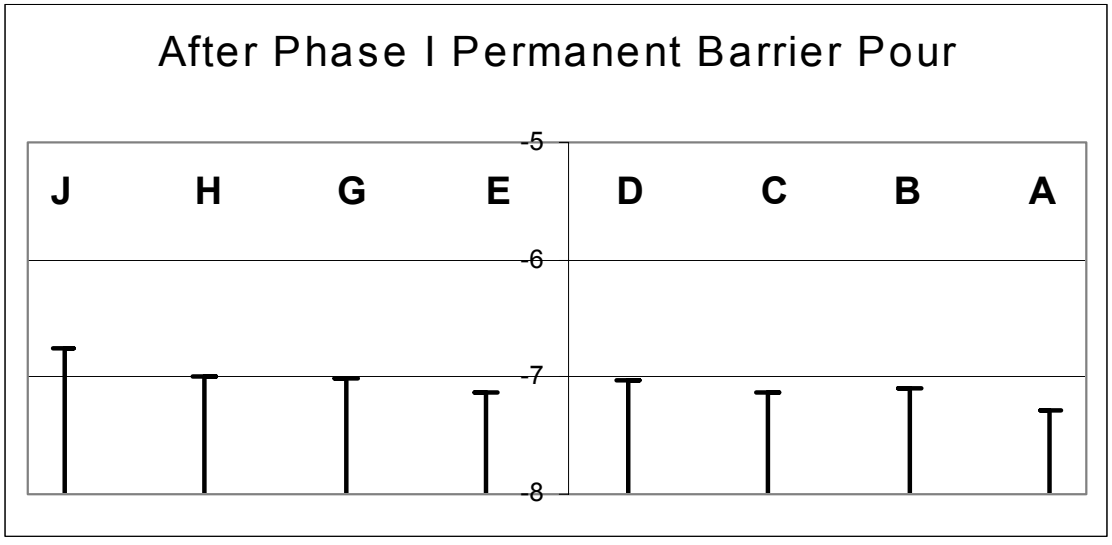

Figure B-47: Transverse profile after Phase I permanent rail placement

rized in Table B-53 (27 days). Transverse profile at opening to traffic can be seen in Figure B-48.

	J	H	G	E	D	C	B	A
Beginning elevation	-6.762	-6.987	-7.011	-7.131	-7.029	-7.132	-7.101	-7.283
Final elevation	-7.010	-7.244	-7.240	-7.361	-7.221	-7.299	-7.251	-7.370
deflection	-0.248	-0.257	-0.229	-0.230	-0.192	-0.167	-0.150	-0.087

Temp at beginning	95.32
Temp when finished	89.40

Table B-53: Time dependant girder deflections between Phase I permanent rail and opening to traffic

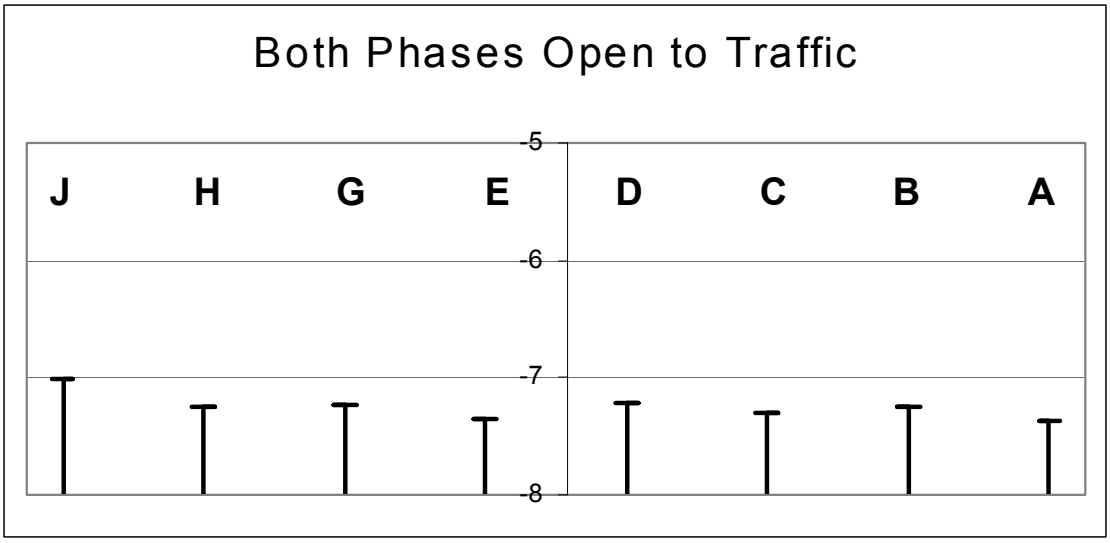

Figure B-48: Transverse deflection Profile when both Phases were opened to traffic

Figure B-49 contains deflection and temperature data for Girder C during these 27 days. Average system temperature varied causing deflection changes. This behavior has been seen previously.

Table B-54 summarizes time dependant deflections between both phases opening to traffic and the last recorded data point March 5, 2001 (205 days). As construction was complete no major events occur during this time.

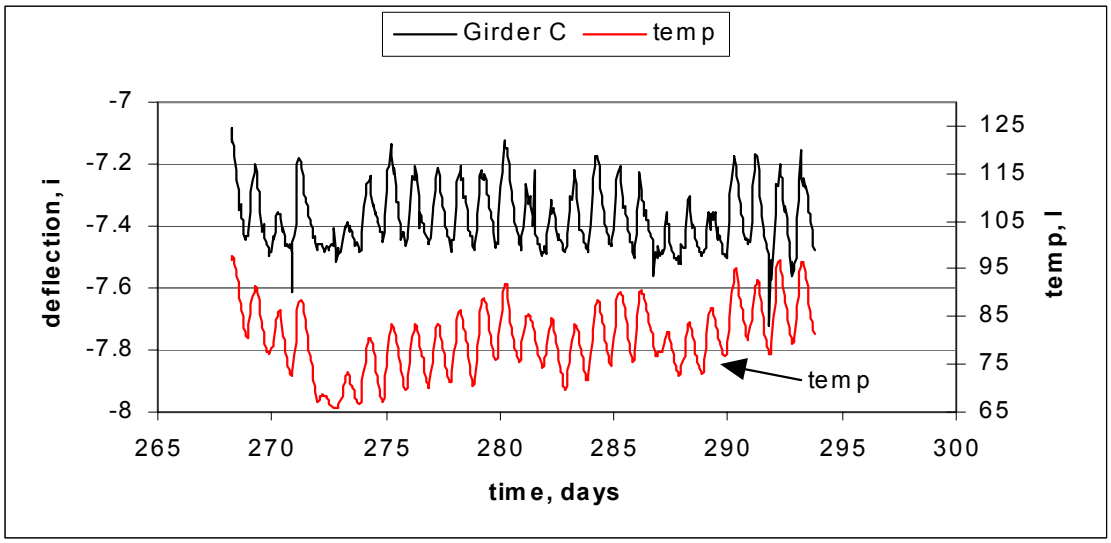

Figure B-49: Temperature and deflection data for Girder C between end of Phase I permanent rail pour and opening to traffic

	J	H	G	E	D	C	B	A
Beginning elevation	-7.010	-7.244	-7.240	-7.361	-7.221	-7.299	-7.251	-7.370
Final elevation	-7.374	-7.390	-7.275	-7.319	-7.142	-7.331	-7.381	-7.593
deflection	-0.364	-0.146	-0.035	0.042	0.079	-0.032	-0.162	-0.223

Temp when opened to traffic	89.40
Temp at last reading	25.88

Table B-54: Time dependent girder deflections between opening to traffic and last measurement on March 5, 2001

Temperature change was very great during this time. The lower temperatures would cause the bridge to lose deflection, not gain deflection. The four outermost girders deflected substantially more though. Figure B-50 is the final transverse profile.

Once again the girders slope away from the closure region, as they once did. The differential elevation at the closure is -0.177" with Girder E lower than D.

Long-term deflections between opening the entire system to traffic and the last measurement for Girders B and H are shown in Figures B-51 and B-52.

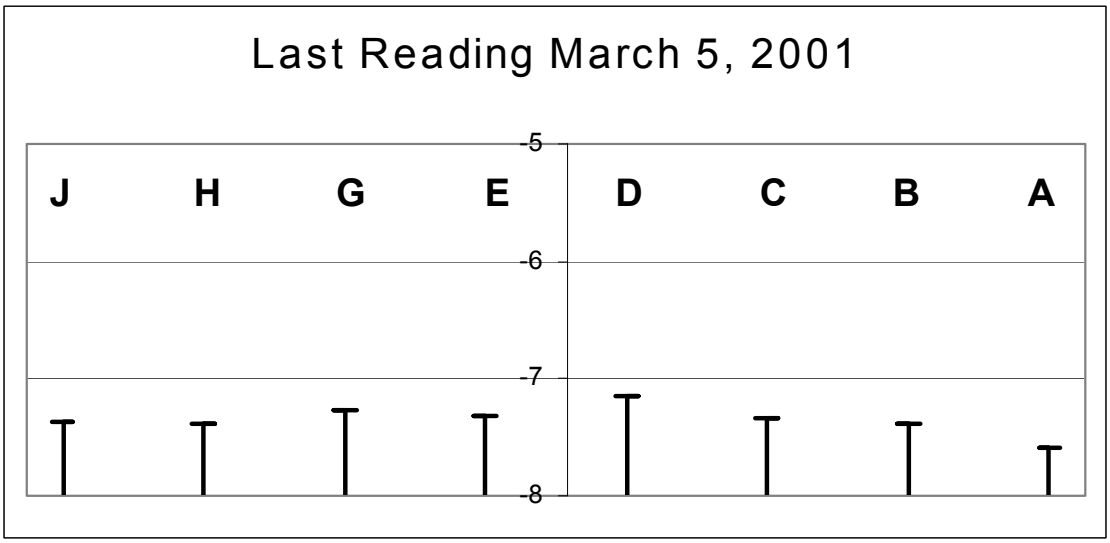

Figure B-50: Transverse deflection profile for last reading taken on March 5, 2001

As the temperature has seasonally dropped, girders lost some deflection while they still vary on a daily basis. No large deflection jumps are present as construction is complete.

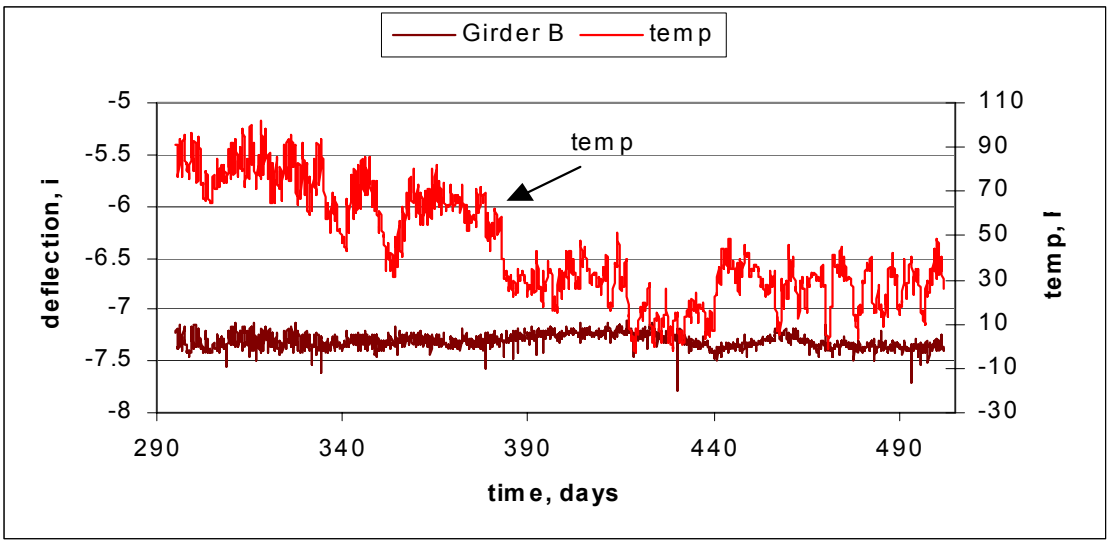

Figure B-51: Girder B long term deflection

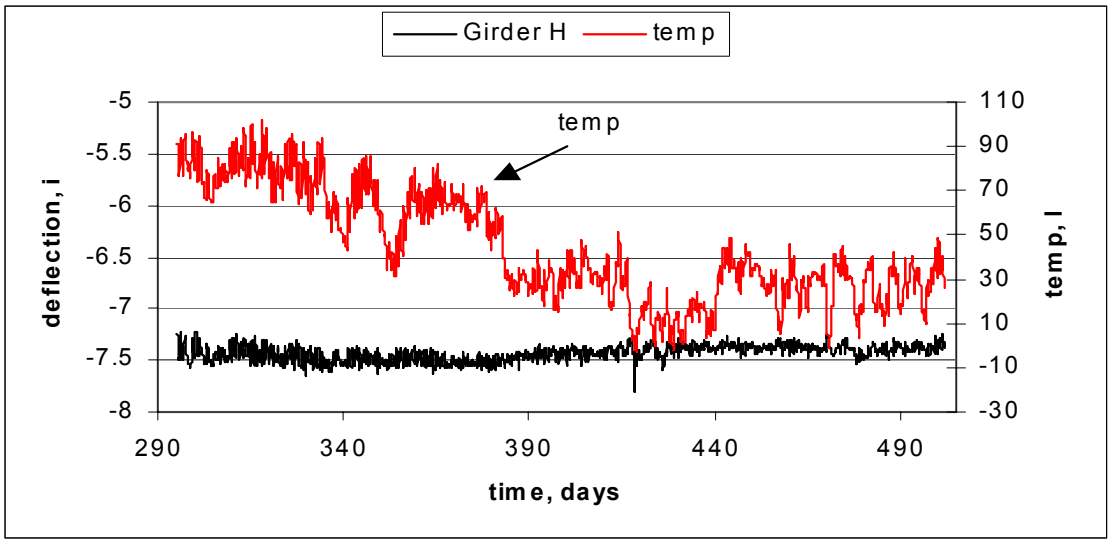

Figure B-52: Girder H long term deflection

B.7 Deflection Comparison During Overlays and Permanent Rail Placement

Symmetric overlay regions and permanent rail locations should cause similar deflections. Deflection comparisons must be made carefully. Girder A deflection for Phase II overlay should be compared to Girder J deflection for Phase I overlay due to symmetry. As Phase I was overlain in two pours, deflections from these pours will be superimposed to compare against Phase II overlay. This superposition for Girders A and B is not possible, as total deflection numbers could not be reported. Overlay deflections for Phase I and Phase II are summarized in Table B-55.

Phase II Overlay Deflections							
J	H	G	E	D	C	B	A
-0.003	-0.121	-0.238	-0.382	-0.539	-0.681	-0.786	-0.902
Phase I Overlay Deflections							
A	B	C	D	E	G	H	J
		-0.196	-0.263	-0.375	-0.459	-0.553	-0.672

Table B-55: Deflection summary for overlay placement on Phases I and II

Clearly deflections are not symmetric. Results can be skewed by the temperature changes during overlays and account for the difference. Live load results showed that the phases deflected similarly with symmetric loads. The same result was expected for overlays and seems reasonable.

Deflection comparisons for permanent rail placement are seen in Table B-56. For the Phase II placement the barrier was placed near Girder A and for Phase I placement the barrier was closest to Girder J.

Phase II Permanent Rail							
J	**H**	**G**	**E**	**D**	**C**	**B**	**A**
0.195	0.041	-0.050	-0.134	-0.248	-0.341	-0.389	-0.486
Phase I Permanent Rail							
A	**B**	**C**	**D**	**E**	**G**	**H**	**J**
0.198	0.251	0.263	0.231	0.155	0.032	-0.131	-0.313

Table B-56: Deflection comparison for permanent rail placement

Deflections from the rail placements are only similar for Girders J and A, which are farthest from the rail placements. Phase II rail placement causes additional deflection for all Phase II girders and some Phase I girders. Once again it appears that girders deflected more for the Phase II operation.

B.8 Transverse Girder Deflection Profile Summary

Figure B-53 displays girder transverse deflections at various Phase I construction stages. Deflection profiles after the positive region pour, negative region pour, after South side temporary barrier placement, North side temporary barrier placement, when Phase I was opened to traffic, and before the closure pour began are all shown. This plot shows a time history of how the transverse profile changes. It is easy to see the effect of adding South and North side barriers. Clearly the side a load is placed on deflects more. Additionally, placing a load on one side can cause the other to lose deflec-

tion. This is contrary to design where all girders are assumed to carry equal load and deflect evenly.

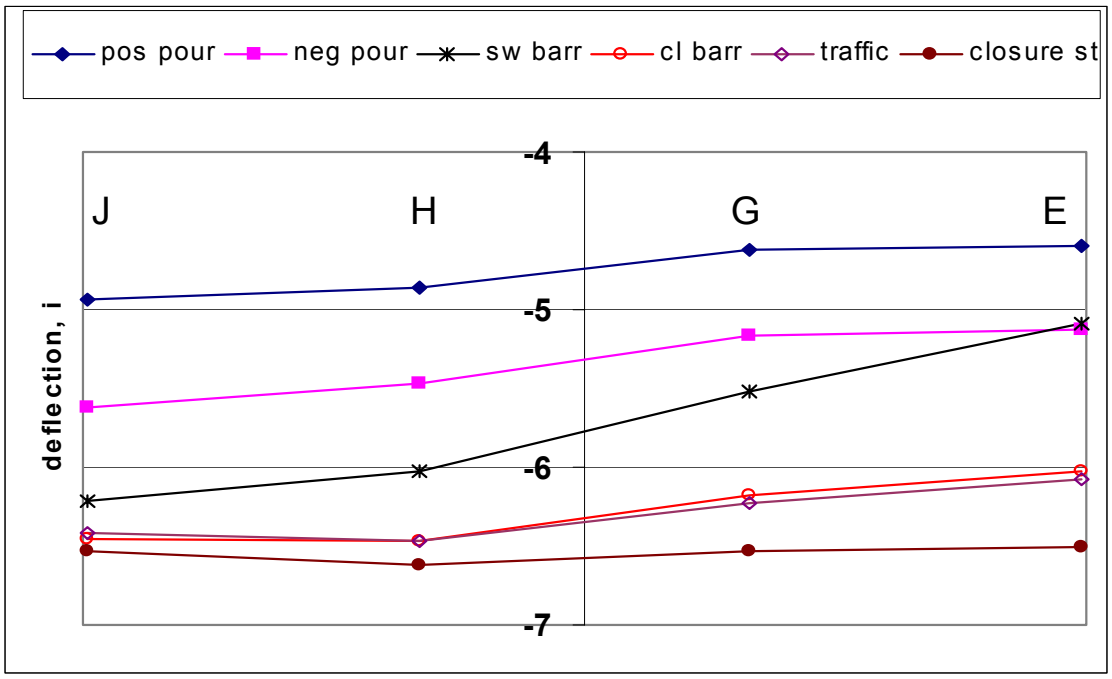

Figure B-53: Phase I transverse girder deflection profiles until closure pour

The same analysis of Phase II transverse deflections can be seen in Figure B-54. Phase II only underwent the positive region pour and negative region pour before closure. The initial transverse profile was maintained until closure. During positive region pours, girders are free to deflect somewhat independently as cross frames provide minimal transverse stiffness. Once positive region concrete has hardened, the section is composite and transverse stiffness forces girders to deflect with each other. The initial transverse profile is mostly maintained during negative pours. This stiffness also affects deflections from load placement as seen in Figure B-53 during barrier placement. As barriers are placed on Phase I girders closest to the addition deflect more while those away can rebound.

At closure, Phase II still has a significant transverse profile in comparison to Phase I. Transverse girder deflections during closure operations can be seen in Figure B-55 through B-57.

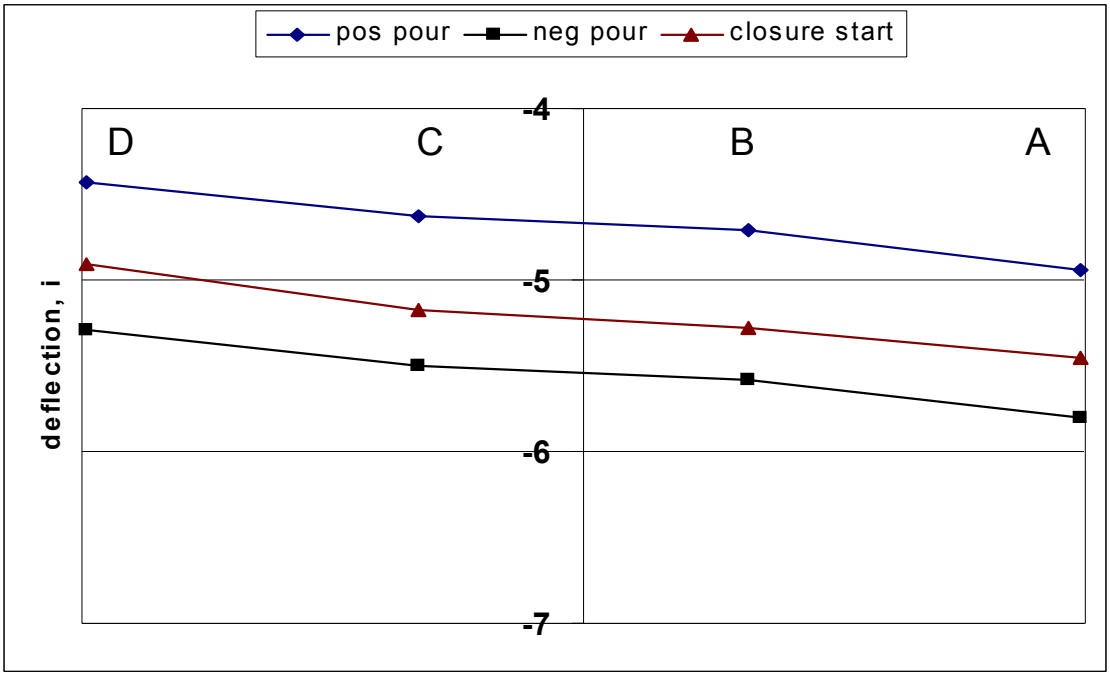

Figure B-54: Phase II transverse girder deflection profiles until closure

Figure B-55 contains data at the start of the operation, after barriers were removed from Phase I near the closure (Phase I North side), and after barriers were removed from Phase I near the sidewalk (Phase I South side).

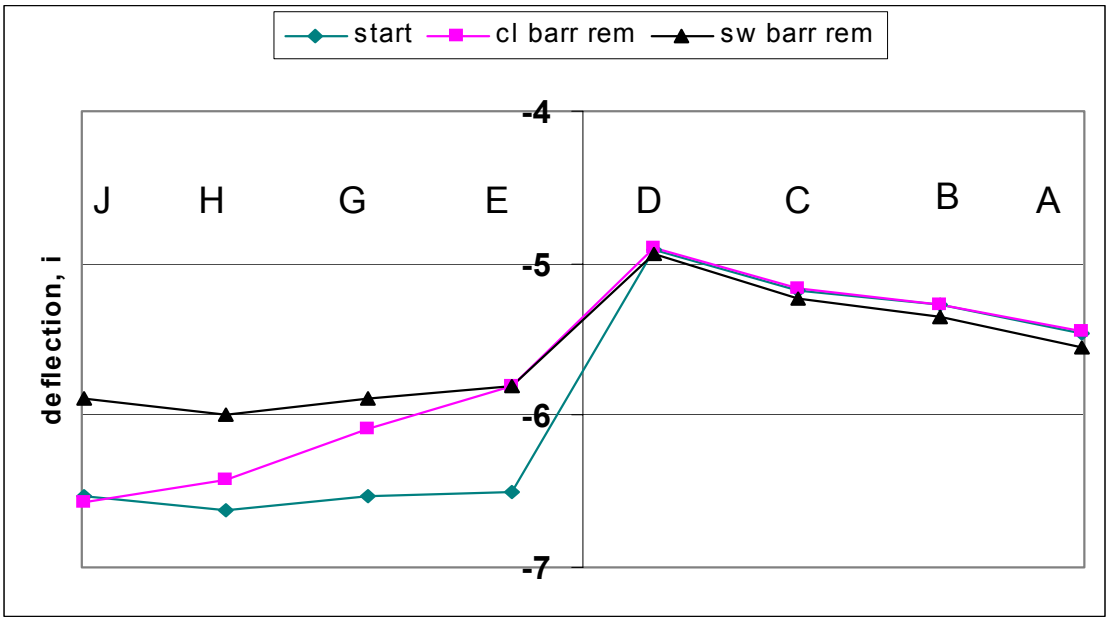

Figure B-55: Transverse girder profiles during closure operations

Figure B-56 contains data from when sidewalk barriers were removed from Phase I (South side Phase I), after barriers were added on east span Phase II, concrete placement start, and concrete placement end.

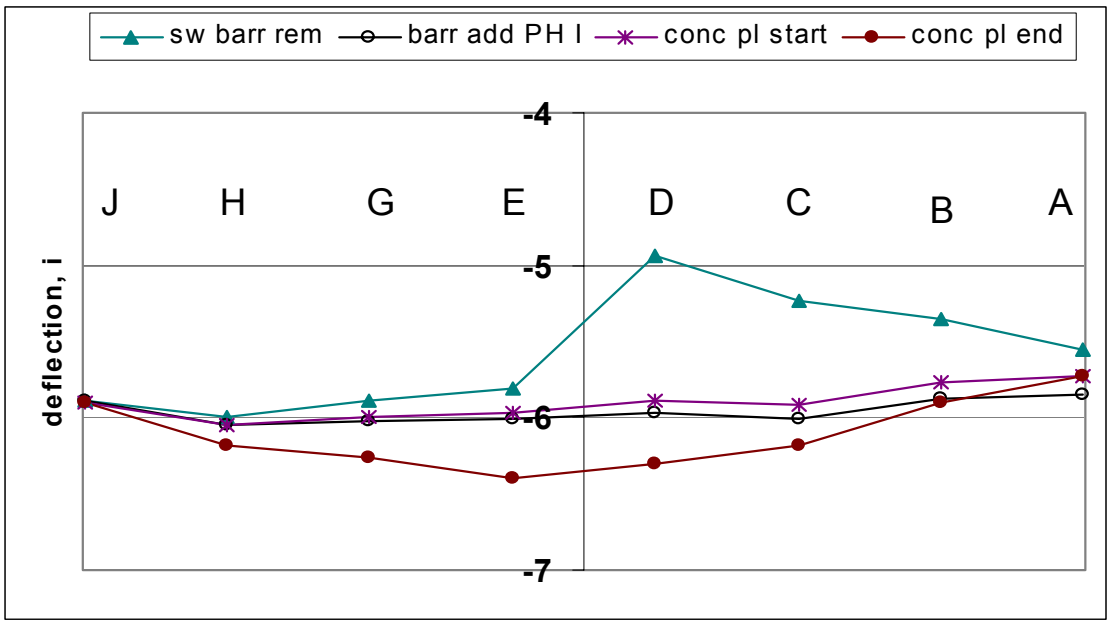

Figure B-56: Transverse girder profiles during closure operations

Figure B-57 contains data from when the closure concrete was all placed to after barriers were moved and Phase I reopened.

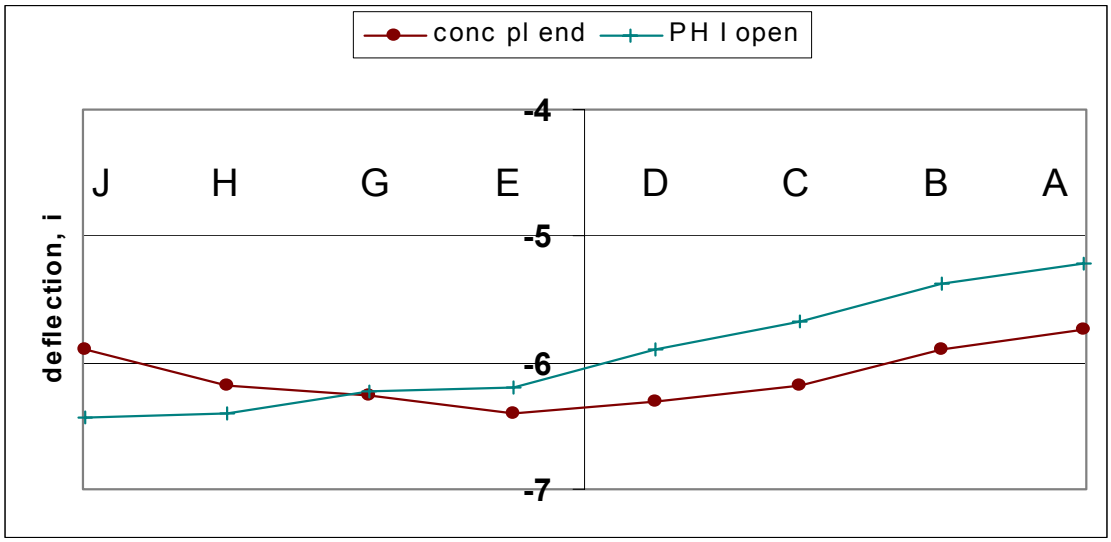

Figure B-57: Transverse girder profile during closure operation

These three figures clearly show effects from adding system loads. Girders do not deflect equally as assumed in design and uplift of some girders is apparent.

Figure B-58 contains transverse girder profiles during Phase II overlay and permanent rail placement operations. Data is shown at overlay beginning, overlay end, start of permanent rail placement, end of placement, and for temporary barriers moved to Phase II. The temporary barriers were moved so Phase II could carry traffic. Adding Phase II loads caused Phase I girders to deflect because of the before mentioned transverse stiffness. Some additions caused Phase I girders to deflect and others to rebound. There seems to be a rotation center near Girder G as it is affected very little for some operations.

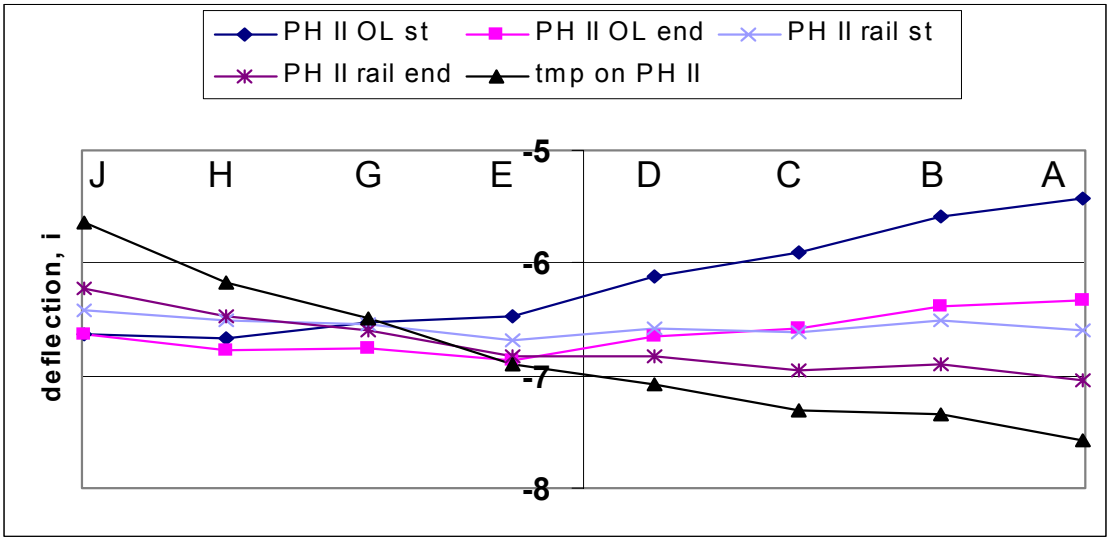

Figure B-58: Transverse Girder profiles during Phase II overlay and permanent rail placement

Figure B-59 contains similar data for Phase I overlay and rail placement operations. Readings are shown for the majority of the Phase I overlay, replacement of concrete temporary barriers with plastic barrels, Phase I sidewalk overlay, Phase I permanent rail placement, both phases open to traffic, and the last reading. Phase I overlay and permanent barrier loads

reduced the transverse profile severity. At the last reading girders are close to the same elevation.

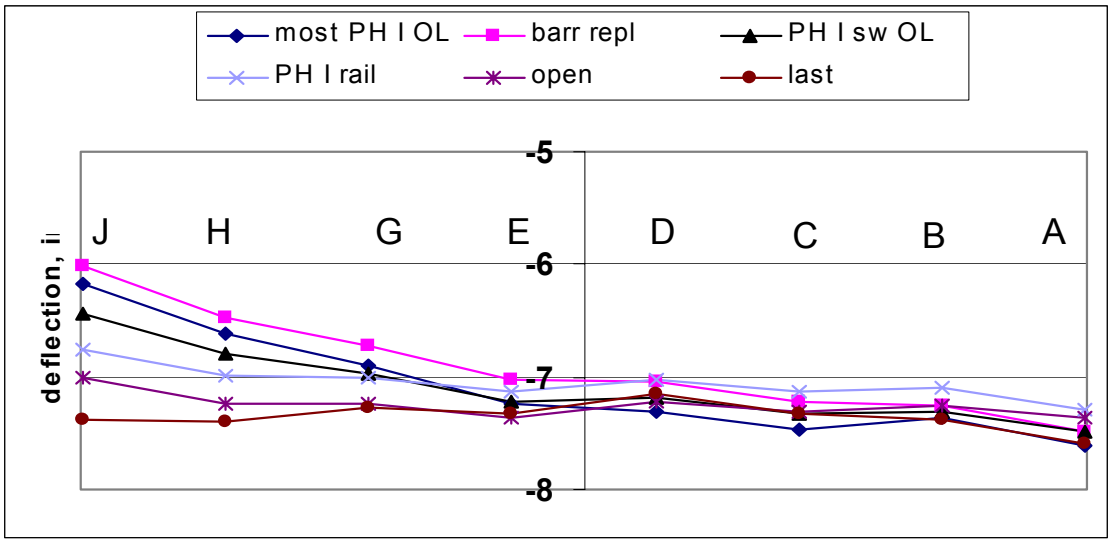

Figure B-59: Transverse girder profiles during Phase I overlay, rail placement, and opening bridge to traffic

In design it is assumed that all girders deflect equally from overlays and barrier placements. This does not appear to be the case as girders closest to loads deflect more. The results obtained in the field are obscured by temperature change. More work needs to be done analyzing system response based on load location. This should be done using a full three-dimensional bridge model in a program such as Ansys or SAP 2000. The computer model may also be able to help explain the behavior during positive region pours, as this also needs more study.

B.9 Differential Deflections of Girders D and E

Girders D and E are closest to the closure pour. If these girders deflect large amounts relative to each other, closure region cracking can occur. It appears deflection is caused by two phenomenons. One is differential bending of the phases and the other is rotation of the section. If girders deflect relative to each other from bending, transverse stresses will be induced in the closure region. If the section rotates as a rigid body, girders

will move relative to each other but no bending stresses are induced transversely. These two different causes of differential elevations are depicted in Figure B-60.

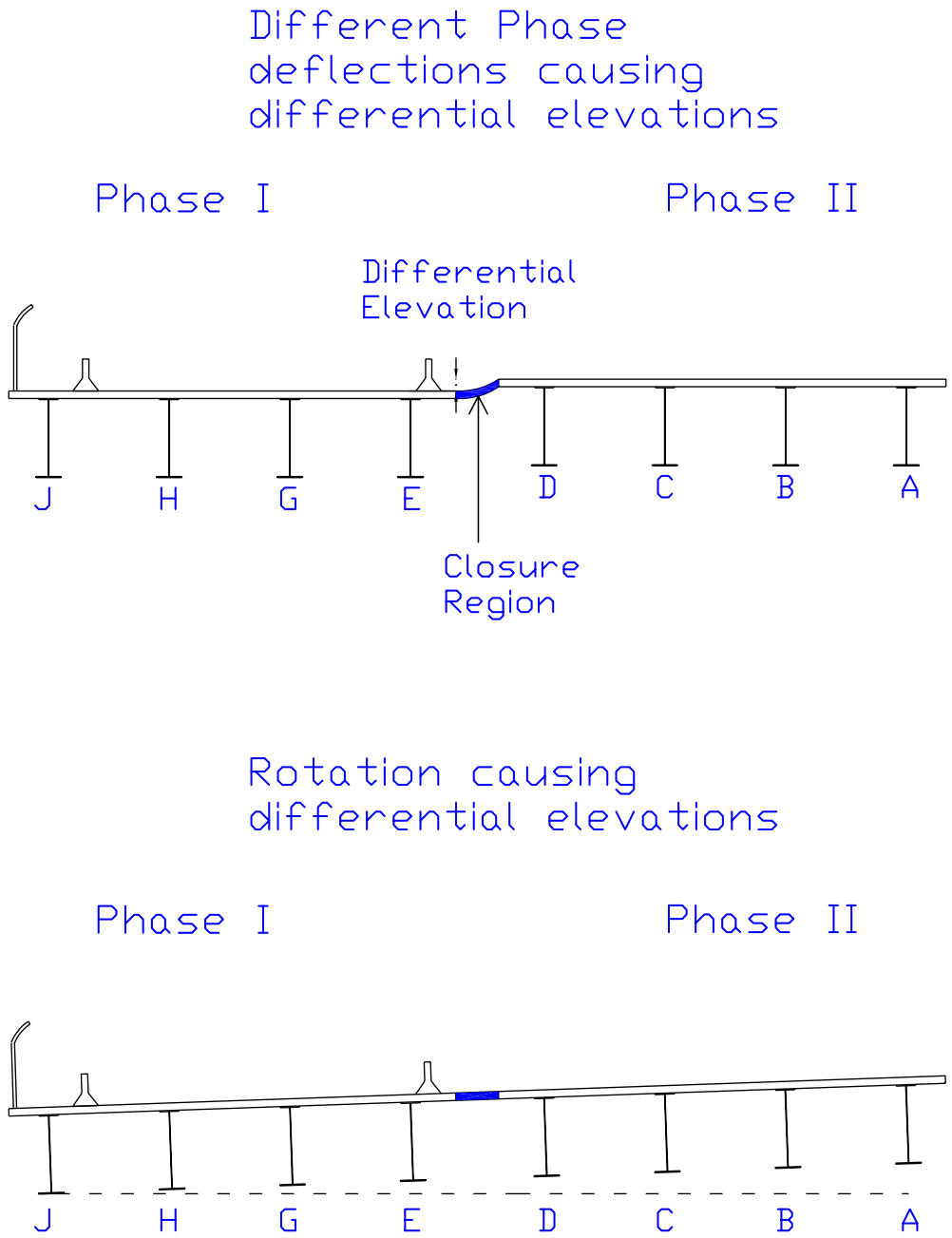

Figure B-60: Two causes of differential elevations

Table B-57 contains Girder E and D differential elevation data from before Phases were joined by the closure until the last reading. A negative number

indicates Girder E is lower than Girder D. It is important to note these girders are 113" apart while the closure is 40" wide. If girders have a 1" differential elevation, the two closure sides have a 40/113 = 0.35" differential. Although differential between girders may look large it is small at the closure.

Operation	Differential
Start of closure concrete placement	-0.085
End of closure concrete placement	-0.103
Barriers removed from PH II and placed on Phase I for traffic	-0.294
Phase II overlay start	-0.364
Phase II overlay end	-0.207
Phase II permanent railing start	-0.107
Phase II permanent rail end	0.006
Barriers moved from Phase I to Phase II. Traffic on Phase II starts	0.172
Most of Phase I overlay start	0.149
Most of Phase I overlay end	0.065
Temporary concrete rail replaced with plastic barrels	0.016
Phase I sidewalk overlay start	0.001
Phase I sidewalk overlay end	-0.028
Phase I Permanent rail start	-0.025
Phase I Permanent rail end	-0.102
Opened to traffic	-0.139
Last reading	-0.179

Table B-57: Differential deflections between Girders E and D from closure to the last reading

These numbers are all small as well as the change between successive numbers. It is the change in differential elevation during and between events that is important. If the girders were to maintain the same differential deflection, closure region cracking would be minimized.

The first three readings show a 0.209" change in differential elevation. This change occurred due to reopening Phase I to traffic after closure. Temporary barrier movement from Phase II to Phase I caused the deflection. As the concrete has not had much time to cure this can induce cracking.

Appendix

C Live Load Testing

RESULTS FROM LIVE LOAD TESTING

C.1 OVERVIEW AND RESULTS

Distribution factors are used in design to approximate the percent of live load carried by girders. Live load tests were performed on Phases I and II so design distribution factors could be compared to test results. The phases were constructed symmetrically so comparisons can also be made between phases to determine if they behave similarly. Tests were performed before the closure pour joined the phases.

On May 3, 2000 tests were performed on Phase I. Phase I was closed for 3 hours for testing. At this time there were temporary barriers in place that will not influence the results. On May 4, 2000 live load tests were performed on Phase II. No temporary barriers were in place on this phase.

The 1998 AASHTO LRFD Bridge Design Specifications were used to compute design live load distribution factors. Tables C-1 and C-2 show the calculated design values:

	1 lane loaded	2 lanes loaded
Int. girder	0.4036	0.6279

Table C-1: Live Load distribution factors from code, interior girder

	Lever rule 1 lane loaded (w/o 1.2MPF)	Special Formula in Commentary (w/o 1.2MPF for L and R lanes)			2 lanes loaded
		Left lane	Right lane	Both lanes	
Ext. girder	1.0726	0.5619	0.4372	0.9991	0.4812

Table C-2: Live Load distribution factors from code, exterior girder

Trucks traversed the bridge in many locations and configurations to simulate traffic. These configurations will be outlined later in this chapter. Maximum experimentally calculated distribution factors from these tests for Phase I and II are in Tables C-3 and C-4, respectively.

Test	J	H	G	E
Lane A	.3683 @ Max -E	.3835 @ Max + E	.2126 @ E4	.1596 @ E7
Lane C	.0675 @ E2	.2002 @ Max - E	.3379 @ Max + E	.4926 @ Max + E
A and C superimposed	.4287 @ E2	.5321 @ Max + E	.5262 @ Max + E	.6448 @ E7
A and C (side by side)	.5180 @ E2	.5446 @ Max + E	.5380 @ Max + E	.5490 @ E7
Middle	.2782 @ Max - E	.2872 @ E6	.3084 @ E6	.2680 @ Max - E

Table C-3: Experimentally calculated distribution factor(DF) for Phase I. Note location where the DF was a maximum is shown. These locations can be seen in Figures C-11 and C-12

In Tables C-3 and C-4 Lane A is the lane away from the closure region and Lane C is near the closure region. Results from testing lane A and lane C were superimposed to obtain the effect of loading both lanes simulta-

Test	D	C	B	A
Lane A	.1511 @ E7	.2179 @ E7	.3542 @ Max + E	.3856 @ max – E
Lane C	.4431 @ Max + E	.3223 @ Max + E	.2414 @ E4	.1351 @ Max - E
A and C superimposed	.5637 @ Max + E	.5271 @ Max + E	.5358 @ E6	.5827 @ E2
A and C (side by side)	.5274 @ E2	.5134 @ Max + E	.5604 @ E6	.5684 @ E2
Middle	.2653 @ Max - E	.3175 @ Max + E	.2722 @ Max + E	.2944 @ Max - E
Train C	.4315 @ E6-W1/W2	.3333 @ E6-W1/W2	.2272 @ E4-W3/W4	.0891 @ E7-CL/W1
Train Middle	.2833 @ E4-W3/W4	.2933 @ E6-W1/W2	.2799 @ E6-W1/W2	.2599 @ E7-CL/W1

Table C-4: Experimentally calculated distribution factor(DF) for Phase II. Note location where the DF was a maximum is shown. These locations can be seen in Figures C-11 and C-12

neously. This can be compared to the lane A and C loaded test. The location where the maximum distribution factor occurred is also shown. Truck positions and locations will be outlined later in this section. Girders A, D, E, and J are exterior girders while Girders B, C, G, and H are interior girders.

Tables C-5 and C-6 compare design values to experimental results for interior and exterior girder distribution factors respectively. From these tables it is clear experimental interior girder distribution factors are close to design values. For exterior girders with one lane loaded the lever rule grossly overestimates the distribution factor. The overestimation is even larger considering that the 1.2 MPF used in design is not included in the calculations. For exterior girders with two lanes loaded the commentary equation overestimates the distribution factor. Consequently, girders designed based on the lever rule and commentary equations will be over proportioned for the live load they experience.

Design		Experimental	
1 lane loaded	2 lanes loaded	1 lane loaded	2 lanes loaded
0.4036	0.6279	0.3835	0.5604

Table C-5: Design calculated distribution factors and experimental results

Design				Experimental	
1 lane loaded		2 lanes loaded		1 lane loaded	2 lanes loaded
Lever rule	commentary	eg	commentary		
1.0726	0.5619	0.4812	0.9991	0.4926	0.4287 to 0.6448

Table C-6: Design calculated distribution factors and experimental results

C.2 Live Load Test Procedure

Tests performed on Phases I and II were conducted in a similar manner. The tests followed a static live load procedure. Specific points were marked on the bridge deck where trucks were to be positioned to obtain the desired measurements. Each day truck axles were weighed with portable scales and those weights recorded. Trucks were guided into position ensuring that they were located correctly. Readings were then taken. Once they were obtained trucks moved to the next position. All tests started at the East abutment and ended at the West abutment. One reading was taken before each test began with trucks off the bridge for a base reading. Trucks were placed at locations symmetric about the completed project centerline so comparisons between the phases could be easily made. Figures C-1 to C-3 are pictures of the different test aspects mentioned above.

C.3 Live Load Test Configuration for Phase I

C.3.1 General

Each construction phase was tested to obtain live load distribution factors. Transverse truck locations were chosen to simulate traffic. The transverse truck locations were symmetric about the project centerline so results from Phase I lane A could be directly compared to Phase II lane A, for exam-

Figure C-1: Example of location to take measurement marked on deck (left) and front truck tire stopped at a location (right)

Figure C-2: Southward view of Phase II lane A live load test. The truck is stopped at a predetermined location. The pier can be seen at the left side and the West abutment is on the right

ple, as seen in Figure C-4. Tests were performed in lanes A and C separately and then a test was performed with both lanes A and C loaded. This allows for comparisons with superposition.

Longitudinal locations were chosen as follows: starting at the center of the bridge, marks were made at 25' intervals to the East and West. Marks were

Figure C-3: Longitudinal view of Phase II lane A live load test. This view is looking West with the man at left standing near the closure region. Men at the right are positioning the truck

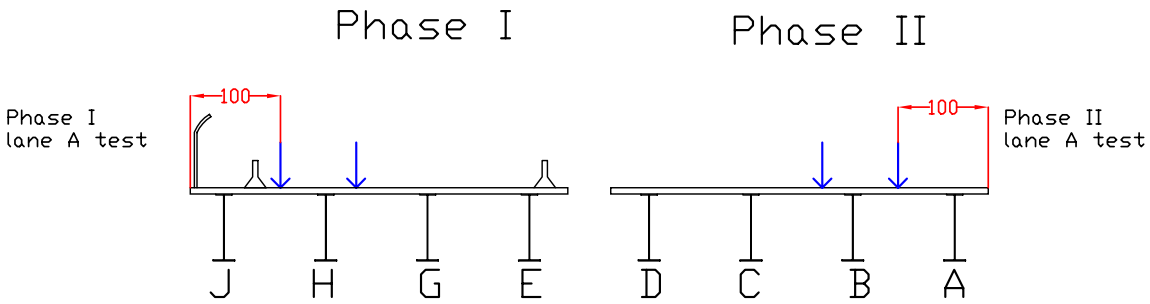

Figure C-4: Symmetry of Phase I and Phase II live load tests. The figure shows the outside wheel distance to the deck edge for the lane A tests. Dimensions are inches. Note temporary barriers on Phase I that do not effect live load results

also made at locations of maximum positive and negative bending moment as calculated from influence lines.

Exact longitudinal and transverse truck locations can be found in the following sections

C.3.2 Phase I Transverse Truck Locations

Live load tests were performed on Phase I May 3, 2000. Although traffic had been switched to Phase I November 15, 1999, the road was closed for 3 hours to perform the tests. The short time allowance limited the tests that

could be performed. Figure C-5 shows truck axle spacings and Figure C-6 shows the axle weights for Phase I tests.

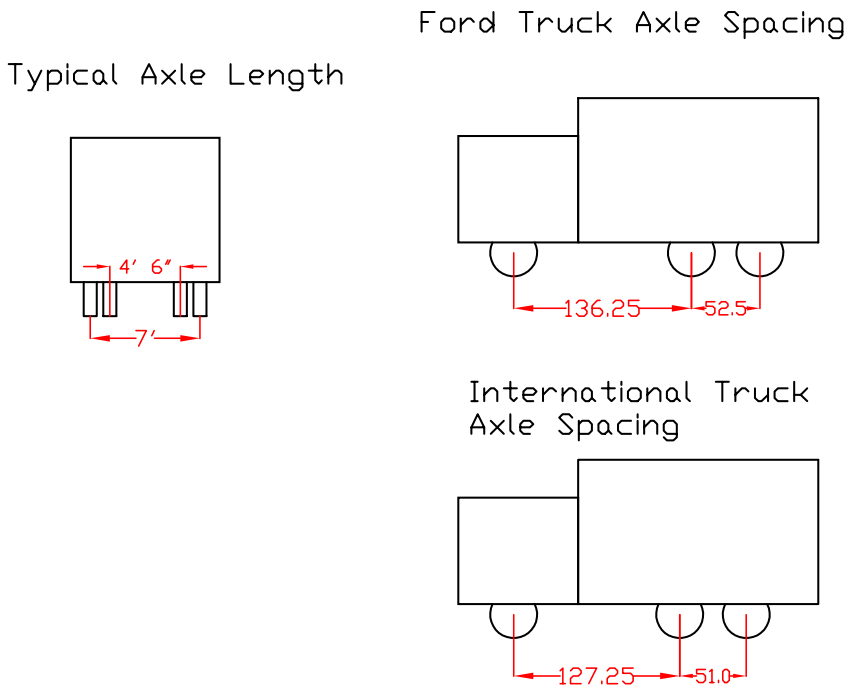

Figure C-5: Axle spacing for Phase I test trucks. Units are inches where not shown

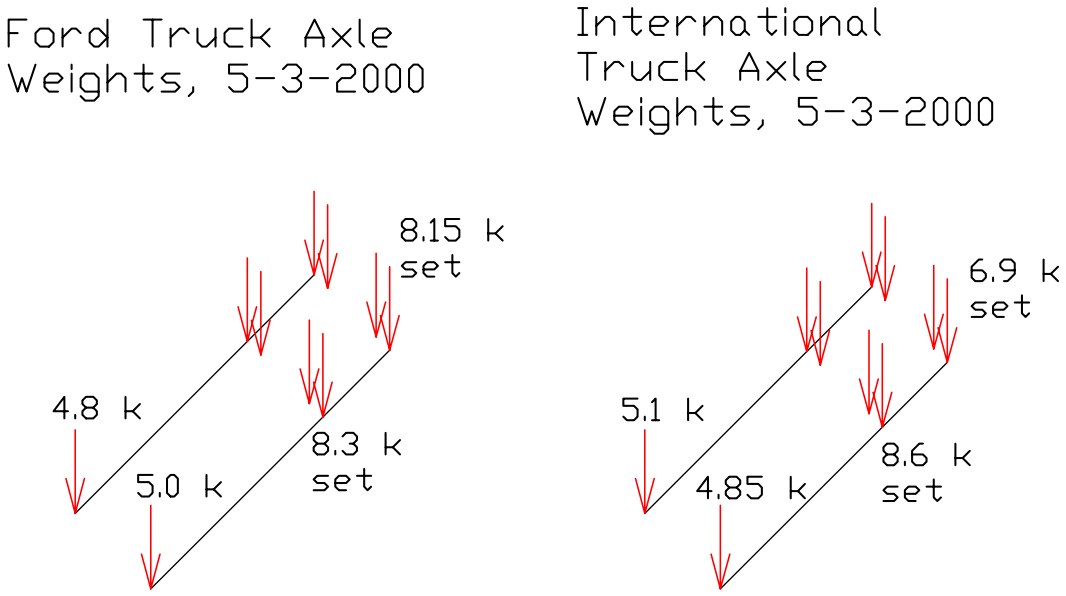

Figure C-6: Axle weights for Phase I tests on 5-3-2000. Time did not allow the weight of all axles to be taken

Individually, lanes A and C were tested as well as a test with both lanes A and C loaded simultaneously. Additionally, a test was performed with a single truck centered on the traffic lanes. Lane A refers to the location away from the closure region and lane C refers to the location closest the closure region. The transverse truck locations for lanes A and C can be seen in Figures C-7 and C-8, respectively. The truck configuration for both lane A and C loaded at once is in Figure C-9. Figure C-10 is the truck configuration when it passes down the middle of traffic lanes.

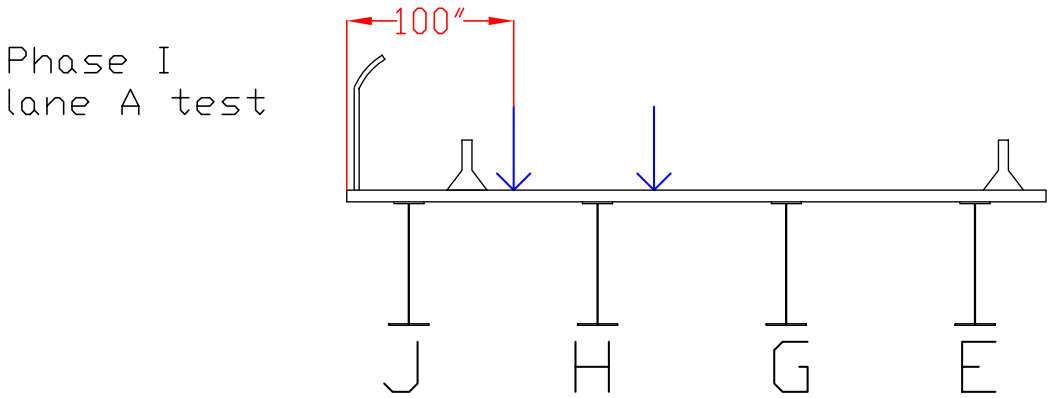

Figure C-7: Truck location for Phase I lane A test. Dimensions are to the center of the front wheel

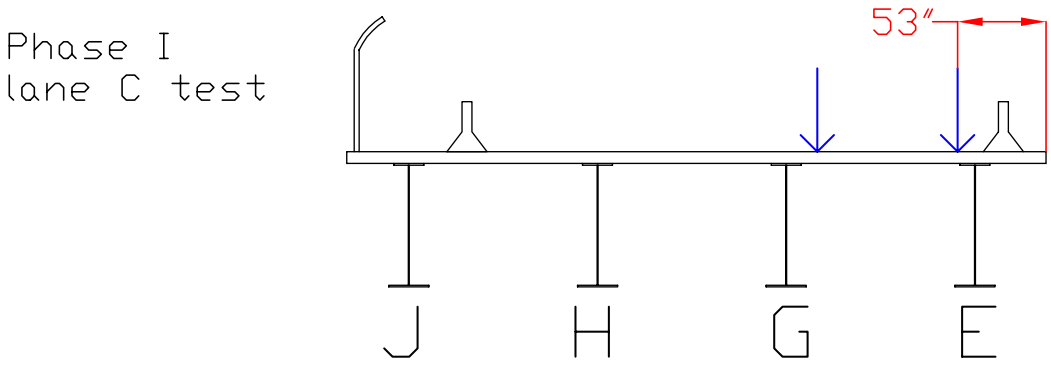

Figure C-8: Truck location for Phase I lane C test. Dimensions are to the center of the front wheel

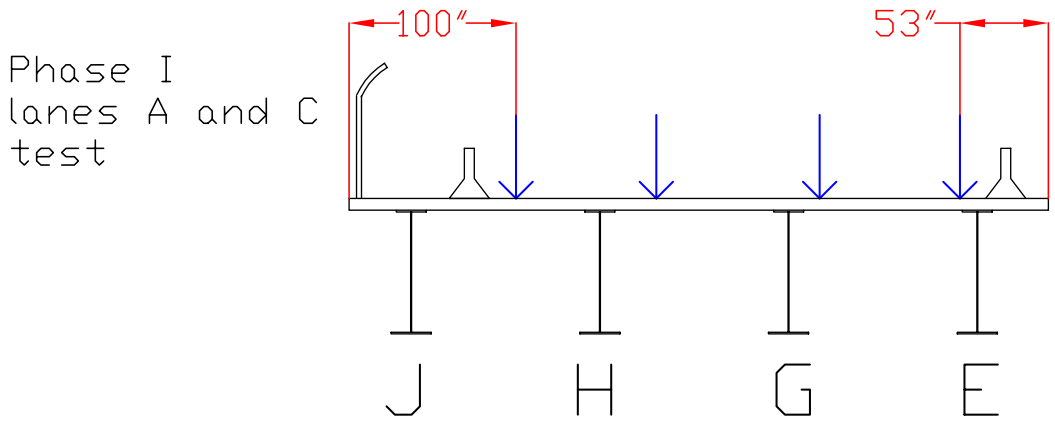

Figure C-9: Truck locations for Phase I lanes A and C test. Dimensions are to the center of the front tire. Note configuration is the same in lanes A and C as they were for lane A loaded only and lane C loaded only

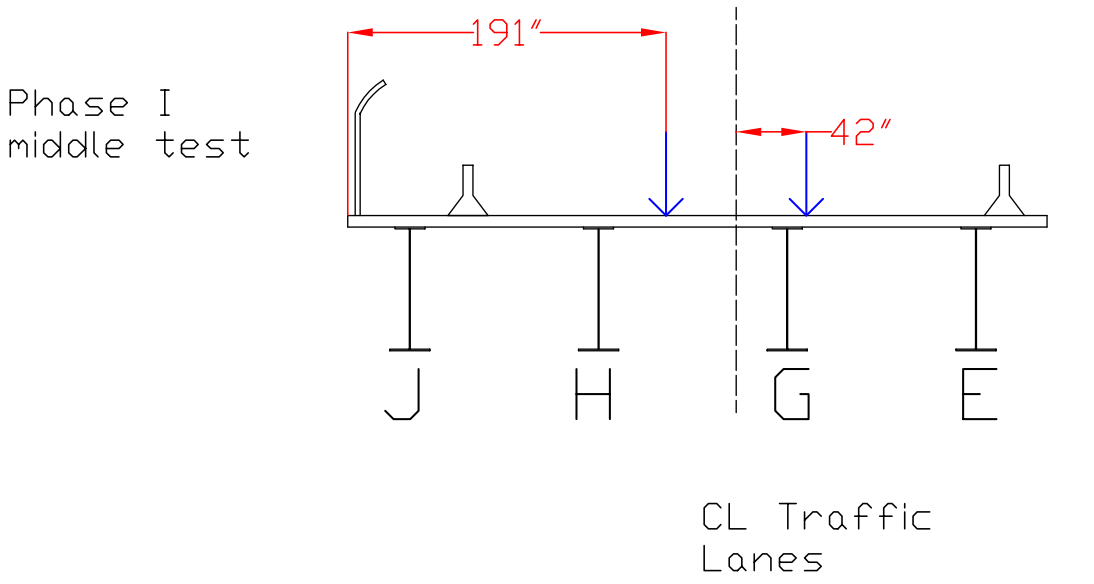

Figure C-10: Truck location for Phase I middle of traffic lanes test. Note dimensions are to center of front tire. The 84" between wheel loads is the 7' axle spacing

C.3.3 Phase I Longitudinal Truck Positions

Longitudinal positions where measurements were taken can be see in Figures C-11 and C-12. Starting at the pier centerline the deck was marked at 25' intervals to define points E1 to E9 and W1 to W9. Using influence lines, the locations on each span that would cause maximum positive and nega-

tive bending moment on the East and West span were determined and labeled EM+, WM+, EM-, and MW-. A lack of time meant readings could not be taken at all positions for the Phase I middle test. Figure C-12 shows the locations readings were observed. Trucks stopped at all locations shown in both figures.

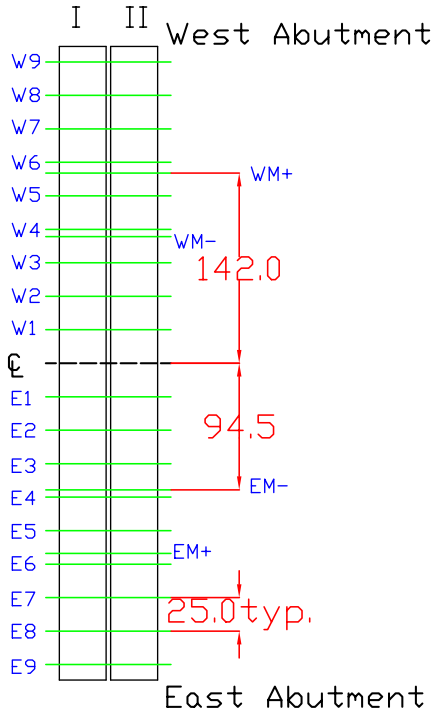

Figure C-11: Longitudinal positions for readings taken for Phase I lane A, Phase I lane C, and Phase I lanes A and C loaded. Note symmetry about the pier centerline. All tests were conducted starting at the East abutment. Units are feet

C.3.4 Phase I Test Summary

Table C-7 summarizes truck locations and longitudinal positions for readings for each test on Phase I. Listed is the test name and truck that was used in each lane. References to figures showing the lateral truck position and the longitudinal positions where readings were taken are included.

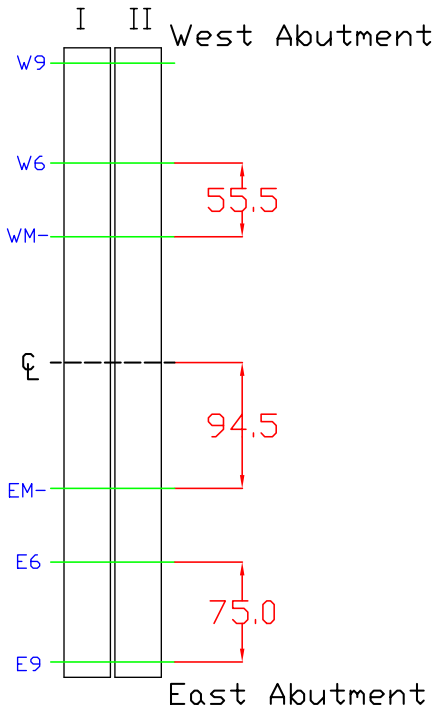

Figure C-12: Longitudinal positions for readings taken for Phase I middle of traffic lanes. Note symmetry about the pier centerline. Units are feet

Test Name	Date	Truck used in position A	Truck used in position C	Truck used in middle of lanes	Truck Location Reference	Longitudinal Locations Reference
Phase I Lane A test	5-3-2000	Inter-national	--	--	Figure C.7	Figure C.11
Phase I Lane C test	5-3-2000	--	Inter-national	--	Figure C.8	Figure C.11
Phase I Lanes A and C test	5-3-2000	Ford	Inter-national		Figure C.9	Figure C.11
Phase I truck in middle of traffic lanes	5-3-2000	--	--	Inter-national	Figure C.10	Figure C.12

Table C-7: Live Load Test Description for Phase I

C.4 Phase II Live Load Test Configuration

C.4.1 General

Phase II was tested May 4, 2000 to obtain distribution factors for this phase. No traffic was being carried by this phase so ample time was available to perform many tests, some of which were not performed on Phase I. Transverse and longitudinal truck positions were similar to Phase I for comparison.

C.4.2 Phase II Transverse Truck Locations

Before beginning tests, axle weights of the two trucks were measured and recorded. Axle spacing and truck weights can be seen in Figures C-13 and C-14.

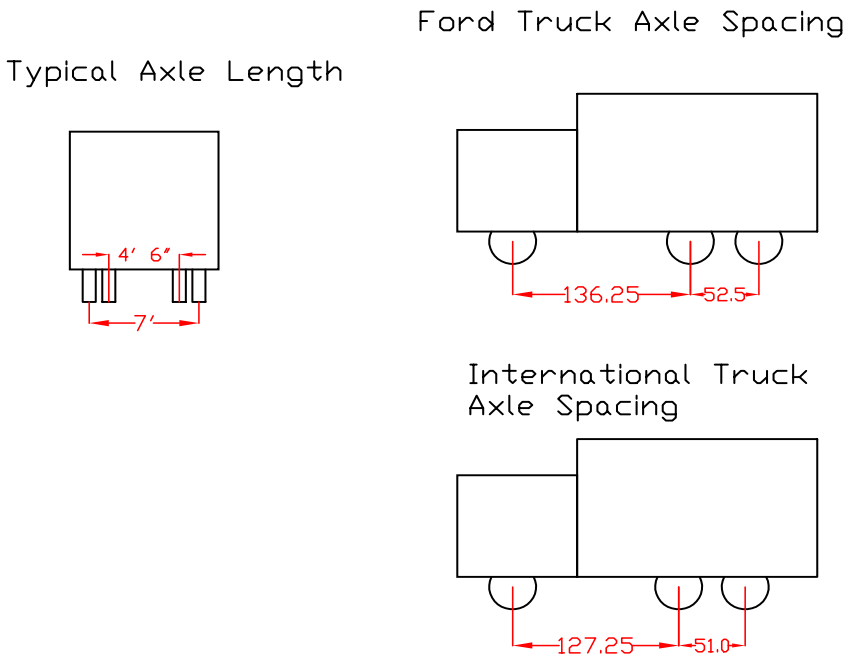

Figure C-13: Axle spacing for Phase II test trucks. Units are inches where not shown

Individually, lanes A and C were tested as well as a test with both lanes A and C loaded. As with Phase I a test was performed with a single truck centered on the traffic lanes. Additional tests for Phase II were conducted, as more time was available. These tests consisted of a two-truck train spaced 189 feet. For one truck train test the trucks were in lane C and in the other

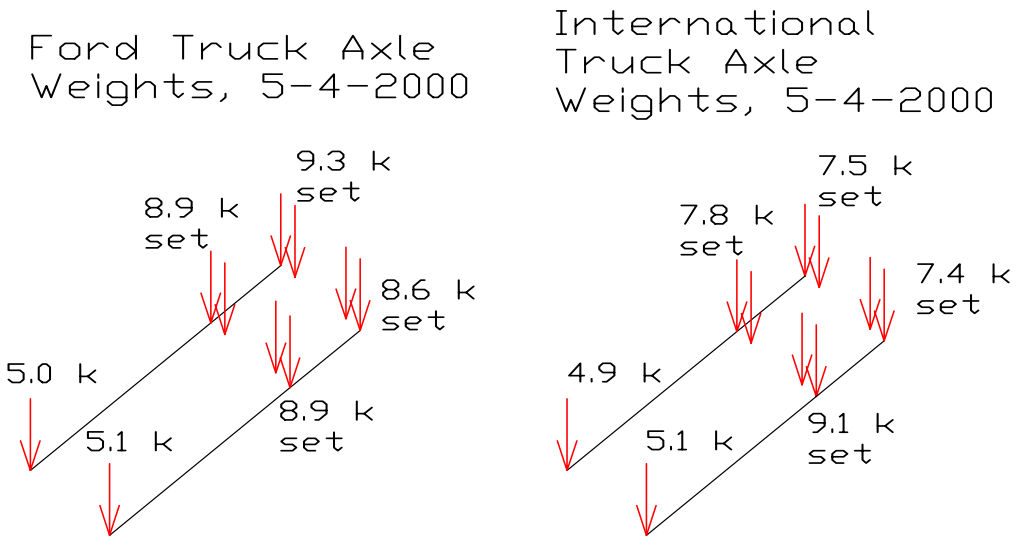

Figure C-14: Axle weights for Phase II tests on 5-4-2000

test the trucks were centered in the traffic lanes. Transverse truck locations for lane A and lane C tests can be seen in Figures C-15 and C-16, respectively. The truck configuration for both lanes A and C loaded at once is in Figure C-17. Figure C-18 is the configuration of the truck when it passes down the middle of the traffic lanes.

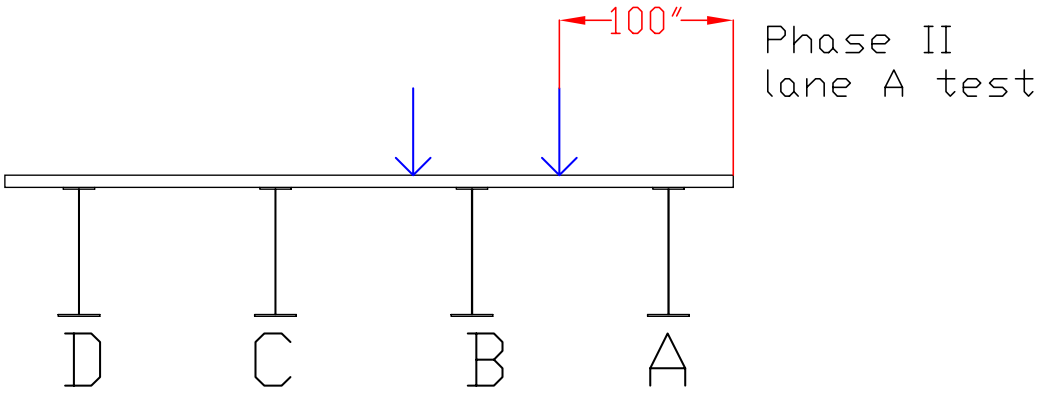

Figure C-15: Truck location for Phase II lane A test. Dimensions are to the center of the front wheel. Note 100" from edge same as for Phase I lane A test

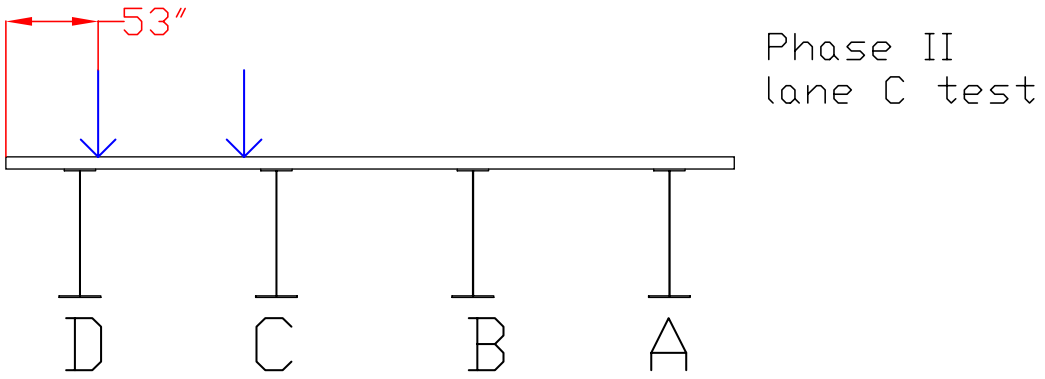

Figure C-16: Truck location for Phase II lane C test. Dimensions are to the center of the front wheel. Note 53" from edge same as for Phase I lane C test

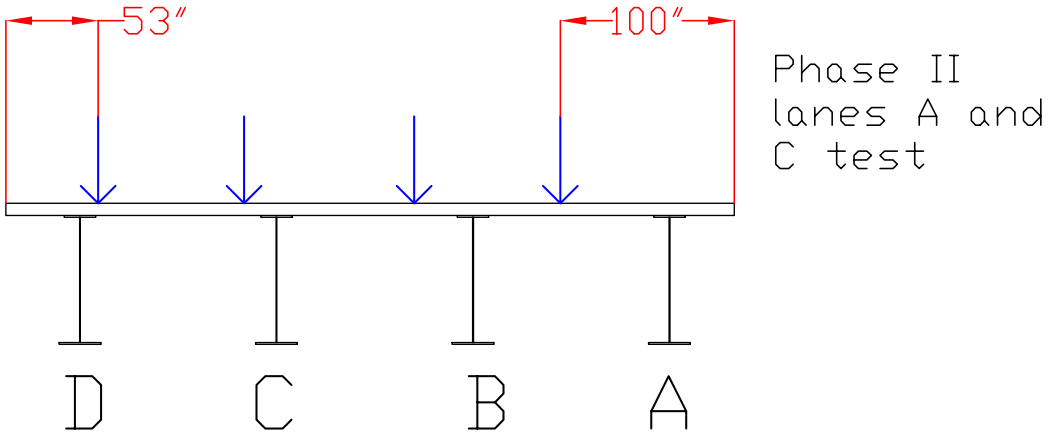

Figure C-17: Truck locations for Phase II lanes A and C test. Dimensions are to the center of the front tire. Note configuration is the same in lanes A and C as they were for lane A loaded only and lane C loaded only

C.4.3 Phase II Longitudinal Truck Positions

Longitudinal positions where measurements were taken for lane A, lane C, lanes A and C, and the truck centered in the middle of traffic lanes can be see in Figures C-19 and C-20 respectfully. Trucks stopped at all locations shown. The dual truck train was spaced such that one truck would stop at the West Max - and the other at the East Max - location, making measurement locations different. These locations are shown in Figure C-20. The front truck of the train always stops at a middle point, i.e. W4-W5, while the rear truck stops at even points as seen in Table C-8.

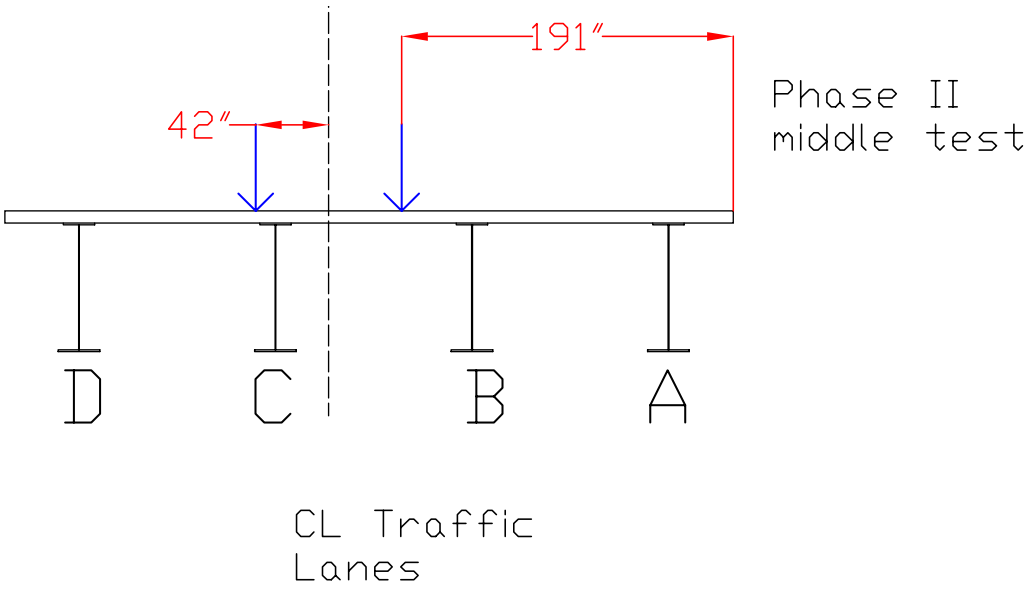

Figure C-18: Truck location for Phase II middle of traffic lanes test. Note dimensions are to center of front tire. The 84" between wheel loads is the 7' axle spacing

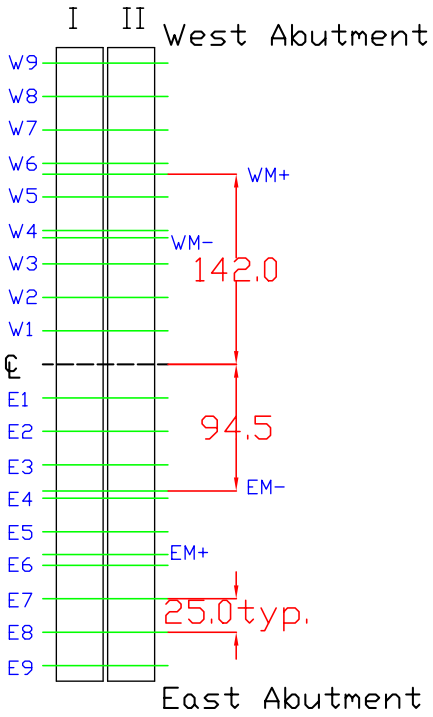

Figure C-19: Longitudinal positions for readings taken for Phase II lane A, Phase II lane C, Phase II lanes A and C loaded, and Phase II middle of traffic lanes. Note symmetry about the pier centerline. All tests were conducted starting at the East abutment

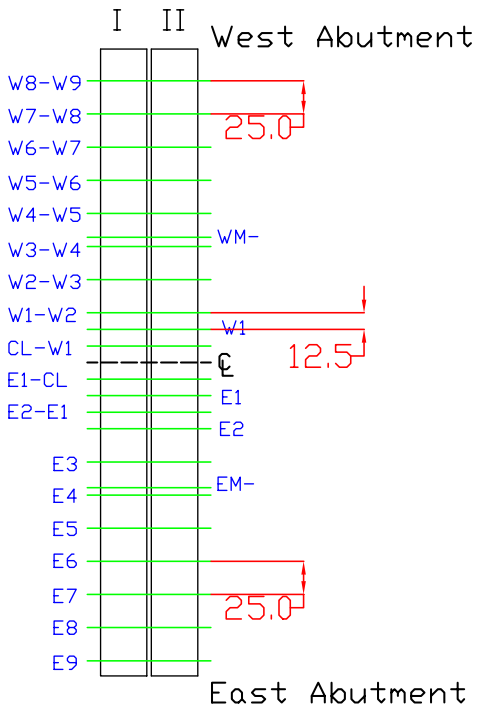

Figure C-20: Longitudinal positions for Phase II truck train readings

Load stage	Rear Truck	Lead Truck
1	E9	E1 – E2
2	E8	E1 – CL
3	E7	CL – W1
4	E6	W1 – W2
5	E5	W2- W3
6	E4	W3 – W4
7	East Max –	West Max -
8	E3	W4 – W5
9	E2	W5 – W6
10	E1	W6 – W7
11	CL	W7 – W8
12	W1	W8 –W9

Table C-8: Locations of readings for dual truck trains

C.4.4 Phase II Test Summary

Table C-9 summarizes truck locations and longitudinal positions for each Phase II test. Listed are the test name and truck that was used in each lane. References to figures showing the truck lateral position and the longitudinal positions where readings were taken are included.

Test Name	Date	Truck used in position A	Truck used in position C	Truck used in middle of lanes	Truck Location Reference	Longitudinal Locations Reference
Phase II Lane C test	5-4-2000	--	Inter-national	--	Figure C.15	Figure C.19
Phase II Lane A test	5-4-2000	--	Ford	--	Figure C.16	Figure C.19
Phase II Lanes A and C	5-4-2000	Ford	Inter-national	--	Figure C.17	Figure C.19
Phase II truck in middle of traffic lanes	5-4-2000	--	Inter-national	--	Figure C.18	Figure C.19

Test Name	Date	Location of Trucks	Lead Truck	Rear Truck	Truck Location Reference	longitudinal Locations Reference
Phase II train in lane C	5-4-2000	South Lane	Inter-national	Ford	Figure C.16	Figure C.20
Phase II train in Middle	5-4-2000	Trucks in Center of Traffic Lanes	Inter-national	Ford	Figure C.18	Figure C.20

Table C-9: Phase II Live Load Test Description

C.5 LIVE LOAD TEST RESULTS

C.5.1 GENERAL

Data of primary interest from live load tests involves deflection and strains at Section 2. Deflection and strain data can be used to compare superposition of lane A and lane C tests with lanes A and C loaded simultaneously. Additionally, deflection and strain data can be used to compare behavior of the phases. Finally, strain data can be used to determine live load distribution factors. Due to the large volume of data collected a representative sample of data will be shown. Further results appear in *Field Monitoring of a Staged Construction Bridge Project* (Swendroski 2001).

C.5.2 Superposition of Test Results

Figures C-21 and C-22 show girder deflections during Phase I lane A test and Phase II lane A test respectively.

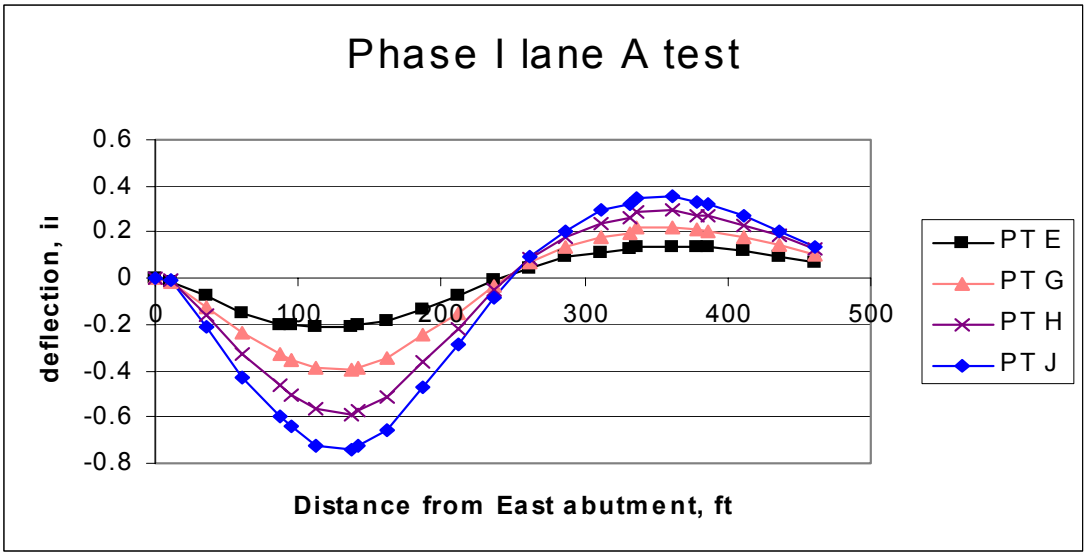

Figure C-21: Deflection of Phase I girders during Phase I lane A test. Girder J is farthest from the closure region

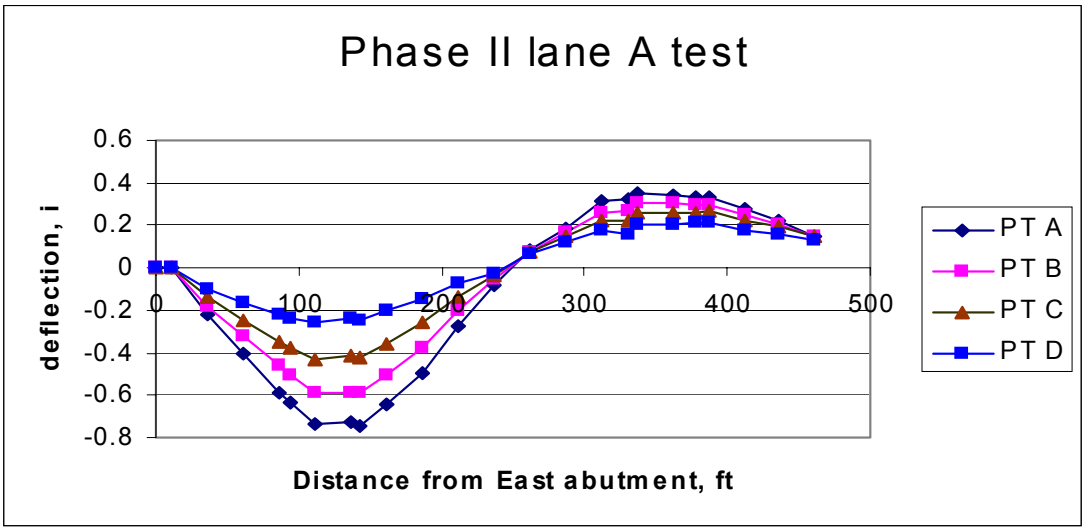

Figure C-22: Deflection of Phase II girders during Phase II lane A test. Girder A is farthest from the closure region

During the lane A tests wheel loads were closest to the outside girders, A and J in this case. It is expected that these girders should deflect more than the girders near the closure region. As seen in the figures, this is the case.

For this test configuration, outside girders deflect nearly 3 times more than the inside girders.

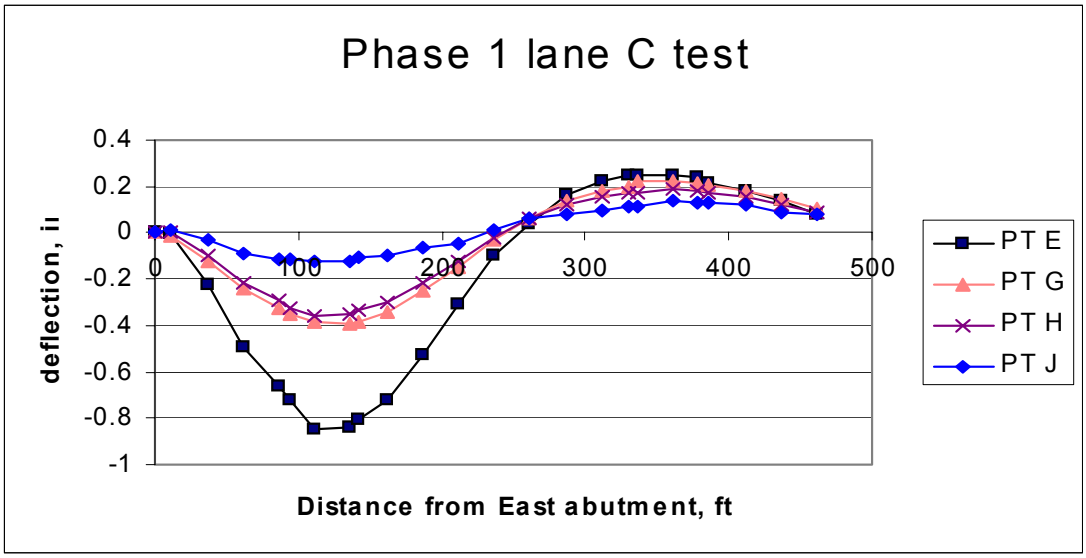

Figure C-23: Deflection of Phase I girders during Phase I lane C test. Girder E is closest to the closure region and deflects the most, as expected

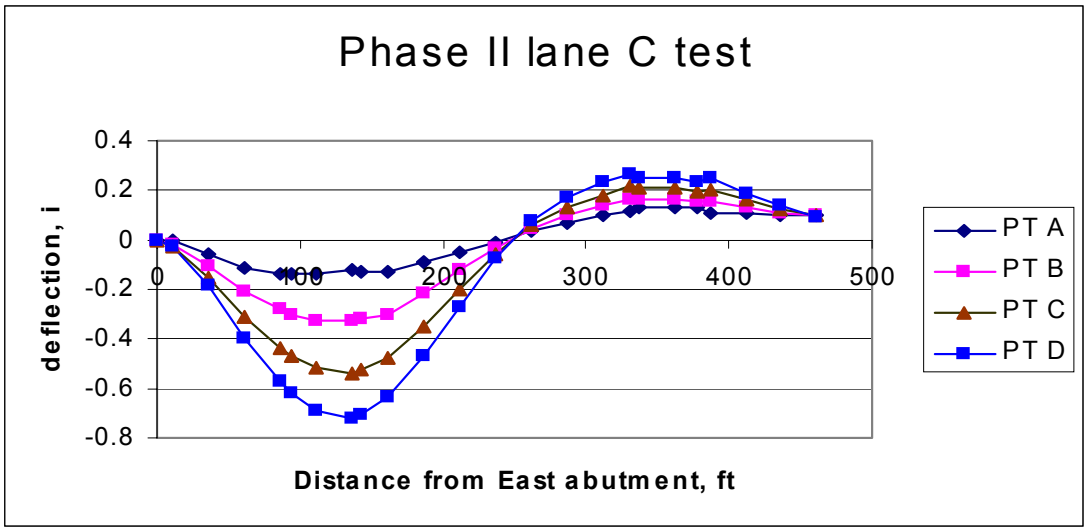

Figure C-24: Deflection of Phase II girders during the Phase II lane C test. Girder D is closest to the closure region and deflects the most as expected

Figures C-23 and C-24 contain deflection data for the Phase I lane C and Phase II lane C tests, respectfully. As the trucks are nearest the closure region Girders E and D should deflect more than the other girders. This behavior is easily seen.

Figures C-21 to C-24 give a very general bridge behavior picture. As expected, girders closest to the loading deflect more than the girders away from the loads.

Superposition of lane A and lane C tests versus simultaneous loadings of lanes A and C are expected to be equal. Suppose a girder deflects X in. when lane A is loaded and Y in. when lane C is loaded. Elastic behavior yields the conclusion that the girder should deflect X + Y in. when both lanes are loaded at once. This assumption can easily be checked as all these load cases were performed. Figures C-25 and C-26 show the resulting girder deflections for the test when both lanes A and C were loaded for Phase I and superposition of lane A and lane C tests, respectively. From these figures it is clearly seen that with both lanes loaded the girders deflect nearly the same amount for all positions along the bridge length. The figures show small discrepancies in total deflection but the difference is less than 0.2 in. This is still very good correlation between the two methods. A deflection comparison for Girder E is in Figure C-27. Girder E shows the highest discrepancy level of any girder using the comparison. The maximum difference in the comparison is 0.14 in.

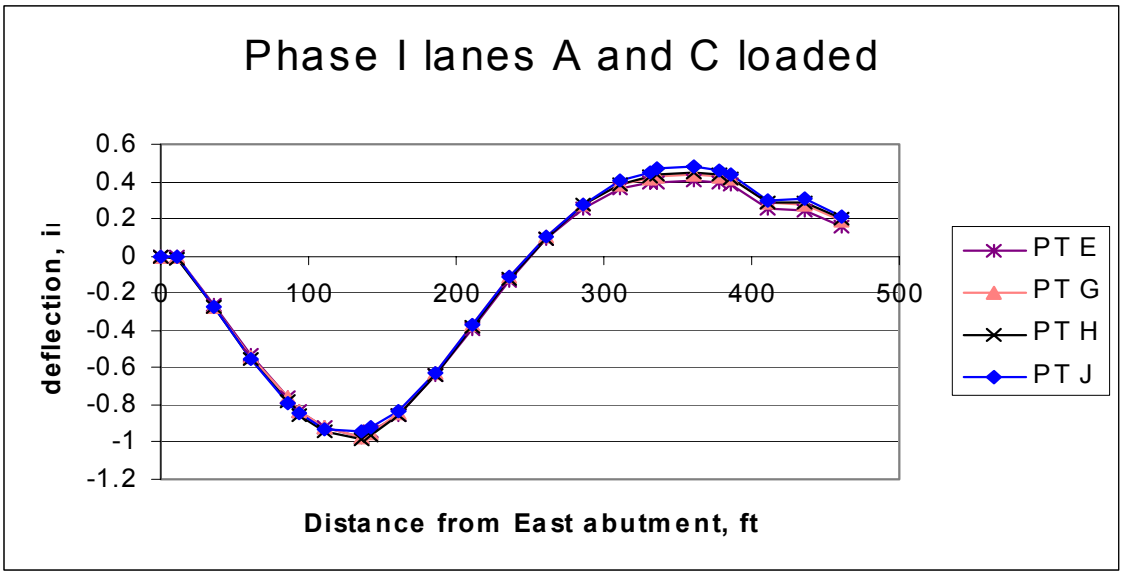

Figure C-25: Girder deflections for Phase I lanes A and C loaded simultaneously

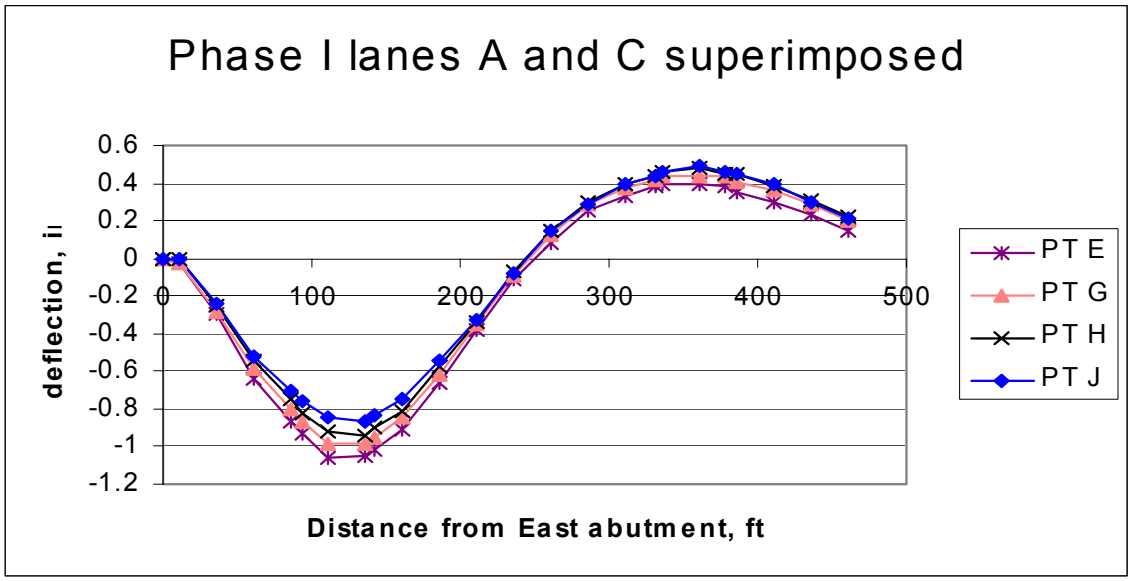

Figure C-26: Girder deflections for the superposition of lane A loaded and lane C loaded for Phase I

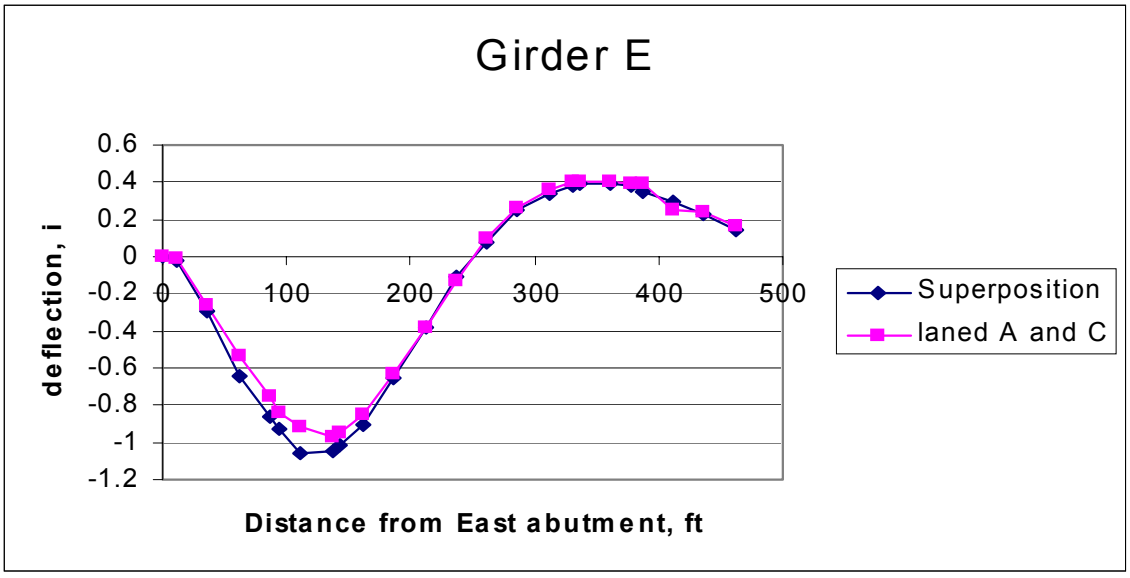

Figure C-27: Comparison between lanes A and C loaded versus superposition of the individual loadings for Girder E. Note maximum difference of 0.14 in is approximately 15% error

Similar comparisons can be made for Phase II. Figures C-28 and C-29 show girder deflections for the case when both lanes A and C were loaded for Phase II and the superposition of the lane A and lane C loadings.

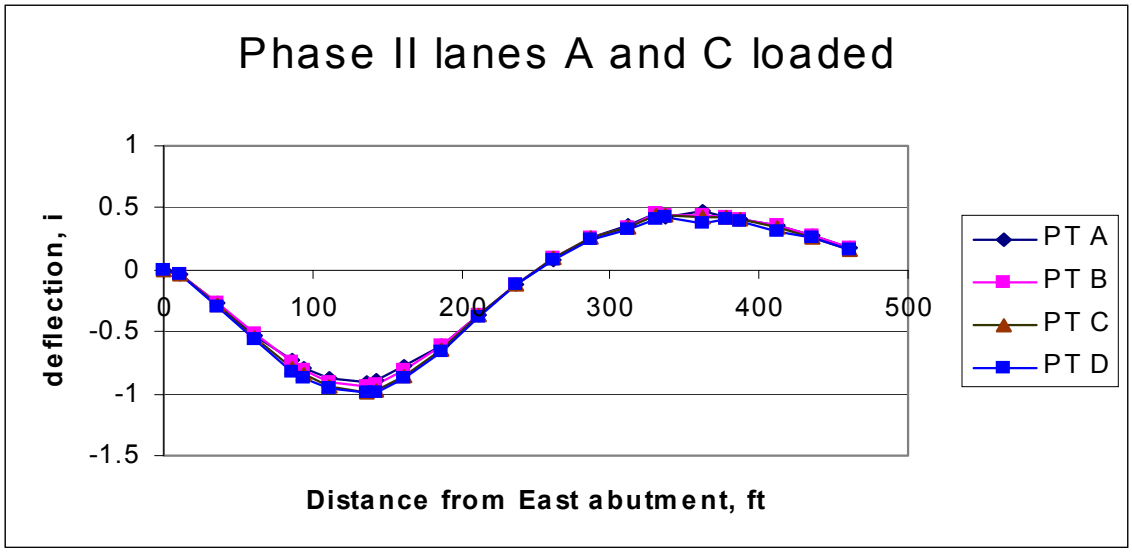

Figure C-28: Girder deflections for Phase II lanes A and C loaded simultaneously

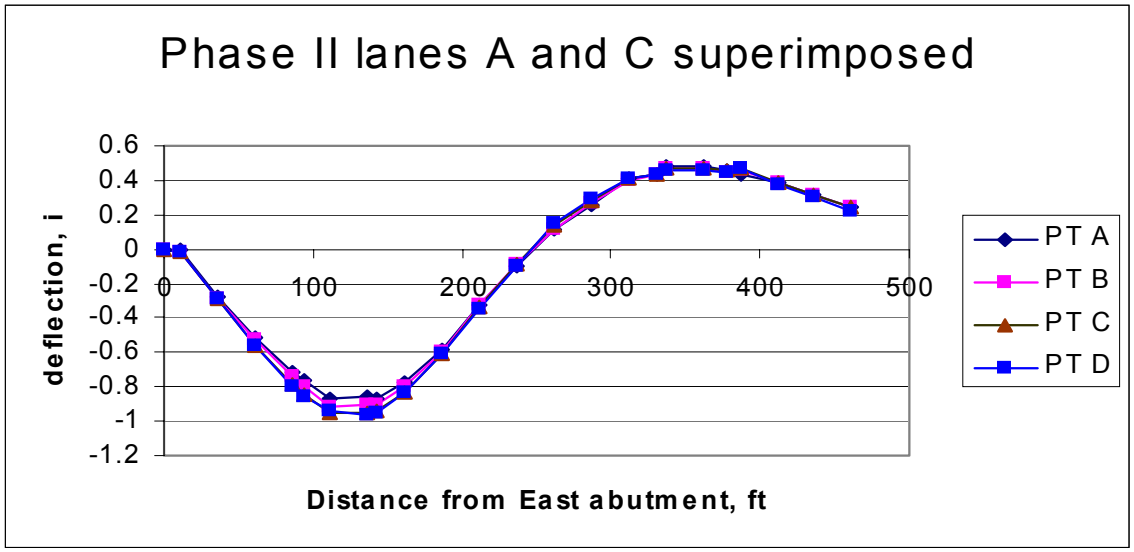

Figure C-29: Girder deflections for the superposition of lane A loaded and lane C loaded for Phase II

While Phase I showed good correlation between the two methods Phase II shows even better correlation. The Girder showing the most discrepancy is

D and a plot of the deflections for this girder using the two methods is in Figure C-30. The maximum difference is 0.04 in.

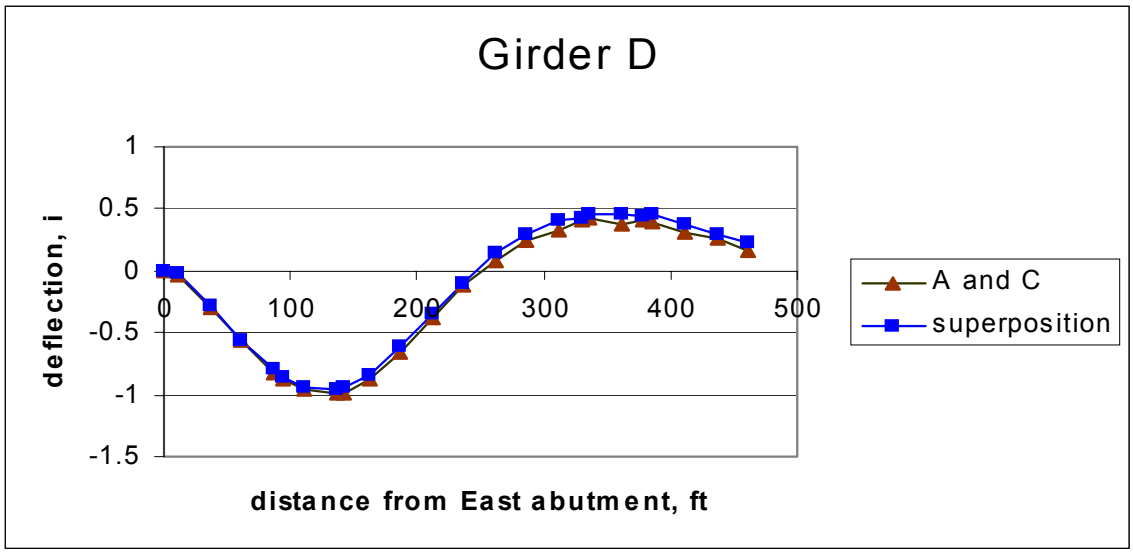

Figure C-30: Comparison between lanes A and C loaded versus superposition of the individual loadings for Girder D. Note maximum difference of 0.04 in is approximately 4% error

Strain data can also be used to verify linear behavior. The superposition of strain data from lanes A and C loaded separately should equal the case of lanes A and C loaded simultaneously. This can be seen in Figure C-31.

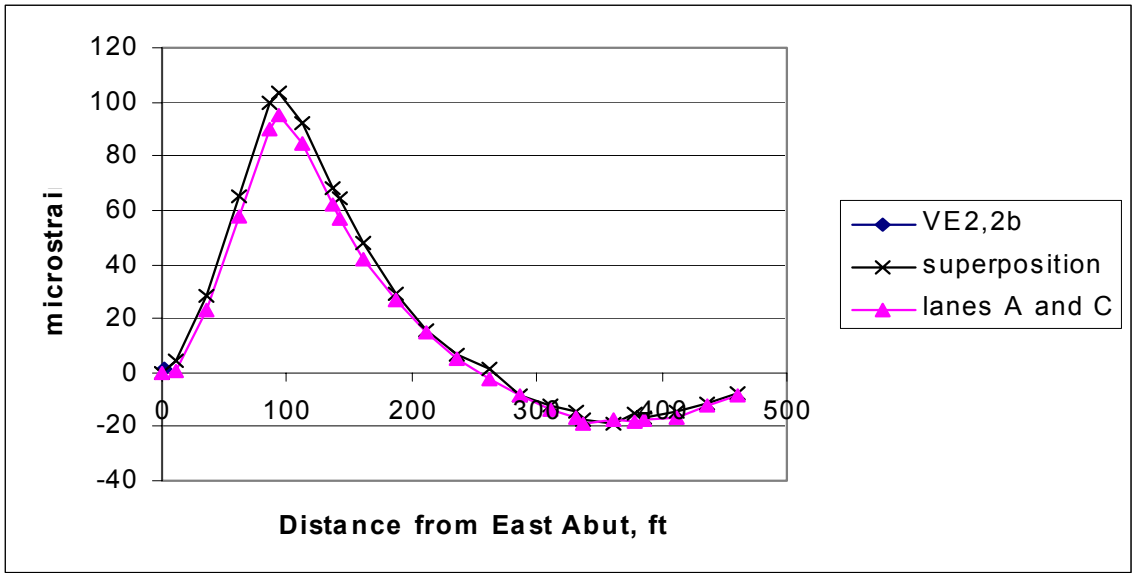

Figure C-31: Gage VE2,2b strain data comparison

Figure C-31 also supports superposition. Embedment gages record concrete strain during tests and should also show superposition. Figure C-32 displays similar data for gage E6 which is positioned over Girder H orientated along the bridge length. The correlation is very good when the trucks are close to the gage location (84' 6" from East abutment) but diverge as the trucks progress farther from the gage. Strain magnitudes are small and it appears that when only one truck passes down the bridge more stress is locked into the system due to friction causing the superposition to diverge from the true behavior of both lanes A and C being loaded. With both lanes loaded there is more load to unlock these stresses when the trucks are on the west span.

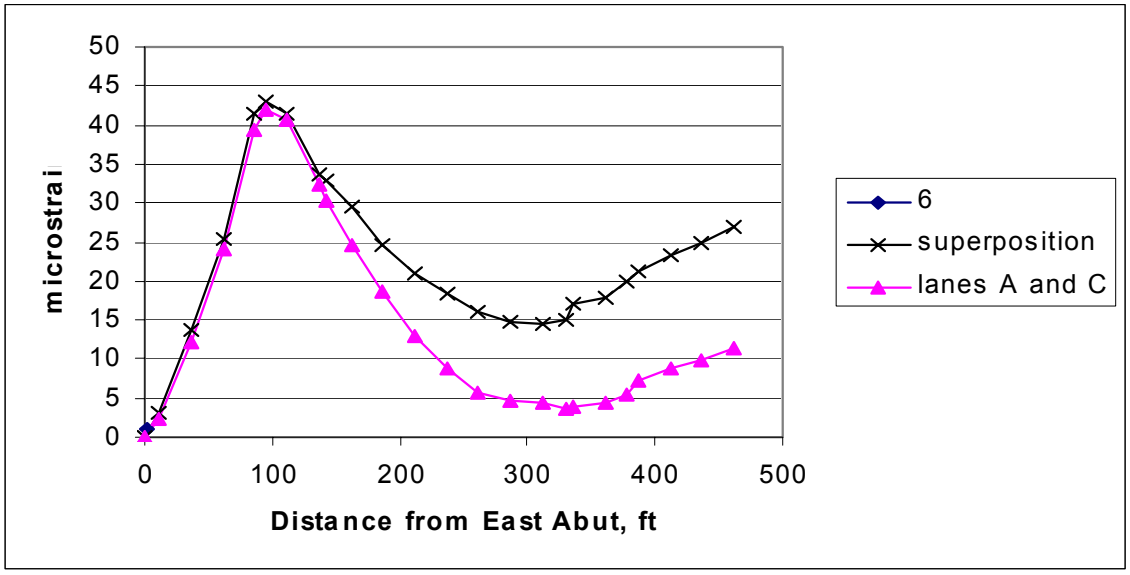

Figure C-32: Gage E6 strain data comparison for superposition versus both lanes loaded. Note positive values indicate compressive strain

In conclusion, data observation supports the linear behavior of the phases. Deflection and strain comparisons for superposition and lanes A and C loaded consistently show good correlation.

C.5.3 Phase I and Phase II Response Comparison

As the two phases are symmetric about the project centerline, behavior should also be symmetric. Tests on lane A, lane C, and lanes A and C loaded

should induce similar responses in both systems as loading was symmetric about the centerline. For comparisons Girder A should be compared to Girder J, B to H, C to G, and D to E. This means a Phase I girder should be compared to its mirror image on Phase II. Due to the number of tests performed only selected comparisons will be shown here. All of the comparisons can be seen in *Field Monitoring of a Staged Construction Bridge Project* (Swendroski 2001).

Figures C-33 to C-35 are comparisons of selected girders for lane A, lane C, and lanes A and C tests, respectively.

Figure C-33: Lane A test comparison for Girders D and E

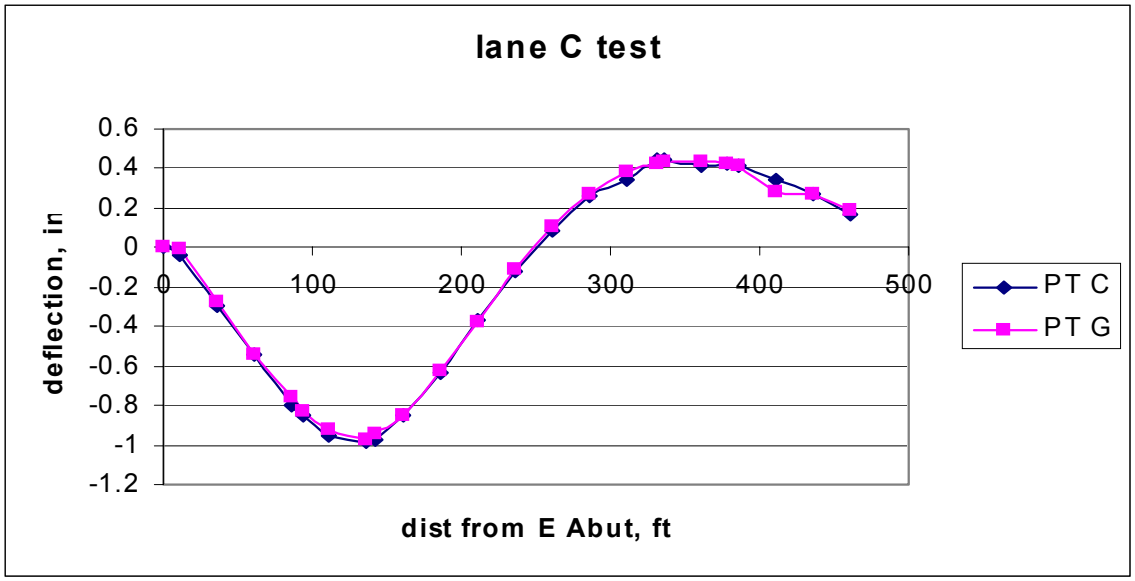

Figure C-34: Lane C test comparison for Girders C and G

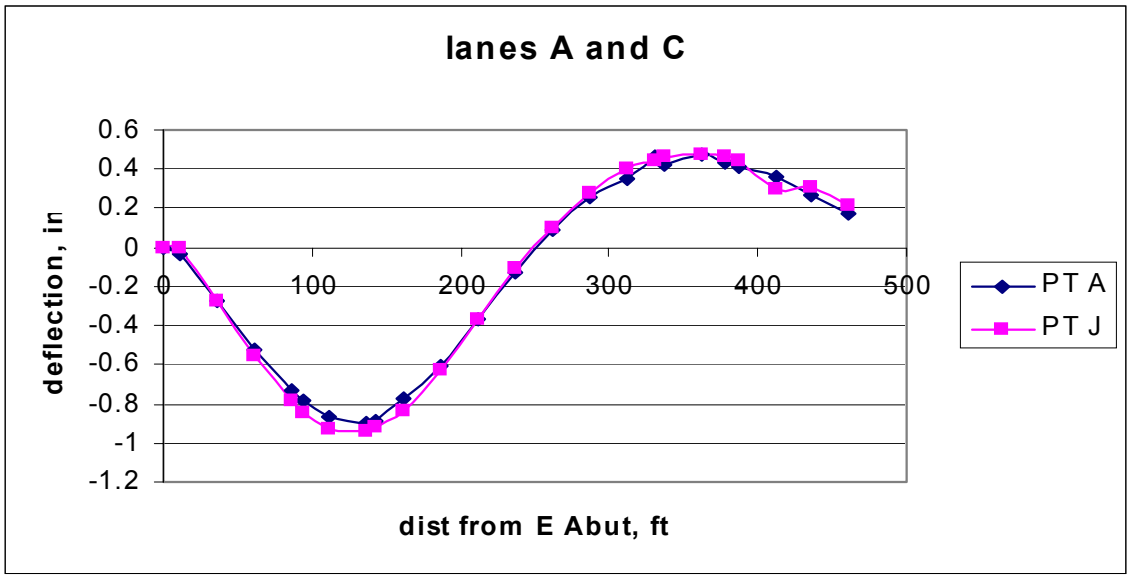

Figure C-35: Lanes A and C test comparison for Girders A and J

Clearly, the above figures show symmetrical behavior. This is exactly what was expected before tests were performed. To further show symmetrical behavior strain data can be compared. Figures C-36 and C-37 show comparisons for the lanes A and C loaded test.

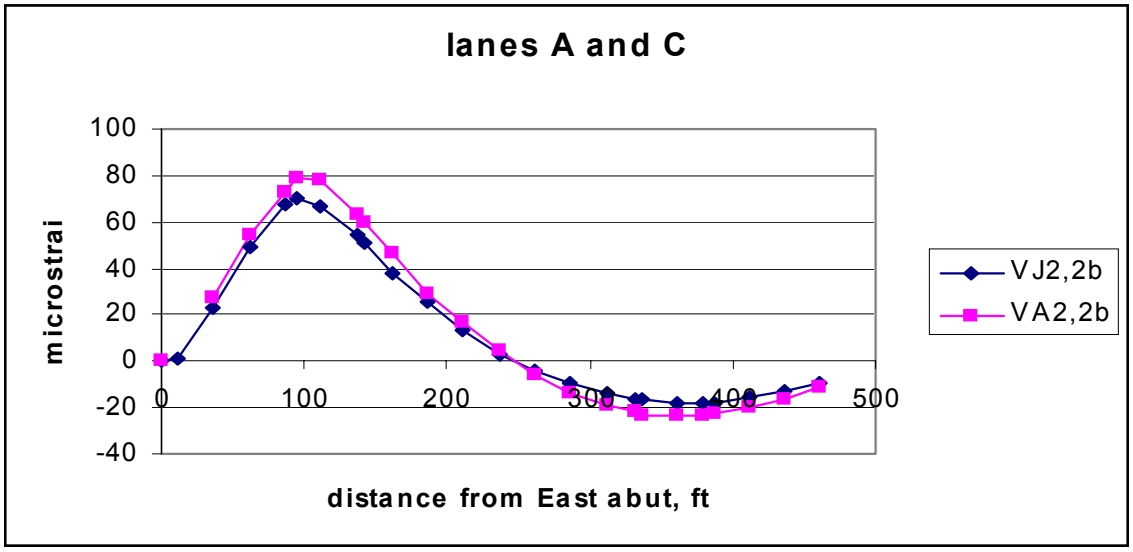

Figure C-36: Strain comparison of Girders A and J, bottom flange at the maximum positive moment region. Note positive strain indicates tension

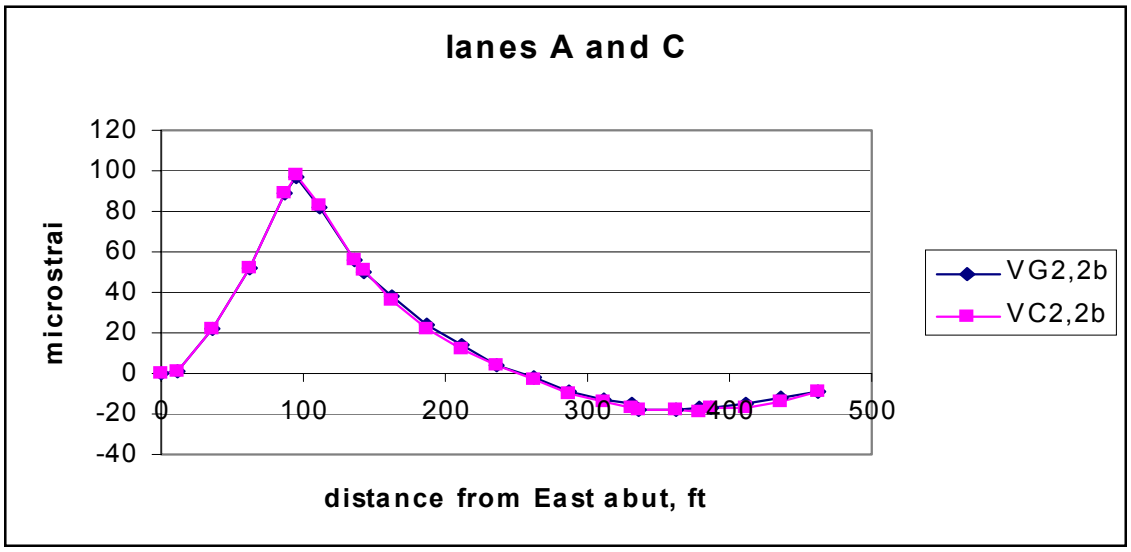

Figure C-37: Strain Comparison of Girders C and G, bottom flange at the maximum positive moment region. Note positive strain indicates tension

Figure C-37 shows a very close comparison between Girders G and C strains. Figure C-36 is not quite as close although curve shapes are similar. This is because the lateral truck position is farther from these girders so more variation can be expected.

A lane C test comparison between Phases I and II appears in Figure C-38. There is a slight difference in strain values but responses are similar.

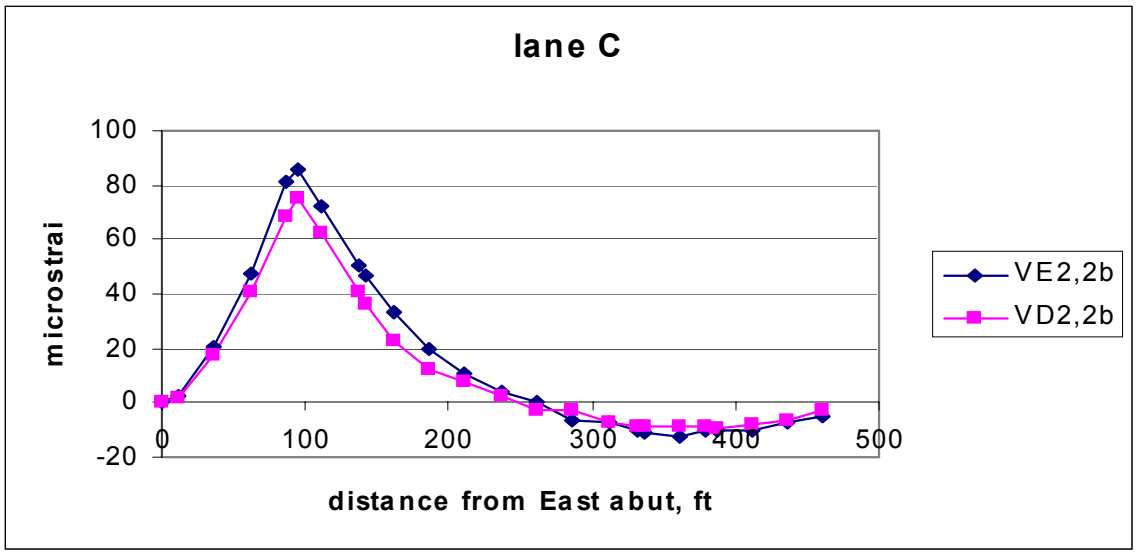

Figure C-38: Strain response of Girders E and D for the lane C test. The gages are located on the bottom flange at the maximum positive moment location

Finally Figure C-39 is a similar comparison for the lane A test. As seen before the responses of the Phase I and Phase II girders are similar.

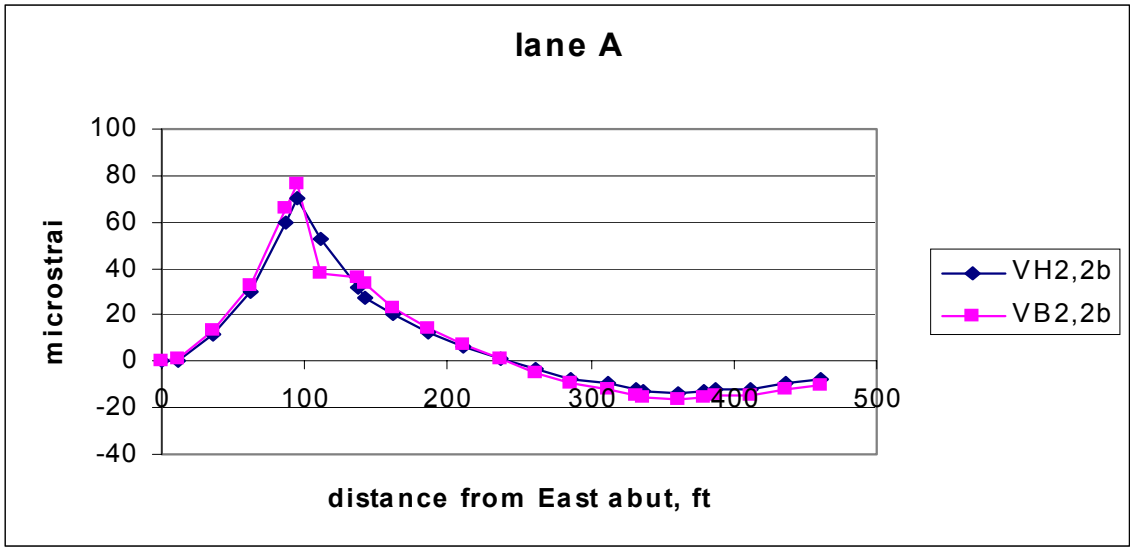

Figure C-39: Strain response of Girders H and B for the lane A test. The gages are located on the bottom flange at the maximum positive moment location

From the deflection and strain data it is clear that the two phases behave similarly under live load conditions. This is what was expected before testing began due to symmetric loading and symmetry of the phases.

C.5.4 Live Load Distribution Factors

The primary objective of the live load tests was to determine live load distribution factors for each phase. The similar behavior shown previously leads to the conclusion that distribution factors for the phases should also be similar.

To determine distribution factors strain data is needed for each girder at a cross section. The data commonly used are bottom flange tensile strains as they have the largest magnitude. Certainly, compressive flange data could be used but due to the smaller strains the calculated distribution factors contain more error. A small tensile strain error has less effect as the total strain is much larger. Calculation of the distribution factors for Phases I and II was based on bottom flange strains at Section 2. Essentially this is the tension flange at a location of high positive moment. Equation C-1 gives the formula to calculate distribution factors from strain data (Stallings and Yoo 1993).

$$DF_i = \frac{n\varepsilon_i}{\sum_{j=1}^{k} \varepsilon_j w_j} \qquad \text{(C-1)}$$

Where

DF_i = Distribution factor for the i^{th} girder
n = Number of loaded lanes
k = Number of girders
ε_j = Bottom flange strain of j^{th} girder
w_j = Ratio of moment of inertia of j^{th} girder to an interior girder

The weighting factor, w_j, is typically taken equal to one. This commonly used assumption means all girders have equal stiffness. A distribution

factor can be computed for every location where readings were taken. The controlling distribution factor is the maximum along the span. However, at some locations the total strain as well as the individual girder strains are relatively small. Any system error in measurements will lead to large errors in calculated distribution factors. This is easily seen in tables to follow. Therefore, locations where the total strains are largest carry more importance than locations where total strain is small. In the tests for Dodge Street over I-480 this leads to more importance being carried on East span readings that are closest to strain gages.

Selected results are shown in Tables C-10 to C-13. These tables contain data regarding where the reading was taken, total bottom flange strain, and the distribution factor for each girder.

From results such as those presented, the maximum interior and exterior distribution factors can be extracted and compared to 1998 AASHTO LRFD Bridge Design Specification recommended values. This was shown earlier in the section in Tables C-5 and C-6. Formulas for interior girders accurately predict distribution factors while the exterior girder DF's are grossly overestimated by the lever rule for one lane loaded. For two lanes loaded the commentary equation once again greatly overestimates the DF. This leads to exterior girders controlling live load design, as is often the case. Girders will be over designed to carry a large live load that they will never experience. A better approach to design would be to design for the two lanes loaded case for interior girders as the 0.6279 calculated DF is larger than any actual DF except for one case for exterior girders. This would still

be acceptable as the 0.6448 experimental DF occurs at E7, away from the maximum positive moment (refer to Table C-3).

		Distribution Factor			
Location	**Total strain**	**Girder E**	**Girder G**	**Girder H**	**Girder J**
E9	2.82	0.2482	0.8511	-0.0709	0.9716
E8	90.2	0.5204	0.4922	0.4745	0.5129
E7	210.42	0.5490	0.4942	0.4904	0.4663
E6	335.54	0.5362	0.5293	0.5305	0.4040
Max +	360.94	0.5256	0.5380	0.5447	0.3916
E5	315.17	0.5353	0.5210	0.5178	0.4259
E4	226.64	0.5459	0.4951	0.4809	0.4781
Max -	208.03	0.5457	0.4845	0.4836	0.4862
E3	154.03	0.5434	0.4908	0.4700	0.4957
E2	99.34	0.5337	0.4832	0.4651	0.5180
E1	54.96	0.5520	0.5022	0.4731	0.4727
CL	15.08	0.6406	0.5305	0.3979	0.4310
W1	-11.98	0.3573	0.3339	0.6845	0.6244
W2	-38.01	0.4530	0.4578	0.5841	0.5051
W3	-56.92	0.4909	0.4708	0.5446	0.4937
Max -	-66.14	0.4941	0.4566	0.5443	0.5050
W4	-71.86	0.5341	0.4926	0.5149	0.4584
W5	-72.17	0.4888	0.4850	0.5182	0.5080
Max +	-72.51	0.4937	0.4634	0.5406	0.5023
W6	-71.92	0.4872	0.4839	0.5200	0.5089
W7	-64.78	0.5199	0.4755	0.5341	0.4705
W8	-52.56	0.4642	0.4718	0.5594	0.5046
W9	-38.24	0.4294	0.4916	0.6015	0.4775

Table C-10: Live Load distribution factors from Phase I lanes A and C loaded. Note small total strain at E9 which is near the East abutment. This small strain leads to a negative distribution factor for Girder H which must be ignored. All other readings are valid as the distribution factors along the bridge length remain relatively constant

		Distribution Factor			
Location	Total strain	Girder A	Girder B	Girder C	Girder D
E9	7.07	0.0000	0.9137	0.4074	0.6789
E8	100.47	0.5367	0.5132	0.4300	0.5202
E7	219.25	0.4951	0.5061	0.4714	0.5273
E6	351.14	0.4147	0.5605	0.5046	0.5201
Max +	381.52	0.4122	0.5601	0.5135	0.5143
E5	334.14	0.4694	0.5398	0.4970	0.4939
E4	240.12	0.5304	0.5168	0.4640	0.4888
Max -	224.12	0.5352	0.5142	0.4572	0.4935
E3	162.91	0.5684	0.5162	0.4401	0.4752
E2	103.19	0.5727	0.5417	0.4299	0.4557
E1	53.71	0.6219	0.5425	0.4290	0.4066
CL	20.12	0.4304	0.5994	0.3598	0.6103
W1	-14.34	0.8298	0.5537	0.4059	0.2106
W2	-42.31	0.6509	0.5067	0.4500	0.3923
W3	-60.31	0.6165	0.5382	0.4503	0.3950
Max -	-70.31	0.6156	0.5251	0.4708	0.3886
W4	-75.72	0.6070	0.5042	0.4649	0.4239
W5	-79.24	0.5858	0.5116	0.4513	0.4513
Max +	-80.53	0.5839	0.5302	0.4597	0.4262
W6	-75	0.6099	0.5413	0.4416	0.4072
W7	-68.95	0.5851	0.4841	0.4827	0.4482
W8	-57.3	0.5654	0.5117	0.4813	0.4415
W9	-38.83	0.5650	0.5300	0.4399	0.4651

Table C-11: Live Load distribution factors from Phase II lanes A and C loaded. Note small total strain at E9 which is near the East abutment. This small strain leads to a 0.0 distribution factor for Girder A which must be ignored. All other readings are valid as the distribution factors along the bridge length remain relatively constant

		Distribution Factor			
Location	**Total strain**	**Girder E**	**Girder G**	**Girder H**	**Girder J**
E9	3.48	0.6724	-0.5460	0.1724	0.7011
E8	48.18	0.1658	0.1993	0.2449	0.3900
E7	107.85	0.1596	0.1956	0.2754	0.3694
E6	169.89	0.1092	0.1984	0.3514	0.3410
Max +	182.77	0.0999	0.1882	0.3835	0.3284
E5	163.4	0.1222	0.2038	0.3244	0.3496
E4	116.18	0.1521	0.2126	0.2711	0.3642
Max -	106.42	0.1666	0.2105	0.2547	0.3683
E3	77.74	0.1830	0.1981	0.2611	0.3577
E2	48.17	0.1841	0.1889	0.2657	0.3612
E1	24.96	0.2171	0.2003	0.2564	0.3261
CL	5.84	0.3801	0.1370	0.1712	0.3116
W1	-7.88	-0.1637	0.3807	0.4442	0.3388
W2	-24.3	0.0893	0.2510	0.3045	0.3551
W3	-32.1	0.1361	0.2087	0.2866	0.3685
Max -	-38.31	0.1099	0.2480	0.3028	0.3393
W4	-42.9	0.1396	0.2238	0.3030	0.3336
W5	-44.73	0.1402	0.2571	0.3085	0.2942
Max +	-42.92	0.1095	0.2563	0.3006	0.3336
W6	-42.76	0.1391	0.2222	0.2877	0.3510
W7	-37.84	0.1176	0.2114	0.3092	0.3618
W8	-31.93	0.1306	0.2286	0.3007	0.3401
W9	-23.75	0.1048	0.2021	0.3284	0.3646

Table C-12: Live Load distribution factors from Phase I lane A loaded. Note small total strain at E9 and all West of CL. This small strain leads to variations in distribution factors for the girders which must be ignored. All other readings between the points E7 and E2 hold the most importance. Note DF for Girder J is largest as the loading is close to girder J

		Distribution Factor			
Location	Total strain	Girder A	Girder B	Girder C	Girder D
E9	3.45	0.0000	0.3304	0.1710	0.4986
E8	44.85	0.1266	0.2419	0.2355	0.3960
E7	97.25	0.0898	0.2145	0.2781	0.4176
E6	157.64	0.0691	0.1872	0.3096	0.4341
Max +	170.37	0.0599	0.1747	0.3223	0.4431
E5	147.27	0.0763	0.2031	0.2977	0.4230
E4	102.96	0.1087	0.2414	0.2573	0.3927
Max -	95.33	0.1351	0.2225	0.2587	0.3837
E3	66.77	0.1712	0.2485	0.2440	0.3364
E2	40.08	0.2081	0.2507	0.2328	0.3084
E1	23.04	0.1810	0.2804	0.2027	0.3359
CL	5.39	0.0482	0.8275	-0.3043	0.4286
W1	-14.89	0.2008	0.2646	0.3613	0.1733
W2	-19.28	0.2806	0.2396	0.3216	0.1582
W3	-28.41	0.2210	0.2401	0.2735	0.2654
Max -	-32.24	0.2618	0.2333	0.2441	0.2609
W4	-35.44	0.2627	0.2325	0.2683	0.2365
W5	-35.81	0.2533	0.2309	0.2617	0.2541
Max +	-35	0.2486	0.2203	0.2757	0.2554
W6	-34.64	0.2373	0.2330	0.2653	0.2644
W7	-32.38	0.2378	0.2378	0.2662	0.2582
W8	-26.87	0.2300	0.2281	0.2944	0.2475
W9	-16.46	0.3123	0.2333	0.3068	0.1476

Table C-13: Live Load distribution factors from Phase II lane C loaded. Note small total strain at E9 and all West of CL. This small strain leads to variations in distribution factors for the girders which must be ignored. All other readings between the points E7 and E2 hold the most importance. Note DF for Girder D is largest as the loading is close to Girder J

C.5.5 Comparison of Phase I and Phase II Distribution Factors

As superposition and comparisons between Phase I and Phase II response have already been shown, a brief distribution factor comparison will be adequate. To compare distribution factors, differences of computed values from similar tests will be used. If the difference is zero the distribution factors are equal. Some variation is expected but differences should be small. Large differences may occur at locations of small total strain as errors occur in calculating the DF's. The comparison between distribution factors for Phase I and Phase II for lanes A and C loaded is in Table C-14.

Location	Total Strain Difference	DF E - DF D	DF G - DF C	DF H - DF B	DF J - DF A
E9	-4.25	-0.4307	0.4437	-0.9846	0.9716
E8	-10.27	0.0002	0.0623	-0.0387	-0.0238
E7	-8.83	0.0217	0.0228	-0.0156	-0.0288
E6	-15.6	0.0161	0.0247	-0.0300	-0.0107
Max +	-20.58	0.0114	0.0246	-0.0154	-0.0205
E5	-18.97	0.0415	0.0240	-0.0220	-0.0435
E4	-13.48	0.0571	0.0310	-0.0359	-0.0523
Max -	-16.09	0.0522	0.0274	-0.0306	-0.0490
E3	-8.88	0.0682	0.0507	-0.0462	-0.0727
E2	-3.85	0.0781	0.0533	-0.0766	-0.0547
E1	1.25	0.1454	0.0732	-0.0695	-0.1492
CL	-5.04	0.0302	0.1707	-0.2015	0.0006
W1	2.36	0.1467	-0.0720	0.1308	-0.2055
W2	4.3	0.0607	0.0078	0.0773	-0.1458
W3	3.39	0.0959	0.0205	0.0064	-0.1228
Max -	4.17	0.1055	-0.0142	0.0192	-0.1106
W4	3.86	0.1102	0.0278	0.0107	-0.1486
W5	7.07	0.0376	0.0337	0.0066	-0.0778
Max +	8.02	0.0675	0.0037	0.0104	-0.0816
W6	3.08	0.0800	0.0423	-0.0213	-0.1010
W7	4.17	0.0718	-0.0072	0.0500	-0.1145
W8	4.74	0.0227	-0.0095	0.0477	-0.0609
W9	0.59	-0.0357	0.0518	0.0715	-0.0875

Table C-14: Comparison of DF's for Phase I and Phase II lanes A and C loaded

The distribution factors rarely have a difference of more than 0.05. Total strains at a section are also very close with Phase II experiencing more strain. The results verify the previous conclusion of symmetric behavior.

To verify superposition, results from lane A loaded and lane C loaded were added together. From this, the results of lanes A and C loaded were subtracted. Results from Phase I tests are in Table C-15 and results from Phase II tests are in Table C-16.

As noted for the symmetry check, the difference in values rarely exceeds 0.05. This also validates the previous result of superposition being valid for the two phases.

Location	Total strain Difference	Girder E	Girder G	Girder H	Girder J
E9	4.77	0.969199	-1.05641	0.36499	-0.27778
E8	3.35	0.097057	0.002363	-0.03783	-0.06159
E7	-3.92	0.095827	-0.00464	-0.03564	-0.05555
E6	0.41	0.060573	-0.00214	-0.02432	-0.03412
Max +	-4.47	0.066856	-0.01189	-0.01261	-0.04236
E5	-1.81	0.068147	0.002891	-0.02208	-0.04896
E4	-2.12	0.073898	0.015678	-0.01597	-0.0736
Max -	-1.23	0.085847	0.014843	-0.02869	-0.072
E3	-2.26	0.093245	-0.01175	-0.01034	-0.07115
E2	-2.84	0.063618	0.018161	0.007567	-0.08935
E1	-6.54	0.110975	0.005042	-0.00353	-0.11249
CL	-1.45	0.291543	0.004428	-0.18813	-0.10784
W1	-0.18	-0.53265	9.19E-05	0.13352	0.399038
W2	-4.67	-0.0188	0.021764	-0.08367	0.080699
W3	-0.54	-0.05859	-0.01369	-0.00171	0.073993
Max -	-4.41	-0.05605	0.030204	-0.01818	0.044025
W4	-3.95	-0.05232	-0.03488	0.022112	0.065087
W5	-8.91	-0.00837	-0.00228	0.010379	0.000273
Max +	-4.15	-0.07064	0.024086	0.011871	0.034688
W6	-4.54	-0.03471	-0.02431	-0.00982	0.068836
W7	-4.65	-0.07689	-0.03612	-0.00016	0.113177
W8	-3.48	-0.04537	-0.02339	-0.03058	0.099344
W9	-4.29	-0.04819	-0.09251	-0.0707	0.211402

Table C-15: Superposition verification of Phase I tests. Values in the columns are the lane A and lane C superimposed minus the lanes A and C loaded results

Location	Total strain Difference	Girder A	Girder B	Girder C	Girder D
E9	-1.39	0	-0.0362	-0.07491	0.111106
E8	-3.16	-0.01564	-0.02251	0.014393	0.023754
E7	0.72	-0.04227	-0.02366	0.024618	0.041316
E6	-4.72	-0.00543	-0.02476	0.012573	0.017622
Max +	4.78	-0.03161	-0.03116	0.013661	0.049106
E5	-53.36	-0.01488	-0.0546	0.002864	0.066618
E4	-6.53	-0.03689	0.001114	0.001794	0.033983
Max -	-9.91	-0.01445	-0.01268	-0.00182	0.028945
E3	-9.26	-0.01302	-0.00569	0.005049	0.013656
E2	-10.02	0.010001	-0.02199	-0.01684	0.028835
E1	-6.11	-0.09559	0.016747	-0.01333	0.092176
CL	-8.09	-0.12314	0.389199	-0.46079	0.194739
W1	-14.73	-0.2856	0.04589	0.141636	0.098073
W2	-9.49	-0.02929	0.028709	0.072672	-0.07209
W3	-11.59	-0.04708	-0.01764	0.024121	0.040594
Max -	-13.8	-0.0187	-0.0046	-0.02829	0.051586
W4	-13.28	-0.0069	0.01394	0.030879	-0.03792
W5	-11.29	0.01816	0.011363	0.012674	-0.0422
Max +	-11.87	-0.00273	-0.03295	0.029424	0.006255
W6	-14.8	-0.02848	-0.05111	0.03436	0.045233
W7	-17.62	-0.01196	0.025319	-0.01033	-0.00303
W8	-13.06	-0.00595	-0.00165	0.019538	-0.01194
W9	-12.71	0.083049	-0.01336	0.07703	-0.14672

Table C-16: Superposition verification of Phase II tests. Values in the columns are the lane A and lane C superimposed minus the lanes A and C loaded results